

CHARACTERIZATION OF GEOMETRIC SURFACE FEATURES USING
STATISTICALLY BASED ANALYTICAL TOOLS

By

Farzad Azimi

A dissertation submitted to the faculty of
The University of North Carolina at Charlotte
in partial fulfillment of the requirements
for the degree of Doctor of Philosophy in
Mechanical Engineering

Charlotte

2019

Approved by:

Dr. Brigid Mullany

Dr. Edward Morse

Dr. Matthew Davies

Dr. Thomas Suleski

Dr. Mohammad Kazemi

© 2019

Farzad Azimi

ALL RIGHTS RESERVED

ABSTRACT

FARZAD AZIMI. Characterization of Geometric Surface Features Using Statistically Based Analytical Tools. (Under the direction of Dr. BRIGID MULLANY)

The nature and quality of a surface's topography can play an important role in a part's performance and expected longevity. The complexity of a surface topography means that while commonly used ISO 25178-2 height based statistical metrics are capable of quantifying periodicity and directionality, they are unable to completely describe geometric isolated surface features, i.e. unwanted processing defects. The same standard does outline other metrics capable to describing geometric features, but these require more processing and user input. This dissertation presents a novel approach for quantifying both surface characteristics and features by calculating simple statistical height data metrics as a surface is rotated about its center and then graphing them in a polar plot format.

Key polar plots metrics such as minimum and maximum radius, number of lobes and difference between their angular locations, etc. can be used to quantify surface isotropy, surface directionality, and surface periodicity. Uniquely, analysis of the polar plots can also provide estimates of the number and geometric sizes of isolated circular and linear geometric surface features. The capabilities and limitations of the approach are outlined, and discussed with respect to actual surfaces topographies. The simplicity, and potential speed of the method addresses the ever-present industrial need for fast, robust methods of surface characterization.

ACKNOWLEDGEMENTS

Throughout my four years of research upon completion of this dissertation many people have helped me and contributed, and I would like to take this opportunity to acknowledge their contributions. First, my PhD advisor, Dr. Brigid Mullany, who had the biggest impact on teaching and developing me as a researcher in the past four years. I am most grateful for her significant mentorship, guidance, and help during my PhD work. Second, Dr. Russell Keanini, one of the kindest persons I have ever met, whom without his help I would not have been able to continue my work here. Third, my dear friend, Dr. Hossein Shahinian, who helped me tremendously from the beginning of my study at the University of North Carolina at Charlotte to date.

I am also very grateful to Dr. Edward Morse, Dr. Matthew Davies, Dr. Thomas Suleski, and Dr. Mohammad Kazemi for their time and consideration on being part of my PhD committee, and Dr. Jimmie Miller for providing feedbacks on this work.

This research was supported by UNC Charlotte's Center for Precision Metrology and partially supported by the National Science Foundation's IRD program. I would like to acknowledge the significant support and help of Center for Precision Metrology (CPM).

I would also like to thank Dr. Richard Leach and Dr. Samuel Mingyu Liu from the University of Nottingham for providing the AFM samples.

I am extremely grateful to my loving parents, my lovely sister, and my dear uncle, Dr. Fakhreddin Azimi, who were there for me no matter what. I cannot thank them enough and their unwavering support was the main foundation supporting me and driving me forward.

Last but not least, my beautiful and lovely friend, Agha Farhad, whom without his presence and positive energy I for sure would not have been able to finish my PhD study.

TABLE OF CONTENTS

LIST OF TABLES	viii
LIST OF FIGURES	ix
CHAPTER 1: INTRODUCTION	1
CHAPTER 2: LITERATURE REVIEW	5
2.1 Introduction	5
2.2 Effects of surface topography	10
2.2.1 Tribology (friction, wear, lubrication)	11
2.2.2 Reflection	12
2.2.3 Fatigue life	12
2.2.4 Corrosion	13
2.2.5 Adhesion	14
2.3 Surface topography measurement instruments	14
2.3.1 Scanning probe microscopes, SPM	16
2.3.2 Stylus instruments	16
2.3.3 Optical methods	18
2.4 Characterization of surface topography	21
2.4.1 Surface profile characterization (2D)	22
2.4.2 Surface areal characterization (3D)	23
2.4.3 Surface visual presentation	25
2.5 Surface inspection	29
2.5.1 Manual inspection	29
2.5.2 Automatic inspection	33
2.6 Conclusion	35
CHAPTER 3: METHODOLOGY	37
3.1 Introduction	37
3.2 Polar plots generation details	38
3.2.1 Rotation in MATLAB	39
3.3 Processing time of generating polar plots	45
3.4 Items affecting polar plots	47
3.5 Unprocessed surfaces	47
3.6 Summary	50
CHAPTER 4: SURFACE CHARACTERIZATION	51

4.1 Introduction	51
4.2 Surface roughness of Gaussian surfaces	51
4.3 Surface isotropy and directionality	54
4.4 Multi directional surfaces	58
4.5 Surface periodic structure	58
4.5.1 Other types of periodic features	65
4.5.2 Identifying different periodic structures	69
4.5.3 Multi directional periodic features	71
4.5.4 Comparison with the power spectral density, PSD, analysis	72
4.5.5 Periodicity in real surfaces	74
4.6 Analysis of real samples	75
4.6.1 Surface roughness of a Gaussian surface	75
4.6.2 Isotropy and directionality	76
4.6.3 Surface periodic structure	81
4.7 Summary	88
CHAPTER 5: SINGLE FEATURE CHARACTERIZATION	90
5.1 Introduction	90
5.2 Single circular feature	90
5.2.1 Feature below or above the surface	92
5.2.2 Estimation of diameter and depth	94
5.2.3 Detectability threshold	97
5.2.4 Analysis of a real surface with a circular feature	100
5.3 Single scratch	103
5.3.1 Estimation of length, width, and depth	106
5.3.2 Detectability threshold	109
5.3.3 Analysis of a real surface with a linear feature	113
5.4 Summary	115
CHAPTER 6: MULTIPLE FEATURES CHARACTERIZATION	118
6.1 Introduction	118
6.2 Multiple circular features	118
6.2.1 Estimation of the number of digs based on the number of peaks	123
6.2.2 Estimation of quantity and diameter of circular features from polar plots	134
6.2.3 Non-circular features	154
6.2.4 Analysis of a real surface with a circular feature	155
6.2.5 Analysis of real surfaces with multiple features	157
6.3 Multiple scratches	160

6.3.1 Non-parallel and identical scratches	161
6.3.2 Non-parallel and non-identical scratches	164
6.3.3 Parallel and identical scratches	165
6.3.4 Different cases of parallel scratches	170
6.3.5 non-straight scratches	185
6.3.6 Analysis of a real surface with a single scratch	186
6.3.7 Analysis of real surfaces with multiple scratches	189
6.4 Multiple linear and circular features on the surface	191
6.4.1 Building blocks for polar plots of multiple linear and circular features	192
6.4.2 A circular and a linear feature on the surface	192
6.4.3 Deconstructing complex cases using building blocks	195
6.4.4 General case of multiple circular and linear features on the surface	196
6.4.5 Peak analysis	198
6.4.6 Analysis of a real surface with mixed features	202
6.5 Obtainable information about the surface from the polar plots	203
6.6 Analyzing polar plots of unknown samples (blind testing)	206
6.7 Summary	212
CHAPTER 7: CONCLUSIONS AND FUTURE DIRECTIONS	216
7.1 Conclusions	216
7.2 Processing time of the approach	221
7.3 Future directions	221
7.3.1 Processing aspects	222
7.3.2 Applications aspects	222
REFERENCES	224
APPENDIX A: STATISTICAL TOOLS	229
A.1 Moment of data	229
A.2 Normal distribution	230
A.3 Chi distribution	230
APPENDIX B: PUBLICATIONS	232
APPENDIX C: MATLAB CODES	233

LIST OF TABLES

Table 4-1: The angles of maximum and minimum radii of the polar plot of Figure 4-6.	65
Table 4-2: c coefficients for different types of periodic structures	67
Table 4-3: Angle difference for σ_{Rq} polar plot of surfaces shown in Figure 4-14.....	69
Table 4-4: Calculated wavelength for different structures based on $\beta=10.6^\circ$	70
Table 4-5: Angle β for different wavelengths and structures.....	71
Table 4-6: Estimated wavelengths from polar plots and the PSD analysis and the associated error.	87
Table 4-7: Polar plot's features, and their ISO 25178-2 equivalent parameters.	89
Table 5-1: Polar plot's features.....	117
Table 6-1: Comparison between single circular feature radius and accepted feature radius, with their minimum radius of the $\sigma_{\mu h}$ polar plots.	149
Table 6-2: Number and radius of multiple circular features combination, and their characteristics in comparison with the accepted feature.....	149
Table 6-3: Scratches' properties from CSI and polar plots.....	191
Table 6-4: Calculated wavelength for different structures based on $\beta=2.0^\circ$	210
Table 6-5: Key metrics from polar plots to analyze different features	215
Table 7-1: Polar plot's key features.	217

LIST OF FIGURES

Figure 1-1: A thresholded surface with three negative circular, and two linear features, b) its $\sigma_{\mu h}$ polar plot.....	3
Figure 2-1: a) Primary profile of a surface and its roughness profile, b) the waviness profile, and c) the form profile. Image taken from [6].....	6
Figure 2-2: Profiles from a) a steel milled surface, b) steel reamed surface, c) steel ground surface and d) steel turned surface	8
Figure 2-3: Field parameters based on ISO 25178-2	9
Figure 2-4: a) NIST scratch grade 0.040 sample, and b) NIST dig grade 0.040 sample measured with ZeGage white light interferometer, 20 \times objective, FoV equal to 417 $\mu\text{m} \times 417\mu\text{m}$	10
Figure 2-5: Steadman diagram showing the range and resolution of available measurement techniques. image taken from [43].....	15
Figure 2-6: Schematic of a stylus instrument, image taken from [47].....	17
Figure 2-7: Reflection of an electromagnetic wave from a solid surface when a) specular only, b) diffusive only, and c) combined specular and diffusive. Image taken from [3]	19
Figure 2-8: Schematic of an interferometer instrument (Linnik interferometer), image taken from [5].....	21
Figure 2-9: Surface topography with ten contour lines (left), and 20 contour lines (right); image taken from [1]	26
Figure 2-10: Dimetric projection of a milled surface with the projection angle equal to 60 degrees. Image taken from [8]	27
Figure 2-11: Example of truncation method on a milled surface. Image taken from [8].....	27
Figure 2-12: Example of truncation and inversion combined. Image taken from [8].....	28
Figure 3-1: Constituent profiles of a 3D height map, the distance between each profile is 30 pixels for demonstration purposes.....	38
Figure 3-2: All the required steps to obtain the σ_{Rq} polar plot.	39
Figure 3-3: a) Original matrix of size $n_{initial} \times n_{initial}$, and b) the same surface when rotated θ degrees with size $n_{new} \times n_{new}$	40
Figure 3-4: a) Initial matrix with a rectangular feature and when it is rotated 40 $^\circ$ clockwise b) with Nearest-neighbor interpolation, c) Bilinear interpolation, and d) Bicubic interpolation method.	41
Figure 3-5: a) Unrotated height map of a surface with Gaussian distribution of heights, b) height map rotated 45 $^\circ$ and the maximum size increase, and c) super imposed rectangle on the height map containing only real height data points.	43
Figure 3-6: a) Initial height map of a surface with Gaussian distribution of heights and the sp histogram of the columns inside the superimposed rectangle, b) initial height map rotated 30 $^\circ$ and the sp histogram of the columns inside the superimposed rectangle, and c) initial height map rotated 45 $^\circ$ and the sp histogram of the columns inside the superimposed rectangle. ...	44
Figure 3-7: a) MATLAB generated surface with Gaussian distribution of heights and its b) σ_{Rq} polar plot, c) Sk_{Rq} polar plot, and d) Ku_{Rq} polar plot.	45

Figure 3-8: a) A MATLAB generated surface without its form removed (the surface is formed with a second degree polynomial), b) the same surface shown in 3D, and c) its σ_{Rq} polar plot. ...	48
Figure 3-9: a) A MATLAB generated planar surface without its tilt removed, b) the same surface shown in 3D, and c) its σ_{Rq} polar plot.	49
Figure 4-1: MATLAB generated surface with Gaussian distribution of heights with Sq equal to a) 0.1 μm , and b) 0.2 μm and their σ_{Rq} , Sk_{Rq} , and Ku_{Rq} polar plots.	52
Figure 4-2: a) A ground steel surface measured with CSI 20 \times objective, b) it standard deviation of Rq histogram polar plot.....	55
Figure 4-3: a) The ground surface shown in Figure 4-2 when rotated such that lay direction is vertical, b) when rotated such that the lay direction is close to vertical, and c) when rotated such that the lay direction is perpendicular to the columns and two sample profiles and the Rq histogram for each case.....	56
Figure 4-4: σ_{Rq} polar plot of the surface shown in Figure 4-2, and b) zoomed in area of the plot in the lobe region.	57
Figure 4-5: a) Grayscale image of a plateau honed surface, and b) its σ_{Rq} polar plot.	58
Figure 4-6: a) A theoretical surface with a sinewave feature of wavelength 300 pixels and a profile along the vertical axis, and b) σ_{Rq} polar plot.	59
Figure 4-7: a) MATLAB TM generated sinewave surface with wavelength of 300 pixels, a vertical profile, and its Rq histogram, b) same surface when features are horizontal, a vertical profile, and its Rq histogram, d) same surface rotated 10 $^\circ$ clockwise, a vertical profile, and its Rq histogram	59
Figure 4-8: a) MATLAB TM generated sinewave surface with wavelength of 300 pixels when rotated 10 $^\circ$ clockwise, b) two randomly selected vertical profiles, and c) the two profiles shown on the second periodic structure.	60
Figure 4-9: Geometrical model of a periodic structure on a surface when it is rotated θ°	61
Figure 4-10: The first upper quarter of the polar plot in Figure 4-6 in Cartesian coordinate.	62
Figure 4-11: Visual representation of the steps involved in finding the length of sections of a periodic structure that has the maximum or minimum range of Rq values	63
Figure 4-12: Standard deviations of Rq values versus the ratio of the size of the moving window over the wavelength of the second periodic feature for a sinewave structure.	64
Figure 4-13: Standard deviations of Rq values versus the ratio of the size of the moving window over the wavelength of the second periodic feature for a) step wave structure, b) sawtooth structure, c) cusp structure, and d) grating structure.....	66
Figure 4-14: Theoretical surfaces with a) sawtooth structure, b) cusp structure, c) step wave structure, d) grating structure, a horizontal profile for each structure, and their σ_{Rq} polar plots.	68
Figure 4-15: σ_{Rq} polar plot for a theoretical surface containing an unknown periodic structure. ...	69
Figure 4-16: Three MATLAB generated highly structured surfaces along with their σ_{Rq} polar plots.	72
Figure 4-17: A theoretical surface with a sinewave structure of 100 pixels wavelength, when a) unrotated, b) rotated 30 $^\circ$ clockwise, and their σ_{Rq} polar plot, and PSD plots.	73

- Figure 4-18: σ_{Rq} polar plot of a) the milled surface in Figure 4-25(a) and, b) the ground surface in Figure 4-20(a). 75
- Figure 4-19: a) A polished glass, b) its σ_{Rq} polar plot. The surface is measured with Zygo ZeGage coherence scanning interferometer (20× objective, piston, tilt and a 4th order polynomial removed from the measurement). 75
- Figure 4-20: a) An Aluminum ground surface, b) its σ_{Rq} polar plot, and c) the zoomed in region of the polar plot around the lobe. The surface is measured with Zygo ZeGage coherence scanning interferometer (20× objective, piston, tilt and a 4th order polynomial removed from the measurement). 77
- Figure 4-21: Superimposed rectangle area on the initial surface when rotated 64.2° clockwise along with the PSD plot and a random horizontal profile from the surface. 78
- Figure 4-22: a) Vibrationally finished aluminum surface, and b) its σ_{Rq} polar plot. The surface is measured with Zygo ZeGage coherence scanning interferometer (20× objective, piston, tilt and a 4th order polynomial removed from the measurement). 79
- Figure 4-23: a) A ground steel surface, and b) a milled steel surface along with their random horizontal profiles and their σ_{Rq} polar plots. 80
- Figure 4-24: PSD plot of the surface shown in a) Figure 4-23(a), and b) Figure 4-23(b). 80
- Figure 4-25: a) A Steel milled surface, b) its σ_{Rq} polar plot, and c) the zoomed in region of the polar plot around the lobe. The surface is measured with Zygo ZeGage coherence scanning interferometer (20× objective, piston, tilt and a 4th order polynomial removed from the measurement). 82
- Figure 4-26: a) Inside the superimposed rectangle when the milled surface is rotated 98.3°, and b) a horizontal profile of the surface. 82
- Figure 4-27: 1D horizontal PSD when the tooling marks are oriented to be vertical. 83
- Figure 4-28 a) A steel reamed surface and, b) its σ_{Rq} polar plot. The surface is measured with Zygo ZeGage coherence scanning interferometer (5× objective, piston, tilt and a 4th order polynomial removed from the measurement). 84
- Figure 4-29: Superimposed rectangle area on the initial surface when rotated 0.4° clockwise along with the PSD plot and a random horizontal profile from the surface. 85
- Figure 4-30: AFM samples after piston, tilt, and a 4th order polynomial is removed from their height map, a random horizontal profile, and their σ_{Rq} polar plots. 86
- Figure 5-1: Schematically depicts a circular feature during rotation. 91
- Figure 5-2: a) MATLAB generated surface with Gaussian distribution of heights, b) its Rq histogram, c) its σ_{Rq} polar plot, d) the same surface with a negative circular feature of 100 pixels diameter, e) its Rq histogram, and f) its σ_{Rq} polar plot. 92
- Figure 5-3: MATLAB generated surface with Gaussian distribution of heights with a) a negative circular feature, and b) a positive circular feature and their σ_{Rq} polar plots. 93
- Figure 5-4: a) MATLAB generated surface with a Gaussian distribution of heights and a negative circular feature, 100 pixels diameter, and its Rsk histogram, b) the same surface when the feature is made positive and its Rsk histogram, and c) the skewness of Rsk histogram for both surfaces and a defect free surface. 94
- Figure 5-5: a) MATLAB generated surface with Gaussian distribution of heights with a negative feature of 100 diameter, b) the Rq histogram of the surface and the Rq threshold. 95

Figure 5-6: a) A circular feature in continuous environment, and b) the same feature in discrete environment.	96
Figure 5-7: Detectable threshold limit for diameter and depth combination.	98
Figure 5-8: MATLAB generated surface with a negative circular feature of diameter 100 pixels and depth of 0.025 μm , and b) the same surface with a circular feature of diameter of 100 pixels and depth of 0.04 μm ; and their Rq histogram.	99
Figure 5-9: a) A measured surface with a negative feature, b) defect free surface of the same sample, c) and d) their σ_{Rq} polar plots.	101
Figure 5-10: Skewness of the Rsk histogram polar plot of the surface and the defect-free surface on the same plot.	102
Figure 5-11: Rq histogram of the surface with the negative circular feature shown in Figure 5-9(a).	102
Figure 5-12: MATLAB generated surface with a Gaussian distribution of heights with a scratch of $250L \times 5w$ pixels, and its σ_{Rq} polar plot, skewness and kurtosis of the Rq histogram polar plots when a) its depth is equal to 0.05 μm and b) its depth is equal to 0.15 μm , (The rotational angle for creating these polar plots is 1°).	104
Figure 5-13: a) MATLAB TM generated surface with a Gaussian distribution of heights with a scratch of $200L \times 5w$ pixels, b) geometrical model of the scratch.	105
Figure 5-14: a) MATLAB generated surface with Gaussian distribution of heights and a scratch of 400×10 pixels, and depth of 0.10 μm , and b) its σ_{Rq} polar plot.	108
Figure 5-15: The Rq histogram of the surface when the scratch is vertical.	108
Figure 5-16: Associated error of scratch's length estimation for depths equal to 0.02 μm and 0.10 μm of a surface comprising 1000×1000 pixels.	109
Figure 5-17: Detectable threshold limits for length and depth combination of a scratch based on equations 5-1.	110
Figure 5-18: Detectable threshold limits for length and depth combination of a scratch based on equations 5-11, 5-12, and 5-13.	111
Figure 5-19: a) MATLAB generated surface with Gaussian distribution of heights and a scratch of $100L \times 5w$ pixels, and depth of 0.02 μm , b) its σ_{Rq} polar plot, c) skewness of the Rq histogram polar plot, and d) kurtosis of the Rq histogram polar plot.	112
Figure 5-20: Detectable threshold limits for length and depth combination of a scratch based on equations 5-1 and 5-11.	113
Figure 5-21: a) A measured surface with a negative linear feature, b) defect free surface of the same sample, c) and d) their σ_{Rq} polar plots.	114
Figure 5-22: Skewness of the Rsk histogram polar plot of the surface and the defect-free surface on the same plot.	115
Figure 6-1: MATLAB generated surface with Gaussian distribution of heights with a negative circular feature and its σ_{Rq} polar plot.	119
Figure 6-2: MATLAB generated surface with Gaussian distribution of heights with a) two negative circular features and its Rq histogram, b) when the surface is rotated 155° CW and its Rq histogram, and c) its σ_{Rq} polar plot.	120
Figure 6-3: Schematic representation of two circular features getting in and out of alignment. .	121

Figure 6-4: a) : MATLAB generated surface with Gaussian distribution of heights with two negative circular features of 50 pixels radius, b) its σ_{Rq} polar plot, and c) the zoomed in region of the lobe in the polar plot.	122
Figure 6-5: MATLAB generated surface with Gaussian distribution of heights with three negative circular features of 50 pixels radius and 0.01 μm depth, and b) its σ_{Rq} polar plot.	123
Figure 6-6: MATLAB generated surface with Gaussian distribution of heights and three negative circular features and its σ_{Rq} polar plot.	124
Figure 6-7: The maximum and minimum values of estimation of circular features.	124
Figure 6-8: a) Histogram of a data set of 1000 normally distributed values with mean and standard deviation, and range equal to 0, 1, and 6.8, b) the same data set when the range is increased to 15.	126
Figure 6-9: a) MATLAB generated surface with two negative circular features, b) the mean of columns plot, c) standard deviation of columns plot, d) the same surface when rotated 90°, e) the mean of columns plot, and f) standard deviation of columns plot.	127
Figure 6-10: σ_{Rq} polar plot and $\sigma_{\mu h}$ polar plot of the surface shown in Figure 6-9(a).	127
Figure 6-11: a) MATLAB generated surface with Gaussian distribution of heights with three aligned circular features, the same surface when it is mapped with b) a second degree polynomial, and c) a fourth degree polynomial.	128
Figure 6-12: a) The surface in Figure 6-11(b) after thresholding, and b) the surface in Figure 6-11(c) after thresholding.	129
Figure 6-13: a) A diamond turned surface with three negative circular features of 30 pixels diameter and 10 nm depth, measured with ZeGage CSI 20 \times objective, and b) the same surface after it is thresholded.	130
Figure 6-14: a) The thresholded $n \times n$ matrix, and b) the new $2n \times 2n$ zero matrix.	131
Figure 6-15: Point p_i and the pd neighboring points in the polar plot.	132
Figure 6-16: a) MATLAB generated surface with three negative circular feature of 50 pixels diameter and 0.1 μm depth, b) its σ_{Rq} polar plot, c) the same surface after it is thresholded and distorted with a fourth order polynomial and d) its $\sigma_{\mu h}$ polar plot.	133
Figure 6-17: a) MATLAB generated surface with three negative circular feature of 50 pixels diameter and 0.1 μm depth, b) its $\sigma_{\mu h}$ polar plot, c) the same surface after it is thresholded and distorted with a fourth order polynomial and d) its $\sigma_{\mu h}$ polar plot.	134
Figure 6-18: Thresholded surface with a circular negative feature with 100 pixels diameter, b) its $\sigma_{\mu h}$ polar plot, and c) columns' mean plot.	135
Figure 6-19: Conversion of a circular feature to a square with equal areas.	136
Figure 6-20: a) Thresholded surface with a circular negative feature with 100 pixels diameter, b) the same surface after the circular feature is converted to a square, c) columns' mean plot of (a), d) columns' mean plot of (b), e) $\sigma_{\mu h}$ polar plot of (a), and f) $\sigma_{\mu h}$ polar plot of (b).	137
Figure 6-21: General form of the graph of columns mean height values for a surface containing a square feature.	138
Figure 6-22: Associated error of the calculated radius of the $\sigma_{h\mu}$ polar plot after converting a circular feature to a square one with equal areas.	139

Figure 6-23: a) A thresholded surface with four negative circular features, b) the same surface after all the circular features are converted to squares with equal areas.	140
Figure 6-24: a) A thresholded surface with four negative circular features, b) $\sigma_{\mu h}$ polar plot and the circle with r_{min_α} radius.....	140
Figure 6-25: a) A thresholded surface with two negative circular features when overlapping exists, b) when overlapping does not exist.	141
Figure 6-26: Schematic representation of the case when all of the circular features are distributed along the diagonal of the surface.	142
Figure 6-27: a) A thresholded surface with multiple negative circular features, and b) a thresholded surface with a single square feature with the same area of the summation of multiple features' area.....	143
Figure 6-28: a) A thresholded surface with the accepted circular feature, and b) the accepted circular feature converted to a square with equal area.	145
Figure 6-29: Number of allowed circular features, α , based on a given accepted feature.	146
Figure 6-30: Number of allowed circular features, α , based on the area of a given accepted feature, A_s	147
Figure 6-31: Number of allowed circular features, α , based on a given accepted feature.	148
Figure 6-32: A thresholded surface with five negative circular and collinear features.	150
Figure 6-33: Behavior of the α versus the minimum radius of the surface with multiple collinear features.....	151
Figure 6-34: A thresholded surface with a) six, and b) eight non-identical circular features. The overall area of the features on both surfaces are equal.	152
Figure 6-35- A thresholded surface with multiple non-identical, and overlapping features.....	153
Figure 6-36: a) A thresholded surface with four negative asymmetric features, b) a thresholded surface with two symmetric and two asymmetric negative features, c), and d) their $\sigma_{\mu h}$ polar plots.....	154
Figure 6-37: a) The thresholded surface with the circular feature, b) its $\sigma_{\mu h}$ polar plot, c) the same surface when the feature is converted to a square, d) its $\sigma_{\mu h}$ polar plot.	155
Figure 6-38: $\sigma_{\mu h}$ polar plot of the thresholded surface with the circular feature.	156
Figure 6-39: Height map of a polished glass.	157
Figure 6-40: a) Original surface, b) its σ_{Rq} polar plot, c) original surface after thresholding, and d) its $\sigma_{\mu h}$ polar plot.	158
Figure 6-41: a) The thresholded and distorted surface, and b) its $\sigma_{\mu h}$ polar plot.....	159
Figure 6-42: a) Polished glass surface measured with CSI 5 \times after processing, and b) the same surface after it is thresholded.	159
Figure 6-43: $\sigma_{\mu h}$ polar of the surface with four negative near-circular features.....	160
Figure 6-44: a) MATLAB generated surface with three scratches, b) the same surface after it is thresholded, and c) its $\sigma_{\mu h}$ polar plot.	162
Figure 6-45: The surface of Figure 6-44(b) when rotated a) 30 $^\circ$, b) 90 $^\circ$, and c) 150 $^\circ$ with the graph of their columns mean height values.	163

Figure 6-46: a) MATLAB generated surface with a Gaussian distribution of heights with three non-identical and non-parallel scratches, b) the same surface after it is thresholded, c) its $\sigma_{\mu h}$ polar plot.	164
Figure 6-47: The surface of Figure 6-46(b) when rotated a) 30°, b) 90°, and c) 150° with the graph of their columns mean height values.	165
Figure 6-48: Thresholded surfaces with one and two features with equal areas, their columns mean height values graph, as well as the histogram of their μh values.....	166
Figure 6-49: Thresholded surfaces with one and two features with equal areas, their columns mean height values graph, as well as the histogram of their μh values.....	167
Figure 6-50: a) A thresholded surface with a single scratch, b) its μh histogram.....	168
Figure 6-51: Schematic model of a scratch rotated equal to its critical angle.	169
Figure 6-52: All possible cases of parallel scratches configuration on a surface, a) all features completely contained within the same number of columns when horizontal, b) all features completely contained with the same number or rows when horizontal, c) non-overlapping features, and d) randomly located.	171
Figure 6-53: a) A thresholded surface with three parallel scratches, and b) its $\sigma_{\mu h}$ polar plot.	172
Figure 6-54: The surface of Figure 6-53(a) during clockwise rotation, a) feature-related columns cross two features, and b) feature-related columns cross one feature.....	173
Figure 6-55: Schematic representation of the configuration of parallel scratches at the angle that the minimum radius of the $\sigma_{\mu h}$ polar plot occurs.....	174
Figure 6-56: a) A thresholded surface with three scratches of the same length and different width, and b) its $\sigma_{\mu h}$ polar plot.	175
Figure 6-57: A thresholded surface with three parallel and aligned scratches, and b) its $\sigma_{\mu h}$ polar plot.	176
Figure 6-58: a) A thresholded surface with three scratches aligned, b) its $\sigma_{\mu h}$ polar plot, c) a thresholded surface with one scratch with its length equal to the cumulative length of three scratches, and d) its $\sigma_{\mu h}$ polar plot.....	178
Figure 6-59: Standard deviation of the μh histogram plotted in Cartesian coordinates.....	179
Figure 6-60: a) A thresholded surface with two scratches of the same width and different length values, and b) its $\sigma_{\mu h}$ polar plot.	179
Figure 6-61: A thresholded surface containing a) two scratch with the same length and different width, b) two scratches with different length and width values.....	180
Figure 6-62: A thresholded surface with three parallel scratches without overlapping, and b) its $\sigma_{\mu h}$ polar plot.....	181
Figure 6-63: a) A thresholded surface with two non-overlapping scratches with the same width but different lengths, and b) its $\sigma_{\mu h}$ polar plot.	182
Figure 6-64: A thresholded surface with two non-overlapping scratches with different widths and lengths, and b) its $\sigma_{\mu h}$ polar plot.....	182
Figure 6-65: a) A thresholded surface with three parallel scratches, and b) its $\sigma_{\mu h}$ polar plot.	183
Figure 6-66: a) A thresholded surface with three randomly located scratches with equal length but different width, and b) its $\sigma_{\mu h}$ polar plot.....	184

Figure 6-67: A thresholded surface with three randomly located scratches with a) equal width but different length, b) different widths and lengths, and c) and d) their $\sigma_{\mu h}$ polar plots.	185
Figure 6-68: a) A thresholded surface with a single non-straight scratch, b) a thresholded surface containing three non-straight scratches, c) and d) their $\sigma_{\mu h}$ polar plots.	186
Figure 6-69: a) The thresholded surface with the single negative linear feature, b) its $\sigma_{\mu h}$ polar plot.	187
Figure 6-70: $\sigma_{\mu h}$ polar plot of the thresholded surface with the negative linear feature.	188
Figure 6-71: a) Polished glass surface measured with CSI 5 \times after processing, and b) the same surface after it is thresholded.	189
Figure 6-72: $\sigma_{\mu h}$ polar plot of the surface with four scratches.	189
Figure 6-73: a) Thresholded surface rotated 34 $^\circ$ clockwise, b) thresholded surface rotated 87 $^\circ$ clockwise, c) thresholded surface rotated 148 $^\circ$, and d) thresholded surface rotated 170 $^\circ$ clockwise along with their columns mean height graph.	190
Figure 6-74: a) A thresholded surface with a linear feature, b) a thresholded surface with a single negative circular feature, and c) a thresholded surface with two negative circular features and their $\sigma_{\mu h}$ polar plot.	192
Figure 6-75: a) A thresholded surface with a negative circular feature and a scratch, b) its $\sigma_{\mu h}$ polar plot.	193
Figure 6-76: $\sigma_{\mu h}$ polar plot of the surface in Figure 6-75(a) with its constituent elements.	194
Figure 6-77: a) A thresholded surface with a negative circular and a linear feature, b) its $\sigma_{\mu h}$ polar plot, c) the same surface when it is rotated 136 $^\circ$, and d) when rotated 156 $^\circ$	195
Figure 6-78: a) A thresholded surface with a pair of negative circular features, and a scratch, and b) its $\sigma_{\mu h}$ polar plot.	196
Figure 6-79: a) A thresholded surface with three negative circular features and one linear feature, b) its $\sigma_{\mu h}$ polar plot.	197
Figure 6-80: $\sigma_{\mu h}$ polar plot of the surface shown in Figure 6-79(a).	198
Figure 6-81: a) A thresholded surface with two negative circular features, b) a thresholded surface with a scratch, c) a thresholded surface with two circular and a linear feature, and their $\sigma_{\mu h}$ polar plots.	199
Figure 6-82: a) A thresholded surface with three negative circular, and two linear features, b) its $\sigma_{\mu h}$ polar plot.	201
Figure 6-83: Signature peak of each type of features' combination.	202
Figure 6-84: a) Polished glass surface measured with CSI 5 \times after processing, and b) the same surface after it is thresholded.	202
Figure 6-85: $\sigma_{\mu h}$ polar plot of the surface with mixed features.	203
Figure 6-86: a) A MATLAB generated surface with Gaussian distribution of heights with a defect and its σ_{Rq} polar plot, and a defect free surface with Gaussian distribution of heights along with its σ_{Rq} polar plot.	204
Figure 6-87: $\sigma_{\mu h}$ polar plot of a surface.	205
Figure 6-88: A thresholded surface with two negative circular and one negative linear feature.	205

Figure 6-89: σ_{Rq} polar plot of an unknown sample.	206
Figure 6-90: σ_{Rq} polar plot of an unknown sample.	207
Figure 6-91: σ_{Rq} polar plot of an unknown sample.	207
Figure 6-92: σ_{Rq} polar plot of an unknown sample.	208
Figure 6-93: Image of the sample of the polar plot shown in Figure 6-89.	208
Figure 6-94: Image of the sample of the polar plot shown in Figure 6-90.	209
Figure 6-95: Image of the sample of the polar plot shown in Figure 6-91.	210
Figure 6-96: Image of the sample of the polar plot shown in Figure 6-92.	211

CHAPTER 1: INTRODUCTION

Surface topography greatly affects the performance and functionality, expected life span, and perceived value of a component. The economic advantage achieved by having surfaces with the desired quality, and within the design specifications is one of the main factors motivating studying and developing methods that are capable of characterizing surface topography, and are also able to detect and quantify surface imperfections. Early surface assessment methods were to rub a fingernail across the surface and visual inspection. With the progress in technology, the first approach was implemented as mechanical stylus measurement techniques and the later by optical methods. At the same time, qualitative subjective assessments were replaced by 1D and 3D quantitative metrics developed by researchers in academia and industrial world, and later on organized in international standards. Due to the complex nature of surface topography, popular height based scalar descriptors are not able to completely describe surface characteristics. This issue furthermore shows itself when the desired task is to detect and quantify surface features, such as circular digs or straight scratches. This matter drives the need for visual inspection of the components in some industries in order to detect defects and check if they are within the design specifications or not. Visual inspection was initially all manual where a human inspector performs the inspection process, this method is still in use especially in sensitive applications such as optics industry. However, the drawbacks of manual inspection such as being slow and subjective incentivized researchers to begin developing automatic visual inspection techniques based on computer vision and image processing techniques.

This work presents a new statistically based approach for analyzing surface topography, and obtaining insights on surface characteristics, as well as single and multiple circular and linear surface features, and it was motivated by the prevalence of fast and cheap computing capability in today's computers that was not available when first surface descriptors were developed. In this work a processed surface, i.e. form and waviness removed from the surface height map, is

considered as a set of constituent line profiles. A statistical parameter of choice such as Ra , Rq , etc. is calculated for each one of the profiles, and the resulting distribution is quantified with different orders of moment of data, i.e. standard deviation, skewness, and kurtosis. The surface is then rotated around its center creating another set of profiles, and the process is repeated until a 180° rotation is complete.

Results are presented graphically in a polar plot format and are capable of identifying and characterizing surface characteristics such as isotropy, directionality, and periodicity, also isolating and characterizing single and multiple surface features such as straight scratches and circular digs. This method complements the current statistical parameters defined in ISO 25178-2, and is highly capable of being implemented in automatic inspection and quality control systems.

In chapter two a survey of the importance of the study of surface topography in dimensional metrology is done, development of metrology instruments from simple 2D profilometers to 3D optical measurement instruments will be discussed, the progress of surface texture parameters from 2D metrics to 3D ones will be then talked about. The importance of surface imperfections on the performance and functionality of the samples will be emphasized, and the study of several methods of defect detection and characterization will be presented.

In chapter three the fundamentals of generating the polar plots will be detailed, rotational algorithms will be described and the differences between the discrete environment of the computer systems versus the continuous nature of the analytical aspect of the method will be discussed. Items affecting the behavior of the polar plots will be identified, and briefly explained. For instance, Figure 1-1(a) shows a surface with multiple circular and linear features, and Figure 1-1(b) depicts its $\sigma_{\mu h}$ polar plot. From this polar plot it is possible to identify the different types of features on the surface as well as each one's quantity.

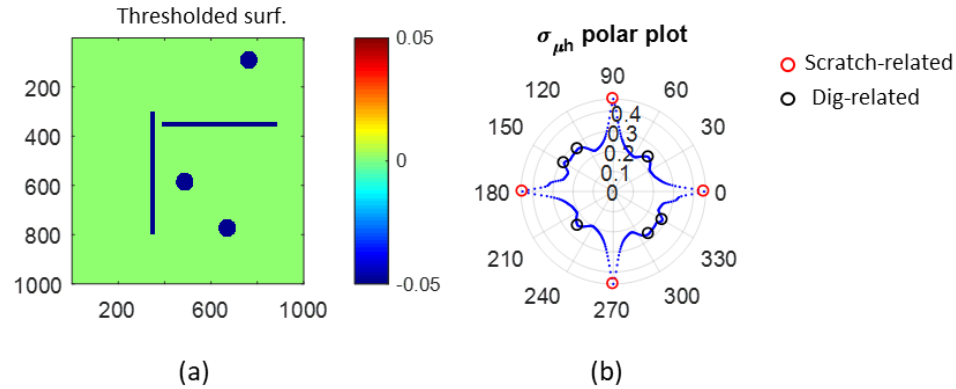


Figure 1-1: A thresholded surface with three negative circular, and two linear features, b) its $\sigma_{\mu h}$ polar plot.

Chapter four of this dissertation focuses on the characterization of surface texture, and details the effect of surface roughness, surface directionality, and surface periodicity on the polar plots. The method for identifying the specific nature of a periodic structure will be introduced and the result of the wavelength calculation with this method will be compared with the power spectral analysis, PSD. Each of the above mentioned capabilities will be tested and verified on real surfaces, and the difference between the model and the real sample will be explained.

In chapter five the effect of an isolated feature, i.e. single circular and single linear feature, on polar plots will be explained. The skewness of the columns Rsk histogram is used, instead of the standard deviation of the columns Rq histogram, to determine whether the feature is on the surface such as a piece of dirt, or is below the surface such as a dig. Estimation of the diameter and the depth of the circular and length, depth, and width of a linear feature from the σ_{Rq} polar plot will be detailed, and a conservative detectability threshold graph for a surface size of 1000×1000 pixels will be generated.

Chapter six focuses on how multiple circular and linear features on the surface will affect the behavior of the corresponding polar plots, and the information contained within the polar plots can provide insights on the surface features. This chapter is divided into three sections, the first section studies surfaces with multiple circular features, the second section will analyze surfaces containing multiple linear features, and the last section will talk about the surfaces that have both linear and

circular features. The real surfaces of fiber optical connectors will be analyzed with the approach and the results will be discussed.

Finally in chapter seven a summary of all the features of the polar plots, and how they can be tied back to surface characteristics and surface features will be discussed. The approach's assumptions and limitations will be presented, and some future work for continuation of this research are suggested.

CHAPTER 2: LITERATURE REVIEW

2.1 Introduction

Perhaps a good starting point for this literature survey would be to ask what is a surface, and why do we need to (and most of the times have to) study and analyze surface topography? Surface by definition is the outer layer of a component or device that interacts with other parts or the environment in which the component is placed [1].

Surface topography importance was the main derive for surface assessment and characterization, early assessment methods were to rub a fingernail across the surface and also by visual inspection of it, with the progress in technology the first one made its way to date as the stylus measurement techniques and the later as the optical methods. At the same time, qualitative assessments were replaced by quantitative metrics developed by researchers in academia and industrial world, and later on organized in international standards.

By looking at technical drawings of engineering components it is clear that they assume that surfaces are perfectly smooth, straight, and free from defects, i.e. the nominal surface, however in reality it is impossible to have a surface that is perfectly smooth, straight, and defect free; and this is due to the fact that the manufacturing method that is implemented to make the parts would leave a micro scale and macro scale finger print on the surface. This finger print is called surface topography [2]. And surface texture is the random or repetitive deviations from the nominal surface [3].

Solid surfaces divide into deterministic and random surfaces. Random surfaces are as well grouped into anisotropic and isotropic types, and finally isotropic surfaces are categorized as Gaussian and non-Gaussian groups [3].

Conventionally surfaces topography constituents are roughness, waviness, and form error [4]. Roughness, which is the focus of this work, is the effect of manufacturing process rather than manufacturing tools that are used and includes tool marks with usually periodic nature, on a finer

scale the waviness is the effect of tool wear and tool tip irregularities, Figure 2-1(a), waviness is mostly related to an individual machine for example unbalanced grinding wheel, or chatter vibrations, Figure 2-1(b); and finally form error is due to the lack of rigidity of the part when mounted in the machine and allowing it to bend or flex, Figure 2-1(c) [2, 5].

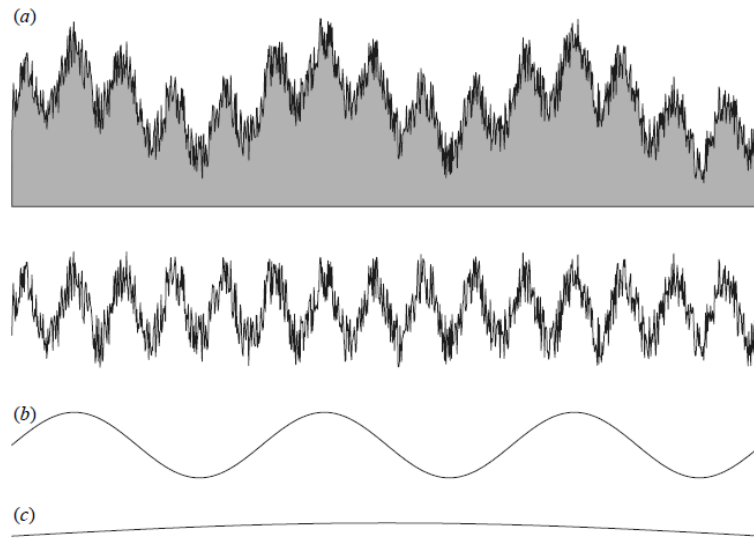


Figure 2-1: a) Primary profile of a surface and its roughness profile, b) the waviness profile, and c) the form profile. Image taken from [6]

Using a filtering method is necessary to be able to extract these different profiles from the primary profile. Filtering is using any means (mostly electronic and computational, and mechanical) for selecting a range of structures [7]. By accepting or rejecting a range of wavelengths or spatial frequencies filters select the desired structure. Roughness profile is the one derived from the primary profile by using a high-pass filter. Waviness profile is achieved by using a band-pass filter to the primary profile. A band-pass filter suppresses wavelengths that are rather longer than roughness but smaller than form wavelengths. These filters select or reject a structure based on its scale in the x-axis, which is in terms of wavelengths or spatial frequencies. A filter that lets the low frequency components pass through is called a low-pass filter, similarly, a high-pass filter preserves the high frequency components. The combination of these two filters to select a restricted range of

wavelengths with both high and low regions is called a band-pass filter [7]. The details about these filters and their values can be found in ISO standards.

The first quantitative 2D instrument for measuring surface topography was developed by Gustav Schmaltz early in 20th century, which was a simple profilometer capable of recording height deviations across a line on the surface after filtering that is critical with respect to separation of roughness, waviness, and form. This profilometer enabled the roughness measurement in terms of peak to valley deviations, and the less extreme average of five highest peaks to the five lowest peaks of the profile. Later on in the UK, the first instrument was developed capable of processing an electrical signal representing the surface height deviations and as a result, a useful parameter, the centerline average roughness (CLA) was calculated with an analogue computer. It is because of the convenience of early analogue instruments of computing the average roughness parameter, *Ra*, that it became the most widely used and accepted surface descriptor to date [2]. Figure 2-2 shows profiles of four different surfaces and their *Ra* values. While this 2D parameter capture the statistical differences, it is inadequate in capturing spatial distribution of the surface. It has been shown that parameters from two different profiles from the same surface can vary up to 50% [8].

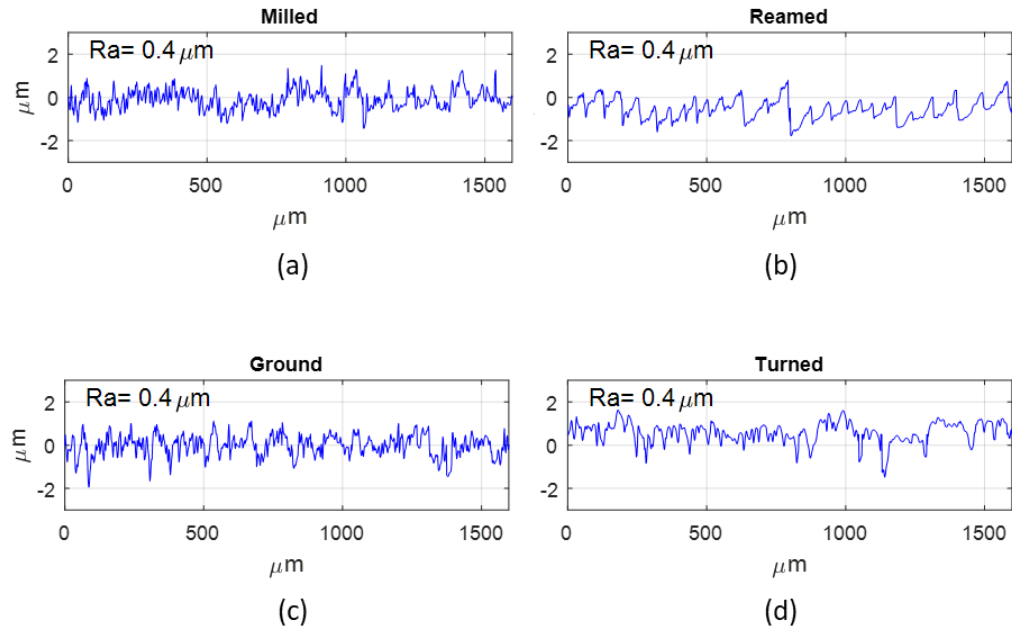


Figure 2-2: Profiles from a) a steel milled surface, b) steel reamed surface, c) steel ground surface and d) steel turned surface

It was in the 1980s when researchers began experimenting surface characterization in 3D trying to correlate surface topography to parts' performance and functionality. 3D characterization is a much better representative of the surface both in terms of statistical and practical point of view since surfaces interact with each other in 3D. Technical committees and working groups were shaped to organize the large number of surface descriptors that were developed especially after the advent of digital computers [9].

ISO 25178-2 categorizes surface parameters into two main groups, namely field parameters that are based on spatial frequency, height amplitude, and material ratio curve shown in Figure 2-3 and feature parameters that are based on subsets of predefined topological features of the surface [10].

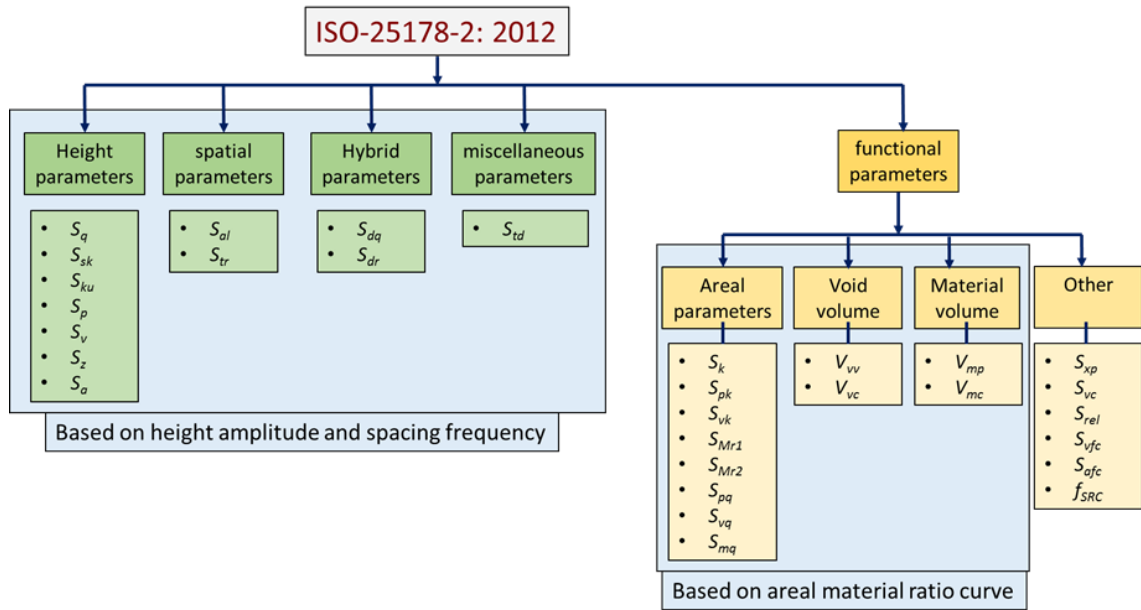


Figure 2-3: Field parameters based on ISO 25178-2

Among these parameters height parameters are mostly used in industry when compared to other parameters because they are an extension of 2D parameters and are well accepted and understood [11].

This issue becomes bolder when surface features such as scratches and digs are taken into account. Because of the nature of the most of the widely used ISO 25178-2 surface parameters which is processing the whole number of data points and reducing it to a number, they are not able to tell the difference between different features on the surface and their properties such as geometrical properties and quantity. Figure 2-4(a) shows surface with a scratch and Figure 2-4(b) shows a surface with a dig and both with equal S_a values. Although ISO parameters such as S_{sk} and S_{ku} are able to distinguish between an ideal and defect-free surface and a defective one, they are not strong tools when comparing two defective surfaces as shown in Figure 2-4. Also, in terms of capability of differentiating perfect surfaces from defective ones, ISO parameters are not able to provide information regarding the source of difference.

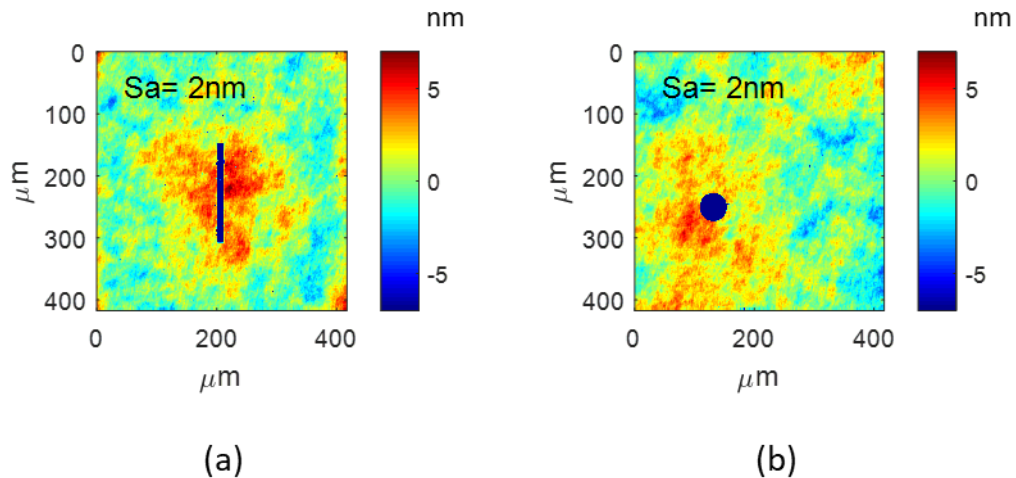


Figure 2-4: a) NIST scratch grade 0.040 sample, and b) NIST dig grade 0.040 sample measured with ZeGage white light interferometer, 20 \times objective, FoV equal to $417\mu\text{m} \times 417\mu\text{m}$

This issue derived the need for visual inspection of the components in some industries in order to detect defects and check if they are within the design specifications or not. Visual inspection began manually where a human inspector performs the inspection process; this method is still in use especially in sensitive applications such as optics industry. However, the drawbacks of manual inspection such as being slow and subjective made researchers to begin developing automatic visual inspection techniques based on computer vision and image processing techniques.

The structure of the rest of this survey is first the effect of surface topography in different applications will be discussed with the emphasize on how surface features affect the final parts' functionality, then the evolution of surface topography measurement instruments will be talked about. In section 2.4 different methods of characterizing surface topography are introduced, and limitations of these methods are described. In section 2.5 an overview of manual and automatic visual inspection techniques are discussed.

2.2 Effects of surface topography

The importance of studying surface topography is because it greatly affects the part's functionality and performance. Tribology which is the science of friction, wear, and lubrication of

moving or stationary parts [3, 12], adhesion, reflection and dispersion of incident electromagnetic rays, fatigue life, corrosion resistance, etc. are all instances that are affected by a part's surface topography [3, 13-15]. An example of the economical aspect of surface importance is that 90% of parts' failure is estimated to be due to the surface effects and are surface initiated, which then highlights the importance of the matter in advanced nation's GDP [16].

2.2.1 Tribology (friction, wear, lubrication)

Properties of surface topography are crucial to understand the nature of surface interactions and affect the real area of contact, friction, wear, and lubrication. Based on an estimate losses associated with ignorance of tribology of components in the United States results in 4% of its gross national product; this emphasizes the importance of friction reduction and wear control [3]. When two nominally flat surfaces are in contact, the actual contact happens at different spot zones because of the surfaces roughness, and the area of real contact is very smaller than the nominal contact area [3, 17]. J. F. Archard studied the contact between a single uniform radius sphere and a flat surface with Gaussian height distribution, he showed that the mean area of all contact spots and their total number increases as the normal load increases [18]. Greenwood et al. studied the general theory of contact between two rough plane surfaces and concluded that the results obtained by modeling the contact between one flat surface and one rough surface remains unaffected, i.e. the load and the area of contact remain almost proportional [19]. Correlation between surface roughness and the friction forces for contact area on a silicon surface with a defined topography (consisting of ridges and groves) was investigated by K. Meine et al. by moving a sliding ball over the surface. They showed that the increase or decrease of the friction force depends on the direction of the sliding ball and is also independent of the material of the tribosystem [4].

One of the most important factors contributing to control and reduction of friction and wear is using lubrication which results in increase of the life span of the moving components and also smoother performance of the system by preventing solid-solid contact [3, 20]. Lubrication separates

two interacting surfaces and thus reduces the wear [12]. The surface roughness plays an significant role in formation of lubricant thin film and contacting performance [21]. In the average flow model developed by Patir and Cheng the actual flow between rough surfaces is equated to an average flow between nominally smooth surfaces, and parameters of roughness is included in Reynolds equation through the flow factors [22]. An average Reynolds equation is defined in terms of pressure and shear flow factors that are functions of surface roughness characteristics [22].

2.2.2 Reflection

Another area that is affected by surface topography and especially surface roughness is reflection and backscattering of electromagnetic waves form surfaces. Schmaltz was probably the first person trying to formalize the effect of reflection of light from a surface, and also he was the first to explore the tactile measurements method [23]. Diffraction and reflection patterns for perfectly smooth surfaces can be calculated by usual methods such as Fresnel and Fraunhofer [24]. However, most of the engineering surfaces are not perfectly smooth and contain surface irregularities and anomalies, therefore many studies have been done to investigate the reflection of a plane electromagnetic wave from mostly rough surfaces to examine the effect of topography of them [25-27]. J. A. Holzer et al. studied the scattering of electromagnetic waves from a Gaussian rough surface without using the small-slope or stationary-phase approximation [25]. For surfaces whose irregularities are not described by Gaussian functions M. J. Kivelson showed that in the small wavelength limit the cross section per unit area for backscattering at an angle ψ with respect to vertical axis is proportional to the probability that the normal to irregular surface makes an angle ψ with respect to the vertical axis [28].

2.2.3 Fatigue life

Fatigue life of components is highly relevant to their surface quality, and fatigue cracks mostly initiate at the surface of a homogenous material [29]. Surface quality in this manner is usually described by three parameters, a geometrical parameter: surface roughness, a mechanical

parameter: residual stress, and a metallurgical parameter: microstructure [30]. Among these factors the effects of surface topography and integrity on fatigue life of components is well recognized by researchers through many experimental and analytical models [31, 32]. M. Suraratchi et al. investigated the effect of surface roughness on the fatigue life of 7010 aluminum and developed a model for fatigue life prediction for aluminum alloys based on finite element analysis of the surface topography [30]. Junbiao et al. studied the fatigue life for surface roughness of typical machined parts with or without surface finishing processes, and proposed a unified model to predict the S-N property that accounts for the effect of surface roughness and defect sensitivity of the microstructure of material, and showed a good agreement between the results of the proposed model and experimental data [33]. P.S. Maiya et al. investigated the effect of surface roughness on the low-cycle fatigue life on 304 stainless steel, and observed at a strain rate of 0.0004 s^{-1} and a total strain range of 1 pct the increase in surface roughness causes the fatigue life to decrease, they also provided information on crack growth versus strain cycles as a function of surface roughness [34]. To establish a method for improving fatigue life prediction of components with rough surfaces Sygmond et al. proposed a model in which microscopic surface measurements, obtained with white light interferometry, are used to generate finite element models of surface topography [29].

2.2.4 Corrosion

Surface topography affects the material's corrosion [35]. Corrosion is the loss of material through electrochemical reactions at the surface, and the localized electrochemical reactions may cause pitting, intergranular or intragranular corrosion [12, 35]. One of the common failure modes in industries such as mining, petroleum, etc. is due to corrosive wear [35]. W. Li et al. investigated the effects of surface topography on corrosion behavior on copper, and by experimental results they showed that an increase in surface roughness will cause higher rates of corrosion of copper [35]. R. Walter et al. showed that surface roughness is a critical factor in corrosion behavior of AZ91

magnesium alloy, and the increase in surface roughness of the tested sample will result in the increase of pitting susceptibility of the alloy [36].

2.2.5 Adhesion

Surface topography is a critical factor in adhesion of two surfaces which is very important in biomedical industry, and is the main reason that microscopic bodies usually do not adhere to each other [17]. K. N. G. Fuller et al. studied the adhesion between two surfaces as a function of surface roughness, they showed that relatively small surface roughnesses (0.12 to 1.5 μm) are sufficient to reduce the adhesion to a very small value [37]. The adhesion of elastic plates to rough surfaces which is relevant to biological systems was studied by Persson B. N. G et al.; they showed how the adhesion is dependent of the nature of the surface roughness of the substrate [38]. P. Linez-Bataillon et al. experimented the role of surface roughness of Ti6A14V on the cell morphology, proliferation, and adhesion particularly on the variation of the expression of cell adhesion proteins, and observed a significant correlation between surface roughness and cell proliferation rate and found a quantitative relationship between surface roughness and cell adhesion [39]. Same results were obtained by investigating the effect of surface roughness of hydroxyapatite (HA) on human bone cell response where cell adhesion, proliferation and detachment strength are sensitive to surface roughness and increased as the HA roughness increased [40].

2.3 Surface topography measurement instruments

Considering the importance of surface topography and the critical role that it plays in functionality of components, as well as the great economic advantages associated with having desired surfaces properties much effort has gone into measurement and characterization of surface topography in both industry and academia. Starting in 1930s when the first stylus instruments were developed the science of surface topography has continuously evolved. Digital techniques were introduced in late 1960s due to the advent of computers enabling researchers of developing

instruments capable of 3D measurements and analysis. The drawback however was the proliferation of parameters addressed by D. J. Whitehouse [41-43].

Figure 2-5 depicts the range and resolution of available measurement instruments and divides them into three main category. Scanning probe microscopy (SPM), and atomic force microscopy (AFM), optical instruments, and stylus instruments. In this graph the range refers to the longest distance that can be measured by the instrument, and the resolution refers to the shortest feature that can be measured [44]. This section will go over the development of these surface measurements instruments. Although some of these instruments do not practically include dimensional metrology of surfaces (such as STM) but for preserving the generality of the discussion they will be briefly introduced in this section.

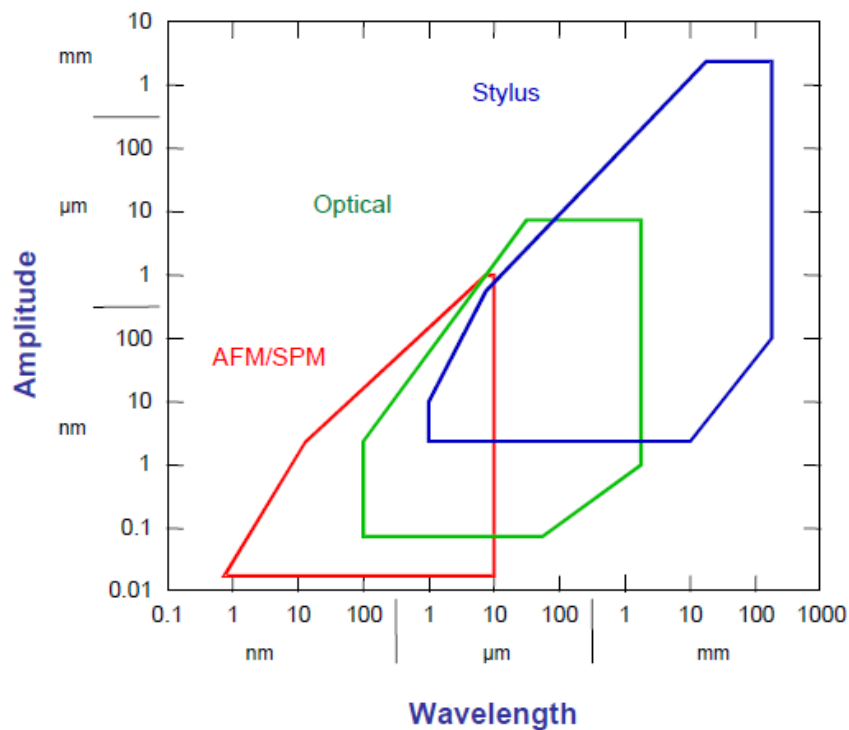


Figure 2-5: Steadman diagram showing the range and resolution of available measurement techniques. image taken from [44]

2.3.1 Scanning probe microscopes, SPM

The scanning probe microscopy is a serial measurement device that uses a nano scale probe to trace the surface, these kind of instruments are usually used when measuring surface topography smaller than conventional stylus or optical instruments [16]. Scanning probe microscopy can be divided into two groups, scanning tunneling microscopy (STM) and atomic force microscopy (AFM) [3].

In an STM system, a sharp metal tip that acts as an electrode of tunneling junction is placed very close to the surface of specimen (0.3-1.0nm) which acts as the second electrode. At this point a convenient voltage that ranges between 10mV to 2V is applied to the tip and causes the tunneling current varies from 0.2 to 10nA which is measurable; the tip is scanned over the surface and the current tunnel is then measured [3, 43]. It should be noted that the issue with STM is that the specimen that is being measured with an STM instrument must be conductive to allow the current to flow from the voltage source to the area that is scanned. Lateral resolution of sub nanometer and vertical resolution of 0.1nm is achievable with STM instruments; sufficient to define the position of a single atom [3].

In 1985 Gerd Binnig et al. developed an instrument capable of measuring both conductive and insulating material called atomic force microscopy (AFM) [45]. Atomic force microscopy is the most common type of SPM, and that is because it overcomes the issue of STM, i.e. a conductive specimen requirement. In an AFM instrument the motion of cantilever beam which is the result of attractive or repulsive forces between the tip, that has an ultra-small mass, and the sample is measured leading to the measurement of very small forces [3, 16].

2.3.2 Stylus instruments

The earliest method of measuring the surface topography was to use the fingernail by rubbing it across the surface of specimen or by making use of sense of sight and subjectively evaluating the surface topography, however, demand for quantitative results led to the development of tactile and

optical methods of surface measurement [7, 46]. Stylus method since its advent has been the most widely used method for measuring surfaces, Figure 2-6 shown a schematic of a stylus measurement instrument [8, 47].

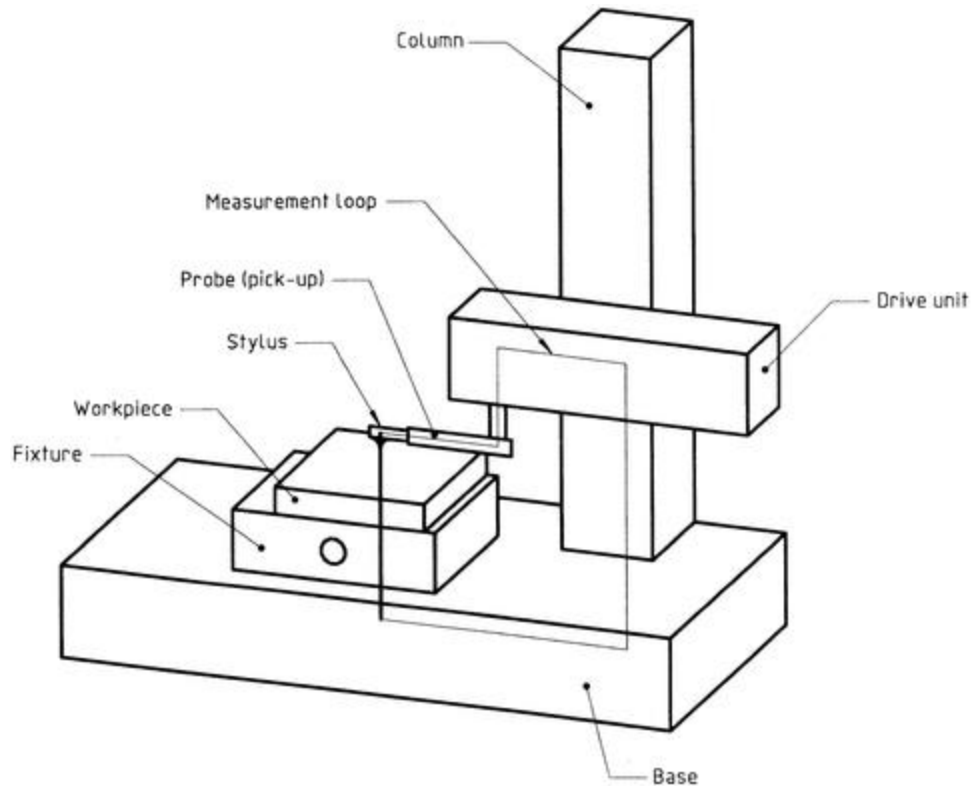


Figure 2-6: Schematic of a stylus instrument, image taken from [48]

Schmaltz was the first person to push the idea of using the fingernail to a mechanical probe, i.e. stylus instrument [49]. In a stylus instrument a diamond tip is dragged across the surface and the vertical motion of the tip is measured [16]. In general a stylus system uses a caliper that has two arms, one of which is in contact with the reference surface and the other is in touch with the surface of specimen that is being measured [46, 49]. In some cases it might be difficult to spot the reference surface, in such case both arms touch the specimen's surface, i.e. skidded instruments. In this case the skid technique provides an intrinsic reference by having one stylus much more rounded than the other, and acts as a mechanical filter having a lower cut-off than the one with sharp tip [46]. It should be noted that what is important in this method is the deviation from an intended

surface and not the actual position of the reference surface relative to the test surface [46]. There are some disadvantages associated with the skidded systems, one being it can distort a surface signal and the other in some cases it can damage the surface, it is worth noting that the skid carries the whole weight of the traverse unit and the stylus is very lightly loaded [49]. To overcome the issues related to skidded instruments skidless systems were developed, in this case an internal precision flat or datum is used to provide reference for the probe. Because of the complexity of these systems they are usually heavier, less portable, and more expensive than skidded ones [50]. A typical stylus instrument consists of five basic components in general, a stylus transducer, an amplifier, a recorder, a traverse unit, and a meter system [43]. Stylus instruments can also produce areal surface measurements by moving a stylus across the surface in a raster form to build up the areal map; however this process, depending of the raster length, could be very time consuming [16]. The range for this type of measurement instruments starts from 1 μm to 100 mm, while the resolution is between 2 nm to 1 mm, see Figure 2-5 [44]. More details about this kind of surface measurement instruments can be found at [1, 3, 7, 16, 43, 46, 49, 50].

2.3.3 Optical methods

In general when an electromagnetic wave is incident on a surface it could be absorbed, transmitted, and reflected either specularly, diffusively or both.

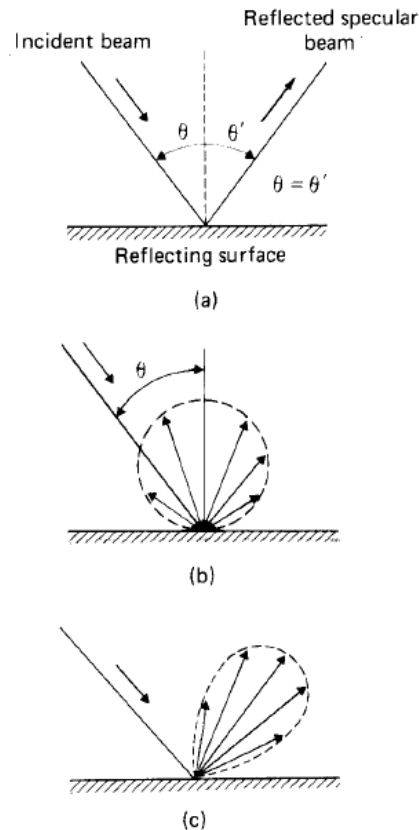


Figure 2-7: Reflection of an electromagnetic wave from a solid surface when a) specular only, b) diffusive only, and c) combined specular and diffusive. Image taken from [3]

On an ideal smooth surface the reflection is totally specular (Snell's law) whereas in rough surfaces as the roughness increases the intensity of specular reflection decreases and the diffracted radiation increases in intensity and becomes more diffusive [3].

Optical methods can mimic either the eye (3D) or the stylus method (2D). In all optical methods, light that sometimes is focused and sometimes is not is projected on the surface. The light can pass by an obstruction before reaching the surface or after it is scattered from it [46]. The light can also be used in coherent and incoherent fashion and the polarization properties can also be used [46].

It is safe to say that since the advent of the first optical methods in 1892 [51] there has been thousands of papers written regarding optical measurements, and it is beyond the scope of this

literature survey to go over all of them. In this section some of the optical techniques that are defined in ISO 4288-1996 specifications [52] are briefly discussed.

2.3.3.1 Optical profilers

The principle of this kind of instruments is analogous to the stylus method with the difference that a beam of light act as the tip of the stylus. This type of instruments splits the image of the specimen into two pieces at the eyepiece and uses two photo detectors one before the image plane and the other equally spaced behind the image plane. Then the signals from the two detectors are balanced and provide micro displacement information. A sub nanometer vertical resolution is obtainable in this case [51].

A special type of optical surface profilers is called confocal microscope that was invented in 1950s [51]. In this case, a point of illumination is focused on the specimen and is scanned using a scanning device controlled by computer. A pinhole filters the image of this illumination and the image is detected via a photodetector. Nanometer vertical resolution is achievable with confocal microscopes.

2.3.3.2 Interferometric microscope systems

Interferometers separate the source light into two paths, one of which hits the surface of the specimen while the other hits a reference surface. The reflection of separated paths are recombined and directed to a digital camera for light intensity measurement. The intensity of this recombined light shows high sensitivity to length variation in pathways. This property is used to evaluate the height variation on the surface and gives nanometer vertical resolution [16].

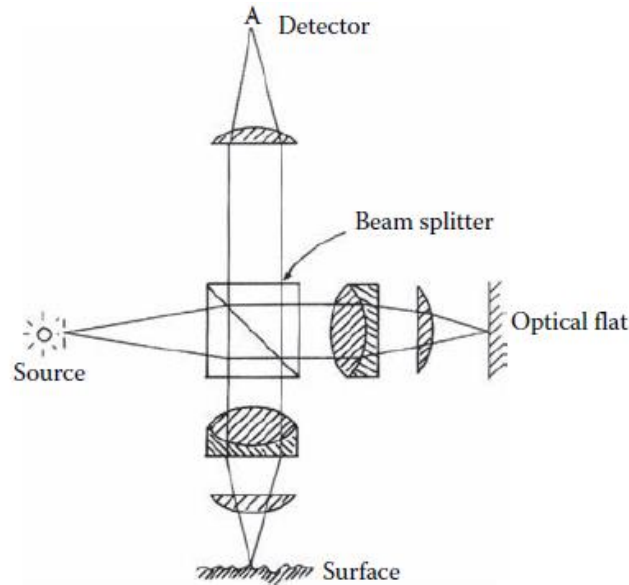


Figure 2-8: Schematic of in interferometer instrument (Linnik interferometer), image taken from [5].

Two major types of these kinds of microscopes exist, interferometers that use the phase shifting technique and evaluate the surface height variations, and those that measure the slope of the surface height changes [3, 53]. The first type performs phase shifting by moving the reference mirror either continuously or by steps of $\pi/2$ using a piezo electric system. Lateral resolution of phase shifting systems is diffraction limited, and also finite numerical aperture causes a limitation of their use on surface heights. Among these interferometric systems white light interferometers are probably the most successful and widely used instruments. The second class of interferometric microscope systems is a differential interference contrast microscope. This type is a shearing interferometer that can be used at very high magnification, and is able to detect defects of 0.1nm level [51, 53].

2.4 Characterization of surface topography

Characterization of surface topography evolved in parallel with the progress in measurement instrument. Characterization of a surface profile or surface area by a parameter or a set of parameters is used to give meaningful and quantitative specific descriptors to a surface that can be

used as a means of communication between the manufacturers and designers, also enables comparison to other machined made surfaces. This section will go over 2D characterization and then the 3D characterization of surface topography in ISO specifications.

2.4.1 Surface profile characterization (2D)

In order to characterize the primary surface profile which is the output of the measuring instrument various aspects of it should be identified, namely form, waviness, and roughness [3, 20].

Using a filtering method is necessary to be able to extract these different profiles from the primary profile. ISO 4287-1997 [54] defines three groups of parameters namely P-parameters for primary profile, W-parameters for the waviness profile, and R-parameters for roughness profile [55]. The focus in the rest of this section would be on the roughness parameters. Parameters can be grouped based on their indication of averages, deviations, extremes, and specific features such as peaks, valleys, etc. [56]. It should be noted that it is important that the profile measurements take place at a direction perpendicular to the lay on the surface.

Amplitude profile parameters only depend on the deviations or heights, they are insensitive to relative positions of the elevations, and are very sensitive to wayward data points [7, 55, 56]. Spacing of some certain topographic features of a profile can be qualified with spacing parameters such as RSm which is the mean width of the profile element width Xs within a sampling length. Hybrid parameters, and curve and related parameters of a profile are all defined in ISO 4287-1997, and their definition and formulas can be found in appendix B of this dissertation. 2D parameters are among the mostly used and widely accepted metrics in the industry, this is due to the ease of use of the 2D measurement instruments, and the fact that it was a 2D profile that was first measured and characterized. However, as was mentioned earlier a 2D profile may not be a perfect representation of surface topography.

2.4.2 Surface areal characterization (3D)

In 1987, the first areal texture measuring instruments were introduced, early areal parameters were simply an extension of 2D parameters such as Ra and Rq to Sa and Sq . In 1993 the ISO technical committee introduced a new concept called Geometrical Product Specifications (GPS) with the goal of unifying specification standards that deal with dimensional analysis and surface texture, and in 2002 the ISO technical committee formed a working group to address the standardization of areal surface texture measurement methods [57]. All these areal standards are part of ISO 25178 that has 19 sections [7].

Based on ISO 25178-2 [10] areal surface characterization unlike 2D profile system does not require three different groups namely primary profile, waviness, and roughness; and uses the concept of scale-limited surface. To remove the unwanted small scale lateral components of the surface such as measurement noise or functionally irrelevant features an S-filter is applied, and to remove the unwanted large scale lateral components an L-filter is applied, and finally to remove the nominal form an F-filter will be applied to surface height map. Scales at which the filters work is controlled by nesting index. An SF surface is equivalent to primary surface; an SL surface is equivalent to roughness surface and by using an L-filter on an SF surface. These SF and SL surfaces are called scale-limited surfaces [1, 7].

Areal parameters in ISO 25178-2 are grouped into two major classes, field parameters that are defined from all the points of a scale-limited surface, and feature parameters that are defined over a subset of predefined topological features from the scale-limited surface. Field parameters themselves are categorized in four groups, height, spacing, hybrid, and function and related parameters [11, 58-60].

2.4.2.1 Field parameters

Height amplitude parameters rely on the height deviations of the surface topography and describe the amplitude related properties of a surface, and are categorized into two groups namely

average of ordinates such as Sa , Sq , Ssk , etc. ,and extreme peak to valley parameters such as Sv , Sp , Sz , etc. Spatial properties of surfaces are described by areal spacing parameters, and they are very useful in distinguishing between highly textured and random surface structure. Two parameters are defined in ISO 25178-2 for this class. Sal which is the autocorrelation length and is defined as the horizontal distance of the autocorrelation function to the fastest decay to a specific value between zero and one. Surfaces with dominant low spatial frequency have a large value of Sal . The other parameter is texture aspect ratio of the surface, Str which is value that identifies texture strength, i.e. the uniformity of the texture aspect. By definition Str is the ratio of the fastest to slowest decay to correlation length, 0.2, of the surface autocorrelation function and its value is between zero and one. Larger values of Str indicates uniformity or isotropy of the surface while lower values show strong directional structure on the surface [7, 10].

Hybrid parameters are those that are based on the amplitude and spatial information of the surface topography. Any change that happens in the either amplitude or spacing may have an effect on hybrid properties. These parameters are especially useful in contact mechanics, for instance the friction and wear between bearing surfaces. ISO 25178-2 defines two parameters in this category, root mean square gradient of the scale-limited surface, Sdq which is useful for assessing surfaces in sealing applications and for controlling surface cosmetic appearance; and the other parameter is developed interfacial area ratio of the scale-limited surface over the definition area. This parameter is useful in applications involving surface coating and adhesion [7, 10]. Finally, the function and related parameters in which the first parameter is *areal material ratio of the scale-limited surface* function, this function can be interpreted as the sample cumulative probability function of height values within the evaluation area. The related parameters are derived from three sections of the material ratio curve: the peaks above the mean plateau, the plateau themselves and the valley between plateau.

2.4.2.2 Feature parameters

One common aspect of all above mentioned surface characterization descriptors is that they use a statistical basis to characterize the whole number of data points in the measurement. These parameters, and especially the profile parameters, were initially developed to monitor production processes. Human's eye does not assess a surface by seeing the filed parameter rather it evaluates the surface by patterns of features and the relationship between them. Pattern analysis works the same way by detecting features and the relationship between them and characterizes the pattern in surface texture. These parameters are called feature parameters; and feature characterization doesn't have a specific feature parameter defined but instead a toolbox of pattern recognition techniques that it utilizes to characterize specific features on a scale-limited surface [61]. Despite the capability of feature parameters to characterize surface texture to some extent it should be noted that surfaces are complex quantities and cannot be described completely by one or a set of parameters [8]. With the advent of computers and to give a better understanding of surface topography visual presentation of surface techniques were implemented.

2.4.3 Surface visual presentation

Visual presentation of surface topography is a unique feature of 3D analysis and in many cases a suitable presentation can give sufficient information about the surface topography [8]. Contour plots and projections are two techniques of surface visual presentation.

2.4.3.1 Contour plots

In a contour plot all the points that have the same height value are connected together via straight lines or curves. Linear interpolation is used to find intersections. Contour lines are a convenient way to represent lines of equal height and are used to define critical points and other concepts such as directional features [1], Figure 2-9 shows an example of a surface topography presented with contour lines.

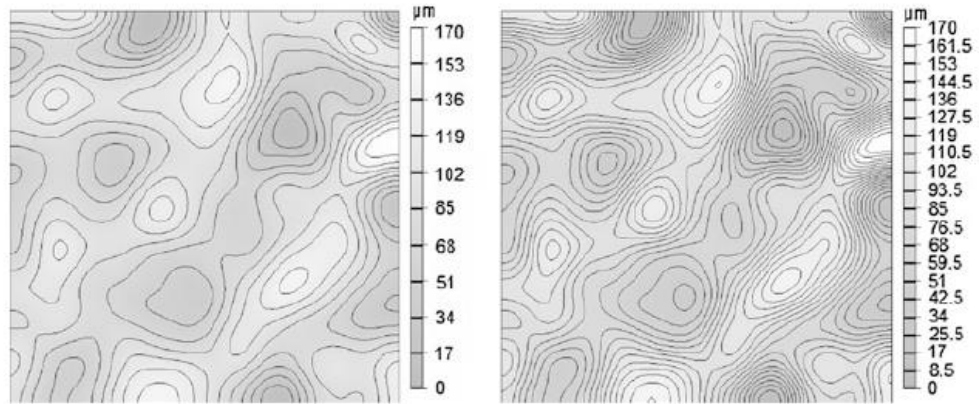


Figure 2-9: Surface topography with ten contour lines (left), and 20 contour lines (right); image taken from [1]

2.4.3.2 Projections

An effective technique of visual presentation is based upon the isometric or dimetric projections. Neighboring points are connected together via straight or curved lines and a hidden line removal algorithm is used to simplify the vision. Projection angle can modify the aspect of representation and defines the viewing direction with respect to the plane. Small projection angles are preferred when amplitudes are of interest, while large projection angles are preferred when surface texture is of interest, see Figure 2-10.

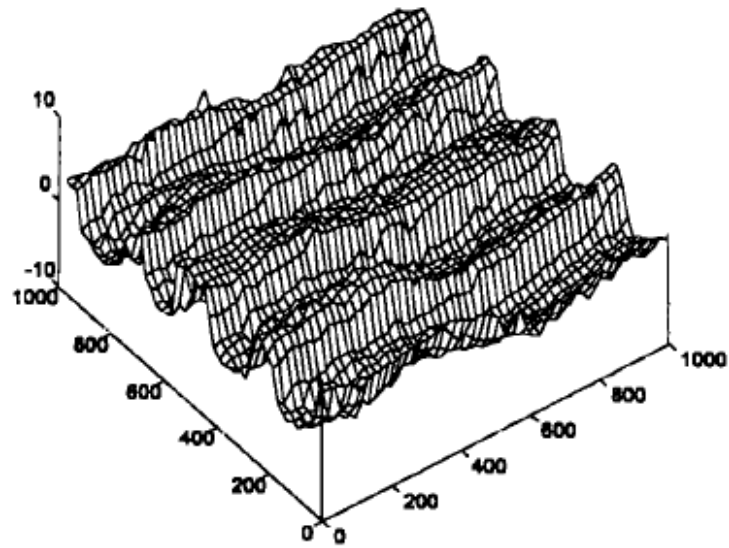


Figure 2-10: Dimetric projection of a milled surface with the projection angle equal to 60 degrees. Image taken from [8]

Some image processing techniques have been used in order to enhance the visual presentation such as truncation, inversion and slope visualization. Truncation is a technique where all the height values above a threshold value are removed, it can be used for instance to visualize the wear process and the bearing area, see Figure 2-11.

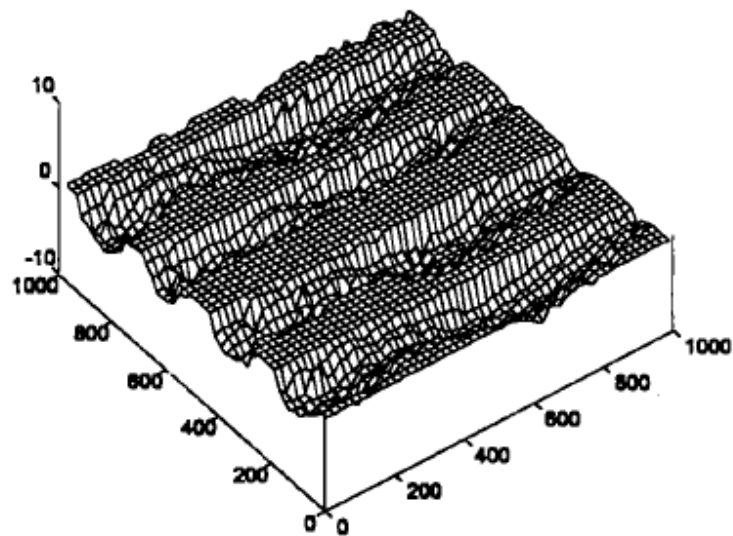


Figure 2-11: Example of truncation method on a milled surface. Image taken from [8]

Inversion is a technique that reverses the height values so that the valleys become summits and can be easily observed. Truncation and inversion can both be done on a surface height data as shown in Figure 2-12. Slope visualization emphasizes the slopes of the surface based on the derivative of the data.

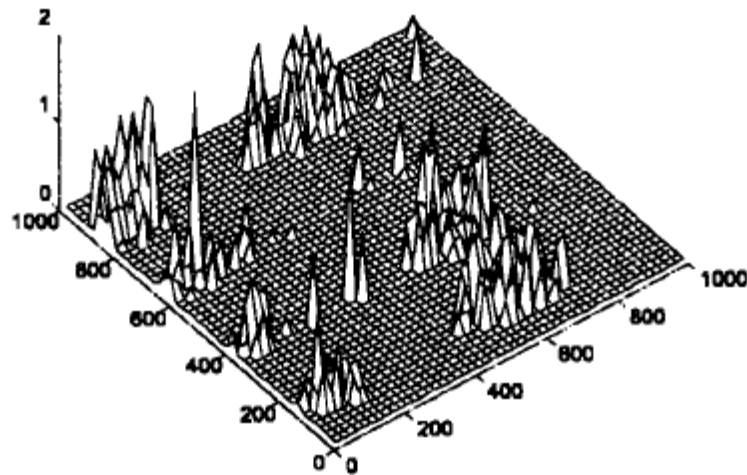


Figure 2-12: Example of truncation and inversion combined. Image taken from [8]

Presence of undesired features or lack of desired features on the surface may have a huge effect on their functionality, especially as we move towards the miniaturized world, these features may be detectable by visual presentation techniques, and however they cannot be characterized by them. Also these features cannot be completely characterized by ISO 25178-2 feature parameters due to the fact that at the end of required steps of feature characterization process a single statistical metric is reported. This single parameter is not able to give much information about the geometrical properties of features, their quantity, their location with respect to surface (above or into), etc... Two different surfaces with different features may exactly have the same parameters as shown in Figure 2-4.

Visual representation and image processing methods are becoming more widespread with the advent of fast computers with large and cheap memory capacity [8]. However before this progress

in technology the human eye was (and still remains) the most powerful and versatile processor of information especially when complicated and ill-defined but patterned data is involved [62]. The capability of this powerful tool is used in surface inspection processes.

2.5 Surface inspection

Product inspection is a very important step in manufacturing processes such as semiconductor industry, optics, metallic parts, aerospace, biomedical, etc. Inspection has been defined as the activity of examining attributes of a part and determining if it conforms to design specifications or not. Such attributes may be quantitative (e.g. dimensions) or qualitative (e.g. appearance) [63-67]. Inspection process is categorized into three groups, manual, automated, and hybrid (partially manual and partially automated) [68].

2.5.1 Manual inspection

Traditionally inspection has been performed manually which is subjective and highly depends on the experience of the human inspector, in addition to that it is a time consuming task, thus it makes the whole process expensive and slow [68, 69]. Manual inspection process involves three steps of search, fault recognition, and decision making [68]. For instance, in wood industry it is the responsibility of a human operator to identify and mark board areas containing defects and decide which characteristics is acceptable and which is not [70, 71]. Inspection procedure in steel surface inspection of steel products that are usually in coil form is done by cutting about 30m of a random coil in a batch and inspecting it by an expert, in this case typically 0.05% of the total steel product is inspected and judged [72].

Special attention has been placed on manual inspection of precision optical components due to their sensitive and important functionalities [65, 73]. The standard practice for optics inspection since 1950s has been to visually inspect the surface for small, localized imperfections and decide if they are acceptable or not. Surface imperfections may occur during or after fabrication. These imperfections may be visible due to the light that they scatter and cause unwanted veiling glare in

an image plane, or they may lead to degradation in signal quality at an image sensor. Imperfections can also cause centers of stress and eventually leading to failure of components that are exposed to high radiation energy densities [74]. Using an appearance comparison scale and with tolerance levels, agreed by the manufacturer and customer, allows a set of classification as “accept” or “reject”. This is a subjective form of inspection which lacks precision but it is fast and economic. Measurement of imperfections is only required as a second stage operation following inspection necessary to select a surface imperfection worthy of study. Surface imperfection tolerances is discussed in ISO 10110-7 [75]. Imperfections are categorized into three groups, namely localized surface imperfections which are produced by improper treatment during or after fabrication or in use (scratches, pits, scuffs, and fixture marks), long scratches that are imperfections larger than 2mm, and edge chip which is localized artifact around the periphery of an element [75]. ISO 10117-7 provides guidelines for tolerances indication in optical drawings.

Methods for inspecting surfaces and measuring grade numbers of imperfections are detailed in two methods in ISO 14997 [74]. In first method, the obscuration of imperfections larger than 10 μ m can be judged visually by comparison of areas of artefacts of known size on a comparison plate. Imperfections with obscuration less than 10 μ m (that are still visible under dark-field illumination) need to be quantified by comparison of their radiometric obscuration with totally absorbing artefact of known size. Every imperfection detected is measured and considered for summation to produce a level of grade for each surface. In this method, a dig is usually fully developed and is quantified by measuring its encircled diameter and then its area is calculated and a grade number is assigned in accordance to ISO 10110-7. By using a comparison plate or a low power microscope the length and width of a scratch with dimensions larger than 10 μ m is measured followed by assigning the grade.

In the second method all of the imperfections, regardless of their width, length or number or whether on or between surfaces of a component, are observed simultaneously and the component is quickly rejected if one imperfection exceeds a predefined level of visibility under controlled

condition illumination and viewing. This method depends on the visibility of the imperfection when viewed by a calibrated eye under controlled conditions of illumination and viewing. By using particular levels of sample illumination any number of imperfections below an acceptance level of severity are rendered invisible for certain classes of components. The component is rejected if any imperfection is visible. The method of specifying imperfection tolerances will be governed by the application and the need for objective measurement of all imperfections (first method) or the desire for a fast overall evaluation of components quality (second method) [74]. However because these ISO standards were too costly to implement due to the fact that they require comparison of every imperfection of the specimen with a comparison plate, and also the accumulation rules are obscure and difficult to implement they have not been fully accepted in the U.S. as a national standard [76].

It was in 1950s and 1960s that first standards for optics In the United States were published, and they originally were for military applications but then were applied across the entire industry [76]. MIL-PRF-13830B [77] currently is what that is referred to as scratch and dig standard, it is based on MIL-O-13830 [78] which was first published in 1954 for military standard purposes [79, 80].

MIL-PRF-13830B is based on visual comparison under specific dark-field lighting conditions between surface imperfections and a comparison standard set to determine the visibility or grade of the imperfection. The scratch and dig grades in this standard are a set of two unrelated numbers separated by a hyphen, scratch grade first and dig grade second. These numbers are assigned by visually comparing the brightness of digs and scratches of a surface to a comparison standard while the specimen and the comparison standard are under specific lighting condition. Scratch number start from 10 to 80 and it indicates the brightness of the scratch that best matches with the one in the comparison standard. The scratch number is not related to the width of scratch and should not be misunderstood with width [81]. The dig number however is a measurable number which is the diameter of the largest specimen's dig given in 1/100 mm, for instance a dig number of 40 means a dig with diameter of 400 μm [77].

The limitation of allowable defects on the surface will be set after the scratch and dig numbers are determined by designer. For scratches, the sum of all scratch lengths with the specific scratch number should not exceed one fourth of the diameter of the optic. For non-circular optics, the diameter of a circle with equal area to that of the optic should be used. For digs the total number of allowable maximum size digs should not exceed the diameter of the optic divided by 20, and also the sum of all digs' diameter should be less than or equal to twice the total number of allowable maximum sized digs multiplied by the specific dig number [77]. Despite the fact there is an expectation that the surface quality will affect the performance of the optics, It should be noted that the scratch and dig standard (MIL-PRF-13830B) is a cosmetic standard and is not a performance standard and should not be used as such [80, 82].

However, the demand in some applications that were sensitive to scratches too small to see, or required a dimensional specification for surface imperfections led to a new set of standards in the U.S. called ANSI/OEOSC OP1.002 [83]. This standard keeps the visibility method from MIL-PRF-13830B and adds a dimensional method of inspection from MIL-C-48497A standard. This standard is equivalent to combination of both ISO 10117-7 and ISO 14997, and to invoke the dimensional method a pair of letters is used such as A-A or E-E [73, 79].

Common factors for all of the aforementioned methods of manual surface inspection are that they all require a human inspector, they are slow (when compared to automatic systems) and thus expensive, and finally they are to some extent still subjective. Among these factors, time plays an important role in the industry. In process automatic inspection systems are preferred and a huge amount of research has been done in this field, for instance a wide variety of computerized visual inspection methods are being investigated by electronics industry where advanced technological capabilities have increased the speed of production and reduced the physical size of components [84].

2.5.2 Automatic inspection

One of the important steps in a production process in industries such as wood, steel, silicon wafer, ceramics, etc. is the product inspection. This is due to the fact that product reliability is of utmost importance in mass production facilities, and as a result the inspection process is normally the largest single cost in manufacturing. One of the advantages associated with automatic visual inspection is the elimination of human inspector which is increasingly expensive, others are the speed of inspection process and diagnostic capabilities. Roland T. Chin lists several practical reasons for automatic inspection including [85, 86]:

- Freeing human from the dull and routine
- Saving human labor costs
- Performing inspection in unfavorable environments
- Reducing demand for highly skilled human inspectors
- Analyzing statistics on test information and keeping records for management decisions
- Matching high speed production with high speed inspection

One of the common issues with the automatic inspection system, especially in the industry where speed is among the most important factors, is that they are computationally expensive, and therefore time consuming. Visual inspection field with computer vision and image processing techniques is so vast and broad and it is beyond the scope of this survey to cover it completely. However one aspect of visual inspection field that is of our interest is surface texture analysis (because in fact the task of detecting defects has been largely viewed as a texture analysis problem), here defects are categorized into two groups, one is the local textural irregularities (which is the main concern of most visual surface inspection applications), and the other is global deviation of pattern or texture where local texture do not exhibit abnormalities [86-88].

Four techniques are used to inspect local textural irregularities namely statistical approaches, structural approaches, filter based methods, and model based approaches.

One of the most widely used approaches for surface texture analysis is the statistical approaches where the spatial distribution of pixel values is being measured. Histogram statistics, co-occurrence matrices, autocorrelation, and local binary pattern are instances of statistical approaches [86]. Mean, standard deviation, variance, median, geometric and harmonic mean are among statistics of a histogram. Histogram statistic techniques have proven to be useful and efficient in applications such as ceramic tiles or fabric defect detection [89]. The accuracy of these approaches can be increased when using histogram statistics of local image regions rather than the global image [90]. I. shou et al. used simple histogram moments such as mean and standard deviation for defect classification in fabrics production by a neural network system [91].

Among the most well-known and widely used texture features are spatial co-occurrence matrices; these that are second order statistics are accumulated into a set of 2D matrices. When given a displacement vector each of which measures the spatial dependency of two grayscales [86]. A. bodnarova et al. used this method (spatial gray level dependence) to identify defects in woven textile fabrics [92]. Lee Hok Siew et al. showed that by using these second order gray level statistics they are able to discriminate of degrees of wear in wool carpet and the capability of the method in quality control process [93]. Jukka Iivarinen et al. proposed a segmentation scheme to detect surface defects using co-occurrence matrices and overcame the issue of threshold selection for the distance between a feature vector and the best matching unit [94]. However it is worth noting that co-occurrence matrices suffer from the fact that there is no generally accepted solution for optimizing the vector of displacement, a poor performance of these methods were observed when compared to other techniques such as filtering based methods [86, 95, 96].

When there are textures on the surface with a repetitive pattern in nature, auto-correlation method that is a second order statistic is useful. It measures the correlation between the image itself and the image when translated with a distance, and shows peaks and valleys in the auto-correlation

measure; and it is related to the power spectrum of Fourier transform. It should be noted that one of the challenges facing the auto-correlation function is that it is not a suitable approach for surfaces with random textures with irregularly arranged textural elements [86, 97].

Local binary patterns (LBP) is a shift invariant complementary measure for local image contrast, and uses a sliding window with the gray scale value of its center pixel as a threshold for surrounding neighborhood pixels. This method is a cheap one in terms of computational expense, and is relatively invariant with respect to change in illumination and image rotation [98]. Matti Nisanen et al. used this method for discriminating defects and sound wood, and showed the high capability of the method in detecting defects with low error scape and false alarm rate [99].

Analyzing surface texture patterns in terms of individual texture primitives and their spatial relationship is called surface structural analysis. In this analysis the two goals are first to extract the surface texture primitives such as a simple individual pixel, a region with uniform gray level or a line segment; and second the modeling of spatial placement rules [100]. These placement rules can be achieved by learning statistical properties of texture primitives or by modeling the geometrical relationship that exists between surface primitives [86]. Jiahan Chen et al. proposed a structural method to detect defects in textile images by thresholding a textured image using histogram analysis, and showed the potential usefulness of the approach in industrial environment [101].

The common factor of all of filter based approach methods is computing the energy of the filter response when filter banks are applied to the image. These methods can be divided into two categories namely spatial domain and frequency domain filtering and joint spatial/spatial-frequency methods [86].

2.6 Conclusion

The importance of surface topography was described both in performance and functionality point of view as well as economic aspect of it. Effect of surface topography in different applications

was discussed. Because of this importance much effort has gone into developing surface measurement instruments, and also surface characterization techniques. Limitation of these parameters in terms of detecting and characterizing surface features made researchers to begin developing visual inspection techniques based on computer vision and image processing methods. However, one of the challenges in the computer image processing techniques used in automated inspection system is their complexity in terms of processing the input data. Algorithms for performing these analyses on the input data are rather complicated, and thus are computationally expensive [86, 91, 96]. However, this matter is manageable and the use of image processing algorithms in the industry is an indicator of its strong capabilities [102, 103].

Fast methods of inspecting components in quality control systems are of great interest in industry, techniques that do not require segmentation and pattern recognition and complicated algorithms are not expected to be computationally expensive and slow. In surface texture analysis methods statistical approaches are among the fastest [86] therefore exploring new statistical approaches is very important and of interest.

CHAPTER 3: METHODOLOGY

3.1 Introduction

A height map of $n \times m$ pixels size consists of n columns and m rows. Conventional amplitude parameters defined in ISO 25178-2 take into account the whole $n \times m$ data points and reduce it to a single statistical parameter such as Sa , Sq , Ssk , and Sku . However, if these constituent line profiles are analyzed individually then more information about the surface topography can be achieved such as directionality on the surface, wavelength of periodic structures on the surface, isotropy/anisotropy of the surface, and also presence and geometrical attributes of surface features such as digs and scratches.

This chapter details all the steps of the approach for creating polar plots from a given height map or a grayscale image. In this approach an areal height map of $n \times m$ pixels, after its form and waviness are removed, is treated as a set of constituent profiles, i.e. columns or rows. Figure 3-1 depicts the constituent profiles of a 1000×1000 pixel areal height map with 30 pixels intervals. Instead of treating the height map as $n \times m$ data points and calculating single statistical parameters such as ubiquitous Sa , Sq , Ssk , or Sku , a statistical parameter of choice such as mean height (μ_h), Ra , Rq , Rsk , or Rku is calculated for each profile of the height map. It should be noted that while these values are calculated as per ISO 25178-2 standard definition, the initial filtering is not done on a profile basis, but instead on the filtered surface. The standard deviation or higher moments of data such as skewness and kurtosis of the resulting distribution is then calculated. In the next step the surface is rotated around its center by some number of degrees, θ , resulting in a new set of profiles, again the μ_h , Ra , Rq , Rsk , or Rku of all profiles is calculated, and so is the standard deviation, skewness, or kurtosis of their distribution. This process is repeated until a 180° rotation of the initial height map is achieved, and finally all the statistical properties of the resultant distributions are plotted versus the angle of rotation in a polar plot formation.

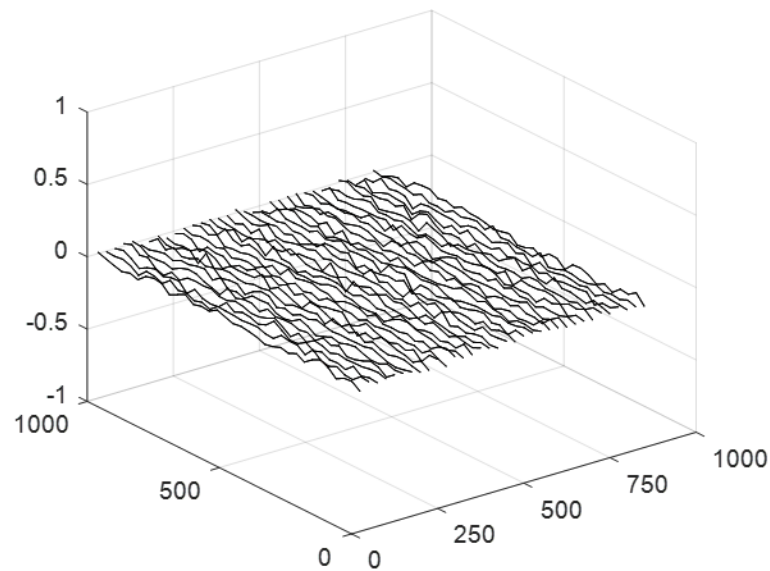


Figure 3-1: Constituent profiles of a 3D height map, the distance between each profile is 30 pixels for demonstration purposes.

3.2 Polar plots generation details

In this method, the process begins with calculating a statistical parameter of choice, sp , for each of the line profiles of the height map. This statistical parameter could be the profiles mean height, μh , its root mean square, Rq , the arithmetic mean of the absolute height values of the profile, Ra , the skewness, Rsk , or the kurtosis, Rku . Calculating the statistical parameter for all of the columns will result in a sp distribution consisting of $n \times sp$ values where n is the smaller value of $n \times m$. This distribution is then quantified based on its standard deviation, skewness, and kurtosis. In the next step the height map is rotated based on a rotational interval around its center creating a new set of profiles and the process of calculating the statistical parameter for profiles and quantifying the resulting histogram is repeated until a 180° rotation is achieved, all of the information from the surface is captured in a 180° rotation, however, in order to have a complete polar plot the second half of it, i.e. 180° to 360° is plotted as well by utilizing the symmetry or results. Figure 3-2 demonstrates all the required steps to create a polar plot where the statistical parameter calculated for columns is their Rq values.

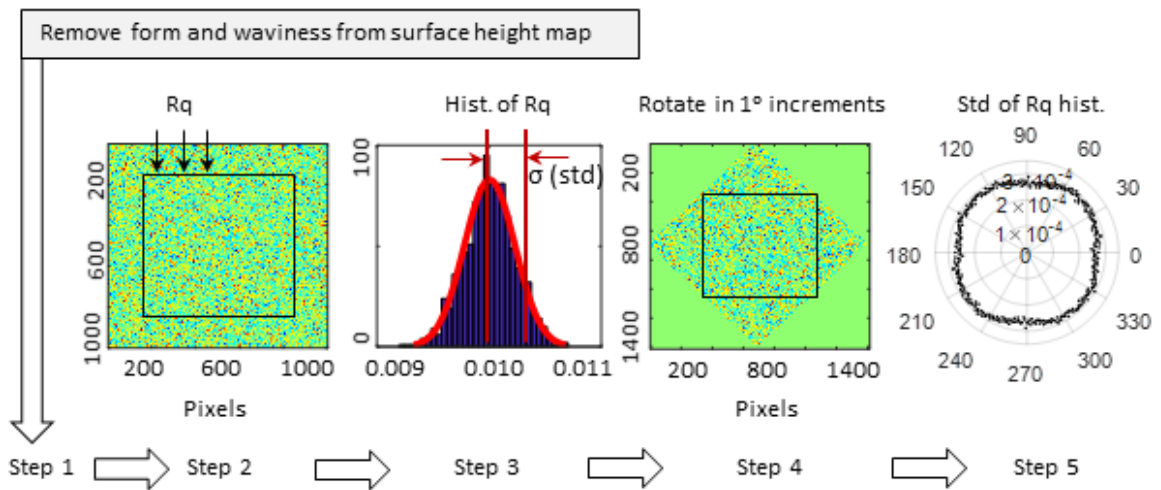


Figure 3-2: All the required steps to obtain the σ_{Rq} polar plot.

3.2.1 Rotation in MATLAB

In this work, the rotation procedure of the height map around its center is done in MATLAB with the `imrotate` command. MATLAB uses three different algorithms to rotate an image or matrix namely Nearest-neighbor interpolation, Bilinear interpolation, and Bicubic interpolation.

In general the relationship between the original coordinate of a point or pixel, $\begin{bmatrix} i \\ j \end{bmatrix}$ and the new coordinate when the point is rotated θ degrees, $\begin{bmatrix} i' \\ j' \end{bmatrix}$ in 2D space is obtained by using the 2D rotational matrix given in equation 3-1.

$$\begin{bmatrix} i' \\ j' \end{bmatrix} = \begin{bmatrix} \cos(\theta) & -\sin(\theta) \\ \sin(\theta) & \cos(\theta) \end{bmatrix} \begin{bmatrix} i \\ j \end{bmatrix} \quad (3-1)$$

Dimension of the rotated matrix when rotated θ degrees increases in MATLAB, and it is given in equation 3-2, see Figure 3-3.

$$n_{new} = n_{initial} [\sin(\theta) + \cos(\theta)] \quad (3-2)$$

Where n_{new} is the dimension of the rotated matrix, and $n_{initial}$ is the dimension of the unrotated matrix.

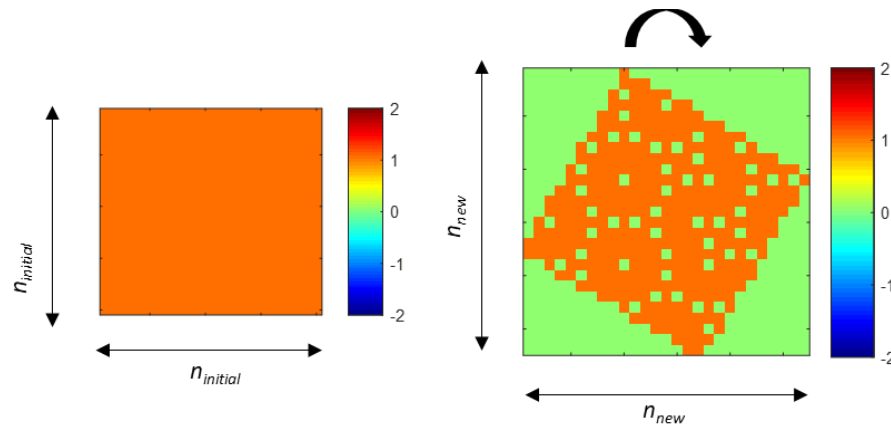


Figure 3-3: a) Original matrix of size $n_{initial} \times n_{initial}$, and b) the same surface when rotated θ degrees with size $n_{new} \times n_{new}$

This increase in size means that there are some new pixels generated, i.e. holes, as shown as green pixels in Figure 3-3. These holes will be filled in depending on the interpolation algorithm in the computer system. In Nearest-neighbor interpolation the value of the new generated pixel will be equal to the value of the nearest neighboring pixel; the advantage of this algorithm in this work is that it uses the real values from the initial matrix and does not generate new values that are not in the initial matrix. In Bilinear interpolation method the value of the newly generated pixel is the weighted average of the four neighboring pixels and thus it is a value that does not exist in the initial matrix. It is the case for Bicubic interpolation method where the value of the newly generated pixel is the weighted average of the 16 neighboring pixels. Figure 3-4(a) depicts a square matrix with a rectangular feature on it, this matrix is rotated 40° clockwise with Nearest-neighbor interpolation method and it is clear that no new value is generated to fill in the holes that is not in the initial matrix, see Figure 3-4(b). When using Bilinear and Bicubic interpolation method to rotate the initial matrix some new values are created and will be used to fill in the holes as shown in Figure 3-4(c) and (d).

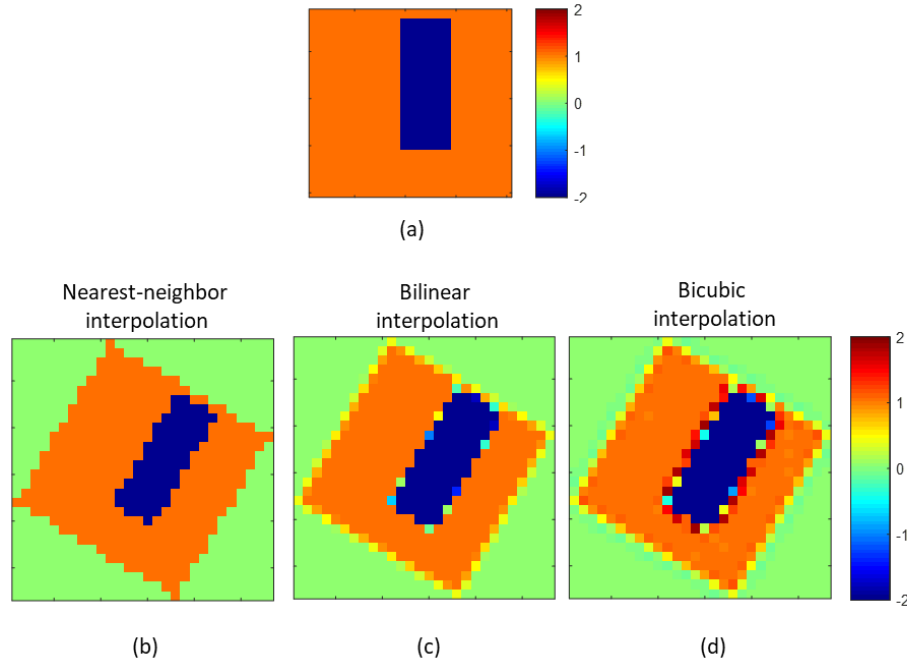


Figure 3-4: a) Initial matrix with a rectangular feature and when it is rotated 40° clockwise b) with Nearest-neighbor interpolation, c) Bilinear interpolation, and d) Bicubic interpolation method.

It should be noted that in theory there is no limitation for the rotational angle and it could be any large or small value. However, MATLAB and other computer systems in general, since their environment is discrete, the resolution of rotation depends on the size of the input image and the angle of rotation. Adjusting equation 3-1 based on the rotation around the center of a matrix in MATLAB is given in equation 3-3.

$$\begin{bmatrix} i' \\ j' \end{bmatrix} = \text{round} \left\{ \begin{bmatrix} \cos(\theta) & -\sin(\theta) \\ \sin(\theta) & \cos(\theta) \end{bmatrix} \begin{bmatrix} i - n_{\text{initial}}/2 \\ j - n_{\text{initial}}/2 \end{bmatrix} + \begin{bmatrix} n_{\text{new}}/2 \\ n_{\text{new}}/2 \end{bmatrix} \right\} \quad (3-3)$$

Moreover, in the discrete environment of computer systems the rotation actually takes place when the size of the rotated matrix, n_{new} , is at least one pixel larger than the size of the initial matrix, n_{initial} . This could be written as:

$$n_{\text{initial}} [\cos(\Delta\theta) + \sin(\Delta\theta)] - n_{\text{initial}} > 1 \quad (3-4)$$

Solving equation 3-4 for $\Delta\theta$ we have:

$$\cos(\Delta\theta) + \sin(\Delta\theta) > \frac{1 + n_{initial}}{n_{initial}} \quad (3-5)$$

The result of the equation 5 is the resolution of rotation for computer systems, $\Delta\theta$. For instance, for a 20×20 matrix the resolution of rotation based on equation 3-5 is equal to 2.94° , which means that the smallest rotational increment has to be more than 2.94° . $\Delta\theta$ for a 1000×1000 pixels matrix is equal to 0.057° .

In rotation process based on equation 3-2 the size of the rotated height map increases at each increasing rotational angle until it reaches its maximum size which is $\sqrt{2}n$ at $\theta=45^\circ$, see Figure 3-5(b). This increase in size means that some zero values are added to the rotated matrix; and these zeros affect the statistical parameters that are calculated for the profiles. For instance, the first and last columns of the surface in Figure 3-5(b) contains zeros except one pixel that belongs to the surface, whereas the column in the middle contains only the surface's height values.

In order to just use the data points that belong to the height map and exclude all the added zeros a rectangle of the size equal to $\frac{n}{\sqrt{2}}$ is superimposed on the height map where n is the smaller of $n \times m$ terms, Figure 3-5(c). This superimposition of the rectangle causes the loss of 50% of the area and 29.3% of the profiles from the initial height map; however, it ensures that only the real surface data is processed.

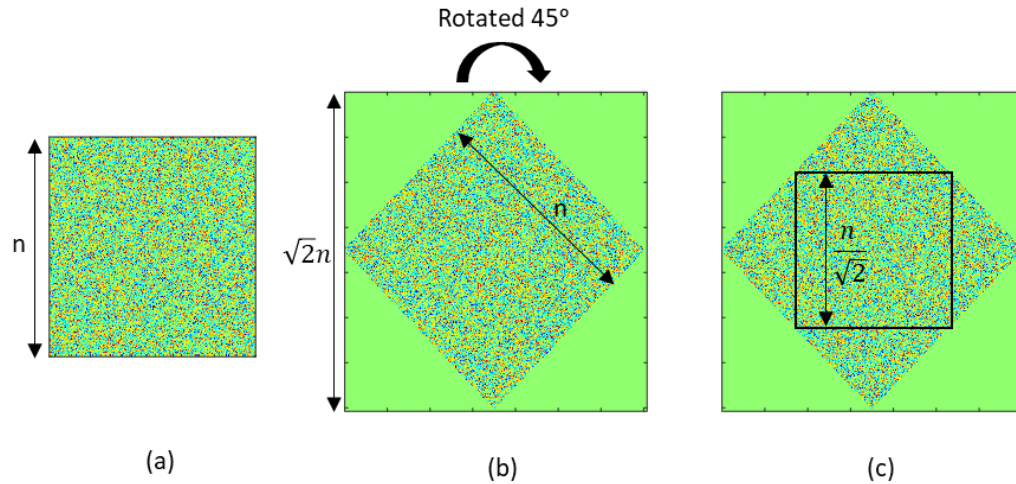


Figure 3-5: a) Unrotated height map of a surface with Gaussian distribution of heights, b) height map rotated 45° and the maximum size increase, and c) super imposed rectangle on the height map containing only real height data points.

At each rotational angle, θ , the statistical parameter, sp , values of all columns inside of the superimposed rectangle is calculated which at the results in a sp distribution shown as sp histogram in Figure 3-6. Each histogram is then quantified in the next step based on its properties such as standard deviation, skewness, and kurtosis. It should be noted that while Figure 3-6 depicts the original surface and when it is rotated 30° and 60° the process of rotating the surface and quantifying the resulting histograms by their properties is repeated until the surface is rotated 180°.

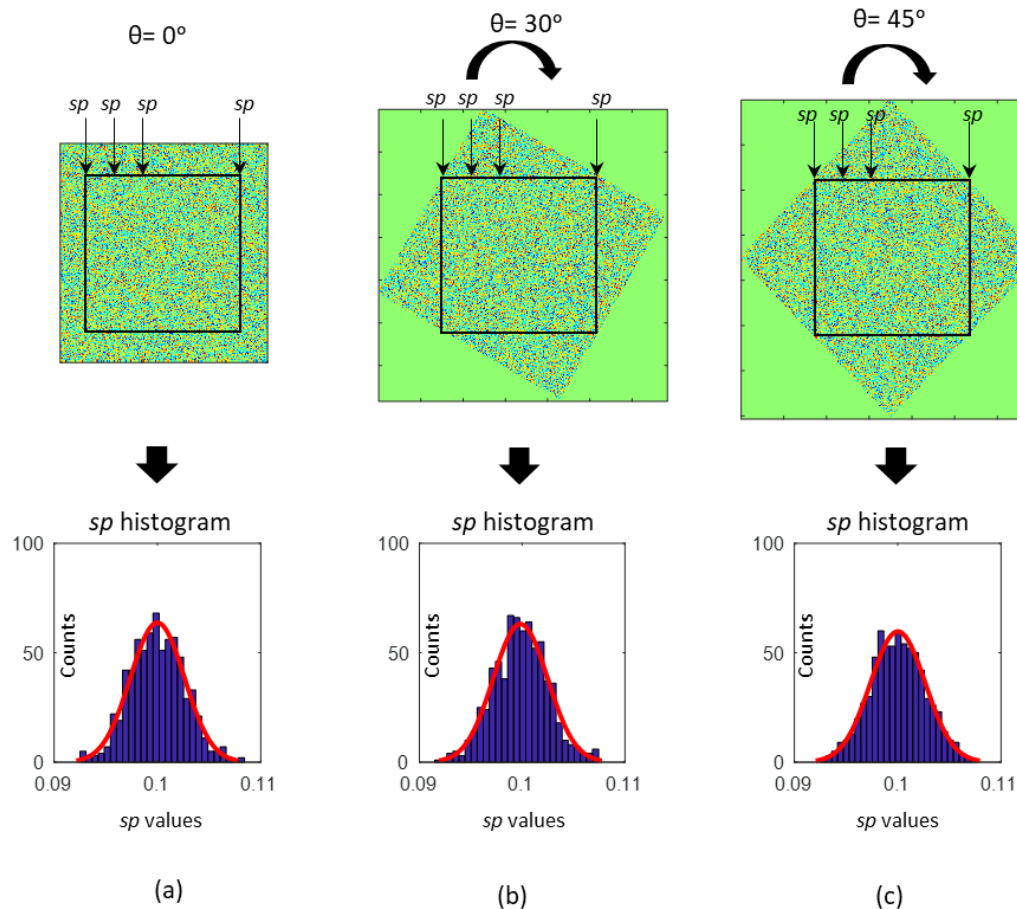


Figure 3-6: a) Initial height map of a surface with Gaussian distribution of heights and the sp histogram of the columns inside the superimposed rectangle, b) initial height map rotated 30° and the sp histogram of the columns inside the superimposed rectangle, and c) initial height map rotated 45° and the sp histogram of the columns inside the superimposed rectangle.

After a 180° rotation, assuming that the rotational increments are in 1° intervals, there will be 180 standard deviation, skewness, or kurtosis values associated to each histogram at each angle of rotation. These values are plotted versus the rotational angle at which they were calculated in a polar plot formation, Figure 3-7 depicts a surface with Gaussian distribution of height and its polar plots when the selected statistical parameter of the profiles is their Rq values, i.e. $sp = Rq$. The second half of the polar plots is generated by utilizing the rotationally symmetric nature of the results of the first half.

It should be noted that the process works if the statistical parameter is calculated for each row instead of each column.

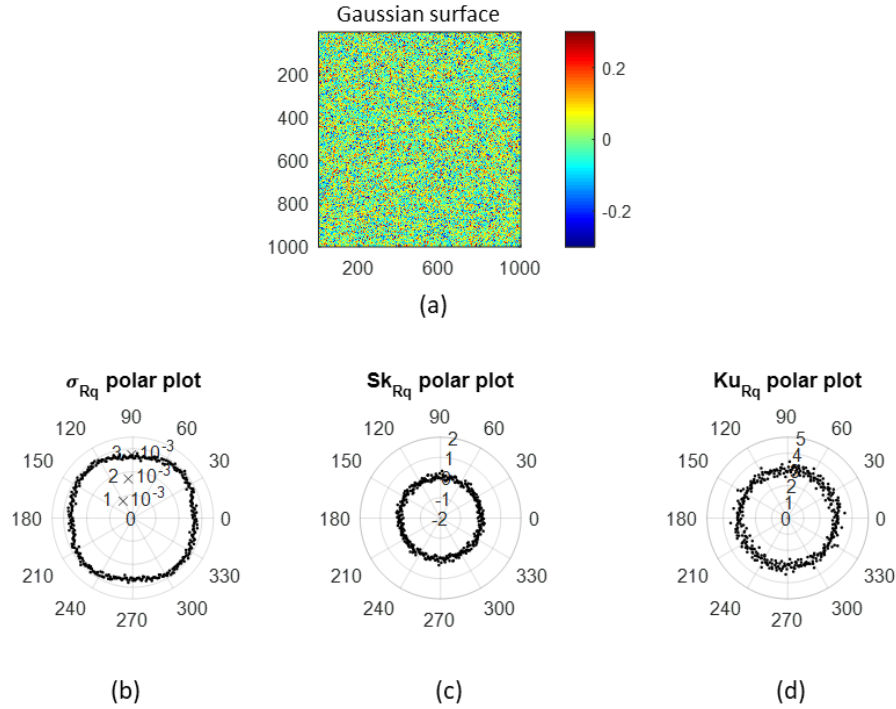


Figure 3-7: a) MATLAB generated surface with Gaussian distribution of heights and its b) σ_{Rq} polar plot, c) Sk_{Rq} polar plot, and d) Ku_{Rq} polar plot.

Figure 3-7(a) shows a 1000×1000 pixels surface with a Gaussian distribution of heights generated in MATLAB with the `pearsrnd` command with its mean, standard deviation, skewness, and kurtosis equal to $0 \mu\text{m}$, $0.1 \mu\text{m}$, 0 , and 3 respectively. Since this surface is statistically stationary the standard deviation, skewness, and kurtosis of the Rq , or any statistical parameter, histogram at each rotational angle is invariant, thus the shape of all three polar plots in Figure 3-7 is nominally circular. Rq histograms for a surface with Gaussian distribution of heights are normal distributions, and for a normal distribution the skewness value is equal to zero as shown in Figure 3-7(c), and the kurtosis value is equal to three as shown in Figure 3-7(d).

3.3 Processing time of generating polar plots

The required steps for generating the polar plots of a surface is shown in Figure 3-2, from this graphical representation step one is only done once and after the form and waviness is removed from the surface this step is finished. Steps two, three, and four are repeated $180/\Delta\theta$ times, this is

due to the fact that all of the information is captured in a 180° rotation, and the results would be symmetrical from 180° to 360° . At this time each rotational angle, θ , and the calculated properties of the sp distribution, i.e. standard deviation, skewness, and kurtosis values are saved. And at the end in step five these results are plotted in a polar plot formation. The processing time of these required steps depends on the size of the matrix and the resolution of the rotation, $\Delta\theta$.

For the typical size of the output of a 3D measurement instruments, that is a height map of 1024×1024 pixels, and when the resolution of rotation is equal to 1° , the whole process of generating σ_{Rq} polar plot, Sk_{Rq} polar plot, and Ku_{Rq} polar plot takes less than 15 seconds in MATLAB installed on a computer with a normal computing power with Intel(R) Core(TM) i7-2600 CPU @ 3.4GH configuration (not a super computer). In this amount of time for processing a surface the `imrotate` command takes about the 80% of the overall time. The overall processing time can be further decreased to 10 seconds by rotating the surface only 90° . In this case at each rotational angle the sp value of the columns and rows of the superimposed rectangle on the surface are being calculated at the same, the calculated values for rows then serve for the polar plot's data points at $\theta+90^\circ$ at each rotational angle, θ .

It was tried to make the whole processing algorithm optimized with the goal of reducing the time of calculations as much as possible, however, it is believed that further optimizations in coding of the process can be done to further increase the speed of process, also it is believed that implementing the whole process of generating polar plots in other programming platforms such as C++ could reduce the overall time of calculations, this is because MATLAB (MATrix LABoratory) is a scripting and mathematical language processor for working with mathematical equations in a matrix base environment, however, C++ is a structured programming language for writing algorithms, and runs as fast as the code written in assembly language.

3.4 Items affecting polar plots

The shape of the polar plots is dependent of the nature of the surface that is being analyzed. Surface topography and surface features are factors that affect the shape of the polar plots and can be divided into two categories naming surface texture characteristics such as tooling marks on a turned surface, and surface features such as circular features, i.e. digs, and linear features such as scratches. These will be discussed in the following chapters.

3.5 Unprocessed surfaces

As was mentioned in section 3.1 calculation of the metric of choice is done once the form and waviness are removed from the surface height map, i.e. surface is post-processed. However, if the form and waviness are not removed from the surface height map the shape of the polar plots would be significantly different when compared to the polar plots of the same surface after it is been processed. Two examples illustrating this point are indicated below, in both examples only form is present on the surfaces, i.e. the surface Sq values are zero in value.

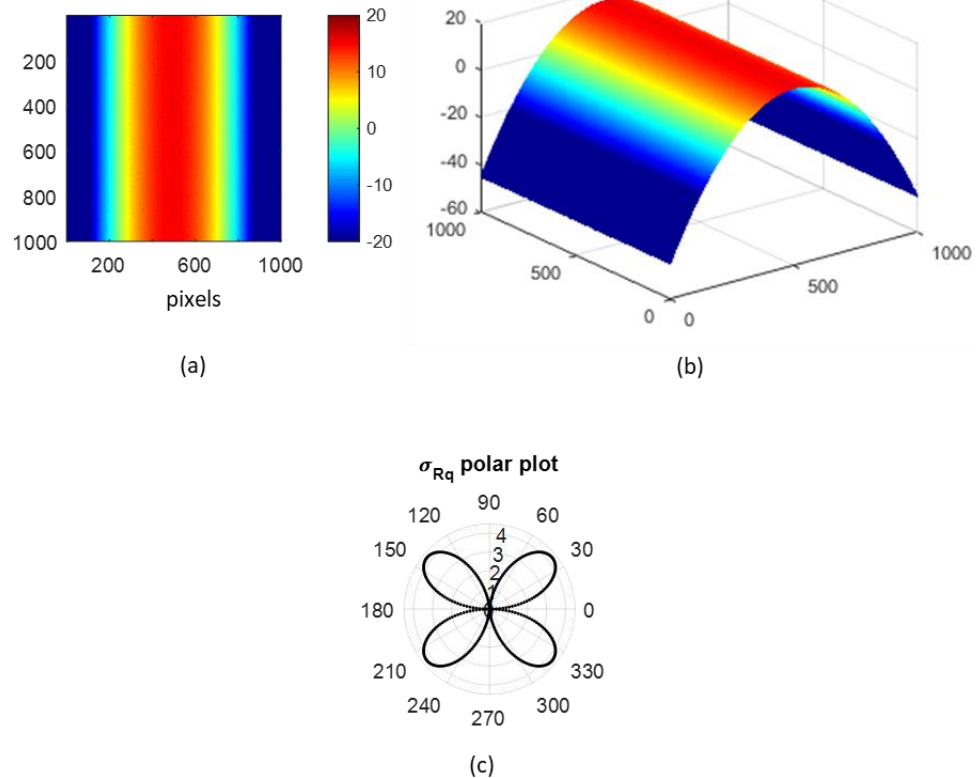


Figure 3-8: a) A MATLAB generated surface without its form removed (the surface is formed with a second degree polynomial), b) the same surface shown in 3D, and c) its σ_{Rq} polar plot.

The shape of the polar plot shown in Figure 3-8(c) is due to the fact that during the rotation of the unprocessed surface, Figure 3-8(a), as the height deviations in the columns varies (because of the presence of the form), the standard deviation of the columns Rq histogram varies significantly, and dominates the shape of the polar plot. Here, the minimum radius of the polar plot happens at two angles; first at the angle where columns are parallel to the axis around which the surface has its curvature, and the second angle where columns are perpendicular to the axis of curvature. In both cases all of the columns are identical, and therefore the standard deviation of their Rq histogram is equal to zero, i.e. the radius of the polar plot is zero. In between these two points the maximum radius of the polar plot occurs at the angle where the range of columns Rq values is maximum. This angle is a function of the geometry of the curvature, and it is thought that similar

to the analysis of the surfaces with periodic features (see section 4.5) it can provide insights on the form of the surface.

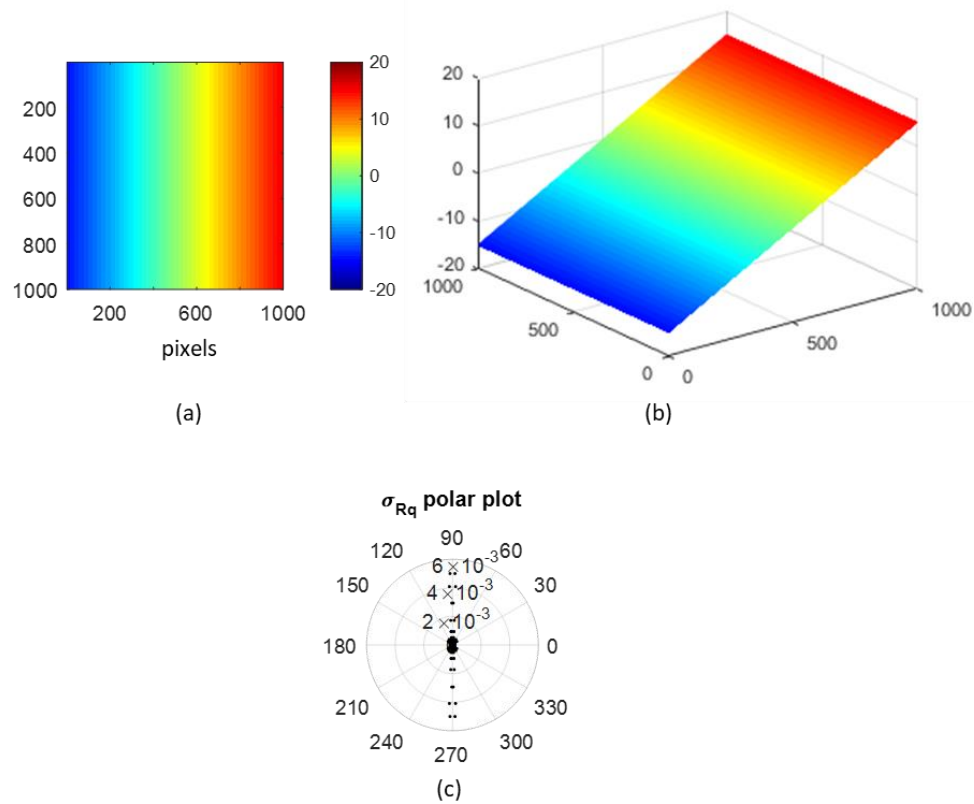


Figure 3-9: a) A MATLAB generated planar surface without its tilt removed, b) the same surface shown in 3D, and c) its σ_{Rq} polar plot.

The surface whose tilt is not removed also affects the behavior of the resulting polar plot as is shown in Figure 3-9. Presence of the tilt in the surface causes the height variations of the columns to vary during rotation, and thus changes the shape of the σ_{Rq} polar plot. In this case the minimum radius of the σ_{Rq} polar plot happens at two angles, first when columns are parallel to the axis around which the surface is tilted ($\theta=0^\circ$, and 180° in Figure 3-9(a)); the average height value for each column is different because of the tilt, however, the standard deviation of their height values is equal to zero; and thus the radius of the polar plot is equal to zero. The second angle is where columns are perpendicular to the tilt axis (90° before or after the angular location of the minimum radius), at this angle all of the columns have the same shape and zero Rq values, therefore the

standard deviation of their Rq distribution which is the radius of the polar plot is zero as well. The maximum radius of the polar plot happens at an angle close to when the columns are perpendicular to the axis of tilt.

The analysis of the effect of the form of the surface on its polar plots has not been covered in this dissertation, therefore further study and research is needed for polar plot analysis of unprocessed surfaces.

3.6 Summary

In this approach the areal map of a surface, after its form and waviness are removed, is treated as a collection of line profiles. A statistical parameter of choice is calculated for each of the profiles and at the end the resulting distribution will be quantified based on its standard deviation, skewness, and kurtosis. The surface is then rotated some number of degrees around its center and the process of calculating the statistical parameter and the properties of the corresponding distribution repeated until the surface is rotated 180° , the second half of the polar plot is then achieved by utilizing the symmetry of the first half. At the final step all the standard deviations, skewness, and kurtosis values are plotted versus the rotational angle at which they were calculated in a polar plot format.

The rotation of the surface around its center can be done in any degree intervals in theory and there is no limitation on it, but in the discrete nature of the computer systems this interval has to be chosen based on the equation 3-5. Since during the rotation the size of the rotated matrix varies a rectangle of size equal to $\frac{n}{\sqrt{2}}$ is superimposed on the initial matrix to make sure that only real surface data is analyzed and not the data added by the numerical algorithm to pad the matrix generated by the 'imrotate' command.

CHAPTER 4: SURFACE CHARACTERIZATION

4.1 Introduction

The shape of the polar plots is dependent on the nature of the surface that is being analyzed. Characteristics such as surface texture directionality, i.e. surface lay, surface periodic structures, surface isotropy/anisotropy, and the surface roughness value, Sq , all affect the polar plots' shape.

In this chapter the effect 1) of surface roughness of surfaces with Gaussian distribution of heights, 2) surface isotropy and directionality, and 3) surface periodicity on the polar plots will be detailed.

The relationship between the surface roughness value Sq and the radius of the standard deviation of the Rq histogram, σ_{Rq} polar plot in a surface with a Gaussian distribution of heights is established, so is the relationship between the wavelength of a periodic structure and the angle between the first global minimum and maximum radii of the polar plots.

The statistical parameter of choice for the columns in this chapter is their Rq values, and the rotational increment is equal to 1° unless otherwise mentioned.

4.2 Surface roughness of Gaussian surfaces

In the unique case of a surface with a Gaussian distribution of heights the radius of the standard deviation of Rq histogram polar plot, i.e. σ_{Rq} polar plot, is a function of the root mean square surface roughness, Sq and the surface size, n . Surfaces with higher values of Sq and equal skewness and kurtosis values will have larger radius in their resulting σ_{Rq} polar plots.

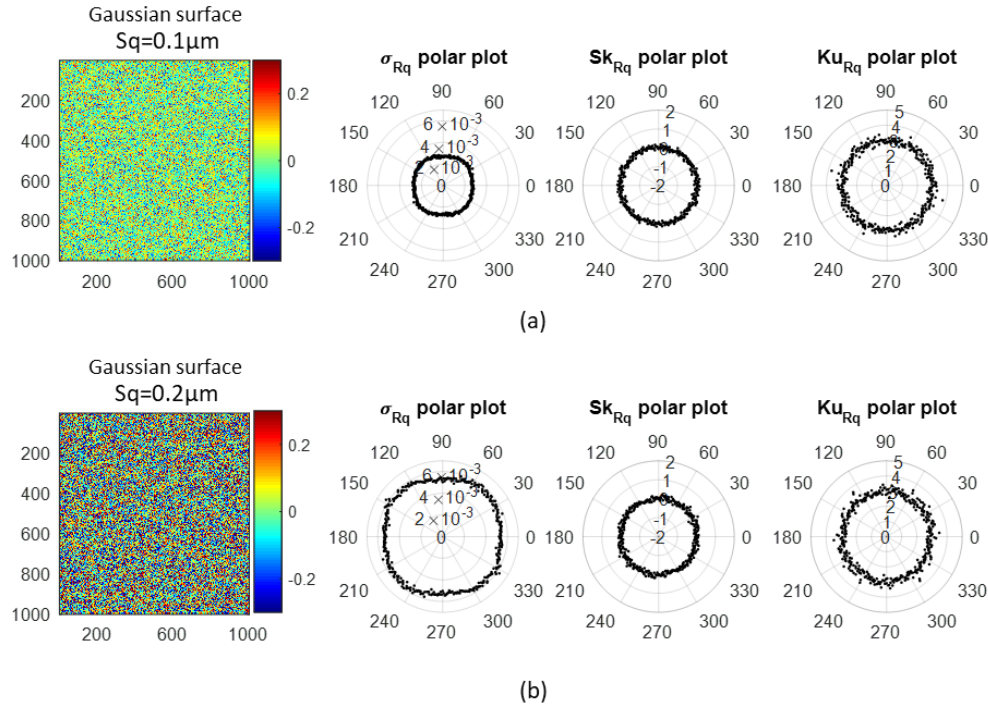


Figure 4-1: MATLAB generated surface with Gaussian distribution of heights with Sq equal to a) $0.1 \mu\text{m}$, and b) $0.2 \mu\text{m}$ and their σ_{Rq} , Sk_{Rq} , and Ku_{Rq} polar plots.

Figure 4-1(a) and (b) show two MATLAB generated theoretical surfaces with Gaussian distribution of heights with their Sq equal to $0.1 \mu\text{m}$ and $0.2 \mu\text{m}$ respectively. The skewness and kurtosis values for both of these surfaces are zero and three respectively. It is clear that the σ_{Rq} polar plot's radius increases as the Sq value of the surface increases, but the radius of Sk_{Rq} and Ku_{Rq} polar plots remains unchanged since their skewness and kurtosis did not change. If the skewness and kurtosis of these surfaces were also changed, their polar plots' radii would change as well.

The relationship between the root mean square roughness of the surface, Sq , with its skewness and kurtosis values equal to zero and three respectively, and the radius of the σ_{Rq} polar plot can be calculated by using the *Chi* distribution properties. In this case dividing all the height values in each column, $h_{i,j}$, by the total root mean square roughness of the surface, Sq , makes them standard normal with the mean and standard deviation equal to zero and one respectively, $h'_{i,j} \sim N(0,1)$. Now let $h_{i,j}$ be all the height values in column j , the variance of this column is given in equation 4-1.

$$\text{var}\left(\frac{h_{i,j}}{Sq}\right) = \sum_{i=1}^k \frac{(h'_{i,j})^2}{k} \quad (4-1)$$

Simplifying equation 4-1 will lead to equation 4-2, which is the definition of *Chi* square distribution.

$$\frac{k}{Sq^2} \text{var}(h_{i,j}) = \sum_{i=1}^k (h'_{i,j})^2 = \chi_k^2 \quad (4-2)$$

Taking the square root of equation 4-2 is equal to the *Chi* distribution. Formulas for mean and variance of *Chi* distribution is given in appendix A. Based on these equations the variance of the *Chi* distribution for degrees of freedom above 20 is equal to $\frac{1}{2}$, and thus the standard deviation of it is equal to $\frac{1}{\sqrt{2}}$.

Rewriting equation 4-2 in terms of standard deviation, σ , we have equation 4-3:

$$\sigma \left[\frac{\sqrt{k}}{Sq} \sigma(hc_j) \right] = \frac{1}{\sqrt{2}} \quad (4-3)$$

And the radius of the polar plot which is the standard deviation of the columns' standard deviations, i.e. Rq , is given in equation 4-4

$$\sigma \left[\sigma(hc_j) \right] = \frac{Sq}{\sqrt{2k}} \quad (4-4)$$

Where k is the size of the super imposed rectangle on the height map, and is equal $\frac{n}{\sqrt{2}}$. Thus,

finally the radius of the polar plot is given in equation 4-5.

$$r_{\sigma_{Rq}} = \frac{Sq}{\sqrt{\sqrt{2}n}} \quad (4-5)$$

For instance, for the surface with $Sq = 0.1 \mu\text{m}$ shown in Figure 4-1(a) the σ_{Rq} polar plot's radius based on equation 4-4 is equal to $2.66 \times 10^{-3} \mu\text{m}$. It should be noted that the units of these equations have the same nature of their input values, for example if the input is in terms of μm then the result of equation 4-5 is in μm as well.

It should be noted that equation 4-5 results in the correct answer of the radius of the σ_{Rq} polar plot if and only if the skewness and kurtosis of the surface is equal to zero and three. For other values of these parameters equation 4-5 does not yield the correct radius of the polar plot. This is due to the fact that in the derivation of this formula the surface is converted to a surface with a standard normal distribution of heights, and a standard normal distribution by definition has its skewness equal to zero, and its kurtosis equal to three.

4.3 Surface isotropy and directionality

In general, the texture aspect ratio, Str , value of a surface is a unitless indicator of surface isotropy/anisotropy, an Str approaching 1 shows that a surface is isotropic and no major directional features are present, whereas an Str value approaching to 0 indicates the presence of directional surface features. Also, the directionality of surface features with respect to the vertical axis is reported by the surface texture direction, Std , value of the surface based on ISO 25178-2 [11].

Surface anisotropy and major surface texture directionality are also captured by the presence of the lobes of the polar plots, i.e. Deviations from a nominally circular polar plot. Figure 4-2 depicts a vibrationally ground steel surface and its σ_{Rq} polar plot generated by rotating the image in 0.2 degrees intervals counterclockwise. In Figure 4-2 the anisotropic nature of the surface is clearly visible from its height map, a fact supported by its Str value which is 0.02, this anisotropic nature is also captured by the non-circular shape of the polar plot. The major surface texture directionality of this surface, Std , is equal to 75.34° , which coincides with the angular location (75.4°) of the local minimum in the lobe in the upper half of the polar plot.

At the angle where the major surface texture directionality is vertical, each of the columns intersects fewer height deviations as a column entrains a surface ridge or valley (which are assumed reasonable smooth), their Rq values are reasonably consistent in magnitude, and as a result the standard deviation of the Rq histogram is low. This creates a local minimum in the σ_{Rq} polar plot, Figure 4-3(a). The standard deviation of Rq values histogram is maximum close to when the surface texture, i.e. the lay is vertical, but not exactly vertical, Figure 4-3(b). When the major surface texture directionality is perpendicular to the columns, the standard deviation of Rq histogram is minimum, at this angle while all the columns intersect all the ridges and valleys of the surface and their Rq value may be high the standard deviation of these Rq values is low, Figure 4-3(c). 90° before or after the angle of the local minimum the range of columns Rq values in a ground surface is larger than this range in the case of a surface with a periodic structure such as a milled surface. This critical factor, i.e. the radius of the polar plot when the major surface texture directionality is perpendicular to the columns, is the main difference between the σ_{Rq} polar plots of a ground surface and a milled surface.

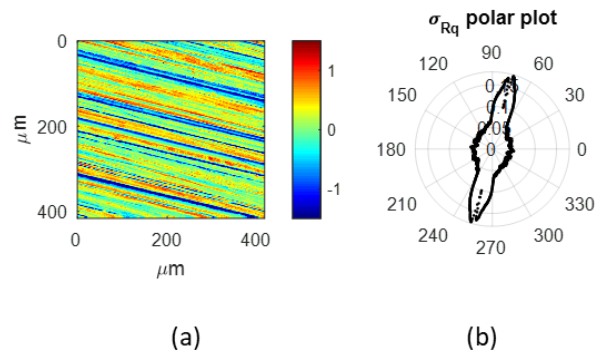


Figure 4-2: a) A ground steel surface measured with CSI 20× objective, b) its standard deviation of Rq histogram polar plot.

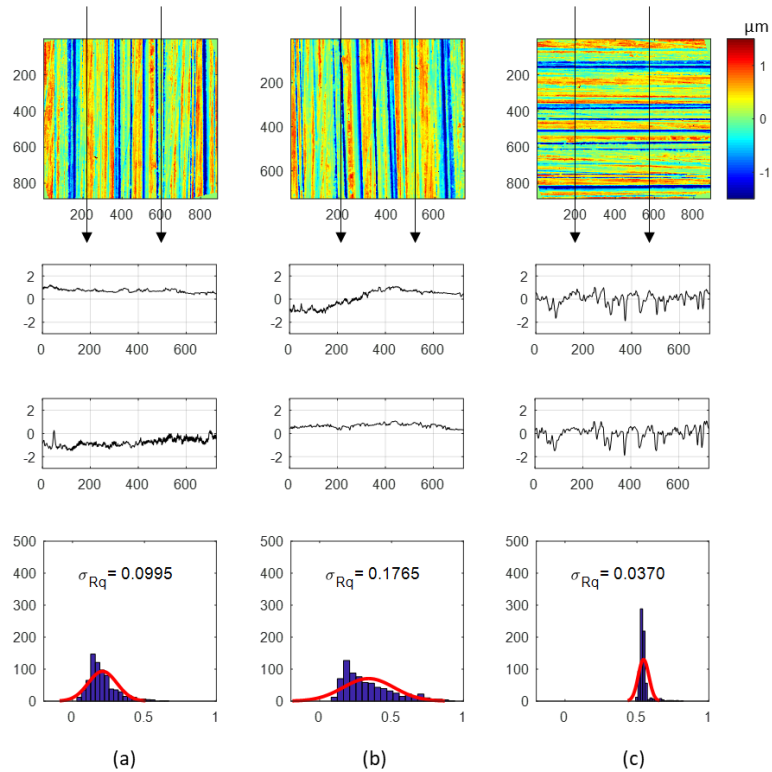


Figure 4-3: a) The ground surface shown in Figure 4-2 when rotated such that lay direction is vertical, b) when rotated such that the lay direction is close to vertical, and c) when rotated such that the lay direction is perpendicular to the columns and two sample profiles and the Rq histogram for each case.

Figure 4-4 depicts the standard deviation of σ_{Rq} polar plot for the ground surface in Figure 4-2, and the zoomed in area of the lobe region in the upper half of the polar plot. As stated above the maximum value of the polar plot occurs close to when the lay direction is vertical, which is $\theta=73.8^\circ$. Two sample profiles at this angle are depicted in Figure 4-3(b), the top profile shows a column that covers a section of a valley and a section of a ridge, and the bottom profile only covers the whole ridge. At this angle some of the columns do not cover the entire ridges or valleys on the surface, and thus the difference between the maximum and minimum Rq values is the largest leading to the maximum standard deviation of the Rq histogram.

When the major surface directionality is vertical, at $\theta=75.4^\circ$, since the majority of the columns encapsulate the entire ridge or valley of the surface there will be a sudden drop in the standard deviation of the Rq values when compared to the previous situation, i.e. a local minimum as

mentioned above. Two sample profiles of the surface at this angle are shown in Figure 4-3(a); the top profile covers a ridge, and the bottom profile covers a valley. Although the average height of these profiles are different their standard deviation which measures their height variations is close to each other and this makes the range of Rq values smaller leading to the local minimum.

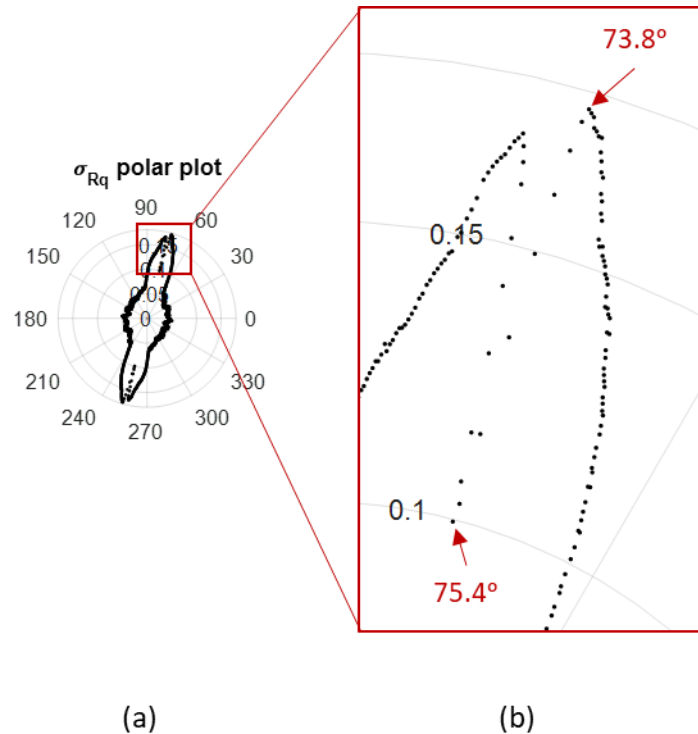


Figure 4-4: σ_{Rq} polar plot of the surface shown in Figure 4-2, and b) zoomed in area of the plot in the lobe region.

Because of the indeterministic nature of the texture of a ground surface it is not possible to mathematically find the angle at which the maximum value of the σ_{Rq} polar plot occurs. However, the angle where the local minimum of the polar plot happens is always the angle where the lay directionality is vertical, and the global minimum of the polar plot occurs when the surface texture is perpendicular to the columns. It should be noted that while the Std parameter of a surface shows the directionality of the major surface texture, the angle of lobes or the local minimums of the polar plots shows the directionality of all of the directional features on the surface.

4.4 Multi directional surfaces

Surfaces that contain multiple directional features affect the behavior of the polar plots such that they create a pair lobes or local minimums on the polar plots whenever each directional feature becomes vertical. The angular location of these polar plot's features in the upper half of the plot indicates the directionality of each feature when it is measured with respect to the vertical axis.

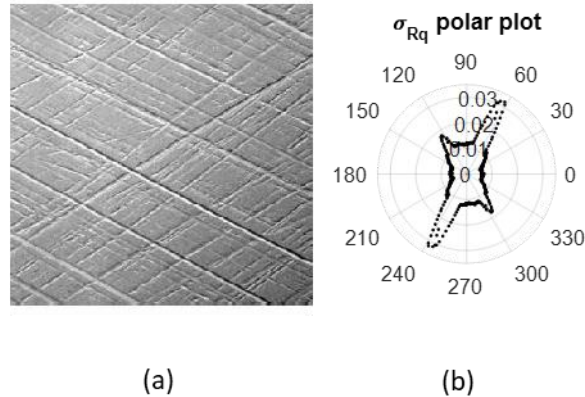


Figure 4-5: a) Grayscale image of a plateau honed surface, and b) its σ_{Rq} polar plot.

Figure 4-5(a) depicts a grayscale image of a honed surface, the σ_{Rq} polar plot of this surface is shown in Figure 4-5(b). In this polar plot there are two local minimums in the lobe region when considering the upper half of the polar plot. The first one occurs at $\theta=62^\circ$, and the second one at $\theta=123^\circ$, these angles are the angle enclosed between each directional feature and the vertical axis.

4.5 Surface periodic structure

Periodicity of a repeating structure on the surface is also reflected on the polar plots and the wavelength of the dominant periodic feature can be calculated from the polar plots.

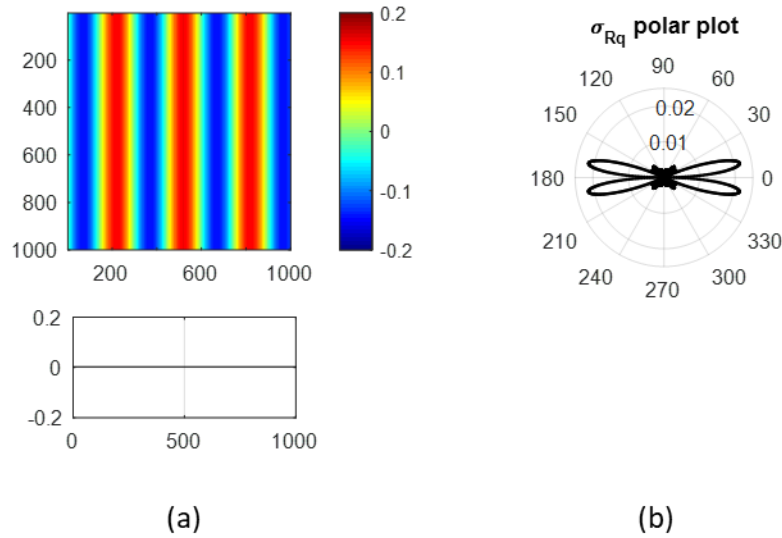


Figure 4-6: a) A theoretical surface with a sinewave feature of wavelength 300 pixels and a profile along the vertical axis, and b) σ_{Rq} polar plot.

Figure 4-6 depicts a theoretical 1000×1000 pixels surface containing a sinewave feature with its wavelength, λ , equal to 300 pixels, and its σ_{Rq} polar plot.

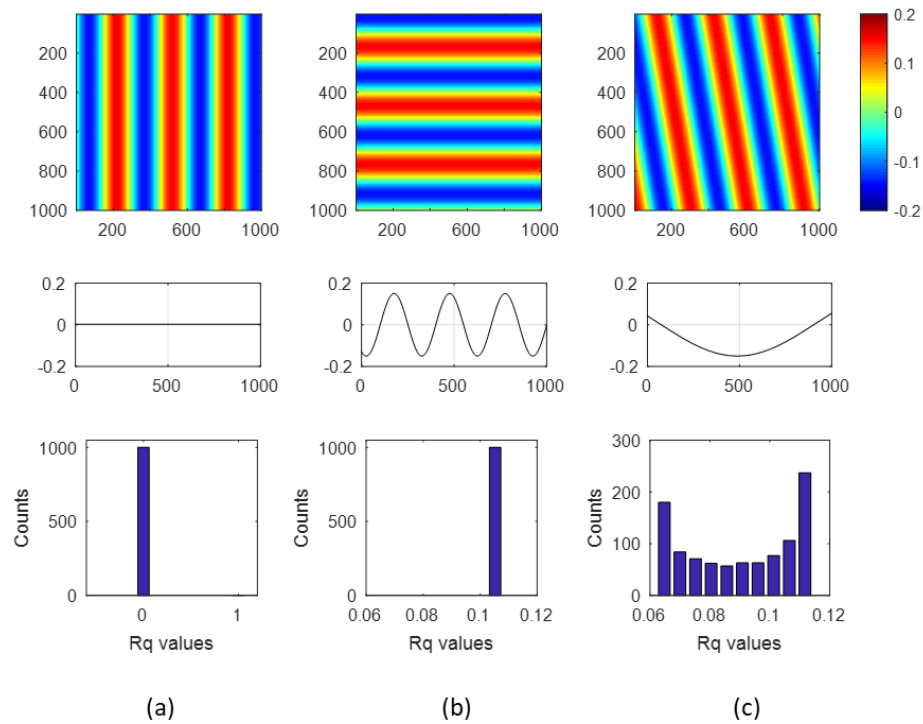


Figure 4-7: a) MATLAB™ generated sinewave surface with wavelength of 300 pixels, a vertical profile, and its Rq histogram, b) same surface when features are horizontal, a vertical profile, and its Rq histogram, d) same surface rotated 10° clockwise, a vertical profile, and its Rq histogram

All the columns at the original orientation have the Rq value equal to zero since the profiles are all along the sinewave, thus the standard deviation of Rq histogram is zero, Figure 4-7(a). When the surface is rotated 90° from its original orientation each column intersects the sinewave at a right angle and all of the profiles are similar, so while the Rq value of the columns is not zero their standard deviation is zero, Figure 4-7(b).

In between these two points at each rotational angle each column is a section of a second periodic feature of the same nature of the periodic structure on the surface, Figure 4-7(c). Figure 4-8(a) depicts the surface with a sinewave feature with the wavelength equal to 300 pixels when rotated 10° clockwise. Figure 4-8(b) shows two randomly selected columns from this surface, as stated above these two columns along with the rest (all 1000 columns) at this angle are parts of another periodic structure which is shown in Figure 4-8(c).

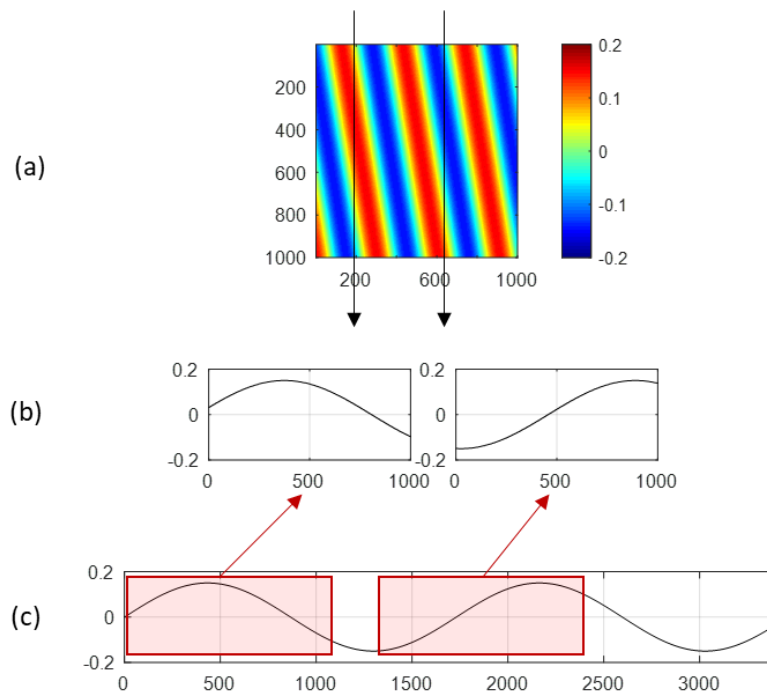


Figure 4-8: a) MATLAB™ generated sinewave surface with wavelength of 300 pixels when rotated 10° clockwise, b) two randomly selected vertical profiles, and c) the two profiles shown on the second periodic structure.

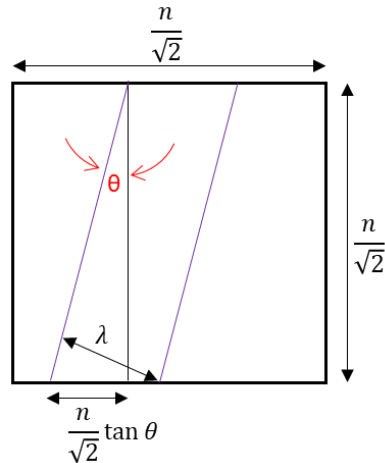


Figure 4-9: Geometrical model of a periodic structure on a surface when it is rotated θ° .

In general, the wavelength of the second periodic structure, λ_θ , is a function of the angle of rotation of the surface, θ , and the wavelength of the periodic structure on the surface, λ . For instance, at the original orientation where all the columns are along the sinewave the wavelength of the second periodic feature is infinity (all straight lines), and when rotated 90° the wavelength of the second periodic structure is equal to the wavelength of the periodic structure on the surface.

Figure 4-9 shows the geometric model of a surface with a periodic structure when rotated θ degrees, only one complete wavelength is demonstrated. From this model the wavelength of the second periodic structure is given in equation 4-6:

$$\lambda_\theta = \frac{\lambda}{\sin \theta} \quad (4-6)$$

And at each rotational angle, θ , the ratio of the length of columns over the second wavelength is given in equation 4-7:

$$\frac{n}{\lambda_\theta} = \frac{n \sin \theta}{\lambda} \quad (4-7)$$

As the surface rotates, for each angle the Rq value of the columns (that are sections of the second periodic structure taken from different positions as shown in Figure 4-8) is calculated, and then the standard deviation of these Rq values is determined. The local maximum and minimum

radii of the standard deviation of Rq histogram polar plot occurs where the range of columns' Rq distribution is maximum and minimum respectively.

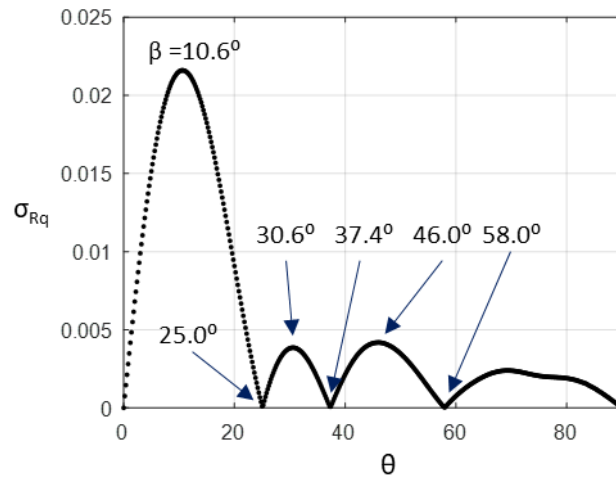


Figure 4-10: The first upper quarter of the polar plot in Figure 4-6 in Cartesian coordinate.

Figure 4-10 depicts the first quarter of the polar plot in Figure 4-6 in Cartesian coordinate, as is seen in this plot there are four maximums and five minimums. The first and last minimums correspond to when the sinewave on the surface is vertical, Figure 4-7(a), and horizontal, Figure 4-7(b), respectively.

To find out when the range of Rq values is maximum and minimum, an iterative approach is taken; in MATLAB a window of variable size is moved across a periodic structure with known wavelength, the Rq value of the portion of the periodic structure inside this moving window is calculated and at the end the standard deviation of these Rq values is calculated. The specific ratio of the window size over the wavelength that leads to the maximum or minimum standard deviations of Rq values is then achieved.

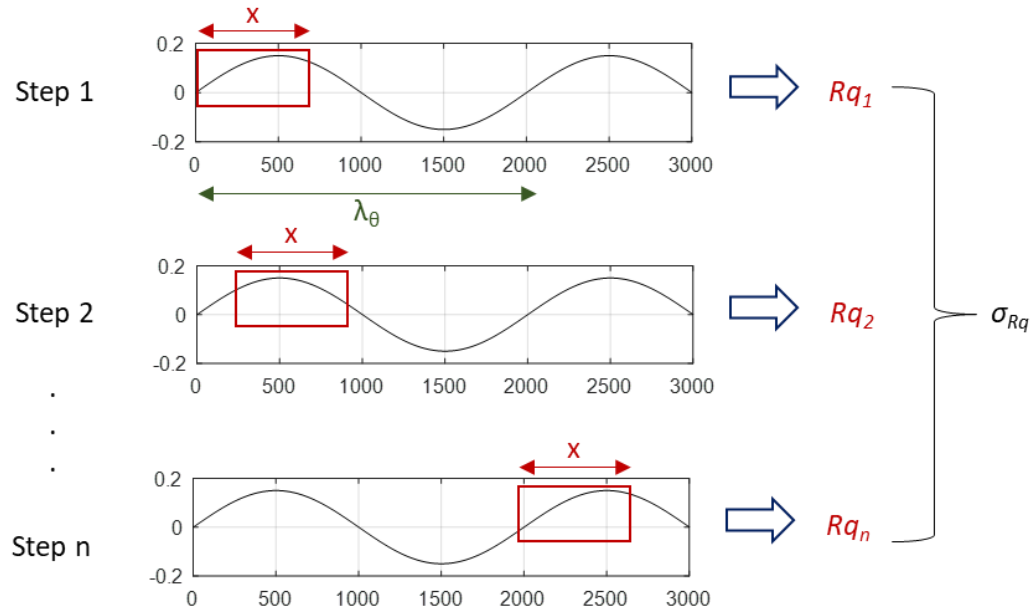


Figure 4-11: Visual representation of the steps involved in finding the length of sections of a periodic structure that has the maximum or minimum range of Rq values

Figure 4-11 gives a visual representation of the steps involved in finding the length of sections of a periodic structure that has the maximum or minimum range of Rq values, first a window of length x is selected from the periodic feature, its Rq value is calculated, in step two the window of size x is moved some number of pixels to the right covering a different section of the periodic feature. At the end the standard deviation of all these Rq values is calculated. Once this cycle is complete the size of the moving window is increased in MATLAB and the procedure again is carried out. The increase in size takes place until the size of the moving window is equal to the length of columns.

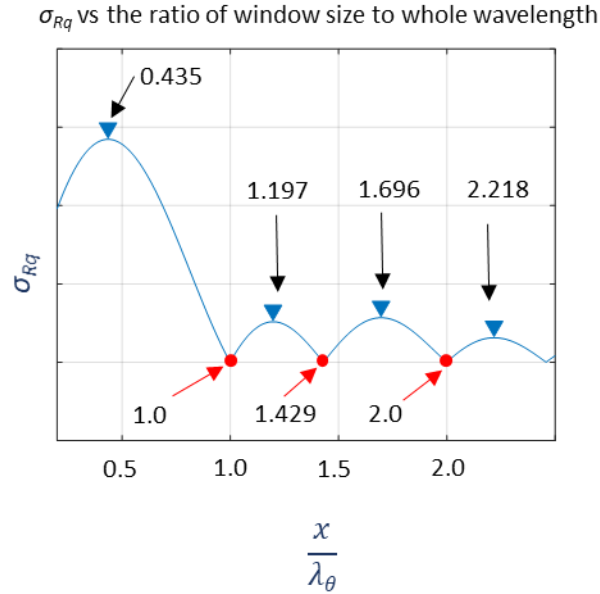


Figure 4-12: Standard deviations of Rq values versus the ratio of the size of the moving window over the wavelength of the second periodic feature for a sinewave structure.

Figure 4-12 depicts the plot of standard deviations of Rq values versus the ratio of the size of the moving window, x , over the wavelength of the second periodic feature for a sinewave structure. The maximum and minimum ratios are shown on the graph.

Based on this graph the first maximum radius of the polar plot occurs when the ratio of the length of the columns, $\frac{n}{\sqrt{2}}$ to the wavelength of the second periodic structure is equal to 0.435, equation 4-8:

$$\frac{n}{\lambda_\theta \sqrt{2}} = 0.435 \quad (4-8)$$

Combining equations 4-6 and 4-8 the wavelength of the sinewave structure on the surface can be estimated with equation 4-9:

$$\lambda_{\text{sinewave}} = \text{round} \left[\frac{n}{0.435 \sqrt{2}} \sin \beta \right] \quad (4-9)$$

Where β is the difference between the angle where the sinewave is vertical and the global maximum of the polar plot, see Figure 4-10.

Knowing the wavelength of the periodic structure and the size of the surface the angles at which the local maximums and minimum happen in the polar plot can be calculated based on equation 4-10:

$$\theta = \sin^{-1}\left(\frac{c\lambda\sqrt{2}}{n}\right) \quad (4-10)$$

Where c is the ratio of the length of the columns over the wavelength of the second periodic structure given in Figure 4-12. For instance, for the surface shown in Figure 4-6 with the wavelength of 300 pixels, the angles of maximum and minimum radii of the polar plot when θ is between zero and 90° are given in Table 4-1, see also Figure 4-10:

Table 4-1: The angles of maximum and minimum radii of the polar plot of Figure 4-6.

c from Figure 4-12	θ from equation 4-10	Local extremes
0.435	10.6	Local maximum
1.0	25.0	Local minimum
1.197	30.5	Local maximum
1.429	37.3	Local minimum
1.696	46.0	Local maximum
2.0	58.0	Local minimum

4.5.1 Other types of periodic features

This method works for other types of periodic features such as sawtooth, step wave, grating, and cusp structure as well. However, the c coefficient to use in equation 4-10 for each type is different and is given in Figure 4-13.

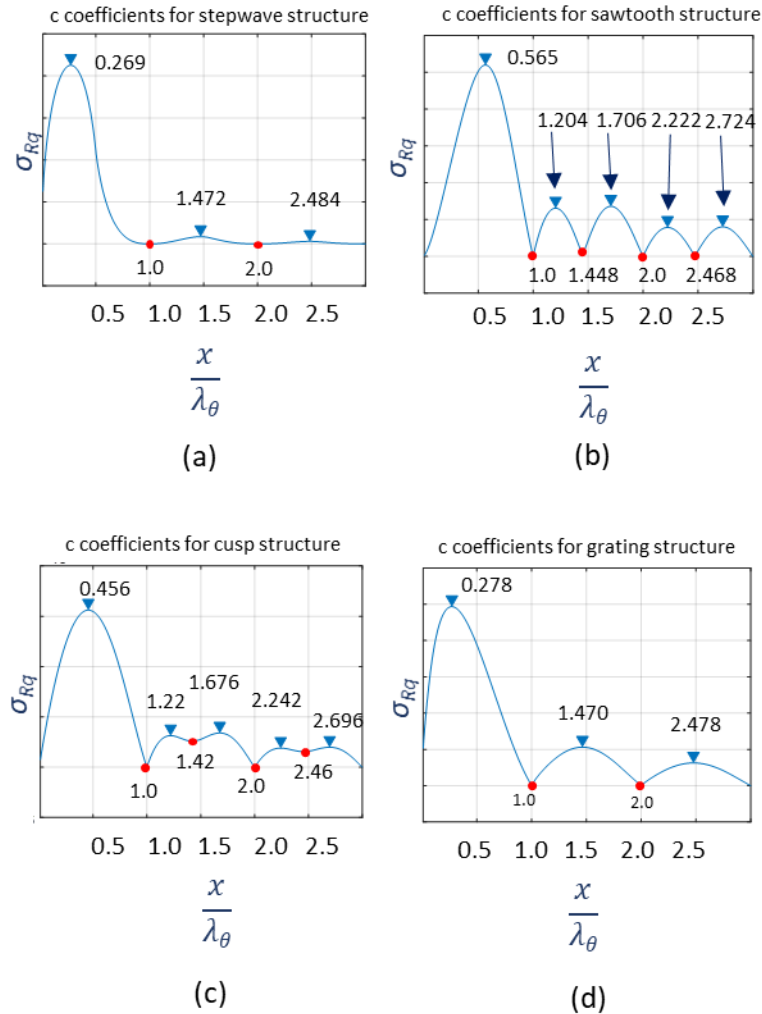


Figure 4-13: Standard deviations of Rq values versus the ratio of the size of the moving window over the wavelength of the second periodic feature for a) step wave structure, b) sawtooth structure, c) cusp structure, and d) grating structure.

It should be noted that the c coefficients shown in Table 4-2 are the first ratio values from Figure 4-13 which correspond to the angle difference between the global minimum, where periodic features are vertical, and the global maximum.

Table 4-2: c coefficients for different types of periodic structures

Type	c coefficient
Sawtooth	0.565
Cusp	0.456
Grating	0.278
Step wave	0.269

Formulas for calculating the wavelength of sawtooth, cusp, grating, and step wave structures are given in equations 4-11, 4-12, 4-13, and 4-14.

$$\lambda_{\text{sawtooth}} = \text{round} \left[\frac{n}{0.565\sqrt{2}} \sin \beta \right] \quad (4-11)$$

$$\lambda_{\text{cusp}} = \text{round} \left[\frac{n}{0.456\sqrt{2}} \sin \beta \right] \quad (4-12)$$

$$\lambda_{\text{grating}} = \text{round} \left[\frac{n}{0.278\sqrt{2}} \sin \beta \right] \quad (4-13)$$

$$\lambda_{\text{stepwave}} = \text{round} \left[\frac{n}{0.269\sqrt{2}} \sin \beta \right] \quad (4-14)$$

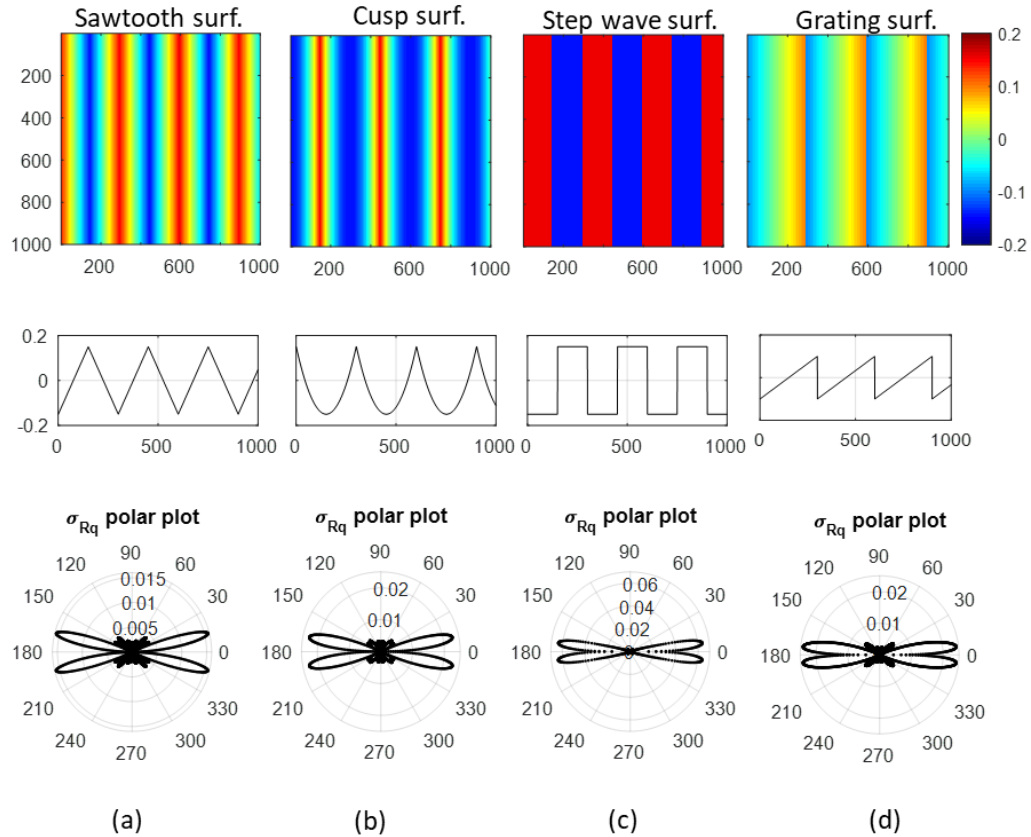


Figure 4-14: Theoretical surfaces with a) sawtooth structure, b) cusp structure, c) step wave structure, d) grating structure, a horizontal profile for each structure, and their σ_{Rq} polar plots.

Figure 4-14 depicts three different periodic structures with wavelength of 300 pixels along with a horizontal profile and their σ_{Rq} polar plot. In all these cases the surface texture directionality with respect to vertical axis, which is 90° , is captured by their polar plots where the first global minimum occurs, i.e. $\theta=0^\circ$.

The difference between each specific type of structure is the angle difference between this global minimum and the global maximum. Based on equation 4-10 this angle for each type shown in Figure 4-14 is as follows:

Table 4-3: Angle difference for σ_{Rq} polar plot of surfaces shown in Figure 4-14.

Type	c coefficient	Angle difference between max. and min. radii
Sawtooth structure	0.565	13.8°
Cusp structure	0.456	11.1°
Grating structure	0.278	7.0°
Step wave structure	0.269	6.5°

4.5.2 Identifying different periodic structures

From the polar plots, it is also possible to find out what type of a periodic structure is present on a surface. In order to do that at the first step is based on equations 4-9, 4-11, 4-12, 4-13, and 4-14 five distinct wavelengths can be assumed for a given polar plot of a surface containing a periodic structure. In the second step a sinewave, a sawtooth, a cusp structure, a grating structure, and a step wave structure with their wavelength equal to the wavelength calculated from equation 4-9 are put on five surfaces, and the angle difference between the first global minimum and maximum radius of the polar plot, β , is compared to the one from the given polar plot, if for any of these structures the β is the same as the one from the given polar plot then the specific type of the structure is identified. If not the second step is repeated but this time for the wavelength calculated based on equation 4-11. This process is repeated until the specific type of the structure is identified.

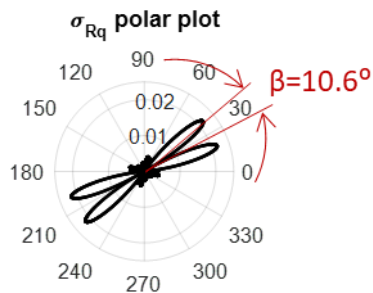
Figure 4-15: σ_{Rq} polar plot for a theoretical surface containing an unknown periodic structure.

Figure 4-15 shows a σ_{Rq} polar plot for a theoretical surface containing an unknown periodic structure. The angle at which the first global minimum radius occurs is equal to 30° meaning that the directionality of the periodic structure with respect to vertical axis is 30° . The angle difference between this global minimum and the maximum radii, β , is equal to 10.6° .

Based on equations 4-9, 4-11, 4-12, 4-13, and 4-14 the five possible wavelengths are as follows:

Table 4-4: Calculated wavelength for different structures based on $\beta=10.6^\circ$.

Sinewave	$\lambda_{\text{sinewave}} = \text{round} \left[\frac{1000}{0.435\sqrt{2}} \sin 10.6 \right] = 299$
Sawtooth structure	$\lambda_{\text{sawtooth}} = \text{round} \left[\frac{1000}{0.565\sqrt{2}} \sin 10.6 \right] = 230$
Cusp structure	$\lambda_{\text{cusp}} = \text{round} \left[\frac{1000}{0.456\sqrt{2}} \sin 10.6 \right] = 285$
Grating structure	$\lambda_{\text{grating}} = \text{round} \left[\frac{1000}{0.278\sqrt{2}} \sin 10.6 \right] = 468$
Step wave structure	$\lambda_{\text{stepwave}} = \text{round} \left[\frac{1000}{0.269\sqrt{2}} \sin 10.6 \right] = 483$

The first step is to put all the possible structures with the wavelength equal to 299 pixels on a theoretical surface and compare the resulting β angle with the β from Figure 4-15. With a sinewave of 299 pixels wavelength the β angle that is produced is equal to the β angle of the polar plot of the unknown structure, this means that the periodic structure is a sinewave and its wavelength is equal to 299 pixels. From Table 4-5 it is clear that no other wavelengths and structures would result in a β equal to 10.6° .

Table 4-5: Angle β for different wavelengths and structures.

λ	β for Sinewave	β for Sawtooth	β for Cusp	β for Step wave	β for Grating
299	10.6°	13.9°	11.2°	6.7°	7.0°
230	8.1°	10.5°	8.6°	5.0°	5.2°
285	10.2°	13.3°	10.8°	6.2°	6.5°
468	16.8°	21.8°	17.6°	10.2°	10.5°
483	17.3°	22.6°	18.0°	10.3°	11.0°

4.5.3 Multi directional periodic features

Structured surfaces such as those that are shown in Figure 4-16 also affect the behavior of the polar plots. In all of these polar plots the angular location of the lobes corresponds to a directionality on the surface. The relationship between these directions and the polar plots, and also how the information of these plots can be related to the wavelength of these repeating structures on the surface has not been completely studied in this work. Therefore, further analysis of these types of surfaces and their polar plots is required to obtain information about the nature of surface features. It is also believed that the presence of irregularities within the structure of the surface would affect the shape of the polar plots, and thus polar plots have a great potential of capturing these irregularities within the structure of the feature that needs to be investigated as well.

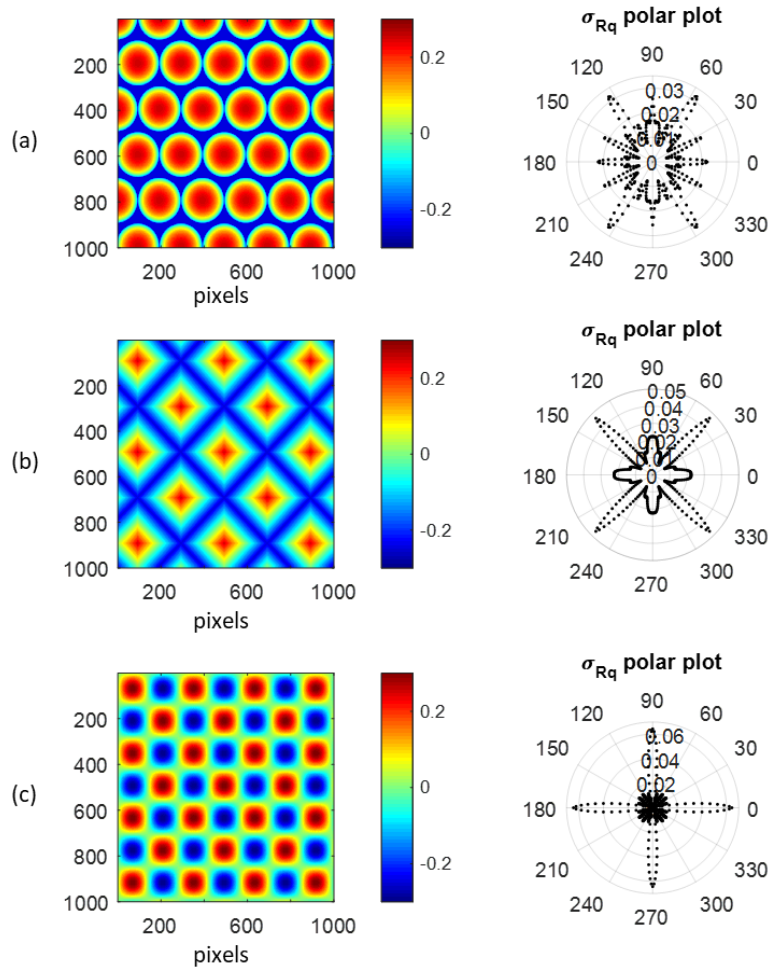


Figure 4-16: Three MATLAB generated highly structured surfaces along with their σ_{Rq} polar plots.

4.5.4 Comparison with the power spectral density, PSD, analysis

The wavelength calculated based on the polar plots is not sensitive to the orientation of the periodic structure on the surface whereas the 1D PSD analysis is; and its results are sensitive to the orientation of the surface texture direction and the direction along which the PSD is being taken.

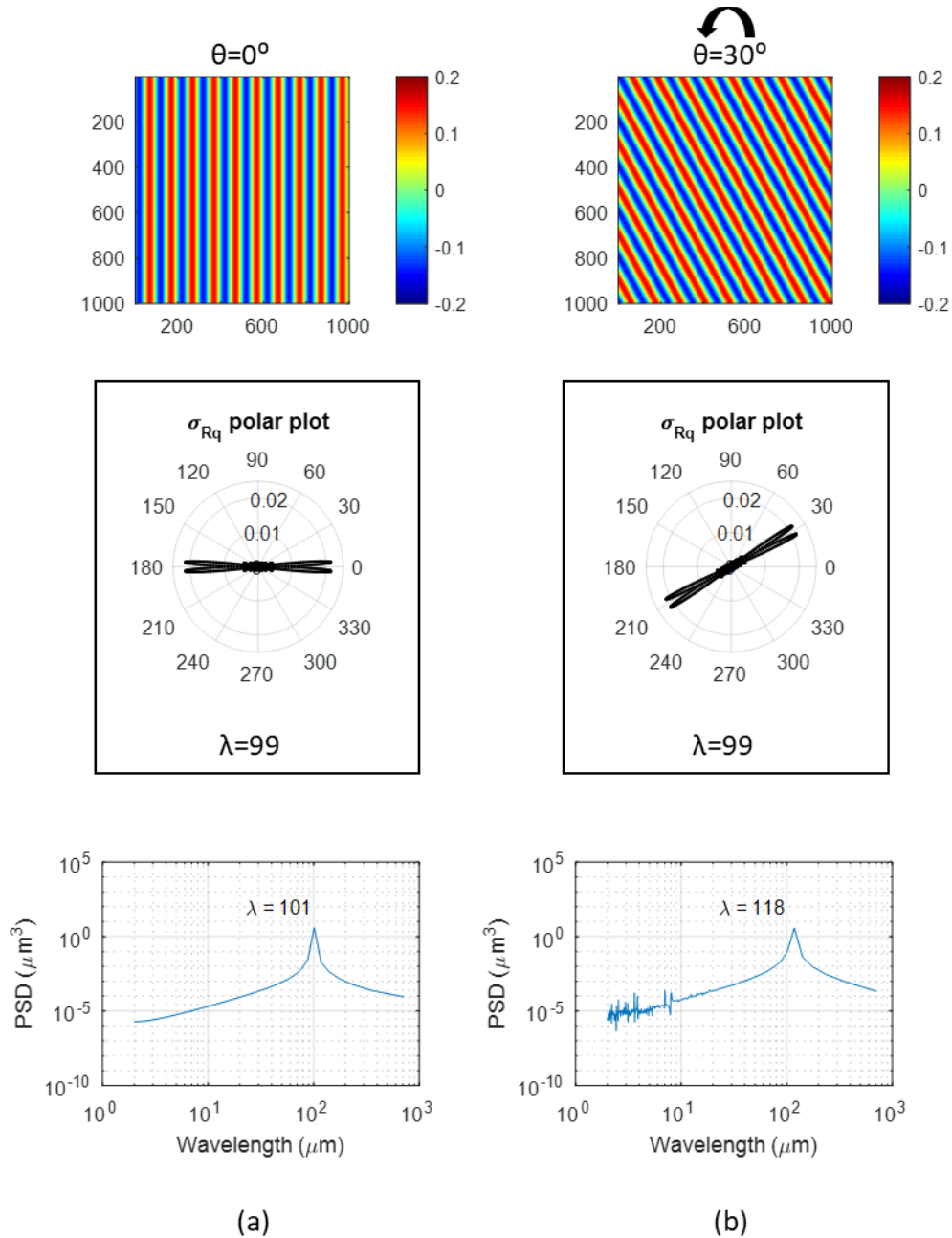


Figure 4-17: A theoretical surface with a sinewave structure of 100 pixels wavelength, when a) unrotated, b) rotated 30° clockwise, and their σ_{Rq} polar plot, and PSD plots.

Figure 4-17(a) shows a theoretical surface containing a sinewave with its wavelength equal to 100 pixels, its σ_{Rq} polar plot, and its PSD when taken along the horizontal axis, from the polar plot and equation 4-9 the wavelength is calculated 99 pixels, and from the PSD analysis, the wavelength is equal to 101 pixels. The same surface is rotated 30° clockwise and is shown in Figure 4-17(b)

with its σ_{Rq} polar plot and PSD plot. In this case, from the polar plot, the wavelength is calculated 99 pixels, but in the PSD analysis in horizontal direction the wavelength is equal to 118 pixels. This shows the advantage of this approach in calculating the wavelength of periodic structures on a surface over the conventional PSD analysis.

4.5.5 Periodicity in real surfaces

All of the above mentioned equations for calculating the wavelength of a periodic structure on the surface rely on the angle difference between the global maximum and minimum radius of the polar plots, β . But it should be noted that the β angle and the equations are meaningful when they are applied to the surfaces with an organized repeating structure, such as a perfect milled surface. The important matter is that this angle, β , may be present in the polar plots of the surfaces that naturally do not have a repetitive pattern, such as a ground surface. However, polar plots are also able to distinguish between the surfaces with organized repeating structures and those that do not have a periodicity on their surface.

The key factor that enables this differentiation is the radius of the polar plot 90° before or after the angular location of the local minimum. This angle corresponds to the orientation where the surface texture is perpendicular to the columns, however, since there is not any organized repeating pattern on the surface the columns Rq values at this orientation are not reasonably close to each other (unlike an organized repeating pattern), and therefore the standard deviation of the columns Rq histogram will not have a minimum value. In other words, the radius of the polar plot 90° before or after the local minimum will not have a near-zero value, whereas this radius in a perfect milled surface is very insignificant, i.e. close to zero. For real milled surfaces the radius of the polar plot at these angles is close to zero, see Figure 4-18(a), whereas this radius for the polar plot of ground surfaces is not a near-zero value as is shown in Figure 4-18(b).

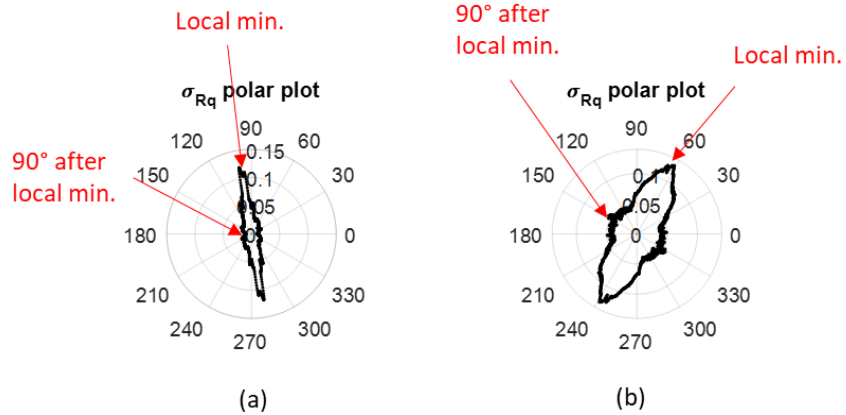


Figure 4-18: σ_{Rq} polar plot of a) the milled surface in Figure 4-25(a) and, b) the ground surface in Figure 4-20(a).

4.6 Analysis of real samples

In this section, the above mentioned capabilities of the polar plots will be studied on real surfaces, and the differences and limitations of the approach for each case will be explained.

4.6.1 Surface roughness of a Gaussian surface

Figure 4-19(a) depicts a polished glass surface measured with Zygo ZeGage coherence scanning interferometer (CSI) 20 \times objective. The field of view of this objective is 417 $\mu\text{m} \times 417 \mu\text{m}$. Skewness of the surface is equal to -2.0, and its kurtosis is equal to 116.91.

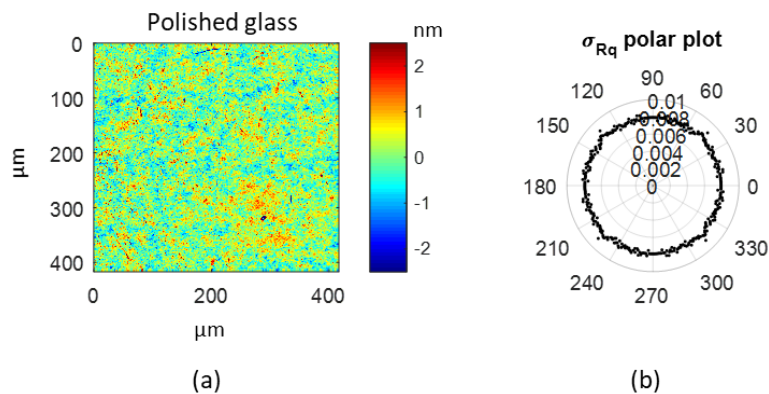


Figure 4-19: a) A polished glass, b) its σ_{Rq} polar plot. The surface is measured with Zygo ZeGage coherence scanning interferometer (20 \times objective, piston, tilt and a 4th order polynomial removed from the measurement).

Figure 4-19(b) shows this surface's standard deviation of Rq histogram polar plot, σ_{Rq} polar plot, the average radius of this polar plot is equal to 84 nm. Using equation 4-5 results in the Sq roughness of the surface which is equal to:

$$r_{\sigma_{Rq}} = \frac{Sq}{\sqrt{\sqrt{2}n}} \rightarrow 0.0084 = \frac{Sq}{\sqrt{\sqrt{2}(1024)}} \rightarrow Sq = 0.56nm$$

And the roughness of the surface calculated with the instrument's software is equal to 0.57 nm. The difference between the Sq roughness calculated via σ_{Rq} polar plot, and the value calculated by the software is less than 1%. This difference could be due to the fact that the polar plot analyzes the smaller rectangle superimposed on the original surface whose dimensions are $\frac{n}{\sqrt{2}}$, whereas the software takes into account the whole $n \times n$ surface. Also, the skewness and kurtosis of the surface that is being analyzed is not equal to zero and three, and therefore these differences induce error on the calculated Sq of the surface via equation 4-5.

The isotropic nature of the polished glass surface is captured by its Str value equal to 0.88, which is supported by the circular shape of its polar plot. The nominally circular shape of the polar plots indicate a lack of any directionality, and thus isotropic nature of the surface.

4.6.2 Isotropy and directionality

Figure 4-20(a) depicts a ground aluminum surface measured with Zygo ZeGage coherence scanning interferometer (CSI) 20× objective with $417 \mu\text{m} \times 417 \mu\text{m}$ field of view. The Str value of this surface, calculated by the instrument's software, is equal to 0.03 which shows a strong anisotropic nature of the surface, and the Std value of the surface that indicates the major directionality of the surface with respect to vertical axis is equal to 64.9° . These properties are also captured by the surface's σ_{Rq} polar plot, the anisotropic nature of the surface is captured by the lobes on the polar plot, i.e. deviations from the nominally circular shape. If the rotational increment used in creating the polar plot is sufficiently small, as is equal to 0.2° in this case, there will be a

local minimum near the apex of the lobe, the angle at which this local minimum occurs is the angle enclosed between the major directionality on the surface and the vertical axis, i.e. equivalent to the Std value of the surface. For this surface this local minimum happens at $\theta=64.2^\circ$. The difference between this value and the Std value from ISO 25178-2 is less than 1.2%; one reason of this difference could be that the polar plot analyzes the smaller rectangle superimposed on the original surface whose dimensions are $\frac{n}{\sqrt{2}}$, whereas the software takes into account the whole $n \times n$ surface.

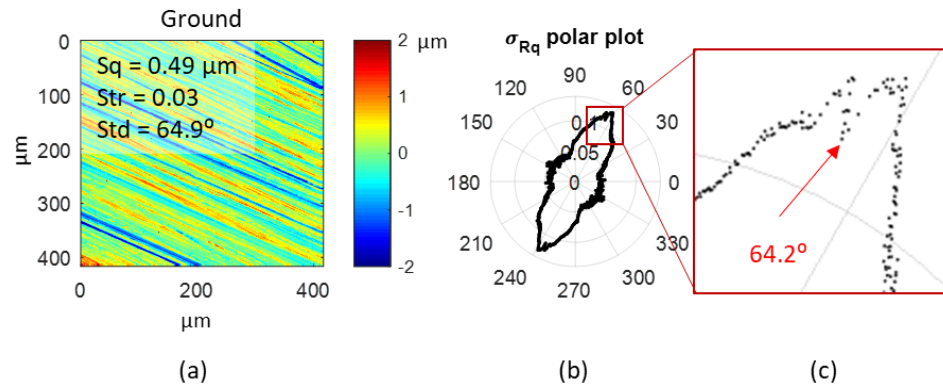


Figure 4-20: a) An Aluminum ground surface, b) its σ_{Rq} polar plot, and c) the zoomed in region of the polar plot around the lobe. The surface is measured with Zygo ZeGage coherence scanning interferometer (20 \times objective, piston, tilt and a 4th order polynomial removed from the measurement).

In Figure 4-20(b) the global maximum occurs at $\theta=61.4^\circ$, and the local minimum at $\theta=64.2^\circ$, the difference between these angles is equal to 2.8° , i.e. $\beta=2.8^\circ$. Using equation 4-9 (that assumes a sinewave structure) to calculate the wavelength of the structure will result in the wavelength equal to 81 pixels:

$$\lambda_{\text{sinewave}} = \text{round} \left[\frac{1024}{0.435\sqrt{2}} \sin 2.8 \right] = 81 \text{ pixels}$$

However, as was mentioned above the radius of the polar plot 90° after the angular location of the local minimum (which is not a near-zero value) indicates that this surface does not have an organized repeating pattern, and thus the calculated wavelength of the periodic structure is meaningless, a fact supported by the PSD analysis of the surface taken perpendicular to the surface

texture direction, see Figure 4-21. In this PSD plot there is no significant peak visible related to the dominant periodic structure on the surface.

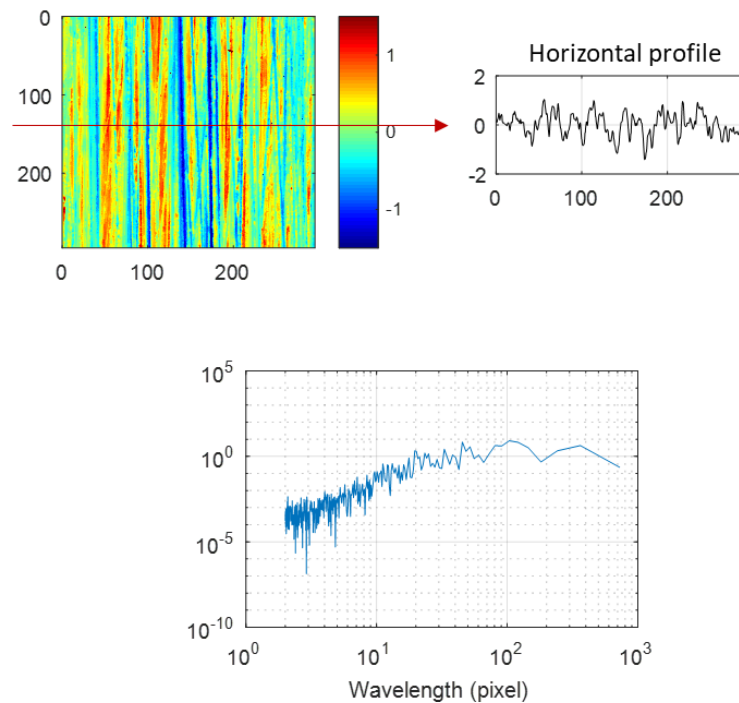


Figure 4-21: Superimposed rectangle area on the initial surface when rotated 64.2° clockwise along with the PSD plot and a random horizontal profile from the surface.

The same surface after it is vibrationally finished is shown in Figure 4-22(a). From the surface's height map it is clear that there is no directionality left on the surface, a fact supported by the surface's high Str value equal to 0.91. This lack of directionality, i.e. isotropic nature of the surface is also reflected on the polar plot where lobes are not present anymore, and the shape of the polar plot is close to a circular shape, see Figure 4-22(b). For this surface, since the distribution of surface height values is not a normal distribution with skewness and kurtosis equal to zero and three respectively equation 4-5 cannot be used to calculate the Sq roughness of the surface.

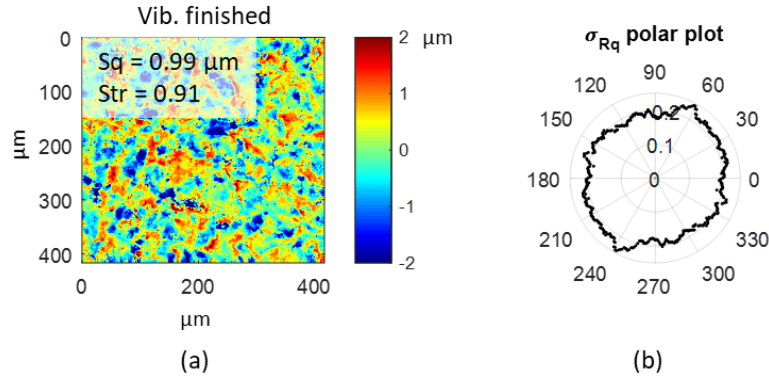
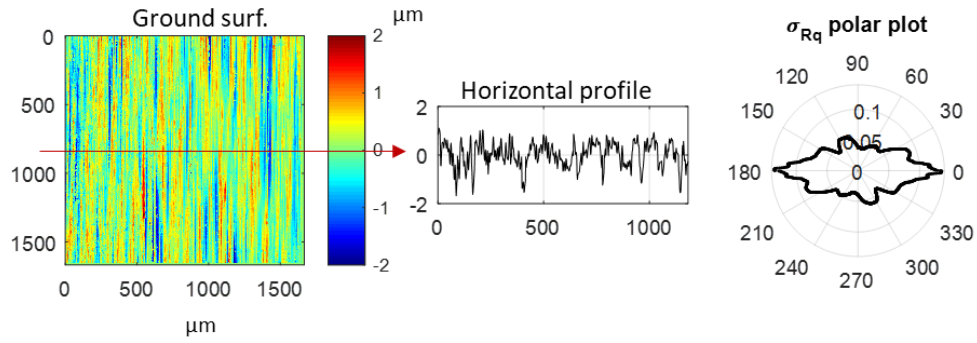
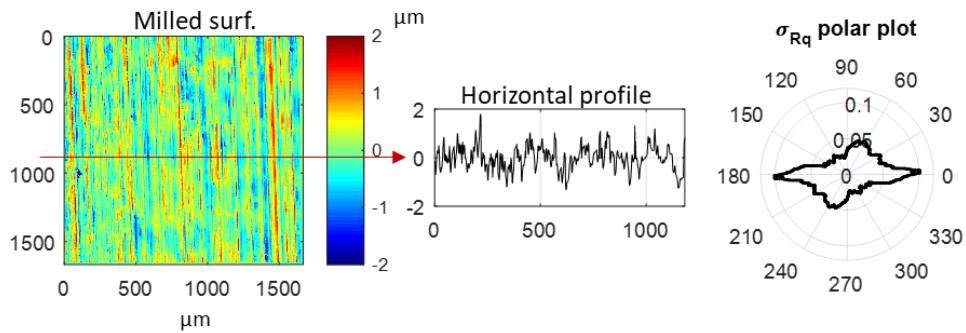


Figure 4-22: a) Vibrationally finished aluminum surface, and b) its σ_{Rq} polar plot. The surface is measured with Zygo ZeGage coherence scanning interferometer (20× objective, piston, tilt and a 4th order polynomial removed from the measurement).

Figure 4-23(a), and (b) depict a steel ground surface, and a steel milled surface along with their random horizontal profiles and their σ_{Rq} polar plots. The global maximum in both polar plots indicates the major surface texture directionality with respect to the vertical axis. In both of these polar plots there is no local minimum in the lobe region, and also there is no near-zero value in the plots. This indicates that both of the surfaces lack a well-organized periodic structure, which is supported by their horizontal profiles. From their random horizontal profiles there is no visible well-organized periodic structure. This behavior of the surface profile is expected for the ground surface since a ground surface naturally does not have a periodic structure, however, for the milled surface this behavior raises the concern that the tool might be worn, or the overall quality of the machining of the part has not been good.

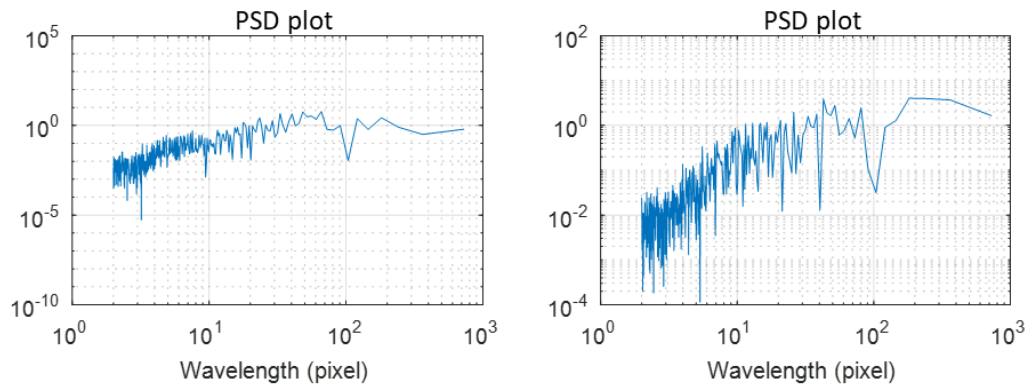


(a)



(b)

Figure 4-23: a) A ground steel surface, and b) a milled steel surface along with their random horizontal profiles and their σ_{Rq} polar plots.



(a)

(b)

Figure 4-24: PSD plot of the surface shown in a) Figure 4-23(a), and b) Figure 4-23(b).

Figure 4-24 depicts the PSD analysis of the two surfaces taken perpendicular to the surface texture direction, clearly there is no dominant peak in either of them which supports the lack of a periodic structure on the surfaces.

4.6.3 Surface periodic structure

Figure 4-25(a) depicts a milled steel surface that is measured with Zygo ZeGage coherence scanning interferometer (CSI) 20× objective with $417 \mu\text{m} \times 417 \mu\text{m}$ field of view. The anisotropic nature of this surface is clearly visible from a glance of its height map, the *Str* value of the surface equal to 0.02 also indicates this property. The angle enclosed between the tooling marks and the vertical axis based on *Std* parameter is equal to 97.0° . As it was mentioned earlier this directionality is also captured by the local minimum radius of the σ_{Rq} polar plot in the lobe region in the upper half of the polar plot. This minimum radius of the polar plot happens at $\theta=98.3^\circ$. The 1.35% difference between this value and the *Std* value could be due to the fact that the tooling marks are curved on this milled surface and this difference in the real surface and the theoretical model contributes to the difference between *Std* value and the angle of the local minimum radius of the polar plot. The rotational increment for generating the polar plots is 0.2° .

It should be noted that in the case of real surfaces, such as this milled surface, there are notable differences between them and the theoretical models of periodic structures on the surface; such as the curvature of the tooling marks, and the fact that it is very unlikely that a profile taken along the length of a valley or peak is perfectly smooth. Nonetheless, the local minimum radius of the polar plot still occurs when tooling marks are vertical, and the angle between this local minimum and the maximum radius of the polar plot, β , can be used to estimate the wavelength of the periodic feature on the surface.

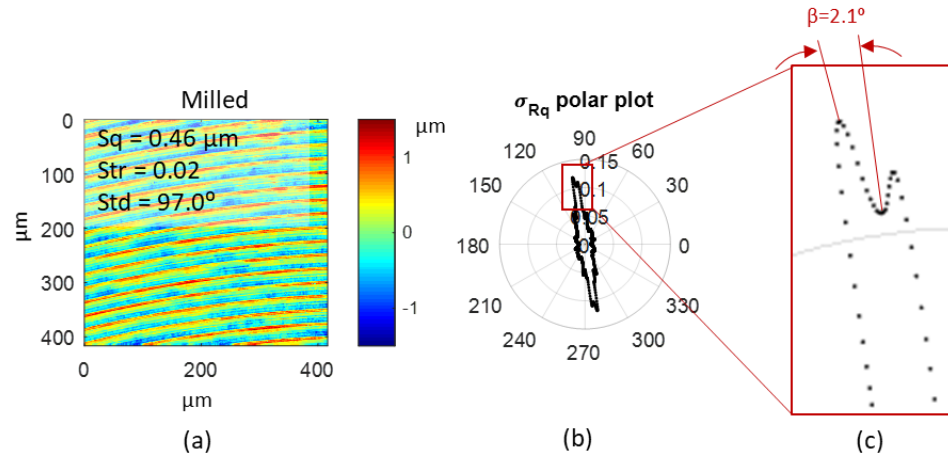


Figure 4-25: a) A Steel milled surface, b) its σ_{Rq} polar plot, and c) the zoomed in region of the polar plot around the lobe. The surface is measured with Zygo ZeGage coherence scanning interferometer (20× objective, piston, tilt and a 4th order polynomial removed from the measurement).

In order to calculate the wavelength of the periodic structure, first the behavior of the periodic structure of the milled surfaces in general should be assumed. Figure 4-26(a) shows the area inside the superimposed rectangle on the initial surface when the surface is rotated 98.3° clockwise. At this angle a horizontal profile is shown in Figure 4-26(b), from this profile if the nature of the periodic structure is assumed to follow a sinewave, then the wavelength of the structure can be calculated from equation 4-9.

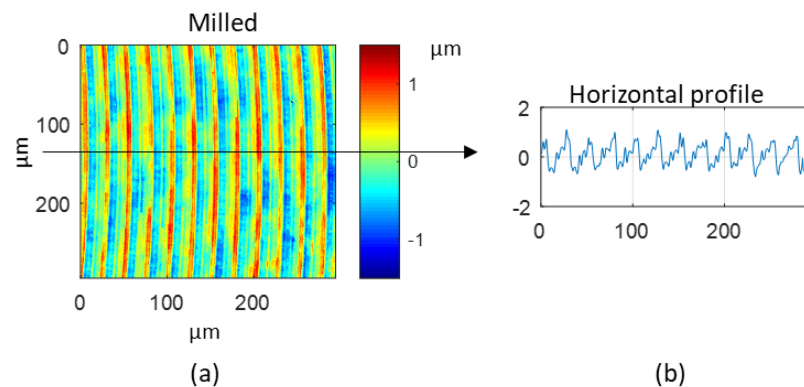


Figure 4-26: a) Inside the superimposed rectangle when the milled surface is rotated 98.3°, and b) a horizontal profile of the surface.

$$\lambda_{\text{sinewave}} = \text{round} \left[\frac{1024}{0.435\sqrt{2}} \sin 2.1 \right] = 61 \text{ pixels}$$

Considering the pixel resolution of the 20× objective which is 0.40 μm the wavelength of the periodic feature on the surface is calculated equal to 24.4 μm . If the nature of the periodic structure is assumed to follow a sawtooth pattern, then its wavelength based on equation 4-11 will be equal to 23.3 μm ; and if it is assumed to simulate a cusp pattern then the wavelength via equation 4-12 is calculated equal to 23.7 μm . Clearly, the profile shown in Figure 4-26(b) does not behave as a step wave or grating structure, and therefore the wavelength equations for a step wave and grating feature should not be used.

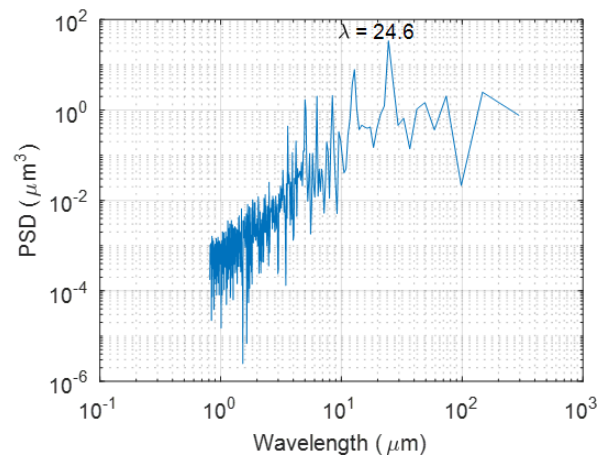


Figure 4-27: 1D horizontal PSD when the tooling marks are oriented to be vertical.

Power spectral analysis, PSD, of the surface in the horizontal direction when the tooling marks are oriented to be vertical is equal to 24.6 μm .

Figure 4-28(a) depicts a reamed steel surface that is measured with Zygo ZeGage coherence scanning interferometer (CSI) 5× objective with 1.6 mm \times 1.6 mm field of view, after its form and waviness is removed. The anisotropic nature of the surface is visible from the tooling marks of its height map, a fact supported by the surface texture aspect ratio, *Str*, equal to 0.02. This property is also captured by the lobes of the polar plot. The surface texture direction value, *Std*, of this surface is equal to 179.5°, and the local minimum in the upper half of the polar plot happens at $\theta=179.4^\circ$. The difference between these two values is 0.05% which indicates the great capability of the polar

plots to capture the directionality of the surface features. The rotational increment for generating the polar plots is 0.2° .

The periodic structure of the surface is obvious from a glance of its height map, a fact supported by the shape of its σ_{Rq} polar plot. In this polar plot there is an angle difference between the local maximum and minimum, and thus the surface may have a well-organized periodic structure. To check if the surface has this type of periodic structure the radius of the polar plot 90° after the angular location of the local minimum is examined. As it is clear from the polar plot shown in Figure 4-28(b) at this angle the radius of the polar plot has a near-zero value, and thus it confirms that there is a periodic structure on the surface.

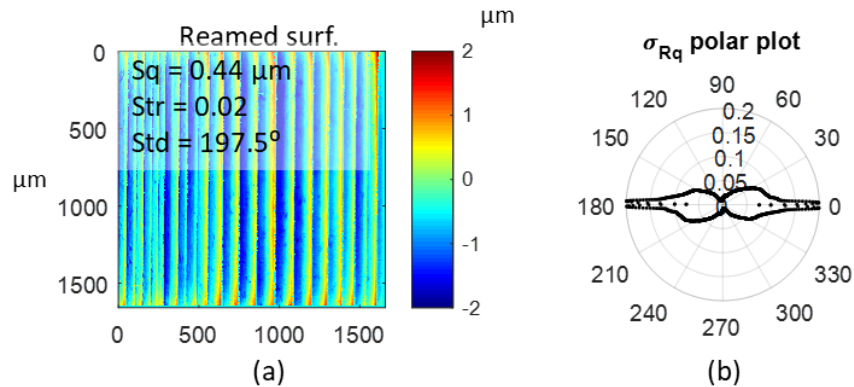


Figure 4-28 a) A steel reamed surface and, b) its σ_{Rq} polar plot. The surface is measured with Zygo ZeGage coherence scanning interferometer ($5\times$ objective, piston, tilt and a 4th order polynomial removed from the measurement).

From this polar plot β is equal to 1.4° , assuming the behavior of the periodic structure follows a grating pattern equation 4-13 can be used to estimate the wavelength of it.

$$\lambda_{grating} = \text{round} \left[\frac{1024}{0.278\sqrt{2}} \sin 1.4 \right] = 64 \text{ pixels}$$

Considering the pixel resolution of the $5\times$ objective equal to $1.6 \mu\text{m}$ the wavelength is equal to $103 \mu\text{m}$.

Figure 4-29 shows the area inside the superimposed rectangle on the initial surface, along with a random horizontal profile. The periodic structure of the surface is clearly visible from the

horizontal profile. The PSD analysis of the surface taken perpendicular to the surface texture has a dominant peak, and the wavelength from 1D PSD analysis is equal to 107 μm . The difference between the wavelength calculated from polar plot and the one from PSD analysis is because of some irregularities in the periodic structure on the surface, i.e. deviation from the theoretical model.

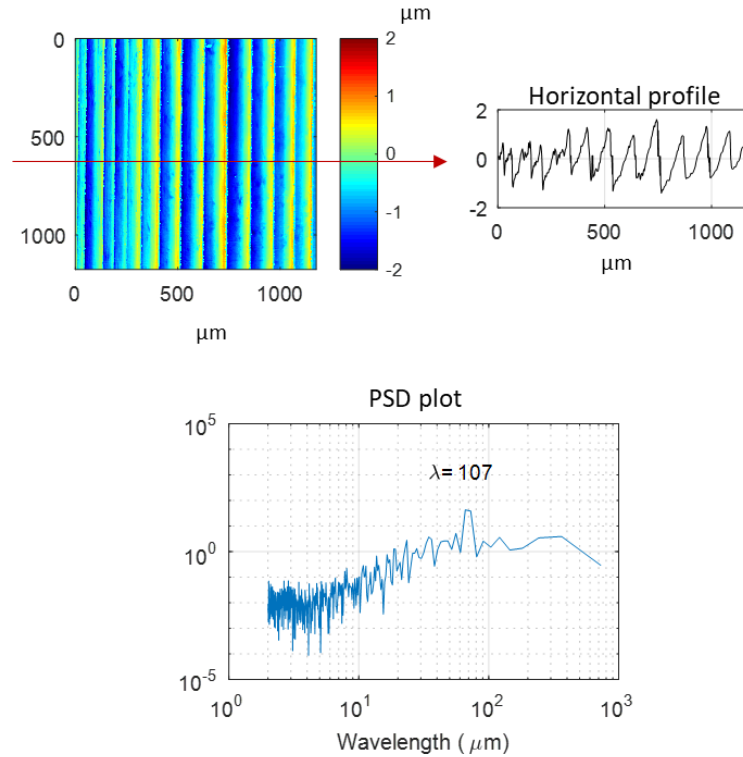


Figure 4-29: Superimposed rectangle area on the initial surface when rotated 0.4° clockwise along with the PSD plot and a random horizontal profile from the surface.

Figure 4-30(a), (b), (c), and (d) depict four AFM samples provided by the Manufacturing Metrology Team at the University of Nottingham, piston, tilt, and a 4th order polynomial are removed from the height maps of 384×384 pixels size. The resolution of rotation used in this approach to create surfaces' σ_{Rq} polar plots is 0.15° .

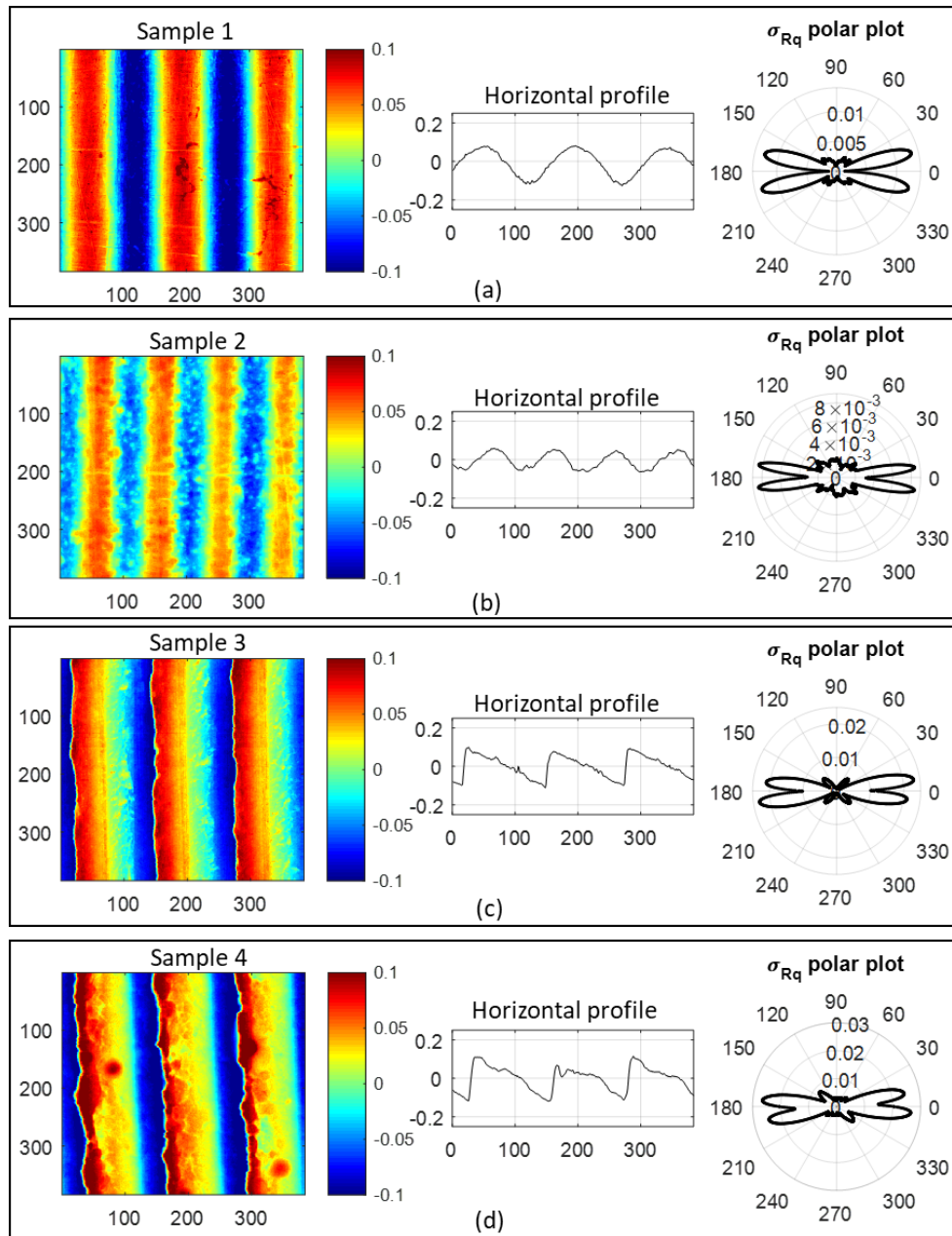


Figure 4-30: AFM samples after piston, tilt, and a 4th order polynomial is removed from their height map, a random horizontal profile, and their σ_{Rq} polar plots.

The angular location of the local minimum in these polar plots corresponds to the angle enclosed between the surface texture and the vertical axis. For each surface a random horizontal profile perpendicular to the periodic structure of the surface is shown in Figure 4-30. From the height map of the samples and their horizontal profiles shown in Figure 4-30(a), and (b) it is clear that they both follow a sinewave structure pattern, and therefore equation 4-9 should be used to

estimate the wavelength of the surface periodic structure. The periodic structures on surfaces shown in Figure 4-30(c), and (d) clearly does not follow a sinewave pattern, nor a cusp one. It also does not comply with the modeled sawtooth pattern that was discussed in section 4.5.1. The closest pattern that these surfaces' features follow can be assumed to be the grating periodic structure.

Table 4-6: Estimated wavelengths from polar plots and the PSD analysis and the associated error.

	β	λ (pixels)		Error %
		Polar plots	PSD	
Sample 1	12.75°	$\lambda_{\text{sinewave}} = \text{round} \left[\frac{384}{0.435\sqrt{2}} \sin 12.75 \right] = 138$	136	1.5
Sample 2	8.0°	$\lambda_{\text{sinewave}} = \text{round} \left[\frac{384}{0.435\sqrt{2}} \sin 8.0 \right] = 87$	91	4.4
Sample 3	7.8°	$\lambda_{\text{grating}} = \text{round} \left[\frac{384}{0.278\sqrt{2}} \sin 7.8 \right] = 133$	136	2.2
Sample 4	8.1°	$\lambda_{\text{grating}} = \text{round} \left[\frac{384}{0.278\sqrt{2}} \sin 8.1 \right] = 138$	136	1.5

The estimation of the wavelength of the periodic structure on each of the samples is summarized in Table 4-6, the calculated wavelength for the sample one has 1.5% error when compared with PSD analysis, and the calculated wavelength from polar plot has 4.4% from the one calculated via PSD analysis for sample two. For these samples although they have a sinewave structure present on their surface, but the structure is not perfect and some irregularities are present as it can be seen from their random profile, this deviation of the perfect sinewave model induces some error on the estimated wavelength. In samples three and four the repeating structure follows a grating type pattern, and samples have some irregularities, thus the estimated wavelength of the periodic structure on their surface has some errors when compared with the result of the PSD analysis.

4.7 Summary

This chapter detailed the capabilities of polar plots in capturing surface characteristics, such as surface directionality, surface isotropy/anisotropy, periodicity of repeating structures on the surface, and in the case of a surface with a Gaussian distribution of heights, the surface roughness Sq .

The analytical relationship between the Sq roughness of a surface with a Gaussian distribution of heights, and the radius of the σ_{Rq} polar plot was established using the *Chi* distribution properties. However, this relationship is limited to the surfaces with their height values following an ideal Gaussian distribution with its skewness equal to zero, and its kurtosis equal to three.

Information about the surface texture aspect ratio, Str , which is an indicator of the isotropy of a surface can also be gained by the overall shape of the surface's polar plots. Nominally circular shape of the polar plots is a sign of isotropic nature of the surface, whereas presence of lobes on the polar plots shows the anisotropic nature of the surface, and is an indicator of the directionality of the major surface texture. The angle of the polar plots at which the lobes or local minimums near them occur corresponds to the angle enclosed between the vertical axis and the surface texture, and it is equivalent of the surface texture direction parameter, Std with this difference that Std shows the directionality of the major surface texture whereas polar plots can show the directionality of all of directional features on the surface. It should be noted that the indeterministic nature of a ground surface makes the formulization of the angle of maximum radius of the polar plot impossible.

It was shown that the wavelength of a periodic structure can also be calculated from the angle difference between the local minimum and the global maximum of the σ_{Rq} polar plot, β . The advantage of estimating the wavelength of a periodic structure on the surface with this approach over the power spectral density analysis, PSD, is that it is insensitive to the surface orientation, whereas the 1D PSD analysis should be done in the direction perpendicular to the surface texture in order to result in the accurate answer. Also, from the information provided by the polar plots

identifying the specific type of the periodic structure on the surface was made possible. Table 4-7 summarizes the key features to consider when analyzing surface's polar plots.

Table 4-7: Polar plot's features, and their ISO 25178-2 equivalent parameters.

Feature	r_{max}	r_{min}	Local r_{min}	Angle between r_{max} and local r_{min}	# of peaks	ISO 25178-2 Equivalent
Surface Sq (Gaussian dist. of heights)						
Isotropy, directionality						<i>Str, Std</i>
Periodicity						PSD

CHAPTER 5: SINGLE FEATURE CHARACTERIZATION

5.1 Introduction

The presence of a single circular or a linear feature on the surface will affect the shape of polar plots. This effect can be used to not only detect the presence of the singular features, but also to back calculate its geometrical properties such as diameter and depth of the circular feature; and the depth, length, and width of the linear feature.

This chapter details the effect of a single feature on the polar plots and explains how to use the wealth of information contained within the polar plots to obtain information about the surface features without the need for segmentation or pattern recognition techniques.

The statistical parameter of columns used in this chapter is their Rq , and Rsk values, and the rotational increment in creating polar plots is 1° unless otherwise mentioned.

5.2 Single circular feature

When a single circular feature is present on the surface, the columns containing the feature have higher Rq values than those feature-free columns. This increases the range of Rq values in the Rq histogram when compared to a surface without any feature. These higher Rq values are found in the bins to the right side of the mean on the Rq histogram, and thus they increase the standard deviation of the Rq histogram.

As the surface rotates around its center, and due to the symmetry of the circular feature, the number of affected columns by it, is equal to the diameter of the circular feature and is a fixed number, see Figure 5-1. As a result, the standard deviation of the Rq histogram remains constant and consequently the shape of the polar plot remains circular, but will increase in diameter.

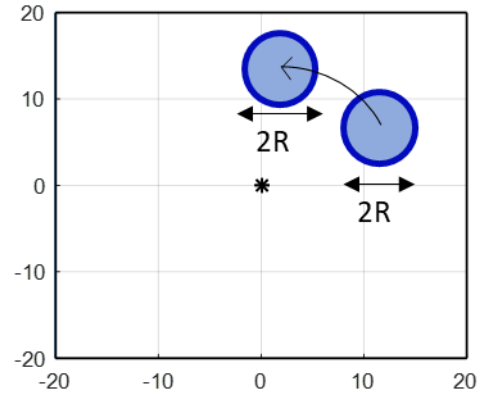


Figure 5-1: Schematically depicts a circular feature during rotation.

Figure 5-2(a) depicts a theoretical surface with Gaussian distribution of heights; this surface does not contain any kind of features so the radius of the standard deviation of Rq histogram polar plot can be found out from equation 4-5. Figure 5-2(b) and (c) are the surface's Rq histogram and its σ_{Rq} polar plot. The same surface when a negative circular feature with 100 pixels in diameter and 0.1 μm in depth is present is shown in Figure 5-2(d), higher Rq values are visible in the Rq histogram, Figure 5-2(e), and the increase in the radius of the polar plot is shown in Figure 5-2(f).

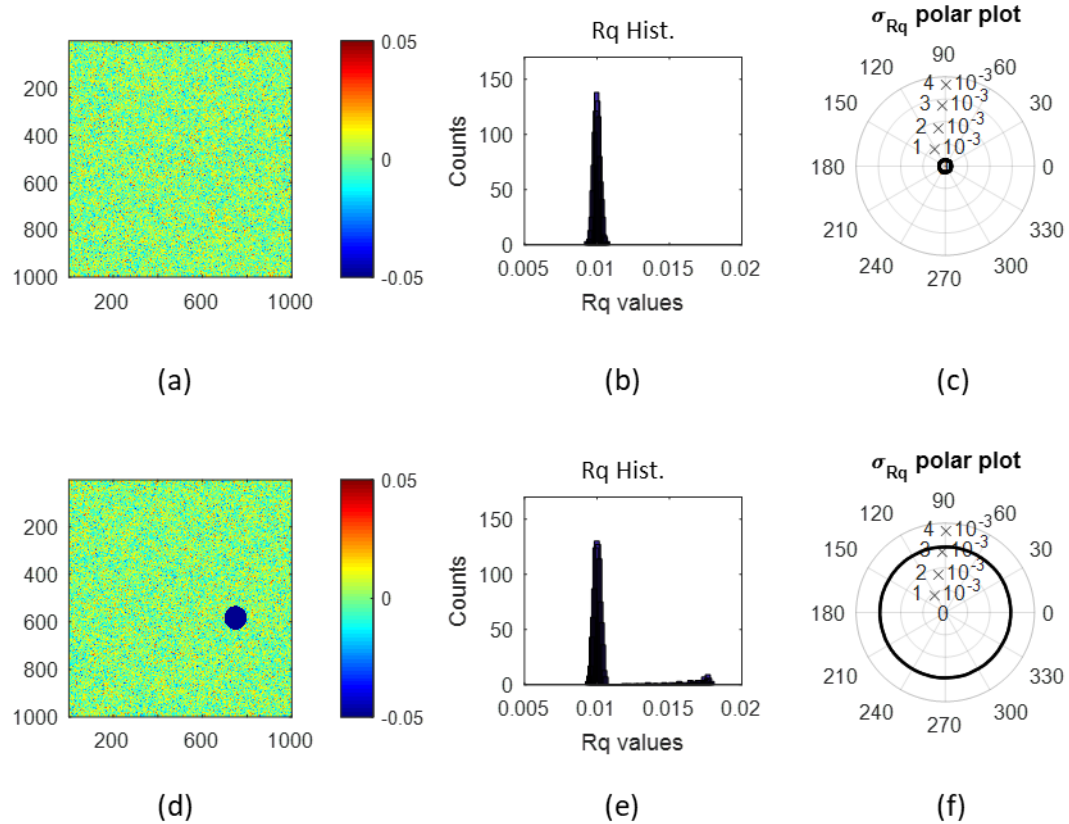


Figure 5-2: a) MATLAB generated surface with Gaussian distribution of heights, b) its Rq histogram, c) its σ_{Rq} polar plot, d) the same surface with a negative circular feature of 100 pixels diameter, e) its Rq histogram, and f) its σ_{Rq} polar plot.

This constant increase in radius when compared to the radius of a defect free surface is an indicator of the existence of a circular feature on the surface with a Gaussian distribution of heights.

5.2.1 Feature below or above the surface

The nature of this circular feature, that is whether it is on the surface (positive) or below it (negative), cannot be identified with the σ_{Rq} polar plot because the Rq and standard deviation are both squared terms, and are always positive values. Figure 5-3(a) shows a surface with a negative circular feature and its σ_{Rq} polar plot, the same surface when the feature is made positive and its σ_{Rq} polar plot is shown in Figure 5-3(b). For both of these surfaces their σ_{Rq} polar plots are similar.

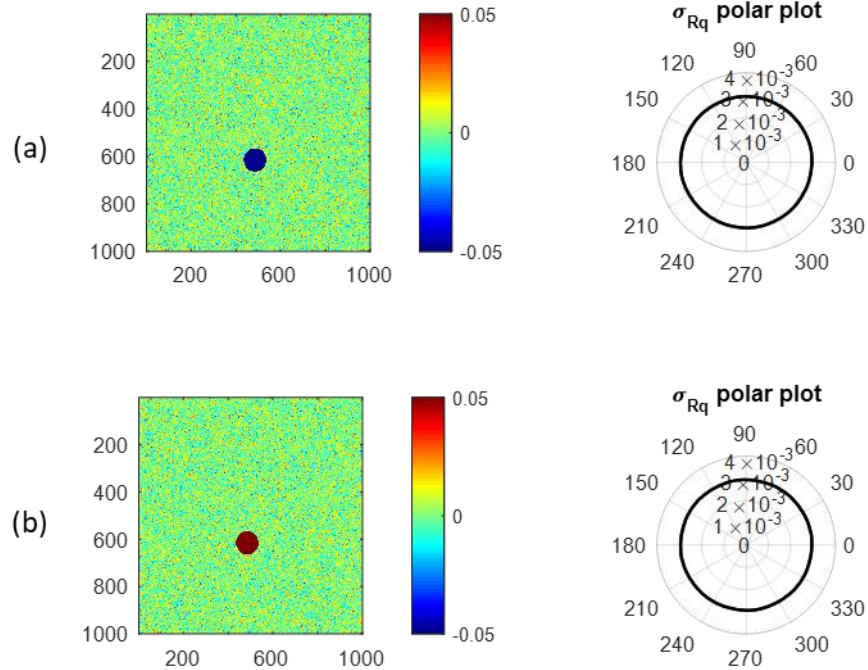


Figure 5-3: MATLAB generated surface with Gaussian distribution of heights with a) a negative circular feature, and b) a positive circular feature and their σ_{Rq} polar plots.

However, in order to determine if the circular feature is positive, i.e. on the surface or negative, i.e. below the surface the third moment of data could be used, i.e. skewness. Since this is a cubic term, it is sensitive to the sign of the magnitude of the feature, and therefore by calculating the Rsk of the columns and then the skewness of the resultant Rsk distribution it is possible to determine whether the feature is positive or negative when compared to the skewness of Rsk histogram polar plot of a defect free sample.

When the feature is negative, the columns containing it have negative skewness values, Rsk , and thus are found to the bins left side of the mean value of the skewness histogram, Figure 5-4(a), and consequently the skewness of this histogram is negative. Similarly, when the feature is positive the Rsk value of the columns containing the feature is positive, and are found to the bins right side of the mean value of the Rsk histogram, see Figure 5-4(b), and thus the skewness value of this histogram is positive.

The skewness of Rsk histogram polar plot of two surfaces with Gaussian distribution of heights containing a circular feature is shown in Figure 5-4(c). The skewness of Rsk histogram polar plot of the surface with the negative feature falls inside the radius of the defect free skewness of Rsk histogram polar plot because of its negative value, and similarly the skewness of Rsk histogram polar plot of the surface with the positive feature lies outside of the radius of the defect free skewness of Rsk histogram polar plot.

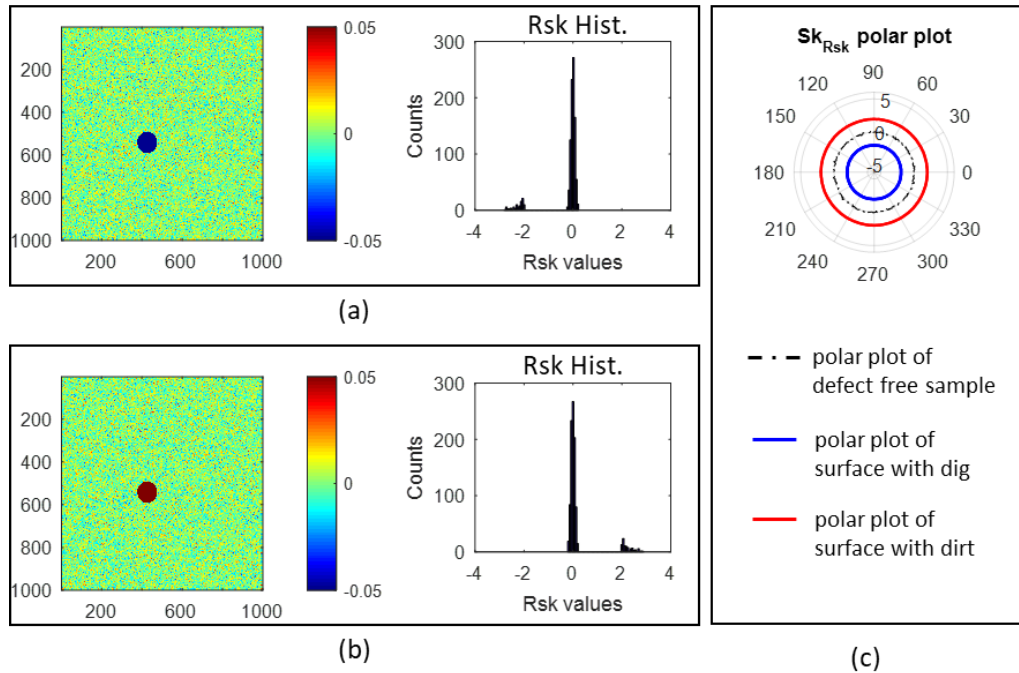


Figure 5-4: a) MATLAB generated surface with a Gaussian distribution of heights and a negative circular feature, 100 pixels diameter, and its Rsk histogram, b) the same surface when the feature is made positive and its Rsk histogram, and c) the skewness of Rsk histogram for both surfaces and a defect free surface.

5.2.2 Estimation of diameter and depth

When the circular feature is sufficiently large or deep, it is possible to estimate its diameter and depth from analysis of columns' Rq histogram without the need for feature recognition algorithms. In order to do this, all the columns that are affected by the feature should be identified, Rq_{defect} . This could be achieved by setting a threshold Rq value such that any column with larger Rq value than it will be considered as a feature-related column.

The Rq histogram of a surface with Gaussian distribution of heights follows a normal distribution, in such distribution the mean value plus or minus 3.2 times the standard deviation will cover 99.9% of the data, and any data point outside of this range would be considered as an outlier. This could be expressed as equation 5-1.

$$Rq_{defect} > Rq_{mean} + 3.2 \times \sigma_{Rq_hist} \quad (5-1)$$

Where Rq_{defect} is the Rq value of the columns containing the feature, Rq_{mean} is the mean value of the Rq histogram of the surface, and σ_{Rq_hist} is the standard deviation of the Rq histogram of a defect free surface with Sq roughness value equal to Rq_{mean} .

The magnitude of the Rq_{defect} term depends on the number of pixels in the column associated with the feature, i.e. its geometric size, and the magnitude of their departure from the nominal surface, i.e. its depth. The sum of all the Rq values greater than the right-hand side of equation 5-1 corresponds to the diameter of the circular feature.

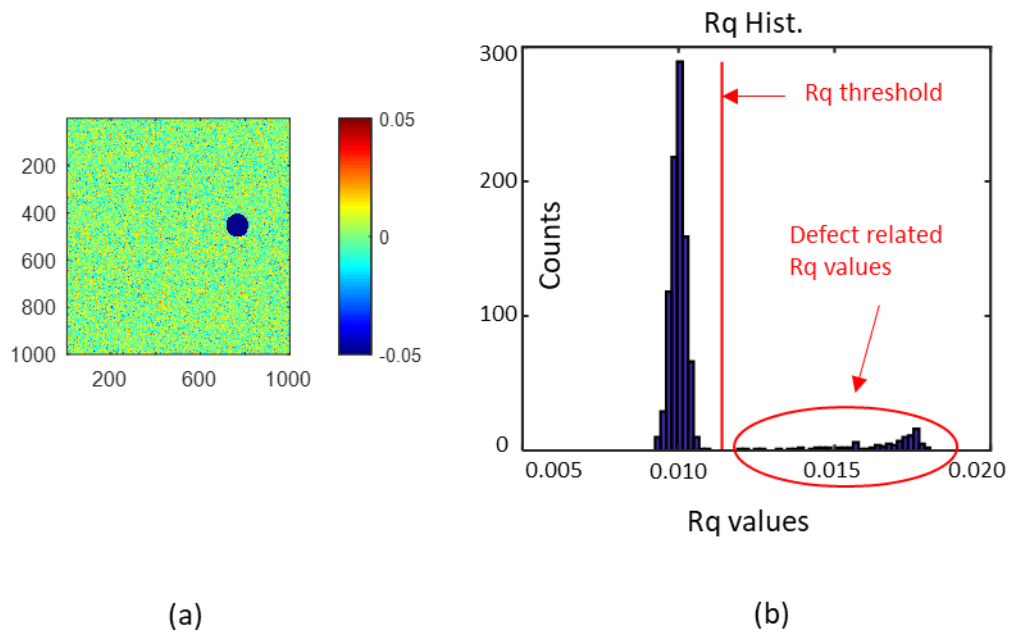


Figure 5-5: a) MATLAB generated surface with Gaussian distribution of heights with a negative feature of 100 diameter, b) the Rq histogram of the surface and the Rq threshold.

Figure 5-5(a) depicts a theoretical surface with Gaussian distribution of heights containing a negative circular feature with 100 pixels diameter and 0.05 μm depth. The Rq histogram of this surface is shown in Figure 5-5(b), the threshold Rq value is calculated based on the right-hand side of equation 5-1, and there are 99 Rq values beyond this threshold corresponding to the diameter of the feature.

It should be noted that because of the pixelization of the circular feature in the discrete environment of MATLAB and other computer systems the outer edges of the feature include a small number of feature related pixels contained within a column. This is shown in Figure 5-6, and therefore irrespective of their magnitude their Rq value might not be larger than the Rq threshold of equation 5-1, and thus the calculated diameter will not be exactly equal to the actual diameter of the feature.

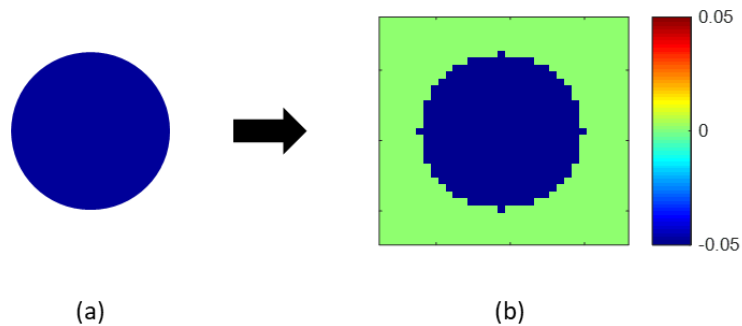


Figure 5-6: a) A circular feature in continuous environment, and b) the same feature in discrete environment.

To calculate the depth of the feature the column with the largest Rq value, Rq_{max} , is that which contains the maximum number of feature related pixels, i.e. corresponds to the column spanning the full diameter of the feature and the number of feature related pixels within the column, l , is assumed to be the same as the number of columns with Rq values above the threshold of equation 5-1. By knowing these two values (Rq_{max} and l) the depth of the feature, d , can be estimated using the formula for calculating standard deviation of a set of numbers, equation 5-2.

$$Rq_{max} = \sqrt{\frac{\sum_{i=1}^{s-l} \left(h_i - \frac{ld}{s} \right)^2 + l \left(d - \frac{ld}{s} \right)^2}{s}} \quad (5-2)$$

Where h_i are the non-feature related height values, l is the number of pixels spanning the feature diameter, d is the depth of the feature, and s is size of the original data set divided by $\sqrt{2}$. It should be noted that this approach assumes that all non-feature related height values have a Gaussian distribution, and the feature has a constant flat depth. For the surface shown in Figure 5-5 the l is equal to 99 pixels and the Rq_{max} is equal to the 0.0179 μm , plugging these numbers in the equation 5-2 the depth is calculated equal to 0.05 μm .

5.2.3 Detectability threshold

From analysis of the Rq histogram, it is possible to create a generalized threshold limit indicating the detectability of a circular feature with different diameters and depths. A feature is defined as detectable if the number of the Rq values of the surface that contains the defect is above the threshold limit of equation 5-1, and is within two pixels of the number of columns spanned by the feature.

For a surface with a Gaussian distribution of heights, this threshold limit is generated in an iterative manner in MATLAB such that for each feature diameter an initial and constant feature depth of a shallow value is first selected, while the other non-feature related pixels are random and have a Gaussian distribution of heights. The Rq histogram of the surface is determined and the number of Rq values that are greater than the right-hand side of the equation 5-1 are counted. If the difference between this number and the number of pixels spanning the full diameter of the feature is equal or less than two then the threshold depth is identified for that diameter, if not the depth value of the feature is increased by 1% of the Sq of the surface ($1.01 \times Sq$), and the process repeated until the threshold depth is identified.

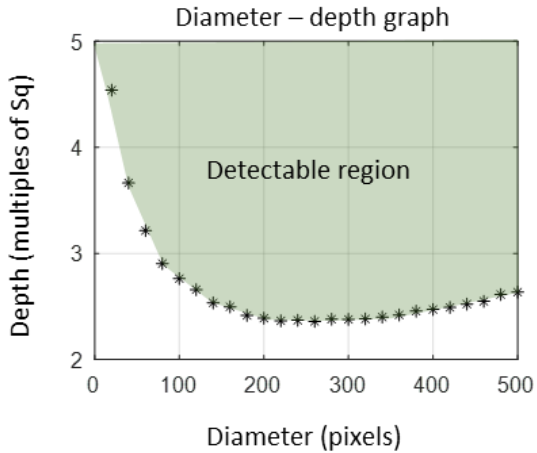


Figure 5-7: Detectable threshold limit for diameter and depth combination.

The process of identifying the detectable threshold limit for a surface comprising 1000×1000 pixels was repeated 500 times on different surfaces with the same Gaussian distribution of heights, and the average calculated height is depicted in Figure 5-7, the standard deviation of each point on this graph is within 0.1% to 0.15% of the average threshold depth, and thus it is too small to be visible on the graph. The diameter of the feature is given in pixels on the horizontal axis, while the depth of the feature is given as a function of the overall surface Sq value on the vertical axis. For other surface dimensions, a different graph would have to be generated.

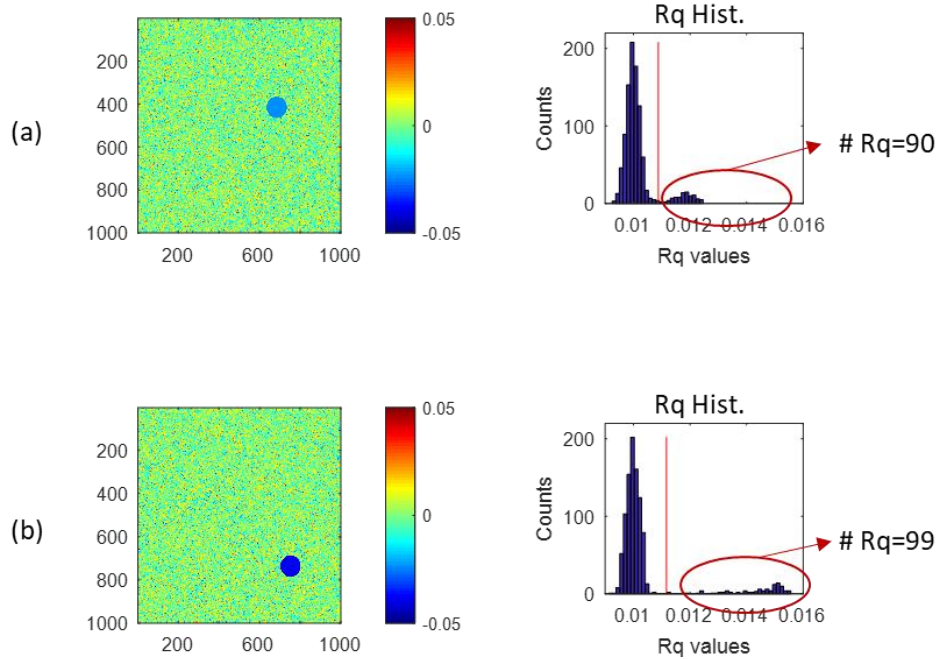


Figure 5-8: MATLAB generated surface with a negative circular feature of diameter 100 pixels and depth of 0.025 μm , and b) the same surface with a circular feature of diameter of 100 pixels and depth of 0.04 μm ; and their Rq histogram.

Based on the graph in Figure 5-7 a circular feature with its diameter equal to 100 pixels on a surface with Sq equal to 0.01 μm should have a depth above 0.028 μm in order to be detectable. Figure 5-8(a) shows a circular feature with 100 pixels diameter and 0.025 μm depth on a surface with Sq equal to 0.01 μm , since this depth is below the detectable region of Figure 5-7 the number of columns that have the Rq value greater than the threshold limit is not within two of the actual diameter, and is equal to 90 pixels. It should be noted that in this case the circular feature's effect is reflected on the columns Rq histogram by creating some number of Rq values larger than the threshold of equation 5-1, i.e. the presence of the feature is detected, however, the radius of the feature is not estimated correctly. This inaccuracy of the estimated radius is because the depth of the feature in the columns close to the edges of the feature, that have a small number of feature-related pixels, is not deep enough to create an Rq value larger than the right-hand side of equation 5-1.

However, when the depth of the feature is increased such that it goes inside the detectable region, i.e. $0.04\ \mu\text{m}$ as shown in Figure 5-7(b), then the number of columns having Rq values larger than the threshold limit is within the two pixels margin of error, and thus is counted as detectable.

This is a conservative approach since it requires nearly all the feature related columns to have Rq values greater than the threshold value of equation 5-1, but nevertheless it has reasonable sensitivity.

5.2.4 Analysis of a real surface with a circular feature

Figure 5-9(a) depicts a polished glass surface from NIST traceable scratch dig standard, dig grade number 0.016, from the specification of the sample the diameter of the dig is equal to $18\ \mu\text{m}$. This surface is measured with Zygo ZeGage coherence scanning interferometer (CSI) $20\times$ objective with $417\ \mu\text{m} \times 417\ \mu\text{m}$ field of view, and the diameter and depth of the feature from the processed measurement height map is equal to $18\ \mu\text{m}$ and $0.060\ \mu\text{m}$ respectively. Figure 5-9(b) shows the same surface when the feature is excluded with its Sq , skewness and kurtosis equal to 1 nm, 0.07 and 2.9 respectively.

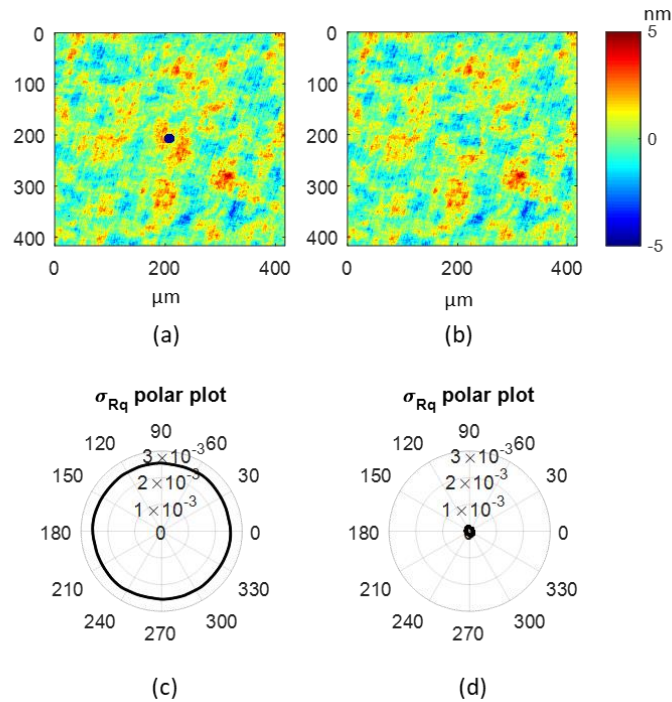


Figure 5-9: a) A measured surface with a negative feature, b) defect free surface of the same sample, c) and d) their σ_{Rq} polar plots.

The presence of a single circular feature is detected with the surface's σ_{Rq} polar plot when it is compared to the polar plot of a defect-free surface of the same kind, Figure 5-9(d). The constant increase of the radius of the σ_{Rq} polar plot, Figure 5-9(c) indicates the existence of a single circular feature on the surface.

In order to determine whether the single circular feature is positive, i.e. on the surface or negative, i.e. below it the skewness of the Rsk histogram, Sk_{Rsk} polar plot, of the surface will be compared to the same polar plot of the defect-free surface. If the Sk_{Rsk} polar plot of the surface with feature is inside the Sk_{Rsk} polar plot of the defect-free surface then it is a negative feature, and if it is outside, then it is a positive feature.

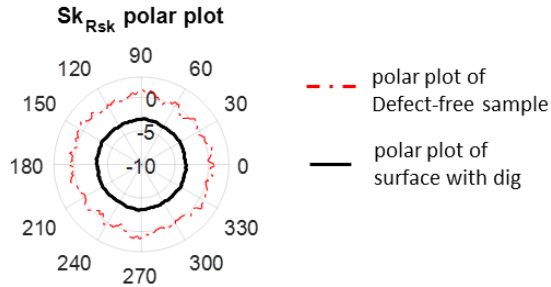


Figure 5-10: Skewness of the R_{sk} histogram polar plot of the surface and the defect-free surface on the same plot.

These two polar plots are shown on the same plot in Figure 5-10, from this plot it is clear that the Sk_{Rsk} polar plot of the surface with the defect is inside the Sk_{Rsk} polar plot of the defect-free surface, meaning that the feature is negative.

To find out the diameter of the feature, first the Rq values of the Rq histogram that are larger than the right-hand side of the equation 5-1 need to be counted.

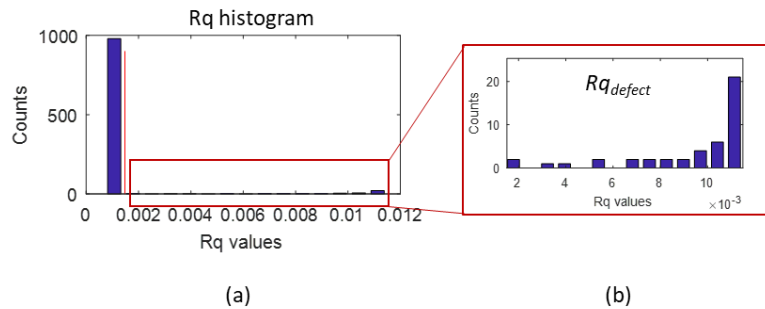


Figure 5-11: Rq histogram of the surface with the negative circular feature shown in Figure 5-9(a).

Figure 5-11 depicts the Rq histogram of the surface containing the circular feature, the right-hand side limit of the equation 5-1 is shown on this histogram by the red vertical line. Any Rq value larger than this limit is a defect-related value, Rq_{defect} , and is caused by the presence of the feature. The area after this threshold Rq value is zoomed in and shown in Figure 5-11(b), and the total number of bins in this area is equal to 45 which corresponds to the diameter of the feature. Considering the pixel resolution of the $20\times$ objective the diameter is calculated equal to $18\ \mu\text{m}$.

The maximum Rq value, Rq_{max} , of this surface's Rq histogram is equal to $0.011\ \mu\text{m}$, and belongs to the columns that has the maximum number of feature-related pixels, i.e. the column that

spans the full diameter of the feature, l . Putting these two values into the equation 5-2 the depth of the feature is calculated equal to 60 nm. From the graph shown in Figure 5-7 the depth for a circular feature with this diameter has to be more than 3.6 times the Sq of the surface in order for it to be detectable with the correct estimate of diameter, which in this case the depth has to be more than 3.6 nm. Since the depth of the feature is equal to 60 nm, this feature is not hard to resolve for its diameter and depth.

5.3 Single scratch

When there is a linear feature on the surface, i.e. a scratch, a pair of lobes will appear on the polar plots. Depending on the geometry of the feature and the resolution of rotation, a local minimum may occur in the vicinity of the apex of the lobe in the σ_{Rq} polar plot. Similar to the circular feature the columns containing the scratch will have higher Rq values than those feature-free columns, and these Rq value are found in bins to the right side of the mean value of the Rq histogram. The angle of the lobe apex or the local minimum of the polar plots shows the angle enclosed between the scratch and the vertical axis, and informs by how much the surface would have to be rotated as to make the scratch vertical.

Figure 5-12(a) depicts a surface with a Gaussian distribution of heights, and Sq value of 0.01 μm containing a scratch of 250×5 pixels length and width respectively. The depth of the scratch is 0.05 μm , and the angle enclosed between the scratch and the vertical axis is equal to 30° . The lobe apex occurs at 30° in all of the polar plots. However, for the same surface when the scratch's depth is increased to 0.15 μm there will be a local minimum in the σ_{Rq} polar plot at 30° , see Figure 5-12(b). The presence of this local minimum is a function of the geometrical properties of the scratch, i.e. its length, width, and depth, and is given in equation 5-7.

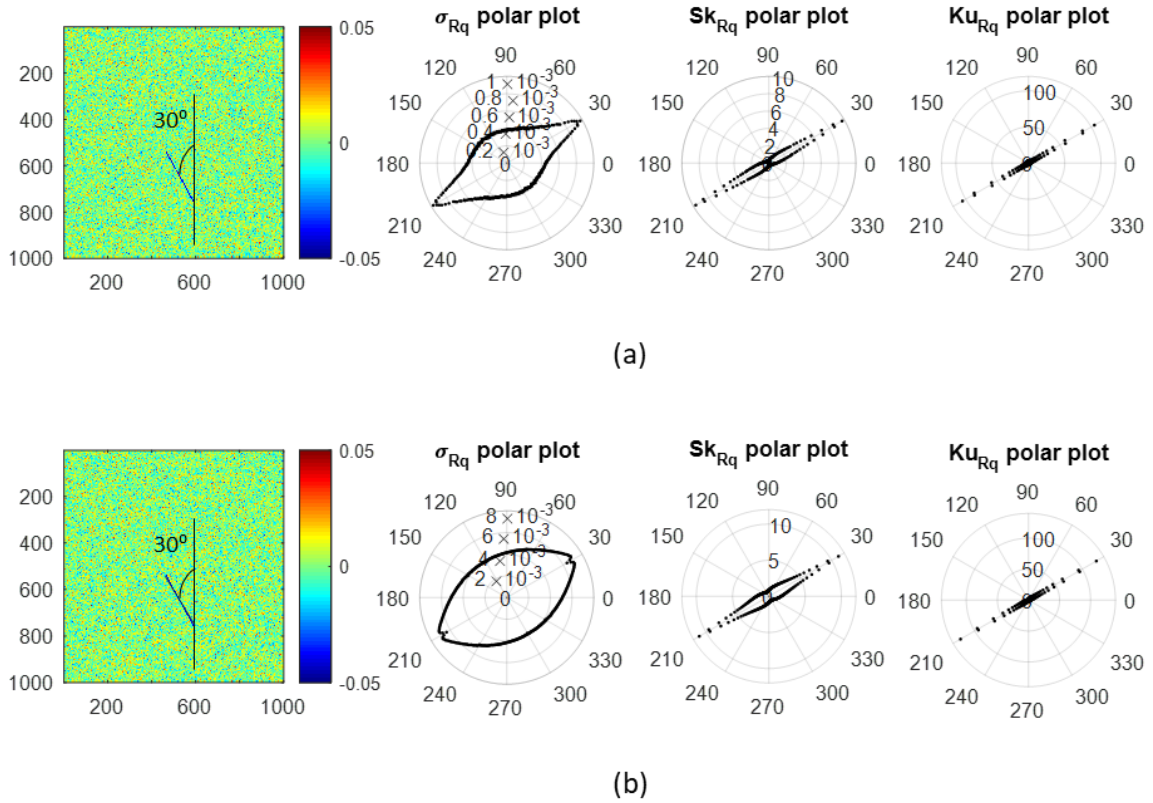


Figure 5-12: MATLAB generated surface with a Gaussian distribution of heights with a scratch of $250L \times 5w$ pixels, and its σ_{Rq} polar plot, skewness and kurtosis of the Rq histogram polar plots when a) its depth is equal to $0.05 \mu\text{m}$ and b) its depth is equal to $0.15 \mu\text{m}$, (The rotational angle for creating these polar plots is 1°).

When the scratch is rotated from its vertical position geometrical analysis states that the number of columns that contain elements of the scratch, $col_{scratch}$ is described by equation 5-3 and the number of pixels in each one of these columns, $Lcol$ is estimated by the equation 5-4.

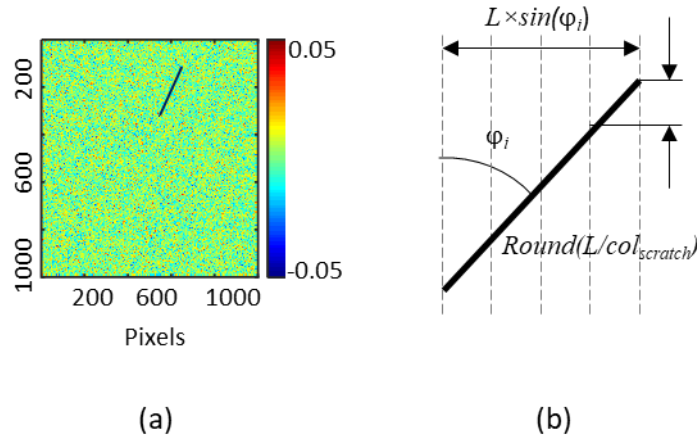


Figure 5-13: a) MATLAB™ generated surface with a Gaussian distribution of heights with a scratch of $200L \times 5w$ pixels, b) geometrical model of the scratch.

$$col_{scratch} = L \times \sin \varphi_i \quad (5-3)$$

$$Lcol = \text{round} \left(\frac{L}{col_{scratch}} \right) \quad (5-4)$$

Where φ_i is the angle enclosed between the scratch and vertical axis at each rotational angle θ , for instance in Figure 5-13(a) at $\theta=0^\circ$, φ is equal to 150° .

At each rotational angle, θ , the Rq value of the defect free columns, Rq_{defect_free} is given in equation 5-5:

$$Rq_{defect_free} = \sqrt{\frac{\sum_{i=1}^s (h_{i,j} - \mu_{df})^2}{s}} \quad (5-5)$$

Where $h_{i,j}$ are height values in the column j , μ_{df} is the average height value of the defect free column j , and s is the size of the superimposed rectangle, i.e. $s = \frac{n}{\sqrt{2}}$.

And the Rq value of all columns containing elements of the scratch, Rq_{defect} , is given in equation 5-6.

$$Rq_{defect} = \sqrt{\frac{\sum_{i=1}^{s-\frac{w}{\sin(\varphi_i)}} (h_{i,j} - \mu_d)^2 + \frac{w}{\sin(\varphi_i)} (d - \mu_d)^2}{s}} \quad (5-6)$$

Where μ_d is the average height value of the defect-related columns, φ_i is the angle enclosed between the scratch and vertical axis at each rotational angle θ , $h_{i,j}$ are height values in the column j containing elements of the scratch, d is the depth, and w is the width of the scratch. The standard deviation of the Rq histogram is equal to the radius of the polar plot at rotational angle θ , r_θ , by using equations 5-5 and 5-6 this radius is given in equation 5-7.

$$r_\theta = \sqrt{\frac{\left\{ (s - L \sin \varphi_i) \left[\sum_{i=1}^s \sqrt{\frac{(h_{i,j} - \mu_{df})^2}{s}} \right] - \mu_{Rq} \right\}^2 + \dots}{\left\{ \left[(L \sin \varphi_i) \left(\sum_{i=1}^{s-w/\sin \varphi_i} \left[\sqrt{\frac{(h_{i,j} - \mu_d)^2}{s}} \right] + \frac{w}{\sin \varphi_i} [d - \mu_d]^2 \right) \right] - \mu_{Rq} \right\}^2}} \quad (5-7)$$

Where μ_{Rq} is the average value of the Rq histogram, w is the width, L is the length, and d is the depth of the scratch respectively. This equation cannot be solved explicitly for the general combinations of the length, width, and depth of a scratch in order to predict for what specific combination of parameters there will be a local minimum or a sharp peak at the angle where the scratch is vertical.

5.3.1 Estimation of length, width, and depth

At each angle of rotation, the number of columns containing elements of the scratch is different and is given in equation 5-4. Assuming the depth of the scratch is large enough to increase the Rq value of these columns such that they become larger than the threshold value of equation 5-1, the length of the scratch can be estimated by dividing the total number of these Rq values by the sine of the angle enclosed between the scratch and the vertical axis; and at the end the estimation of the length is determined by taking the average value of all calculated lengths, equation 5-8.

$$L = \text{mean} \left[\sum_{i=1}^{180} \text{round} \left(\frac{\text{bins}_i}{\sin(\varphi_i)} \right) \right] \quad (5-8)$$

Where bins_i is the total number of Rq values exceeding the limit of equation 5-1, and φ_i is the corresponding angle.

The lobe apex or the local minimum happens at an angle where the scratch of length L is vertical and contained within the minimum number of columns; at this angle, θ_v , the number of columns that have Rq values larger than the threshold of equation 5-1, correspond to the width of the feature, w , equation 5-9.

$$w = \sum_{i=1}^n i \mid (Rq_i > Rq_{\text{mean}} + 3.2 \times \sigma_{Rq_hist}) \text{ at } \theta = \theta_v \quad (5-9)$$

To calculate the depth of the scratch the maximum Rq value, Rq_{max} , at the angle where the scratch is vertical, θ_v corresponds to the column that contains the full length of the feature, L , knowing these two values, (L and Rq_{max}), the depth of the feature can be estimated via equation 5-10 which is the formula for calculating the standard deviation of a set of numbers.

$$Rq_{\text{max}} = \sqrt{\frac{\sum_{i=1}^{s-L} \left(h_i - \frac{Ld}{s} \right)^2 + L \left(d - \frac{Ld}{s} \right)^2}{s}} \quad (5-10)$$

Where h_i are the non-feature related height values, L is the length of the feature, d is the depth, and s is size of the original data set divided by $\sqrt{2}$, ($s = \frac{n}{\sqrt{2}}$).

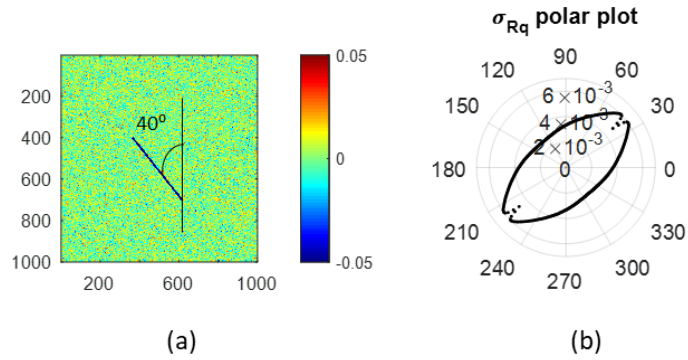


Figure 5-14: a) MATLAB generated surface with Gaussian distribution of heights and a scratch of 400×10 pixels, and depth of $0.10 \mu\text{m}$, and b) its σ_{Rq} polar plot.

Figure 5-14 depicts a surface with Gaussian distribution of heights containing a scratch of 400 pixels length and 10 pixels width, the depth of the scratch is $0.10 \mu\text{m}$ and the angle enclosed between the feature and the vertical axis is equal to 40° . From equation 5-6 the length of scratch, L , is estimated as 398 pixels; from its σ_{Rq} polar plot the local minimum in the upper half of the polar plot happens 40° , thus $\theta_v = 40^\circ$.

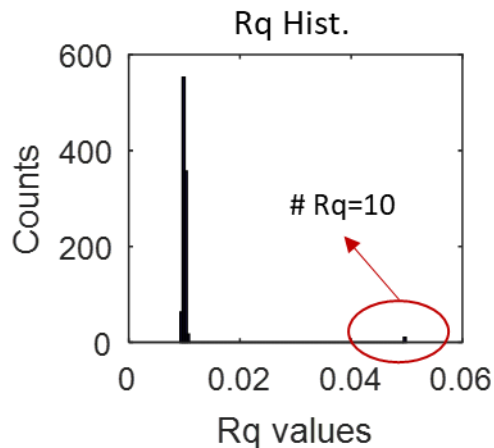


Figure 5-15: The Rq histogram of the surface when the scratch is vertical.

The Rq histogram of the surface at this angle, θ_v , is shown in Figure 5-15, where the number of Rq values greater than the threshold of equation 5-1 is equal to 10 and corresponds to the width of the scratch. In this histogram the Rq_{max} value is equal to 0.0496, plugging this value, and the estimated length ($L=398$) into the equation 5-10 the depth is estimated as $0.101 \mu\text{m}$.

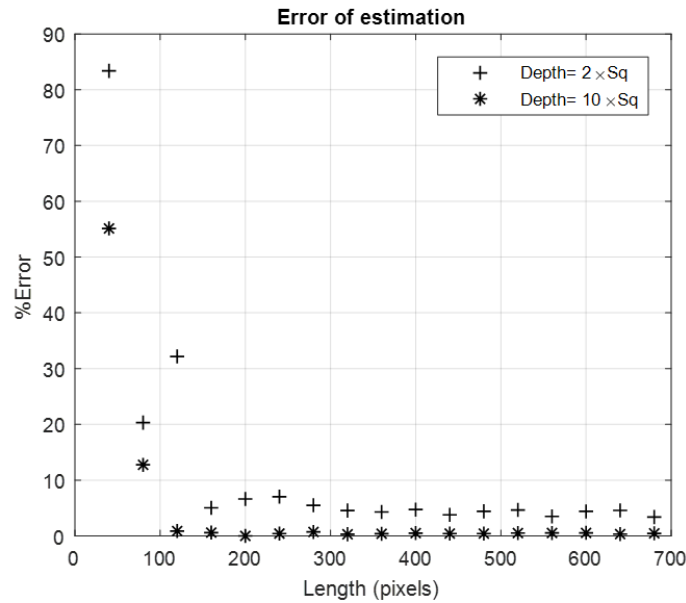


Figure 5-16: Associated error of scratch's length estimation for depths equal to $0.02 \mu\text{m}$ and $0.10 \mu\text{m}$ of a surface comprising 1000×1000 pixels.

To find out the error associated with the estimation of the length of the feature, in an iterative manner in MATLAB a vertical scratch of length L and depth d is placed on a 1000×1000 pixel surface with Gaussian distribution of heights. The length of this scratch is then estimated based on equation 5-8 and the percentage error between this calculated value and the actual value is reported for that specific depth. The process of finding the percentage error for a combination and length and depth is repeated 500 times, and the average value of the error is shown in Figure 5-16 for two fixed depths. From this graph it is clear that the error of estimation of feature's length decreases as the length of the feature increases.

5.3.2 Detectability threshold

Similar to the circular feature by using equation 5-1 the detection threshold can be determined to indicate the geometric limitations of a detectable scratch for a surface comprising 1000×1000 pixels. For each scratch's length when it is vertical an initial shallow depth is first selected, and the number of Rq values in the Rq histogram that are greater than the threshold in equation 5-1 are

counted. If this number is equal to the width of the scratch then the threshold depth for that length is achieved. If not the depth is then increased by 1% of the Sq of the surface ($1.01 \times Sq$) and the process repeated. This iteration process for finding the threshold depth is done 500 times, and the average value is shown on Figure 5-17. Again, similar to the curve for circular feature error bars are within 0.1% to 0.15% of the threshold depth and thus not visible on the graph.

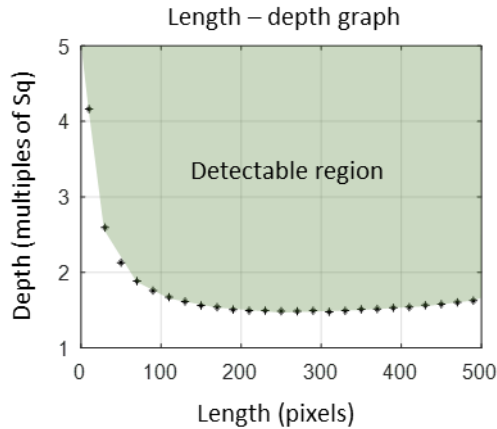


Figure 5-17: Detectable threshold limits for length and depth combination of a scratch based on equations 5-1

The graph in Figure 5-17 utilizes the information of the Rq histogram of a surface; however, since a scratch creates a pair of lobes on the polar plots there is another way of generating the minimum detectable threshold limit for a single scratch directly from the polar plots themselves.

When the scratch is vertical, i.e. contained within a minimum number of columns, the Rq value of these columns must be sufficiently greater than the scratch-free columns to induce an increase in the σ_{Rq} polar plot and hence produce a lobe on the polar plot. The threshold that must be exceeded is given in equation 5-11.

$$\sigma_{Rq_hist} > \sigma_{Rq_hist_mean} + 3.2 \times \sigma_{\sigma_{Rq_hist}} \quad (5-11)$$

Where σ_{Rq_hist} is the standard deviation of the Rq histogram at a particular angle, $\sigma_{Rq_hist_mean}$ is the average of all σ_{Rq_hist} values, and $\sigma_{\sigma_{Rq_hist}}$ is the standard deviation of all σ_{Rq_hist} values. Such

threshold limit cannot be generated for the circular feature due to the circular nature of its polar plot, and absence of a local maximum.

Equation 5-11 uses the standard deviation of the Rq histogram, however, to increase the sensitivity of the approach the higher moments of the Rq histogram could be used such as third order moment, i.e. skewness and fourth order moment, i.e. kurtosis (equations 5-12 and 5-13) of the Rq histogram. Figure 5-18 depicts these threshold limits for a surface dimension of 1000×1000 pixels.

$$Sk_{Rq_hist} > Sk_{Rq_hist_mean} + 3.2 \times \sigma_{Sk_{Rq_hist}} \quad (5-12)$$

$$Ku_{Rq_hist} > Ku_{Rq_hist_mean} + 3.2 \times \sigma_{Ku_{Rq_hist}} \quad (5-13)$$

Where Sk_{Rq_hist} and Ku_{Rq_hist} are the skewness and kurtosis of the Rq histogram at a particular angle, $Sk_{Rq_hist_mean}$ and $Ku_{Rq_hist_mean}$ are the average of all Sk_{Rq_hist} and Ku_{Rq_hist} values, and $\sigma_{Sk_{Rq_hist}}$ is the standard deviation of all Sk_{Rq_hist} values and $\sigma_{Ku_{Rq_hist}}$ is the standard deviation of all Ku_{Rq_hist} values.

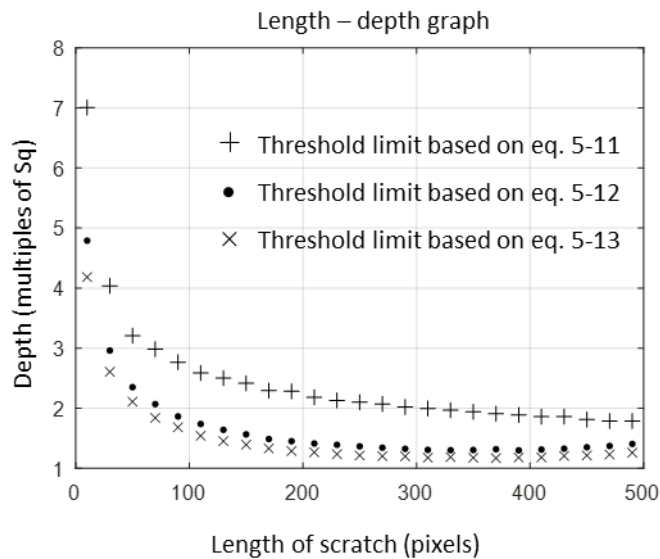


Figure 5-18: Detectable threshold limits for length and depth combination of a scratch based on equations 5-11, 5-12, and 5-13.

Based on this graph a scratch of 100 pixels length on a surface with Sq equal to $0.01 \mu\text{m}$, Figure 5-19(a), when its depth is equal to $0.02 \mu\text{m}$ should not be detected with the σ_{Rq} polar plot, i.e. there will not be a pair of lobes, Figure 5-19(b). Whereas this scratch should be detected with the skewness and kurtosis of the Rq histogram polar plots, and the sensitivity of the detection, i.e. the magnitude of the lobe apex should be higher for the kurtosis of the Rq histogram polar plot, see Figure 5-19(c) and (d).

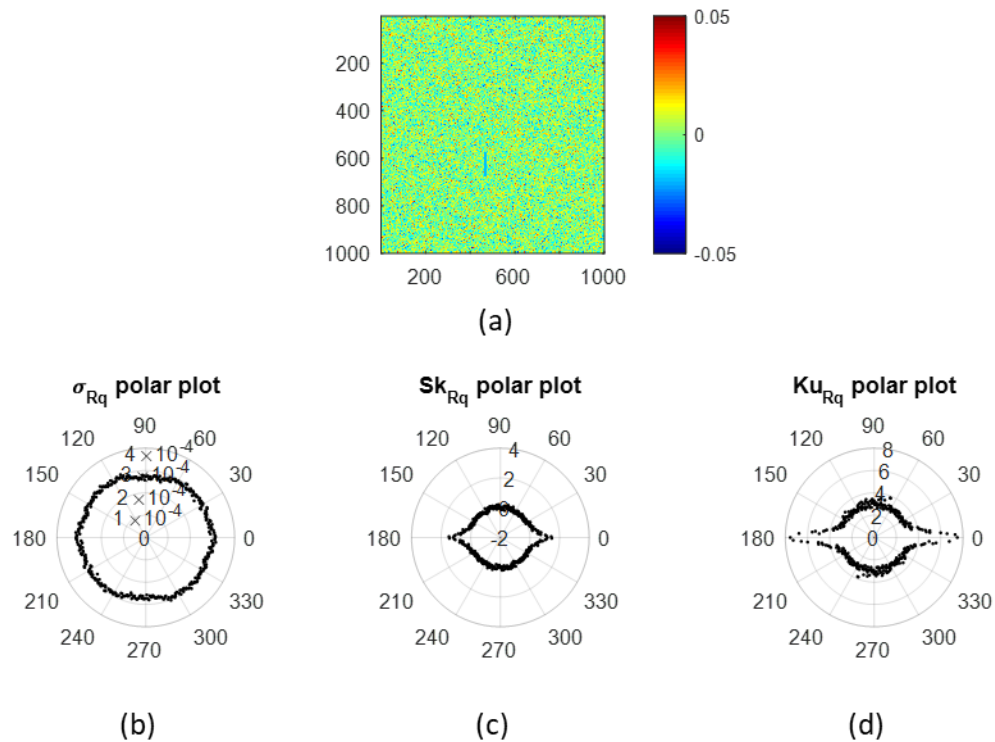


Figure 5-19: a) MATLAB generated surface with Gaussian distribution of heights and a scratch of $100L \times 5w$ pixels, and depth of $0.02 \mu\text{m}$, b) its σ_{Rq} polar plot, c) skewness of the Rq histogram polar plot, and d) kurtosis of the Rq histogram polar plot.

It should be noted that the threshold limit based on the equation 5-11 that directly uses the polar plot itself is more conservative, i.e. less sensitive, when compared to the threshold limit based on the equation 5-1 which is based on the Rq histogram, see Figure 5-20.

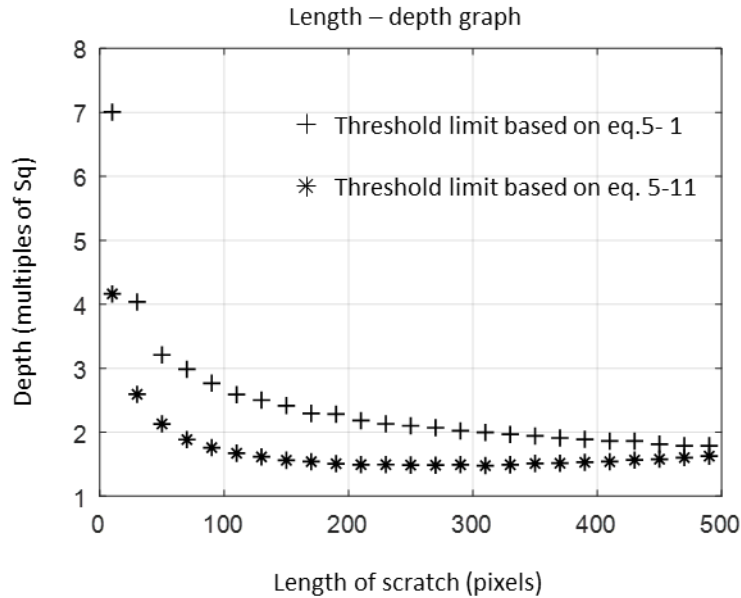


Figure 5-20: Detectable threshold limits for length and depth combination of a scratch based on equations 5-1 and 5-11.

5.3.3 Analysis of a real surface with a linear feature

Figure 5-21(a) depicts a polished glass surface from NIST traceable scratch dig standard, scratch grade number 0.025, from the specification of the sample the length and width of the scratch is equal to 100 μm and 6.3 μm respectively. This surface is measured with Zygo ZeGage coherence scanning interferometer (CSI) 20 \times objective with 417 $\mu\text{m} \times 417 \mu\text{m}$ field of view, and the length, width, and the average depth of the scratch from the processed measurement height map is equal to 102.3 μm , 6.8 μm , and 0.06 μm respectively.

Figure 5-21(b) shows the same surface when the feature is excluded with its Sq , skewness and kurtosis equal to 1 nm, -0.9 and 38.01 respectively.

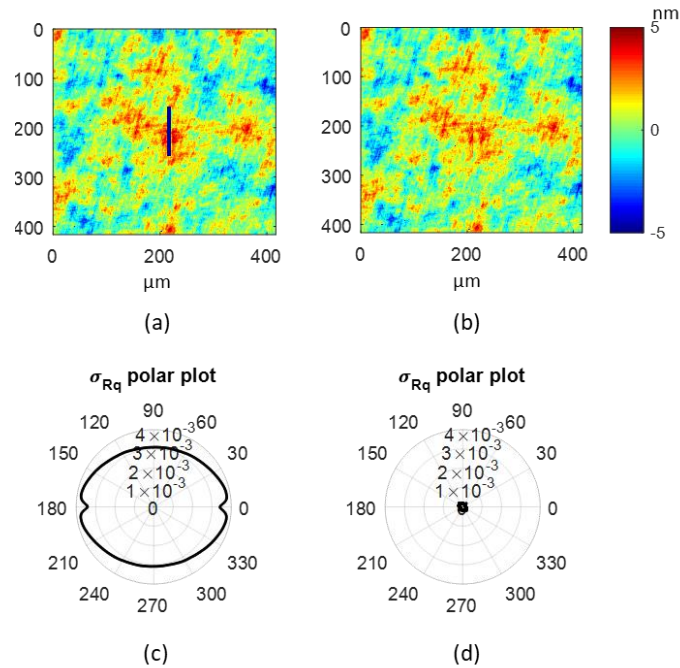


Figure 5-21: a) A measured surface with a negative linear feature, b) defect free surface of the same sample, c) and d) their σ_{Rq} polar plots.

The presence of a single linear feature is detected with the surface's σ_{Rq} polar plot when it is compared to the polar plot of a defect-free surface of the same kind, Figure 5-21(d). The presence of two local minimum in the σ_{Rq} polar plot, Figure 5-21(c) indicates the existence of a single linear feature on the surface.

In order to determine whether the single linear feature is positive or negative the skewness of the Rsk histogram, Sk_{Rsk} polar plot, of the surface will be compared to the same polar plot of the defect-free surface. If the Sk_{Rsk} polar plot of the surface with feature is inside the Sk_{Rsk} polar plot of the defect-free surface then it is a negative feature, and if it is outside, then it is a positive feature.

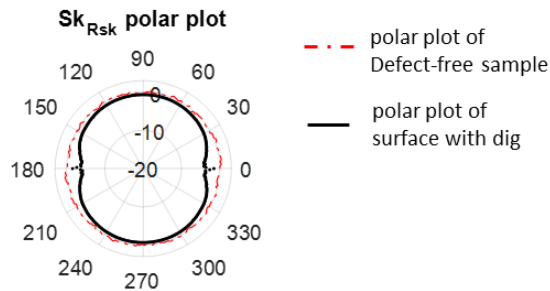


Figure 5-22: Skewness of the Rsk histogram polar plot of the surface and the defect-free surface on the same plot.

From the polar plots of Figure 5-22 the plot of the surface is inside of the plot of the defect-free sample meaning that the feature is negative.

The length of the feature can be calculated via equation 5-8 and is equal to 226 pixels, which is equal to $90.4 \mu\text{m}$ when considering the pixel resolution of the $20\times$ objective. The width can also be achieved by using equation 5-9 and is 25 pixels, equal to $10 \mu\text{m}$. And finally by using equation 5-10 the depth is calculated as $0.060 \mu\text{m}$.

The error of length and width estimation is due to the fact that the surface even excluding the feature is not perfectly Gaussian, and also the scratch is not a perfect rectangle, i.e. there is not a perfect stepped edge between the scratch and the surface.

5.4 Summary

In this chapter the effect of a single circular and linear feature on the surface on the polar plots was investigated. The presence of a circular feature on the surface was detected by comparing the σ_{Rq} polar plot of the surface with the polar plot of a defect-free surface, the increase in the radius of the polar plot is an indicator of the existence of a circular feature.

Since the standard deviation and Rq value are both squared terms their value independent of the magnitude of the feature is always positive. In order to detect whether the feature is located on the surface such as a piece of dirt or below it such a scratch the skewness of the columns Rsk histogram polar plot was used. Skewness is a cubic term and therefore is sensitive to the sign of the magnitude of the feature. If the Sk_{Rsk} polar plot of the surface that is being analyzed is inside the

Sk_{Rsk} polar plot of a defect-free surface then the feature is negative, and if it is outside then the feature is positive.

From the Rq histogram of the surfaces with single features it is also possible to estimate the depth and diameter of a circular feature. The detectability threshold for the circular features can be generated with the information of the columns Rq histogram. From the estimated diameter and the maximum Rq value in the histogram it is also possible to back calculate the feature's depth. Admittedly, this is a conservative approach for detecting a single circular feature since the detectability threshold requires all the feature-related pixels in the feature-related columns to be deep enough to increase the Rq value such that it becomes larger than the threshold Rq value, however, it ensure that the estimated diameter of the feature is within two pixels margin of error of the actual diameter of the feature.

Presence of a linear feature on the surface is also detected by a pair of lobes in the σ_{Rq} polar plot. Similar to the circular feature the Rq histogram of a surface containing a single scratch can be analyzed to estimate the length, width, and the depth of the single linear feature. The length of the linear feature can be estimated by counting the number of Rq values that the scratch creates that are larger than the right-hand side of equation 5-1, and using equation 5-8. At the angle where the scratch is vertical the maximum Rq value in the columns Rq histogram belongs to the column that encapsulates the entire length of the feature, knowing this value and the estimated length, the depth of the feature can also be calculated.

The estimation of length, width, and depth of a single scratch was verified on a real sample. The difference between the theoretical model of a scratch and the real one is that the surface containing the scratch is does not have a perfect Gaussian distribution of heights, the scratch itself is not a perfect rectangle, i.e. there is not a stepped edge between the scratch and surface, and finally the scratch does not have a constant depth at its bottom, i.e. depth variation at the bottom of the scratch.

Presence of the lobes in the polar plots of a surface containing a single scratch can be taken advantage of to increase the sensitivity of the feature detection by using higher orders moments of data, i.e. the skewness and kurtosis of the Rq histogram. However, this is not applicable to the polar plots of a surface that contains a single circular feature for they have nominally circular shape, and do not have any lobes. Table 5-1 summarizes the key features to consider when analyzing surfaces with singular features' polar plots.

Table 5-1: Polar plot's features

Feature	r_{max}	Angle between r_{max} and r_{min}	# of peaks	Rate of slope change
Single circular feature				
Single linear feature				

CHAPTER 6: MULTIPLE FEATURES CHARACTERIZATION

6.1 Introduction

The presence multiple circular features, i.e. digs, and multiple linear features, i.e. scratches also affect the behavior of the polar plots when compared to the polar plots of a defect free surface. Lobes are present on the polar plots depending on the arrangement and the quantity of the features and their magnitude. Similar to the single feature, analysis of the polar plots could be used to detect the presence of multiple features and back calculate the quantity and their geometrical attributes, such as diameter and depth for circular features and length, width and depth of the linear features.

This chapter details the effect of multiple features on the surface and explains different methods to analyze the polar plots in order to obtain insights about the surface features.

The statistical parameter of columns used in this chapter is their Rq , and their mean height, μh , values; and the rotational increment in generating polar plots is equal to 1° unless otherwise mentioned.

6.2 Multiple circular features

Should multiple circular features be present on the surface, their configuration and quantity affect the behavior of the corresponding polar plots by creating some number of lobes. Figure 6-1 depicts a theoretical surface with Gaussian distribution of heights and a negative circular feature; since the number of columns containing the scratch during the rotation process is constant, equal to the diameter of the scratch, the σ_{Rq} polar plot's shape is circular. The assumption in this section is that all of the multiple circular features are identical unless it is specifically mentioned that identity is not a requirement. At the end results of failure to meet this assumption will be discussed.

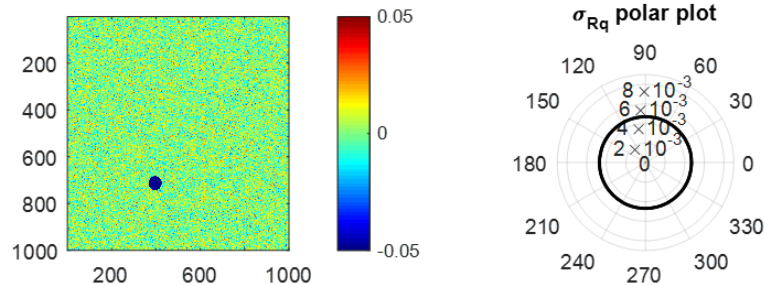


Figure 6-1: MATLAB generated surface with Gaussian distribution of heights with a negative circular feature and its σ_{Rq} polar plot.

Figure 6-2 shows another theoretical surface with its Sq equal to $0.01 \mu\text{m}$, and two negative circular features with 50 pixels radius and $0.1 \mu\text{m}$ depth, these features not only increase the average radius of the polar plot, but also create two lobes on them, Figure 6-2(a). The maximum radius of the polar plot which is the apex of the lobes occur at the angles where both features are perfectly aligned, i.e. are contained within the same columns. At this angle although fewer columns are affected by the presence of the features, but since they contain higher number of feature-related pixels, when compared to the angles that features do not align perfectly, the Rq of these columns further increases, see the Rq histogram in Figure 6-2(b) where both features are completely aligned, therefore the standard deviation of the Rq histogram increases; and it creates a local maximum in the polar plot.

It should be noted that the assumption here is that all of the features should be large and deep enough to significantly affect the Rq value of the columns containing them.

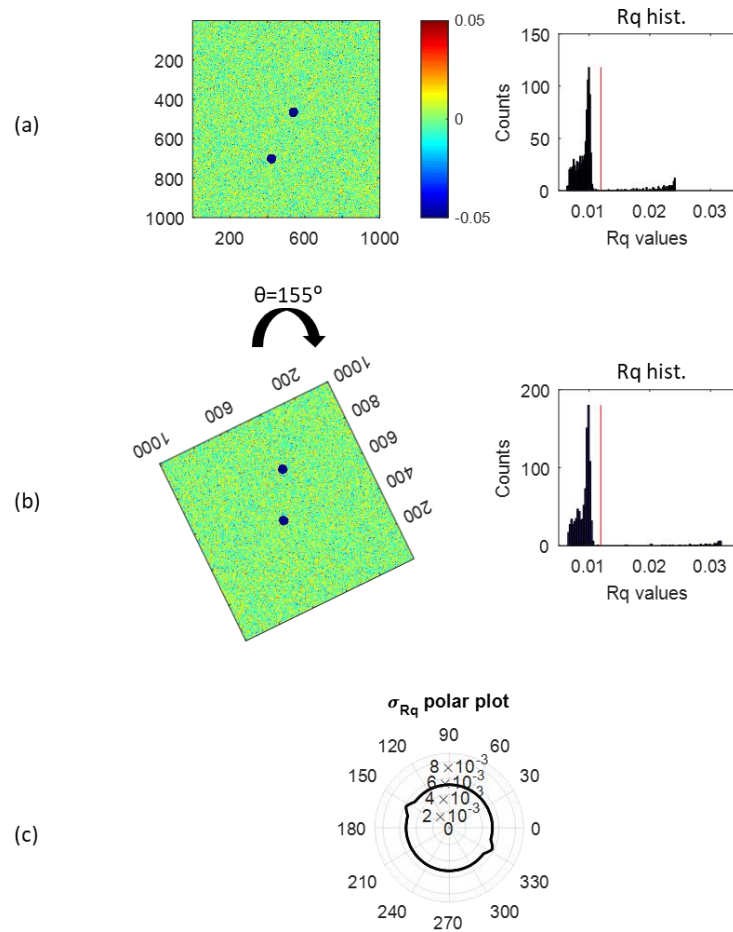


Figure 6-2: MATLAB generated surface with Gaussian distribution of heights with a) two negative circular features and its Rq histogram, b) when the surface is rotated 155° CW and its Rq histogram, and c) its σ_{Rq} polar plot.

Lobes occur at the angles where two or more features align and are contained within the same number of columns. When a column contains sections of multiple features its associated Rq value further increases, so does the standard deviation of the Rq histogram, this increase in standard deviation value continues and reaches to its maximum when features are perfectly aligned, and thus a local maximum on the σ_{Rq} polar plot is produced.

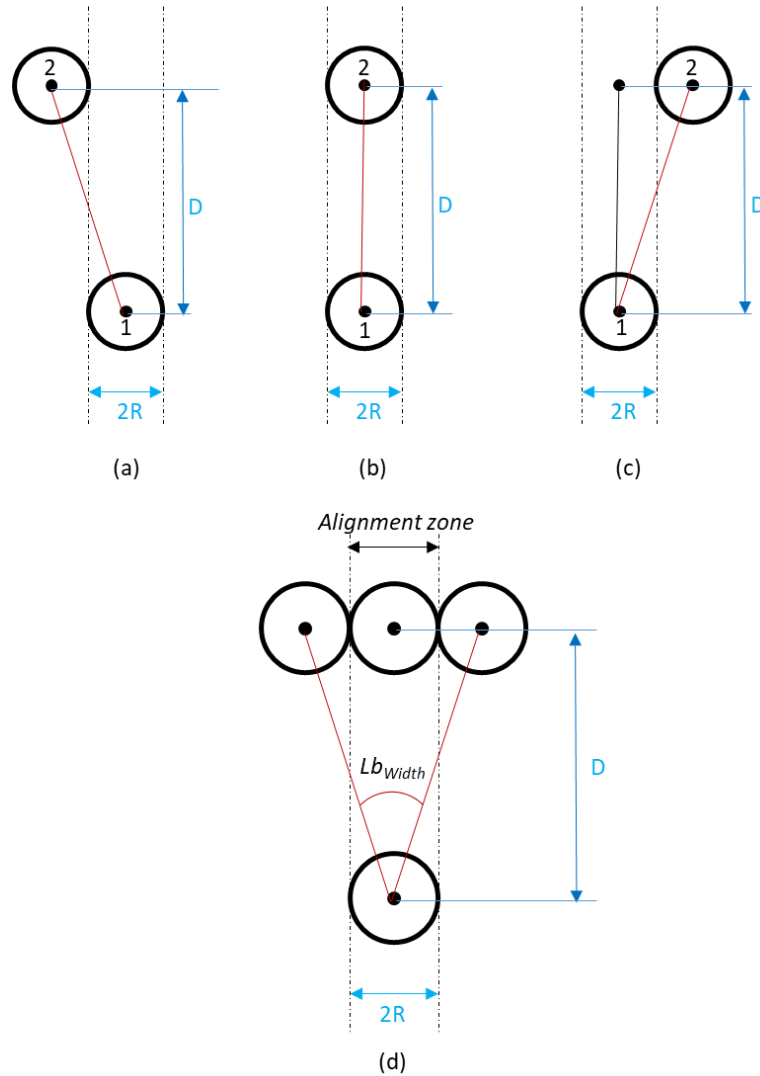


Figure 6-3: Schematic representation of two circular features getting in and out of alignment.

Figure 6-3(a) schematically shows how during the rotation two circular features start aligning, when they are perfectly aligned, Figure 6-3(b), and when they are out of alignment, Figure 6-3(c). Figure 6-3(d) shows these three processes together, from this geometrical model the difference between the angle where one feature starts entering the alignment zone and the angle where the feature is completely out of alignment zone is the width of the lobe, Lb_{width} , in the polar plot, see equation 6-1.

$$Lb_{width} = \text{round} \left(2 \tan^{-1} \left(\frac{2R}{D} \right) - 1 \right) \quad (6-1)$$

Where R is the radius of the circular feature, and D is the center to center distance between two circular features.

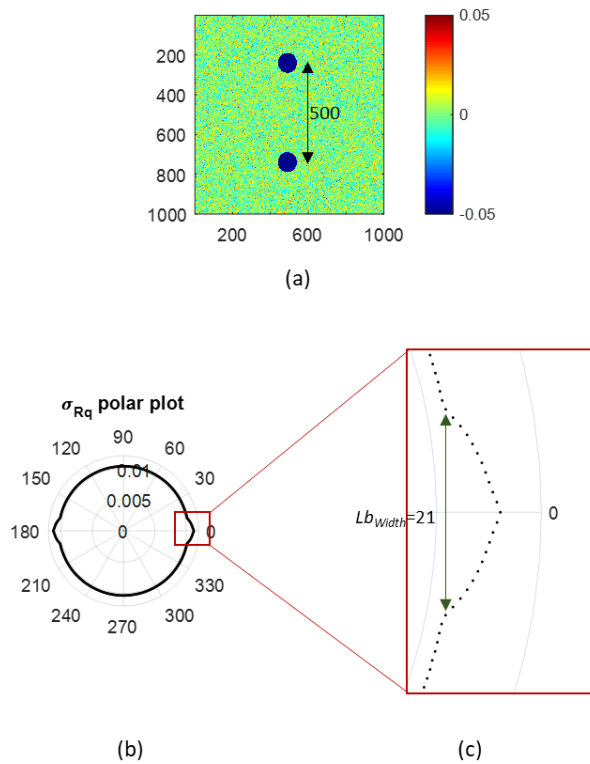


Figure 6-4: a) : MATLAB generated surface with Gaussian distribution of heights with two negative circular features of 50 pixels radius, b) its σ_{Rq} polar plot, and c) the zoomed in region of the lobe in the polar plot.

Figure 6-4 depicts a theoretical surface with a Gaussian distribution of heights with two negative circular features of 50 pixels radius, the spacing between these features from center to center is equal to 500 pixels, the width of the lobe on the σ_{Rq} polar plot based on equation 6-1 is equal to 21 degrees.

6.2.1 Estimation of the number of digs based on the number of peaks

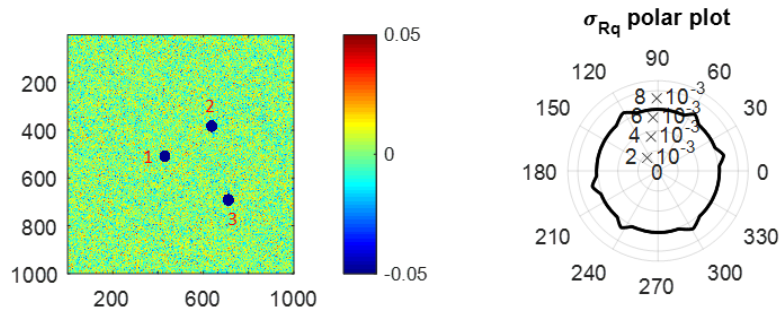


Figure 6-5: MATLAB generated surface with Gaussian distribution of heights with three negative circular features of 50 pixels radius and 0.01 μm depth, and b) its σ_{Rq} polar plot.

In this method of estimating the number of features the identity requirement is not necessary, and the described process works for the circular features that are not identical as well. The number of lobes on the polar plot depends on the location of the features with respect to each other. Figure 6-5 depicts a theoretical surface with its Sq equal to 0.01 μm and three negative circular features of 50 pixels radius and 0.1 μm depth. Based on the systematic analysis of the location of these features with respect to each other it is not possible to have more than two digs aligned at an angle. At each angle where any pair of these features are aligned, a local maximum on the polar plot is produced. Geometrical analysis of the location of the features states that there are three situations, i.e. angles that each different pair can be aligned. These cases are when digs 1 & 2, 1 & 3, and 2 & 3 are aligned in a 180° rotation. However, since in this approach the surface is rotated 360° there will be six angles where two features are aligned and thus six local maximums, i.e. lobes on the polar plot.

In general during rotation when no more than two features align at any one orientation the relationship between the number of features on the surface, f , and the number of lobes on the polar plot, Lb , is equal to twice of the number of all possible connections between any pair of f features, i.e. the combination of two out of f features, see equation 6-2.

$$Lb = \frac{f!}{(f-2)!} \quad (6-2)$$

However, this equation fails to provide the correct number of features if at any orientation more than two digs align. The worst-case scenario is when at one particular orientation all the features align as shown in Figure 6-6. In this case, there is only two lobes on the polar plot, and equation 6-2 results in f equals to two, which is not correct.

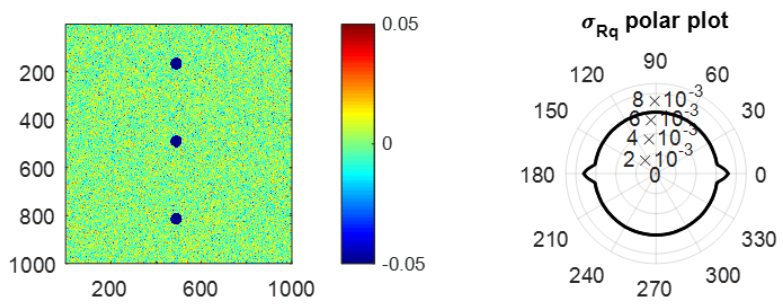


Figure 6-6: MATLAB generated surface with Gaussian distribution of heights and three negative circular features and its σ_{Rq} polar plot.

Figure 6-7 shows the maximum and minimum estimated values of circular features based on the number of lobes on the polar plot, the blue dashed line indicates the ideal case where at each orientation only two features are aligned, and the red dashed line indicates the worst-case scenario where all the features are aligned at a particular orientation.

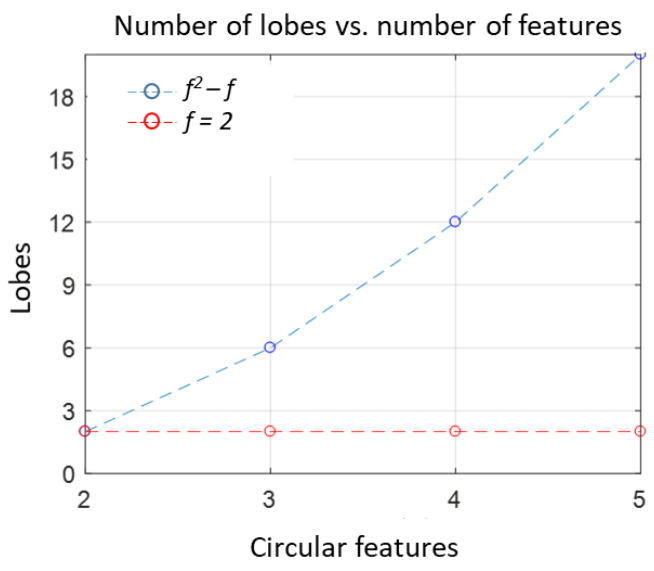


Figure 6-7: The maximum and minimum values of estimation of circular features.

The accuracy of the estimation of the number of features from the number of lobes on the polar plots depends on the ability to 1) identify and 2) count each lobe. For example, for ten circular features on the surface, based on equation 6-2, 90 distinguishable lobes would have to be identified and counted from the polar plot. The maximum number of detectable peaks from the polar plots is given in equation 6-3, and will be detailed in section 6.2.1.4.

In order to identify and count each lobe on the polar plot, and also expand the application of the approach such that it becomes independent of the surface type (milled, ground, etc.), three techniques are used, namely 1) using the mean height value of the columns, $h\mu$, instead of their Rq value in the generation of the polar plot, 2) distortion of the surface, and 3) thresholding.

The first technique makes the magnitude of the lobes at the apex of the lobes larger to help the identification and counting process of lobes. The second technique forcefully removes alignment through imposed distortion of the surface. And the third technique makes the approach less sensitive to non-feature surface texture, it also enables the analysis of the entire field of view.

6.2.1.1 Mean histogram instead of Rq histogram

Standard deviation of a data set is greatly affected by the range of numbers in the data set, larger ranges will lead to larger values of standard deviation. For instance, Figure 6-8(a) shows the histogram for a data set comprising 1000 normally distributed values with their mean and standard deviation equal to zero and one respectively, the range of values for this data set is equal to 6.8. However, if only two values in the same data set are changed to increase the range to 15 the standard deviation increases by 6%, see Figure 6-8(b). Figure 6-8 is an example of how changing the values of only two data points in a distribution consisting of 1000 data points can increase the standard deviation.

This property can be used in order to make the lobes of the polar plots, that are deviations from the circular shape, larger and thus helps the process of identification and counting the lobes on a polar plot.

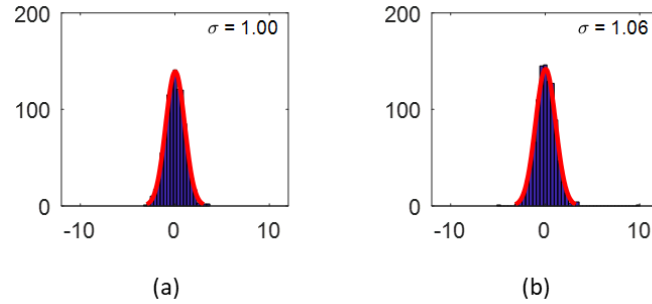


Figure 6-8: a) Histogram of a data set of 1000 normally distributed values with mean and standard deviation, and range equal to 0, 1, and 6.8, b) the same data set when the range is increased to 15.

Figure 6-9(a) depicts a MATLAB generated surface with Sq equal to $0.01 \mu\text{m}$, and with two negative circular features of 100 pixels diameter and $0.1 \mu\text{m}$ depth align at the original orientation, Figure 6-9(c) shows the mean height value of each column, and Figure 6-9(e) shows the Rq value of each column. The same surface is rotated 90° and is shown in Figure 6-9(b), since at this orientation the feature-related columns only contain sections of a single feature their associated mean value decreases and is shown in Figure 6-9(d), so does the Rq values of these columns, see Figure 6-9(f). As is clear from this figure the variations of mean height values is larger than the variations in Rq values, and therefore using the mean height value of columns will lead to larger values of standard deviations.

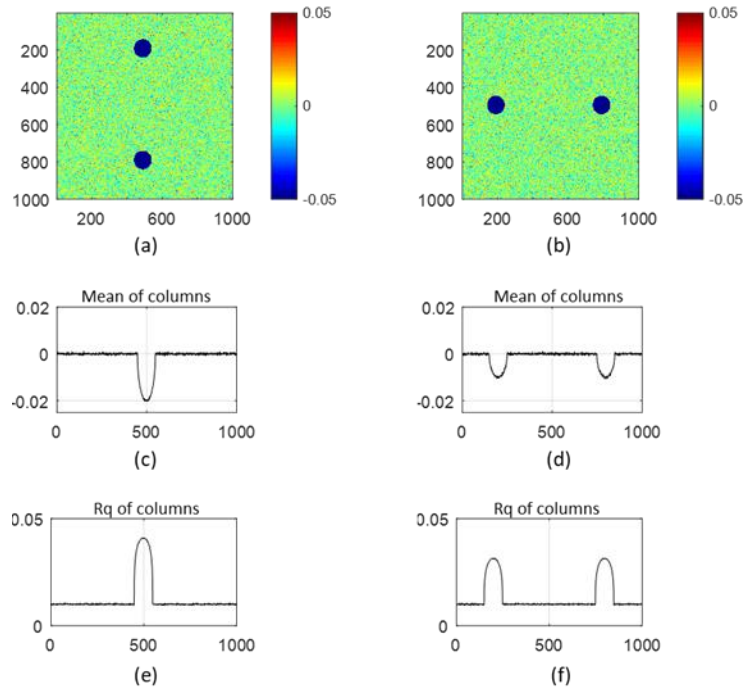


Figure 6-9: a) MATLAB generated surface with two negative circular features, b) the mean of columns plot, c) standard deviation of columns plot, d) the same surface when rotated 90°, e) the mean of columns plot, and f) standard deviation of columns plot.

Figure 6-10 depicts the σ_{Rq} polar plot and $\sigma_{\mu h}$ polar plot of the surface shown in Figure 6-9(a) in one plot. From this figure, it is clear that the deviations of the $\sigma_{\mu h}$ polar plot is larger than the deviation in the σ_{Rq} polar plot. It should be noted that the important point is the deviations of the circular shape, and not the actual magnitude of the points.

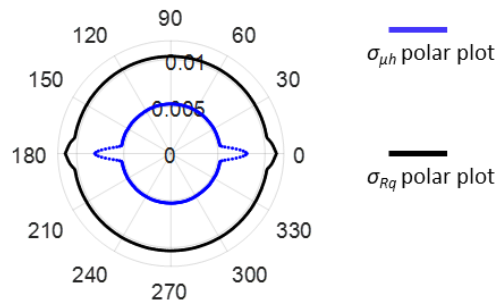


Figure 6-10: σ_{Rq} polar plot and $\sigma_{\mu h}$ polar plot of the surface shown in Figure 6-9(a).

6.2.1.2 Distortion of the surface

In this process, the original surface is distorted in MATLAB with the help of a mapping function. Each pixel in the original surface is an input of the mapping function and the output will

be the mapped value. This mapping function could be an angular mapping function or a polynomial function.

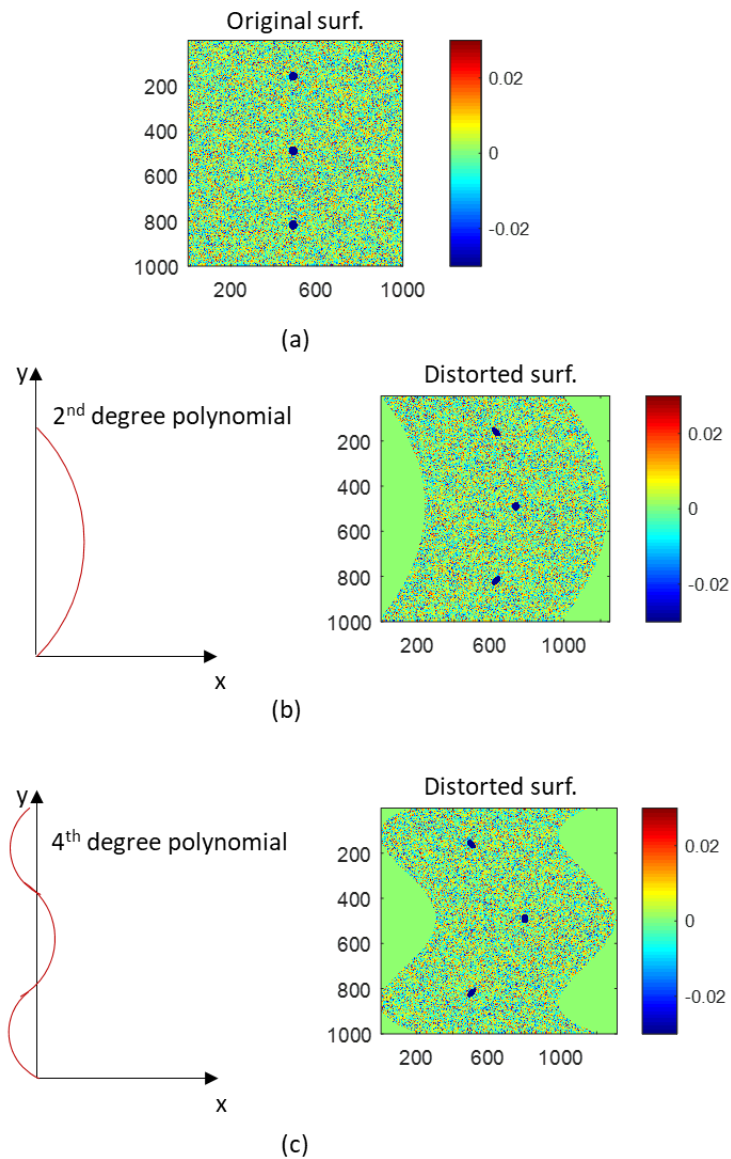


Figure 6-11: a) MATLAB generated surface with Gaussian distribution of heights with three aligned circular features, the same surface when it is mapped with b) a second degree polynomial, and c) a fourth degree polynomial.

Figure 6-11(a) depicts a theoretical surface with three aligned negative circular features of 40 pixels diameter, and 0.05 μm depth. This surface is mapped with a second degree polynomial in Figure 6-11(b), features' location is changed, and it is impossible to have all of them aligned at one particular orientation. Figure 6-11(c) shows the same surface when it is distorted with the help of

a fourth order polynomial, again it is not possible to have more than two features aligned at one particular angle. So, by distorting the original surface the effect of more than two features aligned at each angle is rectified.

Distortion of the original surface will change the shape of surface features and they are not perfectly circular anymore, however since the goal is to count the number of features, and this depends on the number of lobes on the polar plot, this change in the geometry of features will not cause any issue.

The size of the original surface will also change after distortion process, and some zero values are added to the output surface. Thresholding is done to resolve this issue as well.

6.2.1.3 Thresholding

In this technique a threshold height value is selected, all of the height values of the surface that have an absolute value smaller than this threshold value are assigned a zero value, and all of the height values with absolute values larger than this threshold value are assigned an arbitrary non-zero constant value. This process keeps the features on the surface (both positive and negative) and replaces all of the non-feature related height values with zero. Figure 6-12(a) depicts the thresholded surface in Figure 6-11(b), the threshold height is selected equal to $0.04 \mu\text{m}$, and Figure 6-12(b) shows the thresholded surface in Figure 6-11(c).

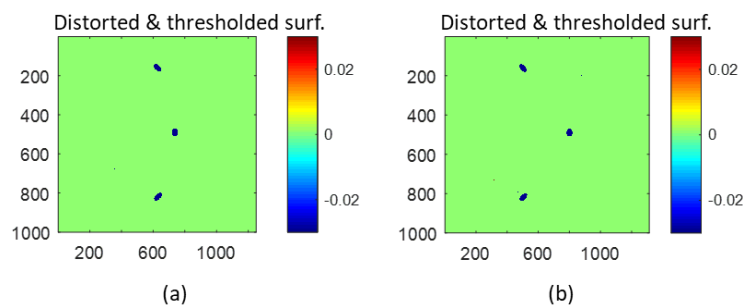


Figure 6-12: a) The surface in Figure 6-11(b) after thresholding, and b) the surface in Figure 6-11(c) after thresholding.

Since this process only keeps the feature-related pixels and sets the rest of the height values to zero every type of surface texture can be analyzed for estimating the number of features present on them. For instance, Figure 6-13(a) shows a diamond turned surface with three negative circular features of 30 pixels diameter and 15 nm depth present on its surface, these features were put on the surface in MATLAB. Setting the threshold height equal to 10 nm, the thresholded surface is shown in Figure 6-13(b). It should be noted that selection of the threshold height value depends on the application of the surface, and the importance and effect of surface features on part's functionality.

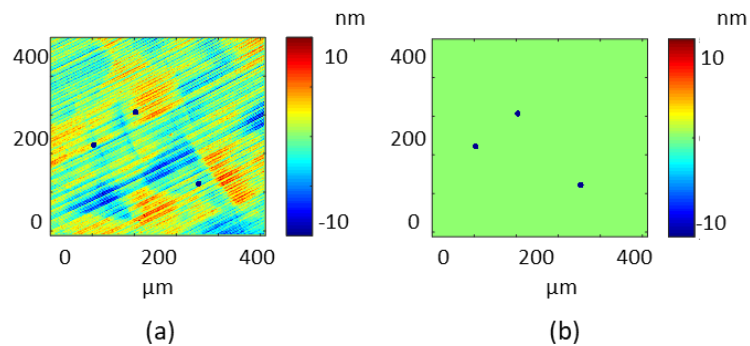


Figure 6-13: a) A diamond turned surface with three negative circular features of 30 pixels diameter and 10 nm depth, measured with ZeGage CSI 20× objective, and b) the same surface after it is thresholded.

This way of thresholding converts all of the features that have an absolute height value greater than the threshold value, therefore all of the positive and negative features will be the same type after thresholding. However, if the thresholding is done such that all of the values that are larger than the threshold height value are set to zero and all of the height values that are smaller than the threshold height value to a negative arbitrary constant, then separation of negative and positive features becomes possible.

Another advantage of thresholding technique is that it makes the analysis of the whole field of view possible by putting the thresholded surface into a bigger zero matrix such that the size of the cropped section of this new matrix, n_{new} , is equal to the size of the original matrix, n , see Figure 6-14.

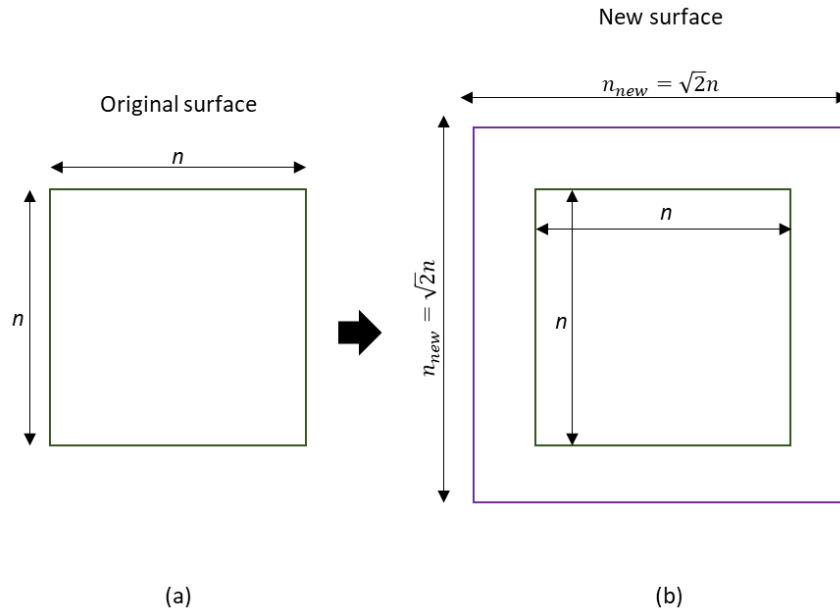


Figure 6-14: a) The thresholded $n \times n$ matrix, and b) the new $\sqrt{2}n \times \sqrt{2}n$ zero matrix.

6.2.1.4 Peak detection details

In order to analyze the polar plot and automatically count the number of peaks the value of each point in the $\sigma_{\mu h}$ polar plot, p_i , is compared to the values of pd neighboring number of points such that the p_i point is the middle point; if p_i has the maximum value in this range then it is counted as a lobe, see Figure 6-15. Based on the selection of pd the maximum number of lobes that can be detected in a polar plot is given in equation 6-3.

$$lobes_{\max} = \frac{360}{\Delta\theta \times pd} \quad (6-3)$$

Where $\Delta\theta$ is the rotational increment.

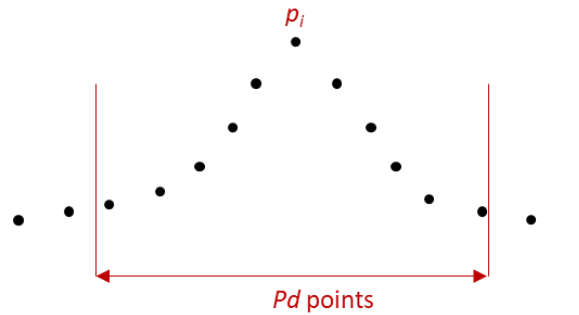


Figure 6-15: Point p_i and the p_d neighboring points in the polar plot.

6.2.1.5 Estimation of number of features on the surface

Figure 6-16(a) depicts the worst case scenario on a theoretical surface with S_q equal to $0.01 \mu\text{m}$ where all of the negative circular features of 50 pixels diameter and $0.1 \mu\text{m}$ depth are aligned at a particular orientation, σ_{Rq} polar plot of this surface is shown in Figure 6-16(b). There are two lobes on this polar plot, thus based on equation 6-2 the number of features is estimated as two, which is not correct. However, if this surface is distorted with respect to a fourth degree polynomial, and then thresholded with a threshold height value equal to $0.04 \mu\text{m}$, see Figure 6-16(c), the final $\sigma_{\mu h}$ polar plot has six lobes, Figure 6-16(d). Consequently using equation 6-2 will lead to the number of features, f , and equals to three.

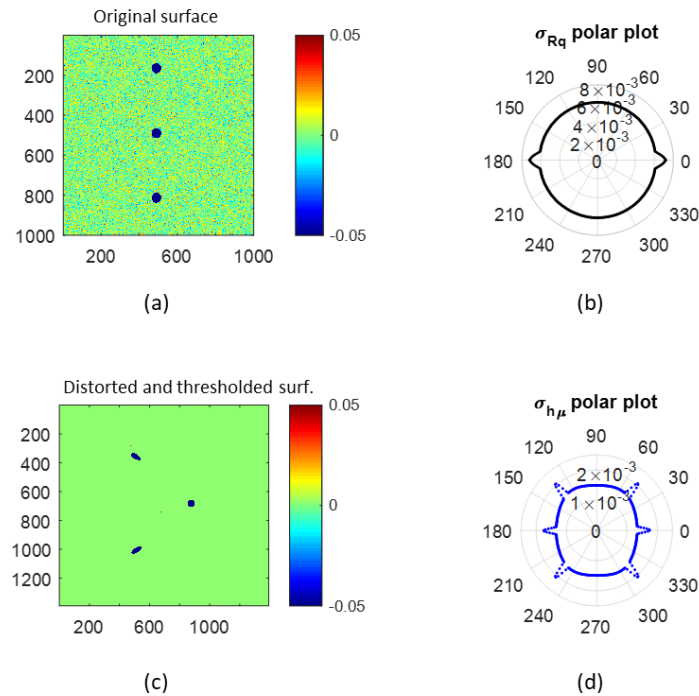


Figure 6-16: a) MATLAB generated surface with three negative circular feature of 50 pixels diameter and $0.1 \mu\text{m}$ depth, b) its σ_{Rq} polar plot, c) the same surface after it is thresholded and distorted with a fourth order polynomial and d) its $\sigma_{h\mu}$ polar plot.

It should be noted that in an ideal case where only two features align at each angle of rotation processing the surface with the three above mentioned techniques will not affect the resulting number of lobes on the polar plot, and thus will not affect the estimation of the quantity of the features. To further explain this case note that Figure 6-17(a) depicts a theoretical surface with three negative circular features of 50 pixels diameter and $0.1 \mu\text{m}$ depth, at any orientation on this surface there is only two features aligned, and thus its $\sigma_{h\mu}$ polar plot has six lobes, Figure 6-17(b). This surface is then mapped with the help of a fourth order polynomial and thresholded with a threshold height value equal to $0.04 \mu\text{m}$, see Figure 6-17(c); and its $\sigma_{h\mu}$ polar plot is shown in Figure 6-17(d) which has six lobes. Therefore, estimation of the number of features based on equation 6-2 results in three features in both cases.

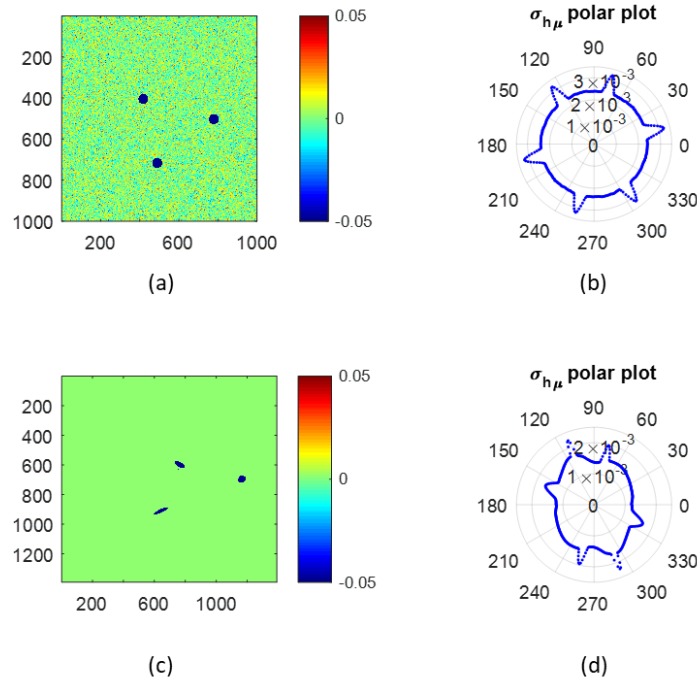


Figure 6-17: a) MATLAB generated surface with three negative circular feature of 50 pixels diameter and $0.1 \mu\text{m}$ depth, b) its $\sigma_{\mu h}$ polar plot, c) the same surface after it is thresholded and distorted with a fourth order polynomial and d) its $\sigma_{\mu h}$ polar plot.

This method, however, is only able to estimate the number of features on the surface, and is not able to provide information about the geometry of the features, i.e. depth and diameter.

6.2.2 Estimation of quantity and diameter of circular features from polar plots

In this method of estimating the number of circular features as well as their diameter two assumptions have to be made. First all of the multiple circular features must be identical (as was mentioned at the beginning of this section), and the second that features must not be collinear in at least one orientation. The details of these constraints and also failure to meet these requirements and its effect on the results will be discussed at the end of this section.

In this approach instead of counting the number of lobes on the polar plot and estimating the number of features based on equation 6-2, the minimum radius of the $\sigma_{\mu h}$ polar plot, r_{min} , is used in order to estimate the number of features as well as their diameter.

6.2.2.1 Governing equations and constraints

Figure 6-18(a) shows a thresholded surface with a single negative circular feature with diameter of 100 pixels and depth of 0.1 μm , the mean height value of the columns of this surface is shown in the graph in Figure 6-18(b), for feature-free columns this mean value is zero, and for the columns containing sections of the feature, i.e. feature-related columns, the mean height value depends on the number of feature-related pixels, and is maximum for the column that contains the diameter of the feature. Standard deviation of this graph is the radius of the $\sigma_{\mu h}$ polar plot and is given in equation 6-4.

$$r = \sqrt{\frac{(n-2R)\left(\frac{-2d}{n^2} \sum_{i=1}^R Y_i\right)^2 + 2 \sum_{i=1}^R \left(\frac{Y_i d}{n} - \frac{2d}{n^2} \sum_{j=1}^R Y_j\right)^2}{n}} \quad (6-4)$$

Where Y_i is the length of the section of the circular feature that is contained within a column, R is the radius of the feature, d is the depth, and n is the size of the surface.

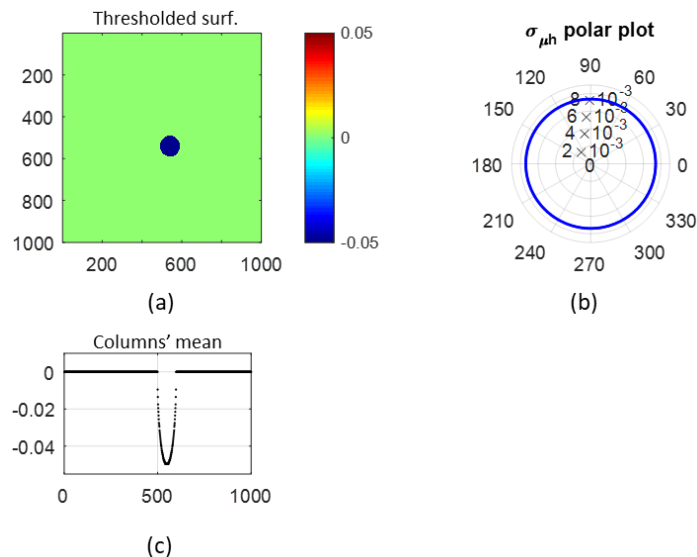


Figure 6-18: Thresholded surface with a circular negative feature with 100 pixels diameter, b) its $\sigma_{\mu h}$ polar plot, and c) columns' mean plot.

Equation 6-4 is rather complicated to solve because of the summations in the numerator, and requires an iterative approach to find its solution. In order to simplify equation 6-4 the circular feature is converted to a square with the same amount of area, see Figure 6-19, the side length of this square is given in equation 6-5.

$$s = R\sqrt{\pi} \quad (6-5)$$

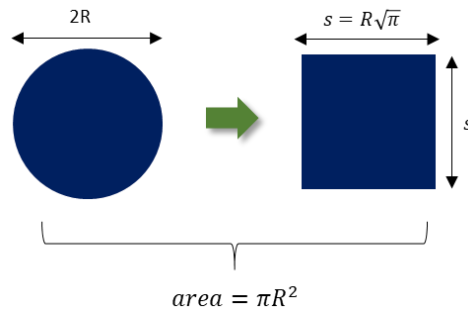


Figure 6-19: Conversion of a circular feature to a square with equal areas.

Figure 6-20 visualizes this conversion, the negative circular feature with the diameter equal to 100 pixels in this thresholded surface, Figure 6-20(a), is converted to a square with the side length equal to 88 pixels, Figure 6-20(b). The area of the features in both surfaces are equal. Figure 6-20(d) shows the mean values of the columns of the surface with converted feature, the standard deviation of this graph is equal to the minimum radius of the surface's polar plot.

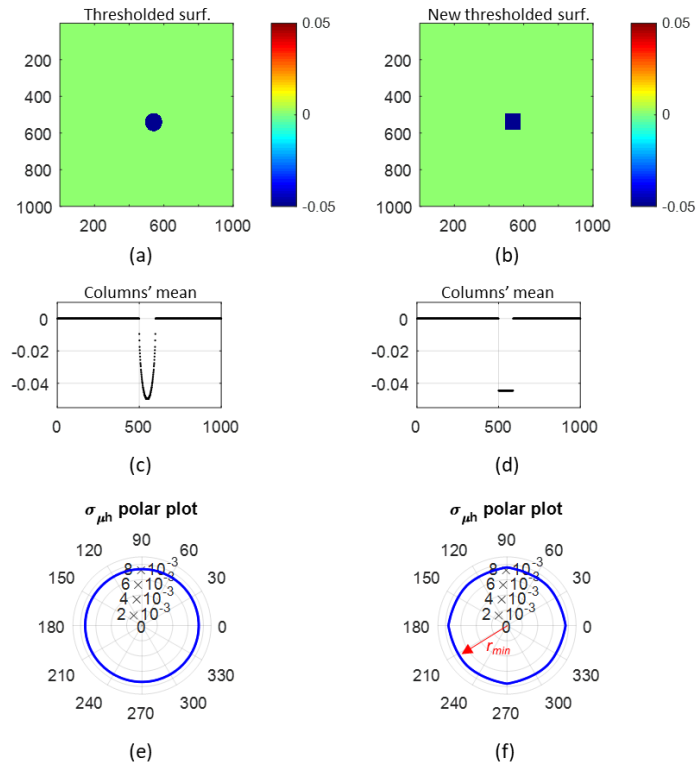


Figure 6-20: a) Thresholded surface with a circular negative feature with 100 pixels diameter, b) the same surface after the circular feature is converted to a square, c) columns' mean plot of (a), d) columns' mean plot of (b), e) $\sigma_{\mu h}$ polar plot of (a), and f) $\sigma_{\mu h}$ polar plot of (b).

Figure 6-21 depicts the general form of the graph of mean height values of the columns of a surface with one square feature with its side length equal to s . This is a set of $\sqrt{2}n$ numbers in which s number of points are non-zero and the rest are zero (the surface is thresholded).

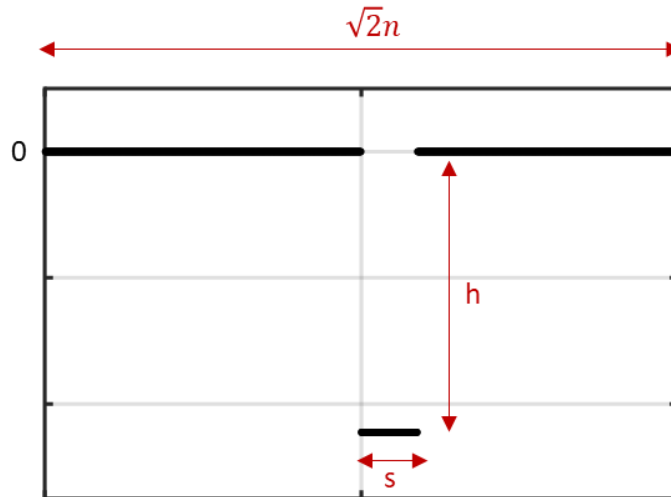


Figure 6-21: General form of the graph of columns mean height values for a surface containing a square feature.

The average value of this set of numbers is equal to:

$$\mu = \frac{sh}{\sqrt{2}n} \quad (6-6)$$

Where s is the side length of square feature, h is the average value of the columns containing the feature, and n is the size of the surface.

The mean height value of each of the columns that contain the square feature is given in equation 6-7:

$$h = \frac{sd}{\sqrt{2}n} \quad (6-7)$$

Where d is the depth of the feature.

Therefore, by replacing h in equation 6-6 with the value of equation 6-7, the mean value of the set of numbers shown in Figure 6-21 is equal to:

$$\mu = \frac{s^2d}{2n^2} \quad (6-8)$$

And the standard deviation of this set of numbers (Figure 6-21) is equal to:

$$\sigma = \sqrt{\frac{(\sqrt{2n} - s)(-\mu)^2 + s(h - \mu)^2}{\sqrt{2n}}} \quad (6-9)$$

By putting equation 6-8 into equation 6-9 and simplifying the result, the standard deviation of the data set which is the minimum radius of the $\sigma_{\mu h}$ polar plot is equal to:

$$r_{\min} = \sigma = \sqrt{\frac{\sqrt{2}nd^2s^3 - d^2s^4}{4n^4}} \quad (6-10)$$

Where r_{\min} is the minimum radius of the $\sigma_{\mu h}$ polar plot, d is the depth of the feature, s is the side length of the square feature, and n is the size of the surface. It should be noted that the $\sqrt{2}$ that appears in these equations is due to the fact that the original surface after thresholding is put into a bigger zero matrix whose dimensions are $\sqrt{2}n$, (see section 6.2.1.3).

The associated error of the calculated radius of the $\sigma_{\mu h}$ polar plot after the conversion of a circular feature to a square one with equal areas is shown in Figure 6-22, in this graph the horizontal axis is given as the percentage ratio of the radius of the feature, R , over the size of the surface, n , it is clear that for radii less than 30% of the surface size the error between the exact and estimate of the radius of the $\sigma_{\mu h}$ polar plot is less than 5%. This graph shows the percentage difference between equation 6-4 and equation 6-10.

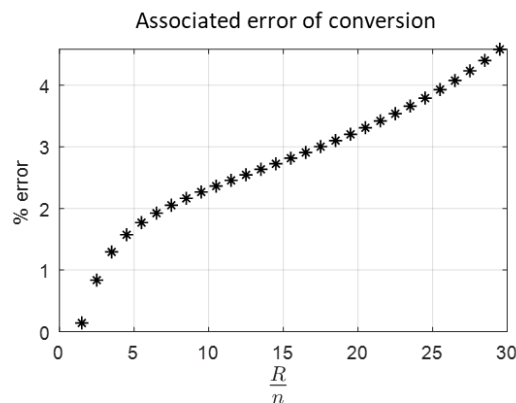


Figure 6-22: Associated error of the calculated radius of the $\sigma_{\mu h}$ polar plot after converting a circular feature to a square one with equal areas.

Same approach that was taken for the single circular feature can be taken for the surfaces with multiple circular features. As is shown in Figure 6-23 each one of the circular features on the surface with their radius equal to R will be converted to a square with equal area, and the side length of s . The minimum radius of the $\sigma_{\mu h}$ polar plot is achieved by modifying equation 6-10 for the surfaces with multiple circular features, and is given in equation 6-11:

$$r_{\min_a} = \sqrt{\frac{\sqrt{2}\alpha n s^3 d^2 - (\alpha d)^2 s^4}{4n^4}} \tag{6-11}$$

Where α is the quantity of the features on the surface, and r_{\min_a} is the minimum radius of the $\sigma_{\mu h}$ polar plot. This minimum radius is the radius from which all the deviation in the polar plot start.

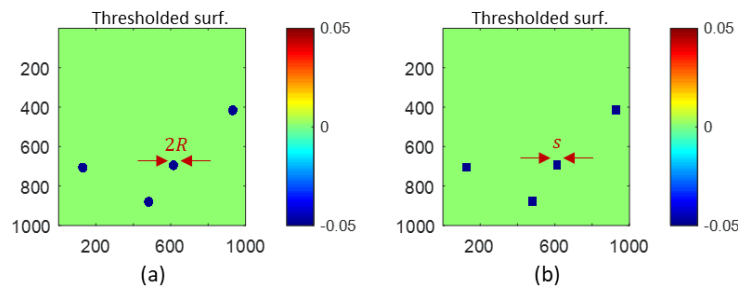


Figure 6-23: a) A thresholded surface with four negative circular features, b) the same surface after all the circular features are converted to squares with equal areas.

Figure 6-24(a) depicts a thresholded surface with four negative circular features, and its $\sigma_{\mu h}$ polar plot, the red circle in Figure 6-24(b) is the circle with its radius equal to the minimum radius, and as stated before all the deviations of the polar plot start from this circle.

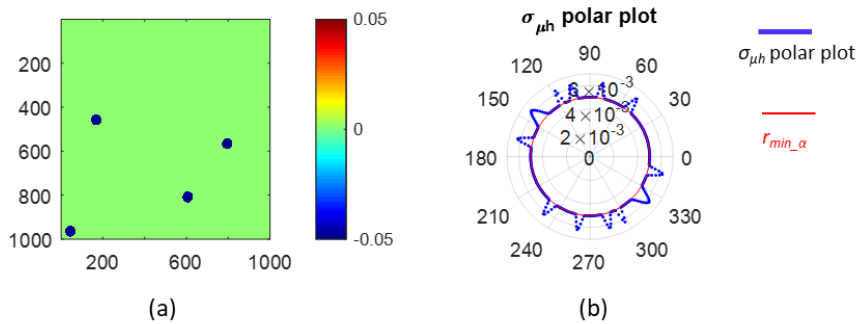


Figure 6-24: a) A thresholded surface with four negative circular features, b) $\sigma_{\mu h}$ polar plot and the circle with r_{\min_a} radius.

Equation 6-11 results in the correct answer if and only if the two mentioned constraints are met, (the first one is that all of the features must be identical, and the other is that there must not be any collinearity between the features in at least one orientation). Lack of collinearity means that at least at one angle of rotation each column must only go through one feature and not more. Figure 6-25(a) shows a surface with two features that are not collinear at θ equal to 0° , whereas in Figure 6-25(b) features are non-collinear and thus the requirement of equation 6-11 is met.

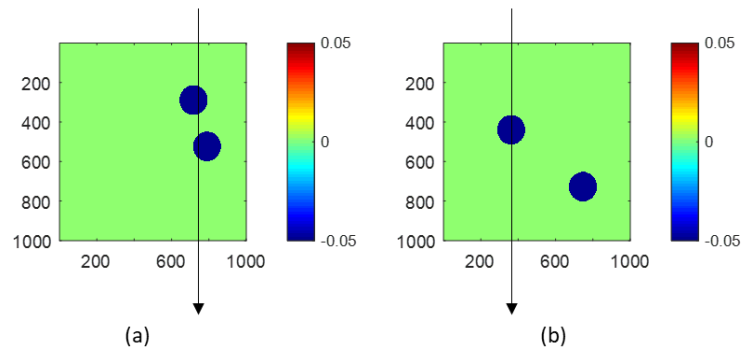


Figure 6-25: a) A thresholded surface with two negative circular features when overlapping exists, b) when overlapping does not exist.

Based on these limitations and in order for the equation 6-11 to be exact, the maximum number of identical features on the surface is when they are distributed along the diagonal of the surface, Figure 6-26, this maximum number is given in equation 6-12:

$$f_{\max} = \text{round}\left(\frac{n}{\sqrt{2}R}\right) \quad (6-12)$$

Where f_{\max} is the maximum number of identical features, n is the size of the surface, and R is the radius of the circular features.

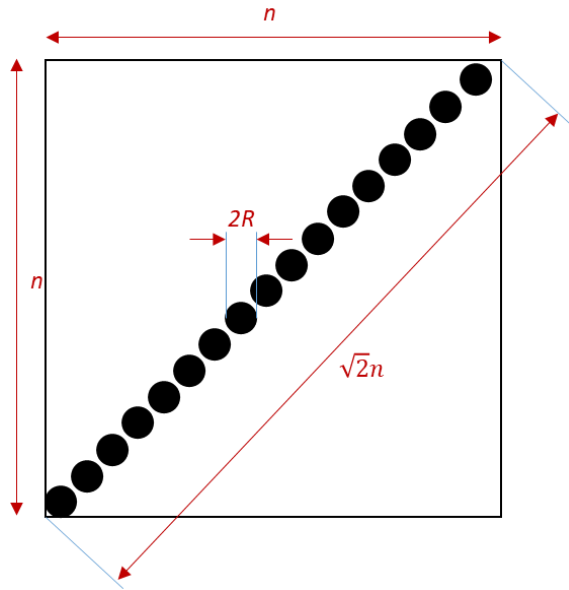


Figure 6-26: Schematic representation of the case when all of the circular features are distributed along the diagonal of the surface.

6.2.2.2 Estimating the quantity and radius of the circular features

Equation 6-10 gives the minimum radius of the $\sigma_{\mu h}$ polar plot for a surface that contains a single circular feature, and equation 6-11 results in the minimum radius of this polar plot for a surface that contains multiple identical circular features. Equation 6-11 has two unknowns that are the quantity of features, α , and s , which is the side length of a square with its area equal to the area of one circular feature. In order to find out these two unknowns a second equation with these two unknowns is needed.

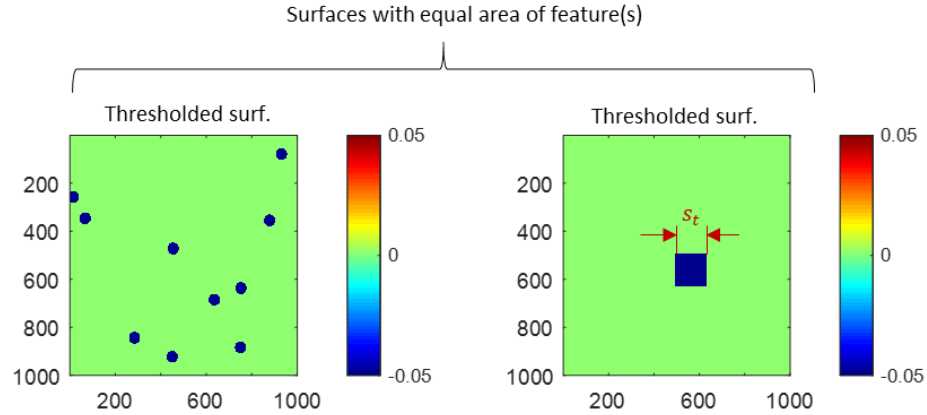


Figure 6-27: a) A thresholded surface with multiple negative circular features, and b) a thresholded surface with a single square feature with the same area of the summation of multiple features' area.

This second equation can be achieved by having a thresholded surface with a single square feature present on its surface with its area equal to the total area of all of the multiple circular features, A_c , see Figure 6-27. The side length of this single square feature is given in equation 6-13.

$$s_t = s\sqrt{\alpha} = \sqrt{A_c} \quad (6-13)$$

Where α is the quantity of the circular features, R is their radius, s is the side length of a square with its area equal to the area of one circular feature, and s_t is the side length of the square with its area equal to the area of all of the circular features.

The minimum radius of $\sigma_{\mu h}$ polar plot, r_{\min_t} , of the surface containing the single square based on equation 6-10 is equal to:

$$r_{\min_t} = \sqrt{\frac{\sqrt{2}nd^2s_t^3 - d^2s_t^4}{4n^4}} \quad (6-14)$$

Replacing the value of s_t in this equation with the right-hand side of equation 6-13 results in:

$$r_{\min_t} = \sqrt{\frac{\sqrt{2}n\alpha\sqrt{\alpha}d^2s^3 - d^2\alpha^2s^4}{4n^4}} \quad (6-15)$$

Equation 6-15 is the second equation along with equation 6-11 that forms a system of equations that can be solved to calculate the quantity of the features, and their radius. This system on equation is given in equation 6-16:

$$\left[\begin{array}{l} r_{\min_t} = \sqrt{\frac{\sqrt{2n\alpha}\sqrt{\alpha d^2 s^3 - d^2 \alpha^2 s^4}}{4n^4}} \\ r_{\min_a} = \sqrt{\frac{\sqrt{2n\alpha}d^2 s^3 - d^2 \alpha^2 s^4}{4n^4}} \end{array} \right] \quad (6-16)$$

Solution of this system of equations for the quantity of the features is given in equation 6-17.

$$\alpha = \left\{ \frac{\sqrt{2n} \left(\frac{r_{\min_t}}{r_{\min_a}} \right)^2}{\left[\left(\frac{r_{\min_t}}{r_{\min_a}} \right)^2 - 1 \right] \sqrt{A_c} + \sqrt{2n}} \right\}^2 \quad (6-17)$$

Where α is the quantity of identical circular features on the surface, r_{\min_a} and r_{\min_t} are known values from the $\sigma_{\mu h}$ polar plots, A_c is also known from counting the non-zero pixels in the thresholded surface in MATLAB (or other computer systems). Once the number of features is calculated their radius can be calculated from:

$$R = \sqrt{\frac{A_c}{\alpha\pi}} \quad (6-18)$$

6.2.2.3 Application in quality control process

The minimum radius, r_{\min} , of the $\sigma_{\mu h}$ polar plot could be used as a measure of surface's quality, when it is compared to the minimum radius of the $\sigma_{\mu h}$ polar plot of a surface with an accepted feature with its radius equal to R_s , see Figure 6-28(a).

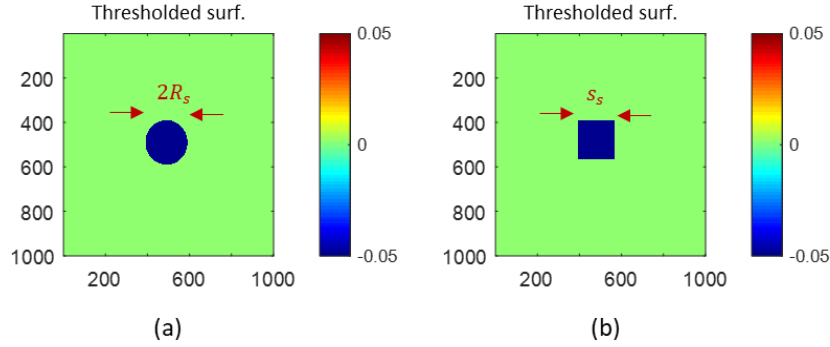


Figure 6-28: a) A thresholded surface with the accepted circular feature, and b) the accepted circular feature converted to a square with equal area.

This accepted circular feature could then be converted to a square with equal area, and the side length of s_s , Figure 6-28(b).

$$s_s = \sqrt{\pi} R_s \quad (6-19)$$

A surface could be defined as acceptable or passed if the minimum radius of its $\sigma_{\mu h}$ polar plot is smaller than the minimum radius of the $\sigma_{\mu h}$ polar plot of the surface with the accepted feature, and similarly a surface fails if its minimum radius is larger than the minimum radius of the surface with the accepted feature.

In order to find out for which combination of numbers of identical circular features and their radius the minimum radius of the $\sigma_{\mu h}$ polar plot of the surface containing them, r_{min_a} , is equal to the minimum radius of the $\sigma_{\mu h}$ polar plot of the surface with the accepted feature, r_{min_s} , their minimum radius equations are set equal to each other:

$$\sqrt{\frac{\sqrt{2n\alpha d^2 s^3 - \alpha^2 d^2 s^4}}{4n^4}} = \sqrt{\frac{\sqrt{2nd^2 s_s^3 - d^2 s_s^4}}{4n^4}} \quad (6-20)$$

Simplifying above equation results in:

$$\alpha^2 s^4 - \sqrt{2n\alpha} s^3 + (\sqrt{2n} s_s^3 - s_s^4) = 0 \quad (6-21)$$

It should be noted that this equation does not depend on the depth of the features, d , as it is a common factor in all of the terms in the numerator of the two equations and cancels out when simplifying equation 6-20.

For a choice of accepted feature size, equation 6-21 could be solved for different values of number of features, α , and s . For instance, on a 1000×1000 pixel surface when the radius of the accepted feature is equal to 75 pixels, $R_s = 75$ pixels, solving equation 6-21 results in the graph of Figure 6-29. The x-axis in this graph is the radius of features given in percentage of the size of the surface, and the y-axis is the number of features.

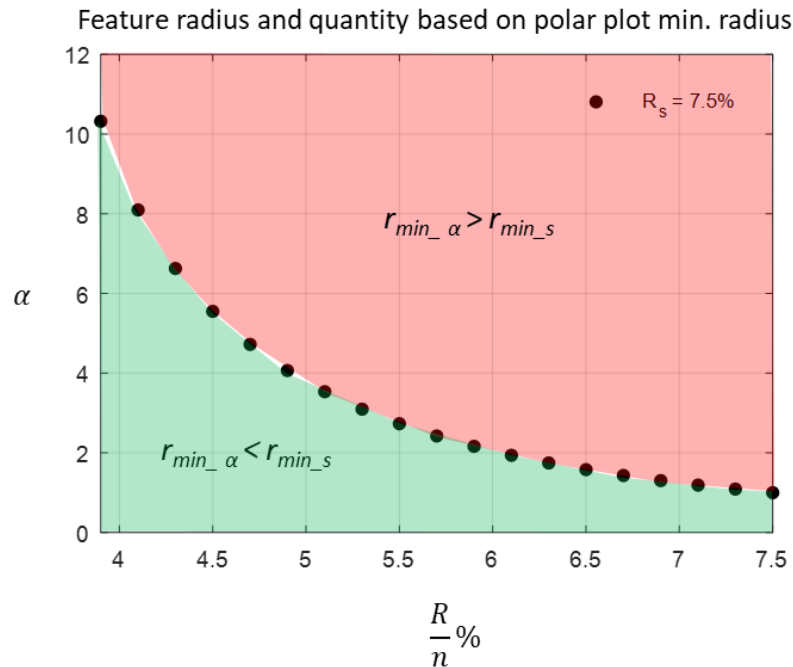


Figure 6-29: Number of allowed circular features, α , based on a given accepted feature.

If the combination of the number of features and their radius is below the curve in the graph in Figure 6-29 then the minimum radius of the surface with multiple features is smaller than the minimum radius of the surface with the accepted feature. Similarly, if this combination goes above the curve then the minimum radius of the surface with multiple features is larger than the minimum radius of the surface with the accepted feature. Finally, if the combination of the number of features and their radius is exactly on the curve then the minimum radius for both surfaces are equal. Similar

graphs for different sizes of surfaces and accepted features could be generated. This graph is based on the minimum radius of the $\sigma_{\mu h}$ polar plot, and the curve is the boundary at which the minimum radius of the surface with multiple features is equal to the minimum radius of the surface with the accepted feature.

Similar graph for a 1000×1000 pixel surface can be generated based on the cumulative area of the features with equal areas, A_c , and the area of the accepted feature, A_s . The curve in the graph in Figure 6-30 shows the boundary at which the cumulative area of all of features on the surface is equal to the area of the accepted feature whose radius is 7.5% of the surface size, i.e. 75 pixels. If the combination of number of features and their radius is below this curve then the cumulative area of multiple features is less than the area of the accepted feature, and similarly if the combination goes above the curve then the cumulative area of features is larger than the area of the accepted feature.

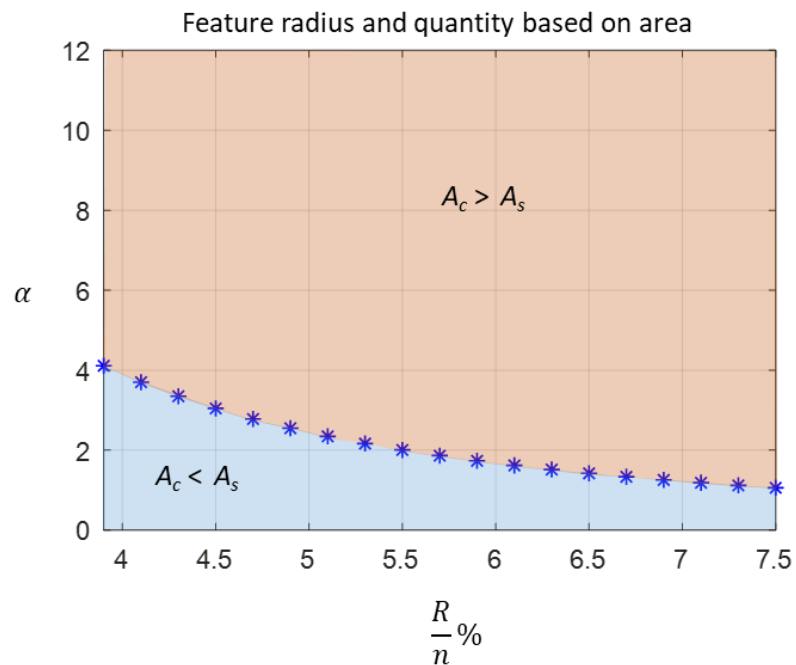


Figure 6-30: Number of allowed circular features, α , based on the area of a given accepted feature, A_s .

Plotting both curves in Figure 6-29 and Figure 6-30 in one graph is shown in Figure 6-31, in this graph region one is the region where the minimum radius and the cumulative area of the

features of the surface with multiple features is smaller than the minimum radius and the area of the accepted feature of the surface with the accepted feature. Region two is where the cumulative area of all of the features is larger than the area of the accepted feature, but the minimum radius of this surface is smaller than the minimum radius of the surface with the accepted feature. And region three is the region where both the cumulative area of all of the features and the minimum radius of the surface containing them is larger than the area of the accepted feature and the minimum radius of the accepted surface.

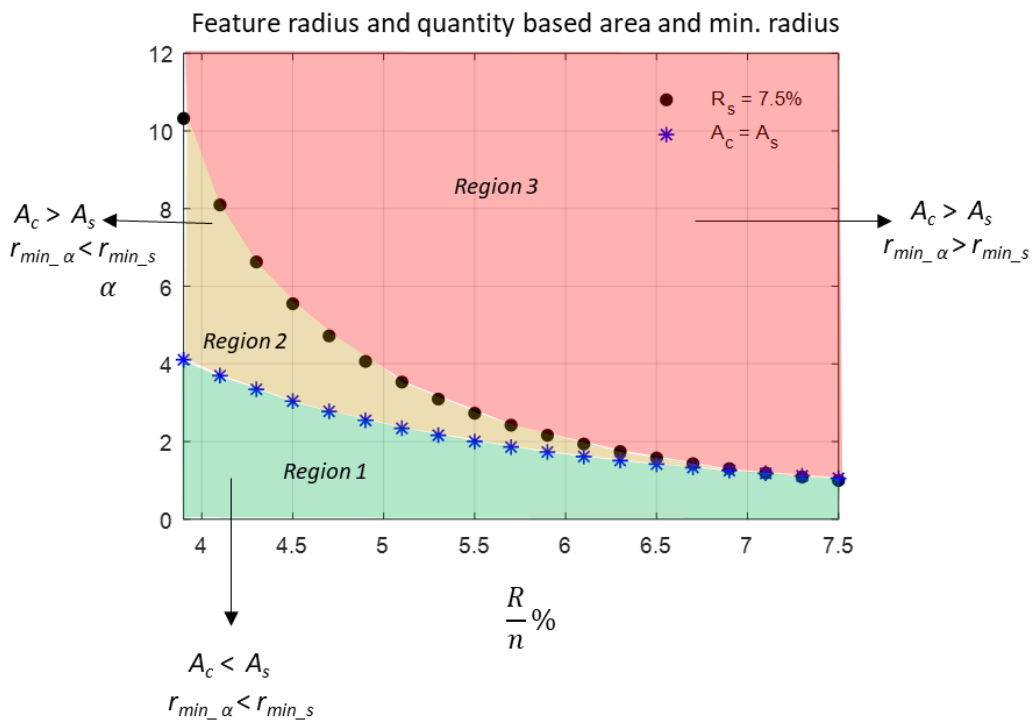


Figure 6-31: Number of allowed circular features, α , based on a given accepted feature.

The minimum radius of a surface with a single circular feature, when compared to minimum radius of the surface with the accepted feature is summarized in Table 6-1.

Table 6-1: Comparison between single circular feature radius and accepted feature radius, with their minimum radius of the $\sigma_{\mu h}$ polar plots.

R : radius of the single feature R_s : radius of the accepted feature	r_{min} : min. radius of the surface's polar plot r_{min_s} : min. radius of the accepted feature surface's polar plot
$R < R_s$	$r_{min} < r_{min_s}$
$R = R_s$	$r_{min} = r_{min_s}$
$R > R_s$	$r_{min} > r_{min_s}$

The minimum radius of a surface with multiple features, α , with their radius equal to R when compared to a surface with a accepted feature based on the graph of Figure 6-31 is summarized in Table 6-2.

Table 6-2: Number and radius of multiple circular features combination, and their characteristics in comparison with the accepted feature.

α : quantity of the multiple features R : radius of each feature	r_{min_α} : min. radius of the surface r_{min_s} : min. radius of the accepted surface A_c : cumulative area of all features A_s : area of the accepted feature
α and R in region 1	$r_{min} < r_{min_s}$ $A_c < A_s$
α and R in region 2	$r_{min} < r_{min_s}$ $A_c > A_s$
α and R in region 3	$r_{min} > r_{min_s}$ $A_c > A_s$

It is worth reminding that all the above calculations are correct when the two requirements, that are identical features, and no collinearity between features in at least one orientation, are met. The next section explains the effect of failure of meeting the requirements in the calculations.

6.2.2.4 Collinear features

Non-collinearity of the features in at least one orientation is a constraint for the equation 6-17 and 6-18 to result in the correct answer. However, when the circular features are located on the surface such that at any orientation two or more than two of them are collinear the results of equations 6-17 and 6-18 are not correct anymore. The quantity of the features is underestimated and the radius of them is overestimated when compared to the situation where features are non-collinear.

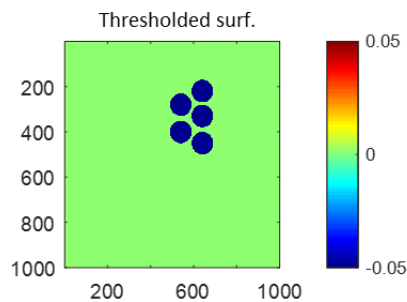


Figure 6-32: A thresholded surface with five negative circular and collinear features.

Collinearity of the features causes the minimum radius of the $\sigma_{\mu h}$ polar plot of the surface that contains them to increase. This increase in the $r_{min,\alpha}$ will decrease the calculated quantity of the features based on equation 6-17, see Figure 6-33, and therefore based on equation 6-18 the decrease in α causes an increase in the calculated radius, R .

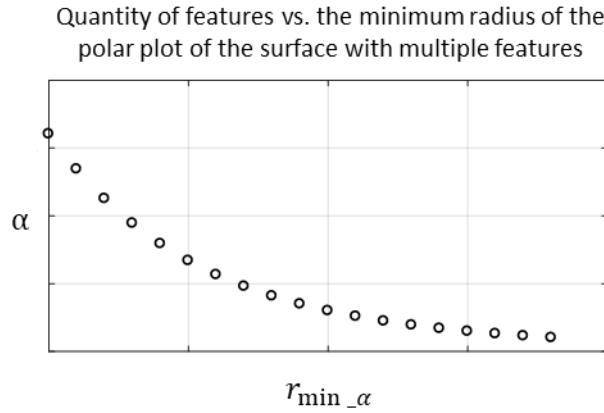


Figure 6-33: Behavior of the α versus the minimum radius of the surface with multiple collinear features.

6.2.2.5 Non-identical circular features

Presence of identical circular features on the surface was another constraint for equations 6-17 and 6-18 to result in the correct answers. Failure to meet this constraint causes the quantity of the features to be underestimated via equation 6-17. To explain this situation suppose that there are multiple circular and non-identical features on the surface with their cumulative area equal to A_c . Using equation 6-17 and 6-18 results in a number for the quantity of the features, α , and a number for their radius, R respectively. This means that A_c is distributed in α number of identical features with their radius equal to R . However, when the features are not identical the total number of them, independent of their radius, must be larger than calculated α in order to have the same amount of overall area, A_c .

$$\alpha_1\pi R_1^2 + \alpha_2\pi R_2^2 + \dots + \alpha_N\pi R_N^2 = \alpha\pi R^2 = A_c \quad (6-22)$$

Where $\alpha_1, \alpha_2, \dots, \alpha_N$ are the quantity of features with their radius equal to R_1, R_2, \dots, R_N respectively. In order for equation 6-22 to be always correct, and given the fact that the quantity of the features on the surface is an integer value, the total number of non-identical features on the surface must satisfy equation 6-23.

$$\alpha_1 + \alpha_2 + \dots + \alpha_N \geq \alpha \quad (6-23)$$

If the left-hand side of equation 6-23 is less than its right-hand side then the initial criterion, equation 6-22, fails. Equation 6-23 means that the number of calculated quantity of the features from equation 6-17 is always equal or less than the actual number of features on the surface. In other words, α is equal to the actual of number of features when they are all identical, and it is less than the actual number of features when they are non-identical.

Figure 6-34(a) depicts a thresholded surface containing four negative identical circular features with their radius equal to 50 pixels, and two features with 35 pixels radius. Figure 6-34(b) has the same amount of cumulative area of features but distributed in two features with 50 pixels radius and six features with 35 pixels radius. For the surface in Figure 6-34(a) equation 6-17 and 6-18 result in the number of identical features equal to 5.51. For the surface shown in Figure 6-34(b), the result of equation 6-17 is equal to 7.25 however; the actual number of features on the surface is equal to eight. Clearly for both of the surfaces the result of equation 6-17 is less than the actual number of features.

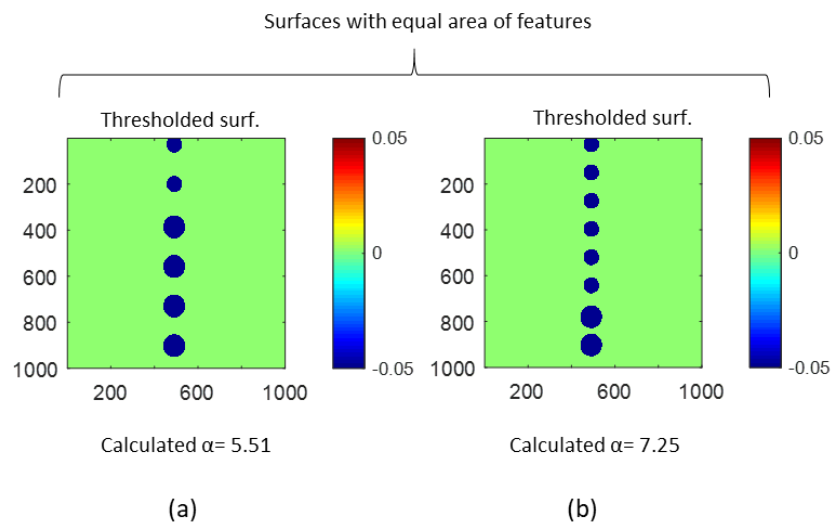


Figure 6-34: A thresholded surface with a) six, and b) eight non-identical circular features. The overall area of the features on both surfaces are equal.

It should be noted that in this case the graph of behavior of α versus the change in $r_{min,\alpha}$ that is depicted in Figure 6-33 does not provide useful information. This is because when the cumulative

area of the features is distributed on the surface such that less than half of the features are smaller than the remaining of the features the minimum radius of the $\sigma_{\mu h}$ polar plot decreases. This decrease causes an increase in the number of calculated features based on Figure 6-33. On the other hand, when more than half of the features are larger than the remaining ones, the r_{min_a} increases, and this increase causes a decrease in the calculated number of features based on Figure 6-33. However, this increase or decrease in α is meaningful when it is compared to a base value. In the case of non-identical features on the surface there is no base value and therefore graph of Figure 6-33 does not provide any useful information.

6.2.2.6 Failure of identical and non-collinear circular features simultaneously

In this case which is the combination of failure of both of the requirements from the results of the previous sections the number of calculated quantity of the features based on equation 6-17 is always less than the actual number of features on the surface.

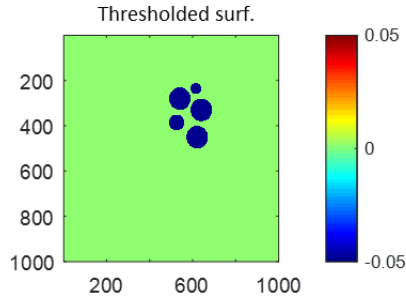


Figure 6-35- A thresholded surface with multiple non-identical, and overlapping features.

This case is shown in Figure 6-35 where three features with radius of 50 pixels, one feature with radius of 35 pixels, and one feature with radius of 25 pixels are present on the surface. Quantity of the features based on equation 6-17 is equal to 2.04, which is clearly less than the actual number of features on the surface.

6.2.3 Non-circular features

All of the calculations and formulas described in section 6.2.2 are based upon the fact that surface features are symmetric with respect to horizontal and vertical axis such as circles and squares. However, when features are not symmetric and have random geometries, then these calculations and formulas will not result in the correct answers and should not be used.

For these asymmetric features the results of section 6.2.1 can be used instead, that is to use the number of peaks on the polar plots to estimate the number of the asymmetric features on the surface, i.e. using equation 6-2.

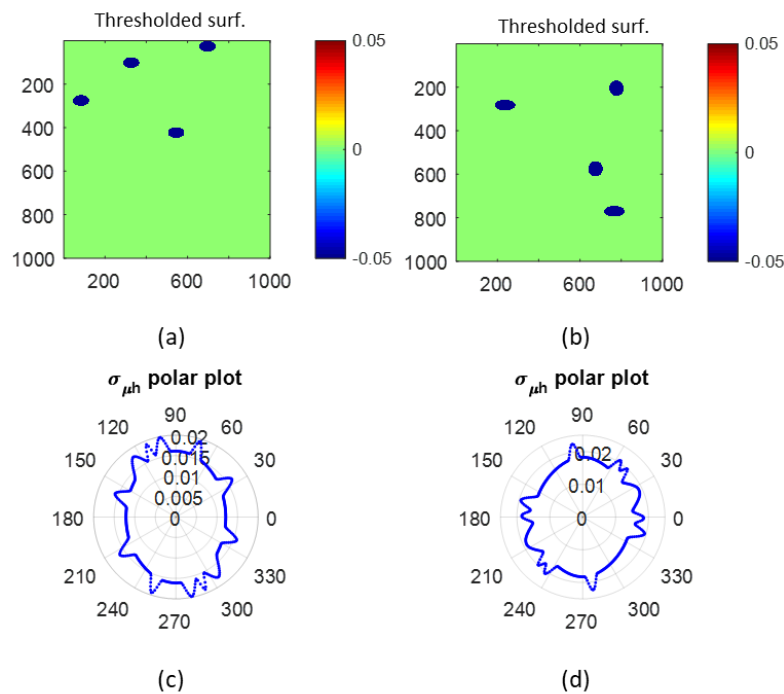


Figure 6-36: a) A thresholded surface with four negative asymmetric features, b) a thresholded surface with two symmetric and two asymmetric negative features, c), and d) their $\sigma_{\mu h}$ polar plots.

Figure 6-36(a) depicts a surface with four non-circular negative features present on its surface, and Figure 6-36(b) shown a surface with two negative circular and two negative non-circular features. From their $\sigma_{\mu h}$ polar plots 12 peaks are detectable. Putting this number into equation 6-2 will result in 4 features. However, no information about the geometry of features or their area can be achieved.

It should be noted that the derivation of the system of equations 6-16 is based on the assumption that features are symmetric without overlapping in at least one orientation, and therefore by using equations 6-17 and 6-18 for asymmetric features no meaningful results can be obtained. In other words, the result of equation 6-17 could underestimate or overestimate the quantity of features depending on the geometry and configuration of them. And equation 6-18 which results in the radius of features is also meaningless because there cannot be a defined radius for a non-circular feature.

6.2.4 Analysis of a real surface with a circular feature

In section 5.2.4 a real surface from NIST scratch dig standard with a single circular feature was analyzed based on its σ_{Rq} polar plot, and its diameter and depth were estimated equal to 18 μm (45 pixels) and 0.060 μm respectively. The same surface can also be analyzed with its $\sigma_{\mu h}$ polar plot and using equation 6-10.

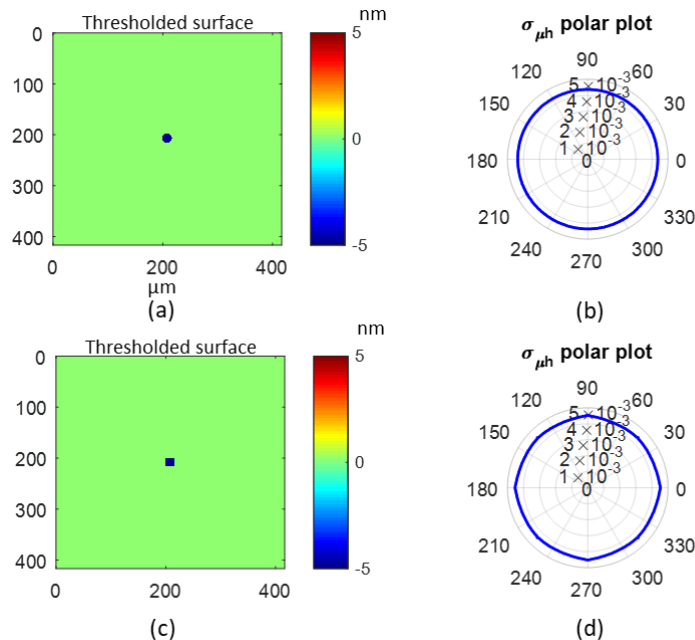


Figure 6-37: a) The thresholded surface with the circular feature, b) its $\sigma_{\mu h}$ polar plot, c) the same surface when the feature is converted to a square, d) its $\sigma_{\mu h}$ polar plot.

For this surface the threshold depth is selected equal to 5 μm , every height value smaller than this limit is set to zero and every value larger than this limit is set to 1, i.e. $d = 1$. This thresholded surface is shown in Figure 6-37(a), and its $\sigma_{\mu h}$ polar plot in Figure 6-37(b). The circular feature is converted to a square with the same area and is shown along with its $\sigma_{\mu h}$ polar plot in Figure 6-37(c), and (d) respectively. The minimum radius of this polar plot in Figure 6-37(d) is equal to 0.0043 nm. Putting these values into equation 6-10:

$$r_{\min} = 0.0043 = \sqrt{\frac{\sqrt{2} \times 1024 \times 1^2 \times s^3 - 1^2 \times s^4}{4 \times 1024^4}} \rightarrow s = 38.64$$

Converting this s value via equation 6-5 to the radius of the circular feature will result in the answer.

$$38.64 = R\sqrt{\pi} \rightarrow R = 21.7$$

The radius of the feature considering the discrete nature of the pixels is calculated as 22 pixels, therefore the diameter of the feature is equal to 44 pixels. This diameter when considering the pixel resolution of the 20 \times objective is equal to 17.6 μm .

In the thresholding process the depth of the feature was assigned a constant value, however, the actual depth can be calculated after the diameter is obtained. In order to do that the surface this time is thresholded such that all the values below the threshold height are set to zero, however, the values larger than this limit will not be changed. The $\sigma_{\mu h}$ polar plot of this new thresholded surface is shown in Figure 6-38.

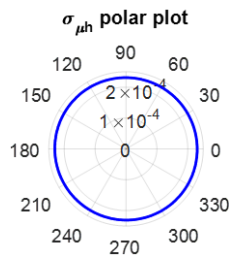


Figure 6-38: $\sigma_{\mu h}$ polar plot of the thresholded surface with the circular feature.

The minimum radius of this polar plot is equal to 0.00026 nm, and s was calculated equal to 38.64. Putting these values in equation 6-10 will result in the average depth of the feature equal to 0.060 μm :

$$r_{\min} = 0.00023 = \sqrt{\frac{\sqrt{2} \times 1024 \times d^2 \times 38.64^3 - d^2 \times 38.64^4}{4 \times 1024^4}} \rightarrow d = 0.06$$

6.2.5 Analysis of real surfaces with multiple features

A height map of a polished glass after its form and waviness are removed is shown in Figure 6-39. The pixel resolution of the surface is equal to 0.55 μm and the field of view of the measurement instrument is equal to 342 $\mu\text{m} \times 342 \mu\text{m}$.

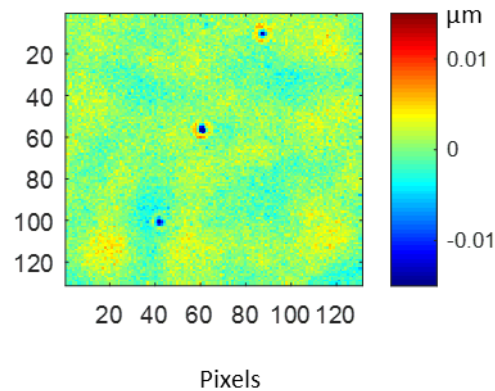


Figure 6-39: Height map of a polished glass.

From the analysis region height map, Figure 6-39, three features are visible. At one angle during the rotation process these three features will be aligned, and therefore they will only create two lobes on the polar plots. However, the size of these features is very small such that there will not be any visible lobes on the σ_{Rq} polar plot with the rotational increment equal to 0.1° , Figure 6-40(b). The Sq roughness of the surface excluding the defects is equal to 3 nm, therefore a threshold height of 0.01 μm is selected and the surface is thresholded with respect to this limit, Figure 6-40(b); all of the height values below this threshold limit are set to zero, and all of those that are larger than the threshold height are set to 1. After thresholding only feature-related pixels

remain on the surface and the rest of the pixel values is equal to zero; the $\sigma_{\mu h}$ polar plot of this thresholded surface is depicted in, Figure 6-40(d). From this polar plot two lobes are visible, and the first one occurs at $\theta=156^\circ$.

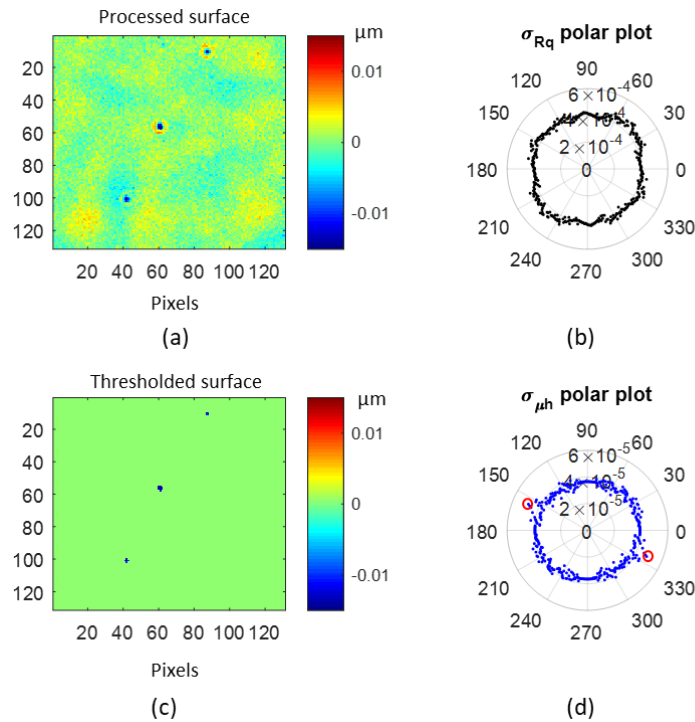


Figure 6-40: a) Original surface, b) its σ_{Rq} polar plot, c) original surface after thresholding, and d) its $\sigma_{\mu h}$ polar plot.

Equations 6-17 and 6-18 that were based on the minimum radius of the $\sigma_{\mu h}$ polar plot will result in the quantity and the radius of the features equal to 2.4 and 3 pixels respectively. However, since the features are not identical the calculated quantity is underestimated. But the quantity of the features can be estimated based on the number of lobes on $\sigma_{\mu h}$ polar plot, however, feature become aligned at one orientation and therefore only two lobes are present on the polar plot.

From this pair of lobes using equation 6-2 will result in two features, which is not correct. So the surface has to be distorted to eliminate the collinearity of the features at $\theta=156^\circ$. This distortion of the thresholded surface is done with the help of a fourth degree polynomial as shown in Figure 6-41(a).

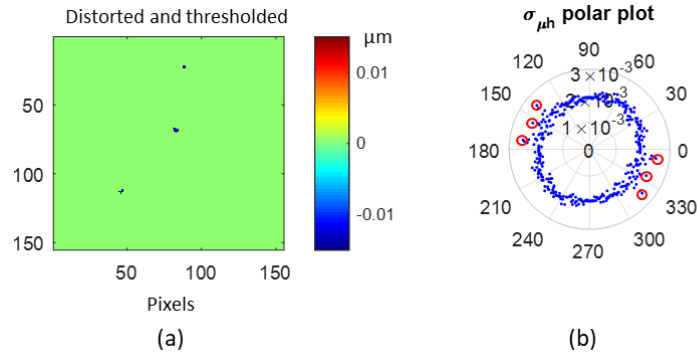


Figure 6-41: a) The thresholded and distorted surface, and b) its $\sigma_{\mu h}$ polar plot.

Geometrical analysis of the surface in Figure 6-41(a) states that there is not any angle at which more than two features can be aligned, therefore during the rotation process six lobes will be generated, Figure 6-41(b). The number of features based on equation 6-2 is now equal to three, which is the correct number of features. As was mentioned earlier by using this approach only the quantity of the features can be estimated and no information regarding their geometrical properties can be achieved.

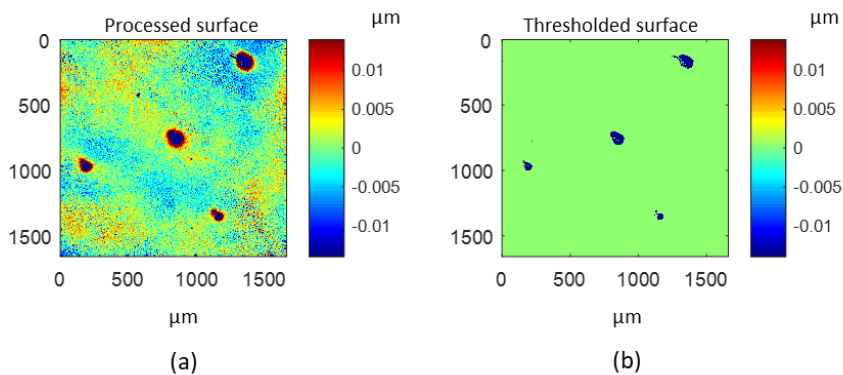


Figure 6-42: a) Polished glass surface measured with CSI 5 \times after processing, and b) the same surface after it is thresholded.

Figure 6-42(a) depicts a BK7 glass polished sample that was measured with Zygo Zegage coherence scanning interferometer (CSI) 5 \times objective with 1.6 mm \times 1.6 mm field of view, and the pixel resolution of 1.6 μ m. Piston, tilt, and a 4th order polynomial is removed from the initial height map. S_q surface roughness of the surface excluding defects is equal to 0.005 μ m. The surface is thresholded with the threshold limit equal to 0.016 μ m and is shown in Figure 6-42(b), all of the

height values larger than this limit are set to 1; this threshold value is selected to be 3.2 times larger than the Sq of the surface because in a surface with Gaussian distribution of heights 3.2 times the standard deviation covers 99.9% of the data, and any value above it is considered as a outlier, i.e. defect. From the thresholded surface four near-circular features are visible.

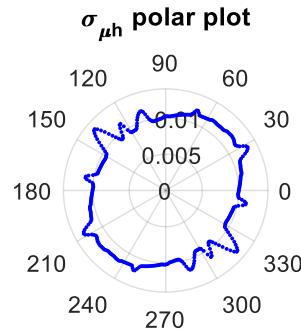


Figure 6-43: $\sigma_{\mu h}$ polar of the surface with four negative near-circular features.

Figure 6-43 depicts the $\sigma_{\mu h}$ polar plot of the thresholded surface, from this plot 12 peaks are visible, therefore by using equation 6-2 the number of features is calculated equal to four.

6.3 Multiple scratches

Presence of multiple linear features, i.e. scratches on a surface would also affect the shape of polar plots. A single scratch would create two lobes on the polar plots, while multiple scratches create multiple lobes on the polar plots depending on their relative orientation with respect to each other. Similar to the polar plots of surfaces with multiple circular features, the number of lobes can provide some insights about the quantity of scratches on the surface, and their geometrical properties such as length, and width. Thresholding and using columns' mean height value instead of their Rq value is also used in linear features analysis due to the fact that they make the formulization of the radius of the $\sigma_{\mu h}$ polar plot simple.

In order to analyze surfaces with multiple scratches two scenarios have to be considered, first when none of the scratches on the surface is parallel to each other, and the second when all of the

scratches are parallel to each other. Each of these situations will be discussed in the following sections of this chapter.

6.3.1 Non-parallel and identical scratches

In this case, where none of the identical scratches is parallel to each other, each individual scratch will create two lobes on the polar plot, and thus the number of lobes on the $\sigma_{\mu h}$ polar plot is equal to twice the number of scratches on the surface.

$$Lb = 2 \times \alpha_{scr} \quad (6-24)$$

Where Lb is the number of lobes on the $\sigma_{\mu h}$ polar plot, and α_{scr} is the quantity of the non-parallel scratches on the surface.

The maximum number of lobes that can be detected from the polar plot is given in equation 6-3, and therefore the maximum number of scratches that can be estimated is given in equation 6-25:

$$\alpha_{scr_max} = \frac{180}{\Delta\theta \times pd} \quad (6-25)$$

Where α_{scr_max} is the maximum number of detectable scratches from the $\sigma_{\mu h}$ polar plot.

Figure 6-44(a) depicts a theoretical surface with its Sq equal to 0.01 μm , and three non-parallel identical scratches of 400 pixels length, 10 pixels width, and 0.1 μm depth. This surface is thresholded with the threshold height value equal to 0.05 μm , and is shown in Figure 6-44(b); each lobe on the upper half of the $\sigma_{\mu h}$ polar plot in Figure 6-44(c) is created by one scratch, and the angle at which the lobe occurs corresponds to the angle enclosed between the scratch and the vertical axis.

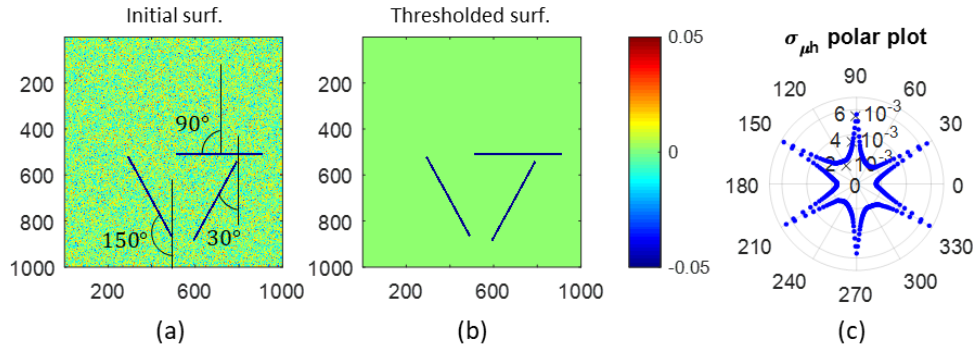


Figure 6-44: a) MATLAB generated surface with three scratches, b) the same surface after it is thresholded, and c) its $\sigma_{\mu h}$ polar plot.

In order to find out the quantity, width, and length of each scratch the following steps has to be followed.

The first step is divide the total number of counted lobes, Lb , by two to obtain the quantity of the scratches, α_{scr} . Figure 6-44(c) has six lobes, so based on equation 6-24 the number of scratches is equal to three, $\alpha_{scr}=3$. The second step is to rotate the thresholded surface based on the angle of each lobe in the upper half of the $\sigma_{\mu h}$ polar plot in order to make each one of the scratches vertical at a time. Lobes in the upper half of the $\sigma_{\mu h}$ polar plot in Figure 6-44(c) occur at 30°, 90°, and 150°; so by rotating the thresholded surface equal to each one of these three angles in a clockwise direction every one of the scratches becomes vertical.

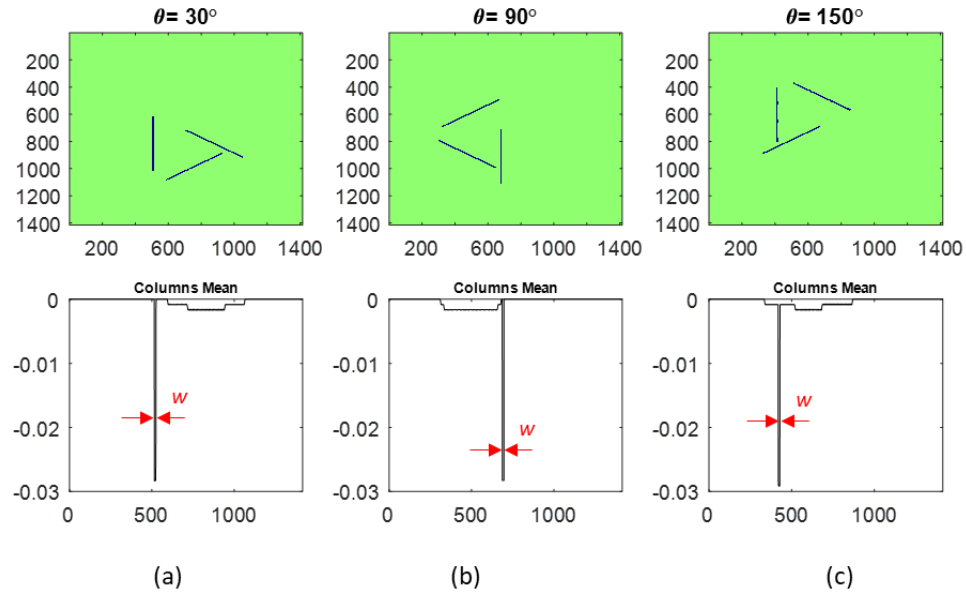


Figure 6-45: The surface of Figure 6-44(b) when rotated a) 30° , b) 90° , and c) 150° with the graph of their columns mean height values.

Once each scratch is vertical, from the columns mean height value graph it is possible to estimate the width of each one. At each one of these angles the mean height value of the columns that do not contain any sections of the scratches, non-feature-related columns, is equal to zero, columns that contain sections of scratches, feature-related columns, have non-zero mean values; and among these columns those that contain the vertical scratch have the maximum absolute value of mean height. The width of each scratch is equal to the number of non-zero values in the columns mean height value graph that are greater than 95% of the absolute maximum value of the graph, μh_{max} . This 95% value is selected to filter out the non-zero values that do not belong to the vertical scratch.

From step one the quantity, α_{scr} , and from step two the width, w , of scratches is estimated. The final step is to estimate the length of scratches. The length of identical scratches can be estimated from equation:

$$L = \frac{A_{total_scr}}{\alpha_{scr} w} \quad (6-26)$$

Where A_{total_scr} is the total area of all of the features, i.e. total number of non-zero values in the thresholded surface, α_{scr} is the quantity, L is the length, and w is the width of the non-parallel scratches.

6.3.2 Non-parallel and non-identical scratches

If the multiple non-parallel scratches on the surface are not identical, the quantity and width of each one of them can be calculated similar to step one and two for calculating the quantity of width of multiple non-parallel and identical scratches described in section 6.3.1. However, for estimating the length of each scratch at step two where the surface is rotated such that at each angle only one scratch is vertical by knowing the absolute maximum value of the feature-related columns mean height value the length of the scratch can be calculated via equation:

$$L = \frac{n(\sin \theta + \cos \theta) \times \mu h_{\max}}{d} \quad (6-27)$$

Where μh_{\max} is the absolute maximum value of the columns mean height values distribution, d is the assigned depth of the features after thresholding the surface, θ is the rotational angle, and n is the size of the rotated surface.

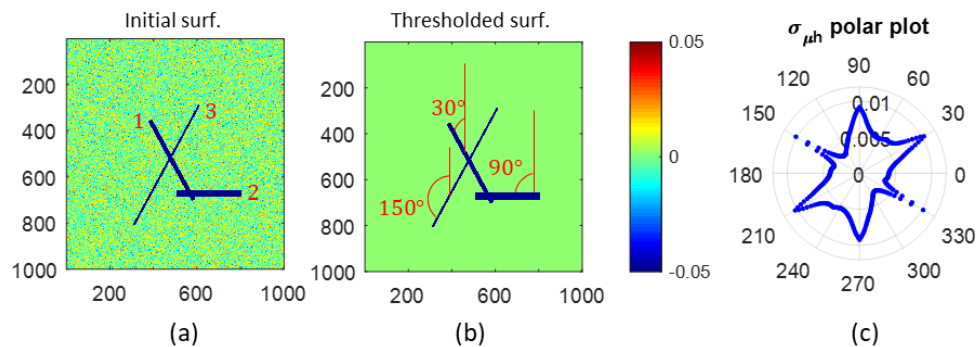


Figure 6-46: a) MATLAB generated surface with a Gaussian distribution of heights with three non-identical and non-parallel scratches, b) the same surface after it is thresholded, c) its $\sigma_{\mu h}$ polar plot.

Figure 6-46(a) depicts a surface with one 400×20 pixel (labeled as 1), one 300×30 pixel (labeled as 2), and one 500×10 pixel (labeled as 3) scratches present. This surface after thresholding

is shown in Figure 6-46(b), so is the angle enclosed between each feature and the vertical axis. The $\sigma_{\mu h}$ polar plot is shown in Figure 6-46(c) with six lobes present, and therefore the quantity of scratches based on equation 6-24 is equal to three, $\alpha_{scr}=3$. The surface is rotated based on the angle of the lobes on the polar plot, and from the columns' mean height value graph the width of each one can be calculated, see Figure 6-47.

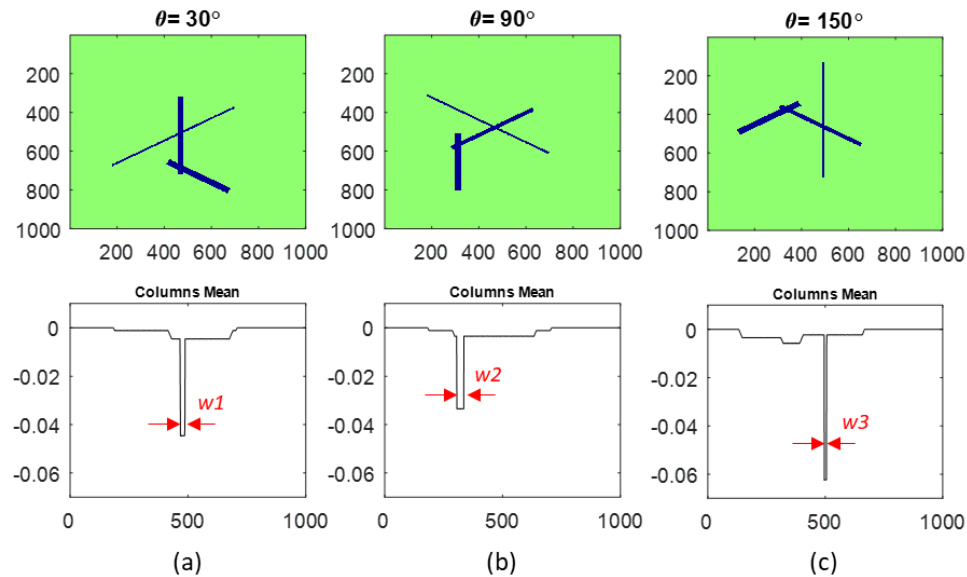


Figure 6-47: The surface of Figure 6-46(b) when rotated a) 30° , b) 90° , and c) 150° with the graph of their columns mean height values.

The length of each one of these scratches can then be calculated via equation 6-24.

6.3.3 Parallel and identical scratches

When there are only parallel scratches on the surface independent of their quantity, the number of lobes on the $\sigma_{\mu h}$ polar plot will not be equal to twice the number of scratches, therefore the correct number of scratches cannot be determined by dividing the number of lobes by two. So other key metrics of the polar plot should be used in order to obtain insights on the surface features. Figure 6-48(a) depicts a thresholded surface with two parallel identical scratches with 400 pixels length, and 20 pixels width, the graph of mean height values of the columns of this surface is shown in Figure 6-48(c), and their histogram is shown in Figure 6-48(e). If these two features are combined

together to form a single scratch on another thresholded surface as shown in Figure 6-48(b), the graph of mean height values of the columns of this new surface as well as their histogram looks exactly the same, see Figure 6-48(d) and (f).

This is due to the fact that the distribution of columns' mean height values is a function of the total number of feature-related pixels in each one of the feature-related columns, and is independent of the configuration/location of these pixels within a column, i.e. scattered in different groups or lumped together.

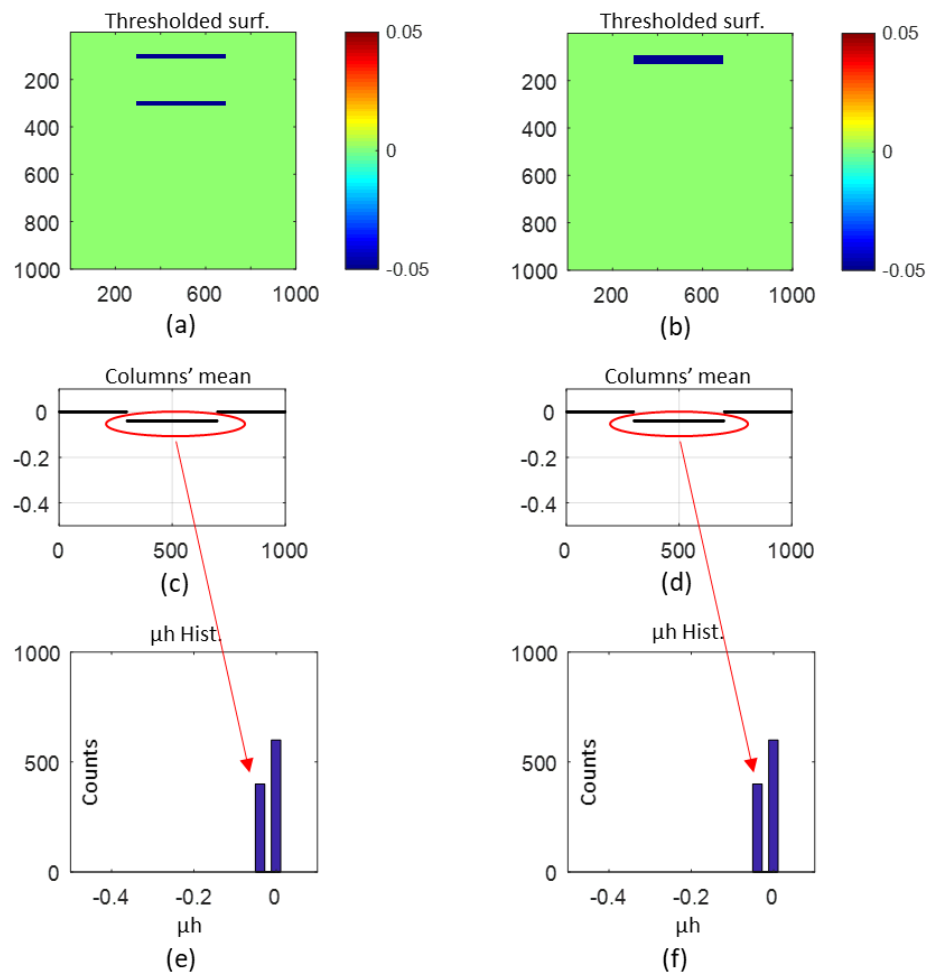


Figure 6-48: Thresholded surfaces with one and two features with equal areas, their columns mean height values graph, as well as the histogram of their μh values.

The same argument holds true when all of the parallel scratches are vertical as shown in Figure 6-49. In this figure the mean height values of the feature-related columns are scattered in two groups

in Figure 6-49(c), and lumped together in Figure 6-49(d). However, as stated above their histogram looks exactly the same, Figure 6-49(e), and (f).

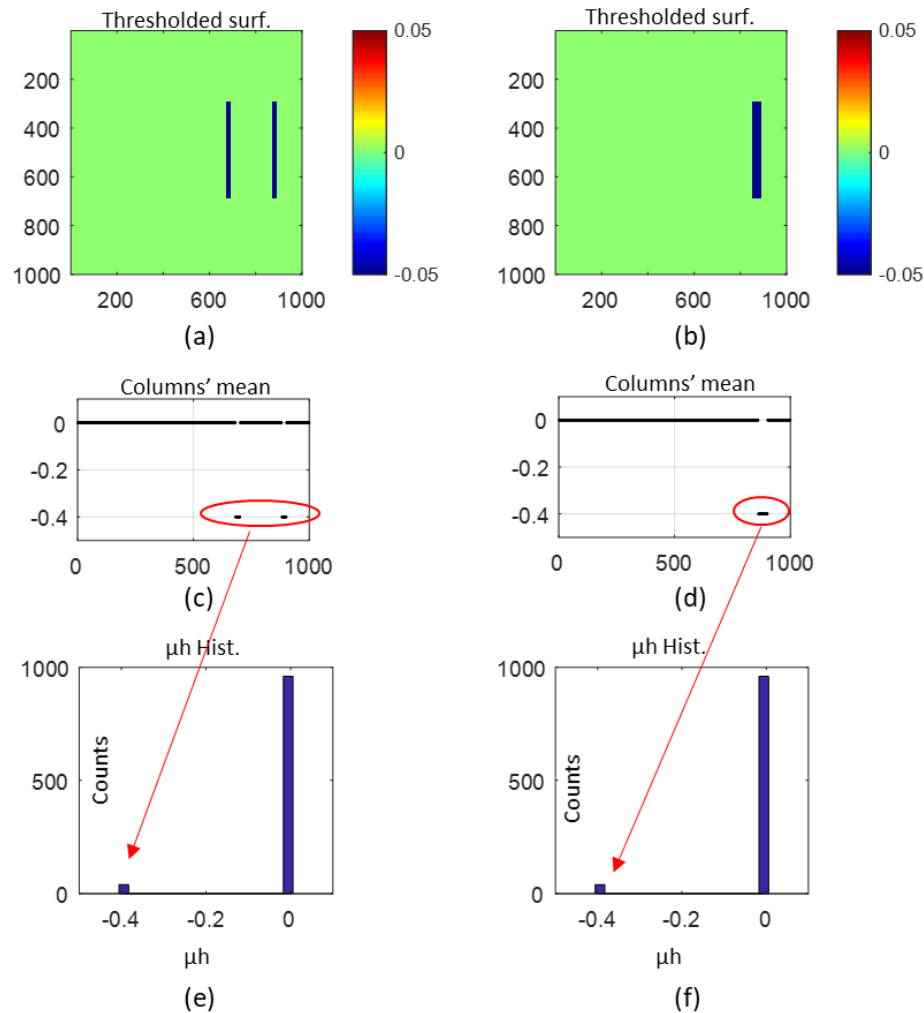


Figure 6-49: Thresholded surfaces with one and two features with equal areas, their columns mean height values graph, as well as the histogram of their μh values.

The radius of the $\sigma_{\mu h}$ polar plot, that is the standard deviation of μh histogram, is directly proportional to the total number of feature-related pixels in each feature-related column. The key point is that this radius is maximum, r_{max} , at an angle where all of the features are vertical, i.e. the number of feature-related pixels in the feature-related columns is maximum; and this radius is minimum, r_{min} when the number of feature-related pixels in the feature-related columns is minimum. 90° before or after the angle at which r_{max} occurs is the angle where all of the features

are horizontal, $r_{max \pm 90^\circ}$. The knowledge of these three parameters makes the analysis of the surface with multiple identical parallel scratches possible.

It also makes possible to formulate the radius of the $\sigma_{\mu h}$ polar plot of a thresholded surface with a single scratch present on its surface at any angle θ .

6.3.3.1 Radius of the $\sigma_{\mu h}$ polar plot for a single scratch on a thresholded surface

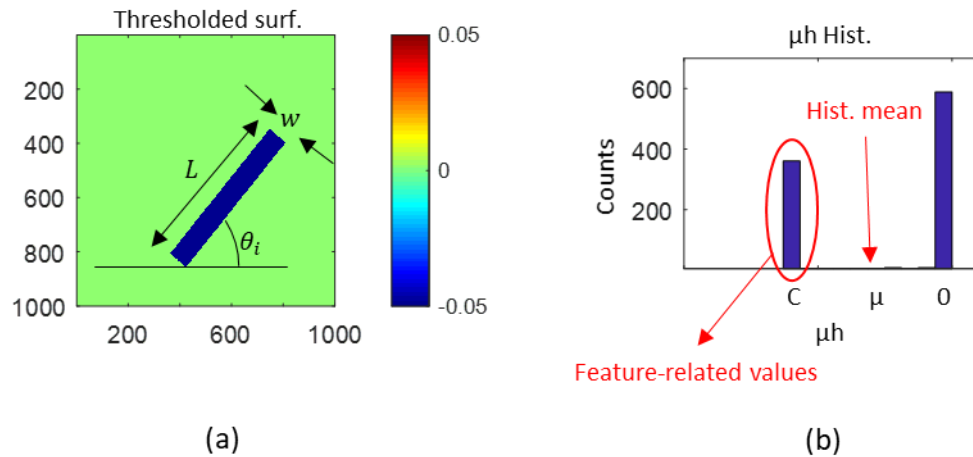


Figure 6-50: a) A thresholded surface with a single scratch, b) its μh histogram.

At any angle of rotation the mean height value of the feature-related columns, C , is equal to:

$$C = \frac{wd}{\sqrt{2n} \cos |(\theta - \theta_i)|} \quad (6-28)$$

Where θ_i is the initial angle enclosed between the scratch and the horizontal axis, θ is any angle of rotation, w is the width, and d is the depth of the scratch, see Figure 6-50.

The mean value of the histogram of these values, μ , is equal to:

$$\mu = \frac{wdL}{2n^2} \quad (6-29)$$

And the standard deviation of the columns' mean height histogram, μh histogram, is given in equation 6-30.

$$\sigma = \sqrt{\frac{(\sqrt{2n} - L |\cos(\theta - \theta_i)|)(-\mu)^2 + L \cos(\theta - \theta_i) |C - \mu|^2}{\sqrt{2n}}} \quad (6-30)$$

Finally the radius of the $\sigma_{\mu h}$ polar plot at any angle, θ , is achieved by simplifying equation 6-30 and is equal to:

$$r_{\theta} = \sqrt{\frac{\frac{\sqrt{2n}Lw^2d^2}{|\cos(\theta - \theta_i)|} - (Lwd)^2}{4n^4}} \quad (6-31)$$

Where r_{θ} is the radius of the $\sigma_{\mu h}$ polar plot at angle θ .

However, when the angle of rotation, θ , becomes closer to the initial angle of the scratch with respect to horizontal axis, θ_i , the cosine of the difference of these angles approaches to infinity, in order to resolve this limitation, the critical angle of a scratch should be defined, θ_c , this is the angle where a column includes the hypotenuse of the scratch as shown in Figure 6-51. This angle is only a function of the scratch geometry, i.e. length and width.

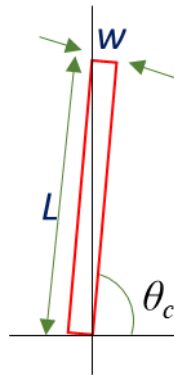


Figure 6-51: Schematic model of a scratch rotated equal to its critical angle.

The critical angle is the angle enclosed between the scratch and the horizontal axis and is given in equation 6-32

$$\theta_c = \tan^{-1}\left(\frac{L}{w}\right) \quad (6-32)$$

At the critical angle geometrical analysis of the scratch in Figure 6-51 states that:

$$\frac{L}{\sin(\theta_c)} = \frac{w}{\cos(\theta_c)} \quad (6-33)$$

Replacing the cosine term in equation 6-31 with its sine equivalent from equation 6-33 resolves the infinity limit of the equation 6-31 for angles larger than $\theta_c + \theta_i$ and smaller than $\pi - \theta_c + \theta_i$, and is equal to:

$$r_o = \sqrt{\frac{\frac{\sqrt{2}nwL^2d^2}{|\sin(\theta - \theta_i)|} - (Lwd)^2}{4n^4}} \quad \text{for} \quad \theta_c + \theta_i < \theta < \pi - \theta_c + \theta_i \quad (6-34)$$

6.3.4 Different cases of parallel scratches

All of the formulas for calculating the length, width, and quantity of multiple parallel scratches are derived based upon the assumption that all of the features are identical. When this requirement is met the results from equations that lead to the length and width of the features can be meaningfully interpreted, as will be detailed in the following sections. However, when this requirement is not met, the polar plots are not able to provide information about the geometry of features, or their quantity and configuration on the surface.

Four possible situations of the surfaces that contain a fixed number of parallel scratches are as follows:

- All features exactly below each other when horizontal, Figure 6-52(a)
- All features align when horizontal, Figure 6-52(b)
- Non-overlapping when all features are horizontal, Figure 6-52(c)
- Randomly located, no restrictions about overlapping, Figure 6-52(d)

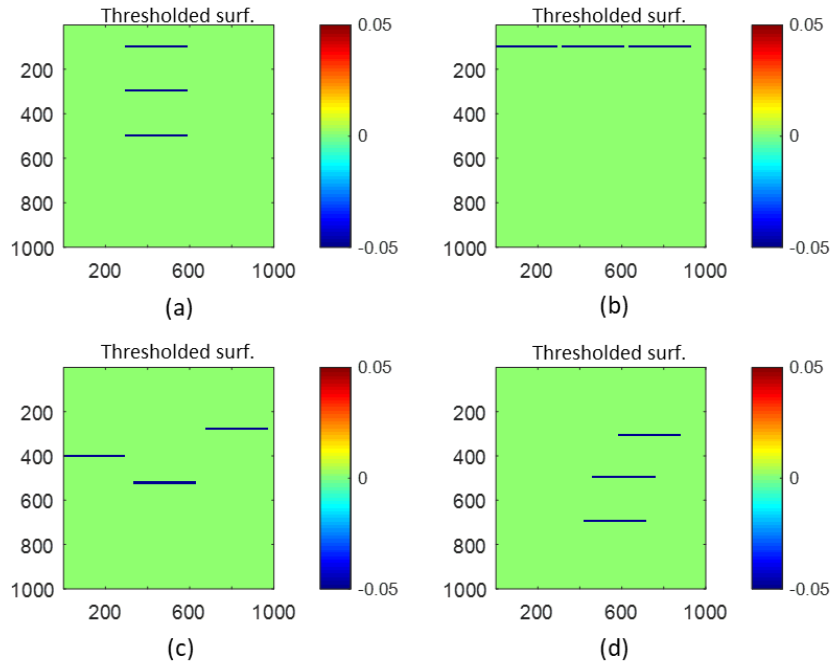


Figure 6-52: All possible cases of parallel scratches configuration on a surface, a) all features completely contained within the same number of columns when horizontal, b) all features completely contained with the same number or rows when horizontal, c) non-overlapping features, and d) randomly located.

Each one of these cases will be explained based on the assumption that features are identical, and then the results of failing this assumption will be discussed.

In order to analyze each case of parallel scratches three key metrics should be identified, first the maximum radius of the $\sigma_{\mu h}$ polar plot, r_{max} , which corresponds to the orientation where all of the features are vertical, 90° before or after the angle of maximum radius, $r_{max \pm 90^\circ}$, that corresponds to when all the features are horizontal, and the minimum radius of the $\sigma_{\mu h}$ polar plot, r_{min} , that corresponds to the orientation where the number of feature-related pixels in the feature-related columns is minimum.

6.3.4.1 All features exactly below each other when horizontal

This case is shown in Figure 6-53(a) where three identical scratches with 400 pixels length and 20 pixels width are completely contained within the same number of columns when features

are horizontal, and the spacing between them is equal to 200 pixels. $\sigma_{\mu h}$ polar plot of this surface is shown in Figure 6-53(b) along with its three key metrics.

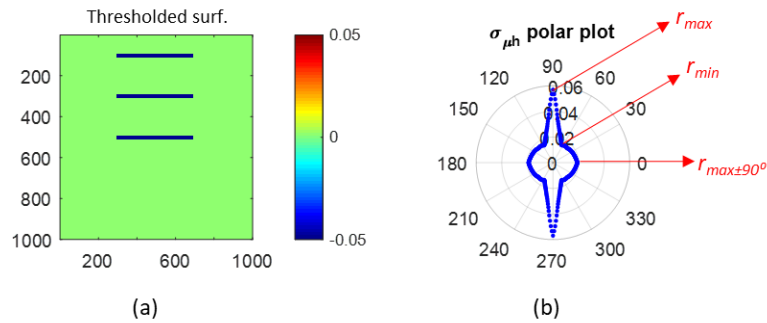


Figure 6-53: a) A thresholded surface with three parallel scratches, and b) its $\sigma_{\mu h}$ polar plot.

When the surface is rotated 90° from its original orientation all of the features become vertical and the number of feature-related pixels in the feature-related columns becomes maximum, therefore the maximum radius of the polar plot occurs at 90° .

The angle between the features and the horizontal axis at the initial orientation of the surface is equal to 0° , the critical angle of each of these features based on equation 6-32 is equal to 87.13° , since 90° is larger than the critical angle, the maximum radius of the polar plot can be calculated from equation 6-31, which is equal to:

$$r_{\max} = \sqrt{\frac{\sqrt{2}nw_{\text{total}}L^2d^2 - (w_{\text{total}}Ld)^2}{4n^4}} \quad (6-35)$$

It should be noted that in equation 6-35 the cumulative width of all features is used, w_{total} . As mentioned in section 6.3.3 the standard deviation of μh histogram is only dependent on the number of feature-related pixels, and is independent of whether they are scattered or lumped together.

The cumulative area of all of the features, that is the total number of feature-related pixels, is equal to:

$$A_{\text{total_scr}} = w_{\text{total}}L \quad (6-36)$$

Where w_{total} is the cumulative width of all of the identical features, and L is their length.

Substituting the cumulative area into equation 6-35 and solving the result for L will give the length of each scratch:

$$L = \frac{4n^4 r_{max}^2 + A_{total_scr}^2 d^2}{\sqrt{2nA_{total_scr} d^2}} \quad (6-37)$$

Where r_{max} is the maximum radius of the polar plot and is a known value, A_{total_scr} is the cumulative area of all of the features and is a known value, d is the depth after thresholding the surface and is a known value, and n is the size of the surface.

Once the length is calculated, the cumulative width of the features can then be found out by using equation 6-36.

90° before or after the angle of r_{max} is where all of the features are horizontal, $r_{max \pm 90^\circ}$. In between these two orientations at a specific angle the number of feature-related pixels in the feature-related columns becomes minimum.

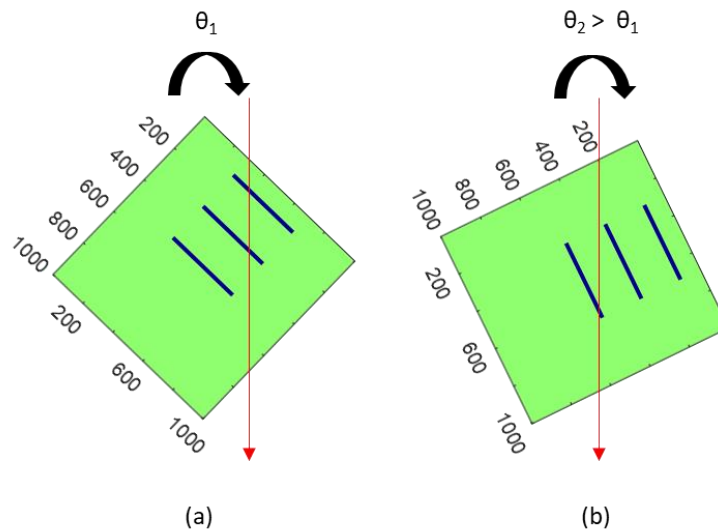


Figure 6-54: The surface of Figure 6-53(a) during clockwise rotation, a) feature-related columns cross two features, and b) feature-related columns cross one feature.

For the surface in Figure 6-53(a) at its original orientation, every feature-related column crosses all of the features, and therefore the number of feature-related pixels cannot be minimum. During the rotation the number of features that a column crosses becomes smaller as shown in

Figure 6-54(a), at this orientation each feature-related column goes through only two features. As the surface keeps rotating there will be an angle where a column crosses only one feature such that the number of feature-related pixels in it is a minimum, Figure 6-54(b). This angle is where the minimum radius of the polar plot occurs, and can be found by the geometrical analysis of the features and spacing between them as shown in Figure 6-55.

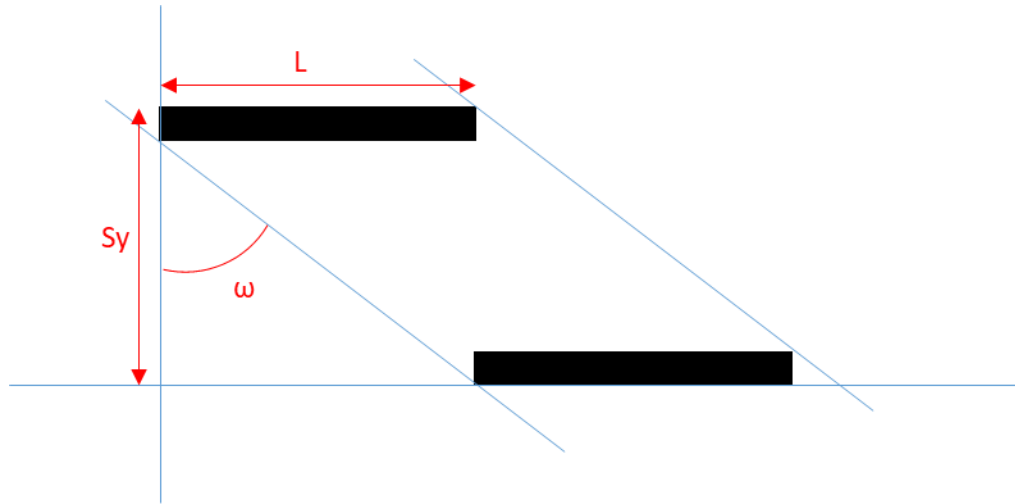


Figure 6-55: Schematic representation of the configuration of parallel scratches at the angle that the minimum radius of the $\sigma_{\mu h}$ polar plot occurs.

From this analysis the angle where a feature-related column contains the minimum number of feature-related pixels, ω is equal to:

$$\omega = \tan^{-1}\left(\frac{L}{Sy}\right) \quad (6-38)$$

Where L is the length of each scratch, and Sy is the spacing between each feature.

By knowing the angle of the minimum radius of the polar plot, ω , and the length of each feature, L , the spacing between each feature, Sy can be calculated from equation 6-38. Based on this spacing the maximum number of possible features on the surface, \max_{α_scr} is equal to:

$$\max_{\alpha_scr} = \text{round}\left(\frac{n}{Sy}\right) \quad (6-39)$$

In order to find out the quantity of the features, some number of scratches ranging from two to $max_{\alpha_{scr}}$ are put on a new thresholded surface such that their cumulative width is equal to w_{total} , and their spacing equal to S_y . The number of scratches that makes the minimum radius of the new surface $\sigma_{\mu h}$ polar plot equal to the minimum radius of the $\sigma_{\mu h}$ polar plot of the surface that is being analyzed is equal to the number of scratches present on the initial surface, i.e. α_{scr} is identified.

When the length of the features are equal, but their width is not equal to each other as shown in Figure 6-56, the length of them can be calculated via equation 6-37, and their cumulative width via equation 6-36. In this case independent of the spacing between the features, calculating the quantity of them is not possible because there is no information available about how to divide the total area of features into several scratches with their length equal to L , but having different widths.

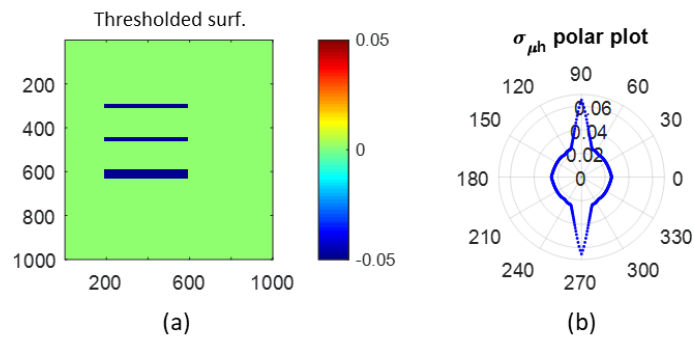


Figure 6-56: a) A thresholded surface with three scratches of the same length and different width, and b) its $\sigma_{\mu h}$ polar plot.

It should be noted that if the identical parallel scratches are not equally spaced, it is again not possible to estimate the exact number of features, and only their length and cumulative width is achievable. This is due to the fact that no information about the spacing between the scratches can be achieved from the polar plots. Also, when features are not identical, i.e. having different length values no information from the polar plots regarding their length, and width can be achieved.

Characteristics of the $\sigma_{\mu h}$ polar plot, see Figure 6-53(b), of the surfaces containing this configuration of identical scratches are:

- Only four lobes exist on the polar plot.
- R_{max} occur at the angles where the features are vertical.
- $r_{min} \neq r_{max \pm 90^\circ}$

6.3.4.2 All features align

This case is depicted in Figure 6-57(a) where three identical scratches with 300 pixels length and 20 pixels width are completely aligned, and are completely contained within the same number of rows when horizontal. Typical $\sigma_{\mu h}$ polar plot of this surface is shown in Figure 6-57(b) along with the three key metrics.

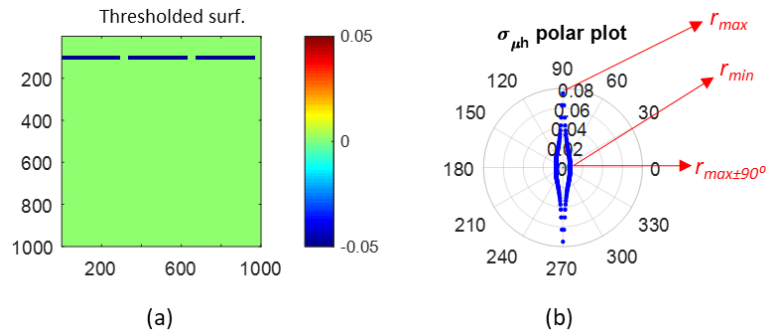


Figure 6-57: A thresholded surface with three parallel and aligned scratches, and b) its $\sigma_{\mu h}$ polar plot.

When the surface in Figure 6-57(a) is rotated 90° all of the features become vertical, at this orientation each feature-related column encapsulates the total length of all of the three scratches, therefore the number of feature-related pixels in these column is maximum leading to the maximum radius of the polar plot. The cumulative area of the features in this case is equal to:

$$A_{total_scr} = wL_{total} \quad (6-40)$$

Where L_{total} is the cumulative length of all scratches.

The angle between the features and the horizontal axis at the initial orientation of the surface is equal to 0° , the critical angle of each of these features based on equation 6-32 is equal to 86.18° , since 90° (orientation where all features are vertical) is larger than the critical angle the maximum

radius of the polar plot can be calculated from equation 6-34, substituting the total area of features in this formula the cumulative length of features can be calculated:

$$L_{total} = \frac{4n^4 r_{max}^2 + A_{total_scr}^2 d^2}{\sqrt{2nA_{total_scr}} d^2} \quad (6-41)$$

Once the cumulative length is known the width of each scratch can be calculated from equation 6-40.

Three unknown are length, width, and the quantity of the features. The cumulative length can be achieved via equation 6-41, the width can be calculated via equation 6-38, however, there is not any other formula to solve for the third unknown, i.e. α_{scr} . Therefore, it is not possible to calculate the number of features in this configuration.

It should be noted that the $\sigma_{\mu h}$ polar plot of a surface containing multiple aligned features with their cumulative length equal to L_{total} pixels, Figure 6-58(b) is very similar to the $\sigma_{\mu h}$ polar plot of a surface with a single scratch of length L_{total} pixels, Figure 6-58(d).

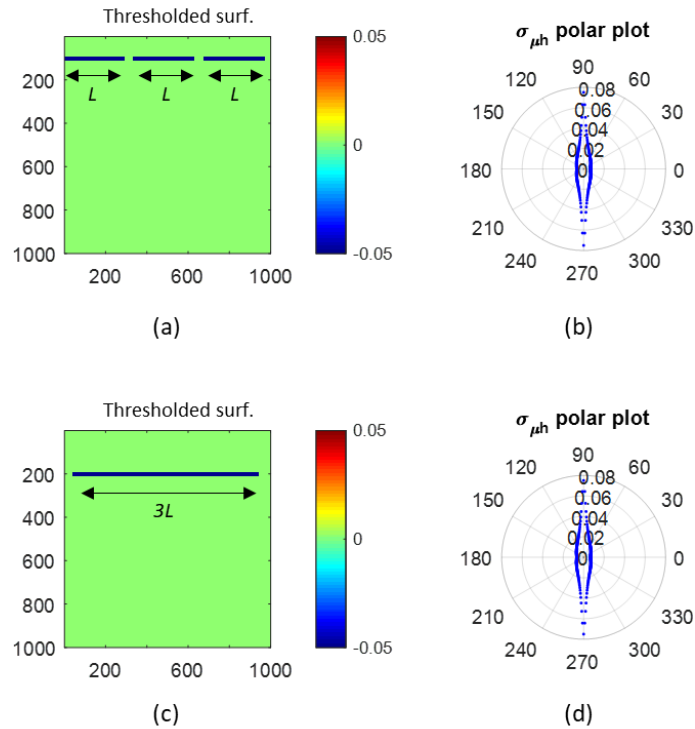


Figure 6-58: a) A thresholded surface with three scratches aligned, b) its $\sigma_{\mu h}$ polar plot, c) a thresholded surface with one scratch with its length equal to the cumulative length of three scratches, and d) its $\sigma_{\mu h}$ polar plot.

However, the rate of change of the radius around the lobes of the polar plots are slightly different, and this property helps identify whether the polar plot belongs to a surface with a single scratch or to a surface with multiple aligned scratches. This rate of change of radius is larger for the single scratch, and falls above the radii values of the polar plot of a surface with multiple aligned scratches. Figure 6-59 shows the graph of standard deviation of columns mean height values plotted in Cartesian coordinates to clearly show the different rates of change.

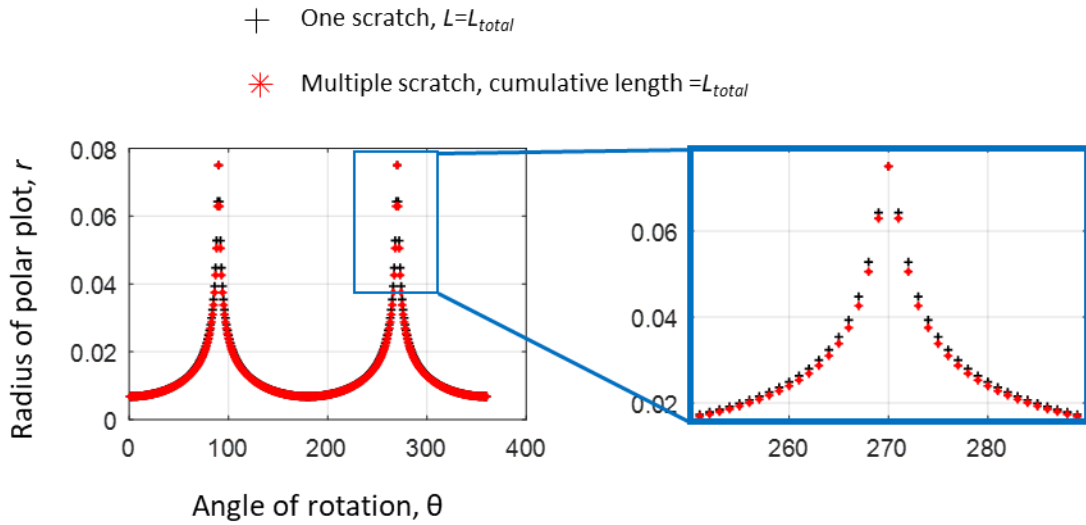


Figure 6-59: Standard deviation of the μh histogram plotted in Cartesian coordinates.

In this case when features have the same width but have different length values, Figure 6-60, their width along with their cumulative length can be calculated as mentioned above.

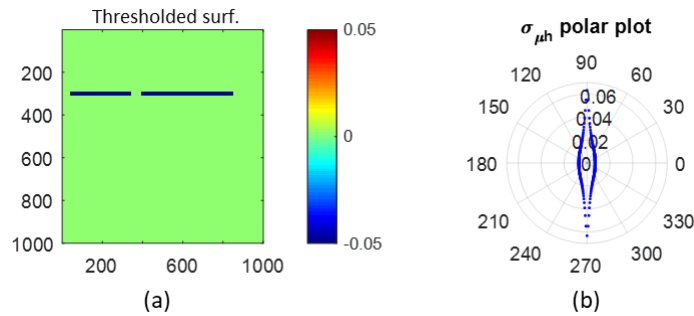


Figure 6-60: a) A thresholded surface with two scratches of the same width and different length values, and b) its $\sigma_{\mu h}$ polar plot.

However, if the width of features is different from each other, see Figure 6-61, independent of the length of them no information about the width or cumulative area can be obtained from the polar plots.

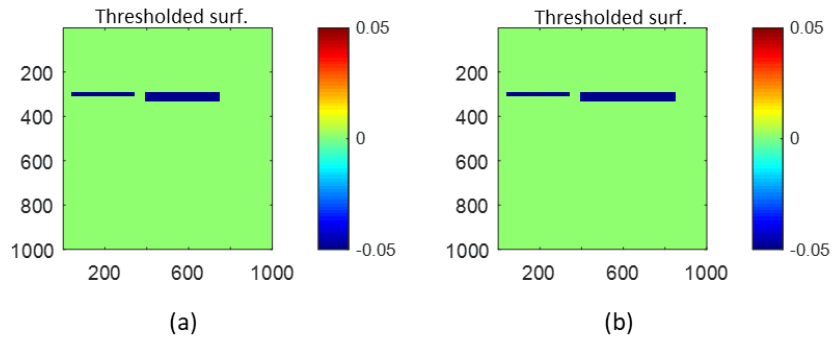


Figure 6-61: A thresholded surface containing a) two scratches with the same length and different width, b) two scratches with different length and width values.

Characteristics of the $\sigma_{\mu h}$ polar plot, see Figure 6-57(b), of the surfaces containing this configuration of features are:

- Only two lobes exist on the polar plot.
- R_{max} occur at the angles where the features are vertical.
- $r_{min} = r_{max \pm 90^\circ}$

6.3.4.3 Not-overlapping when all features are horizontal

This situation is depicted in Figure 6-62(a), where identical parallel scratches with 300 pixels length and 20 pixels width are located on the surface such that at the angle where the features are horizontal each column crosses only one scratch, i.e. there is no overlapping between scratches at this angle. Typical $\sigma_{\mu h}$ polar plot of this surface is shown in Figure 6-62(b).

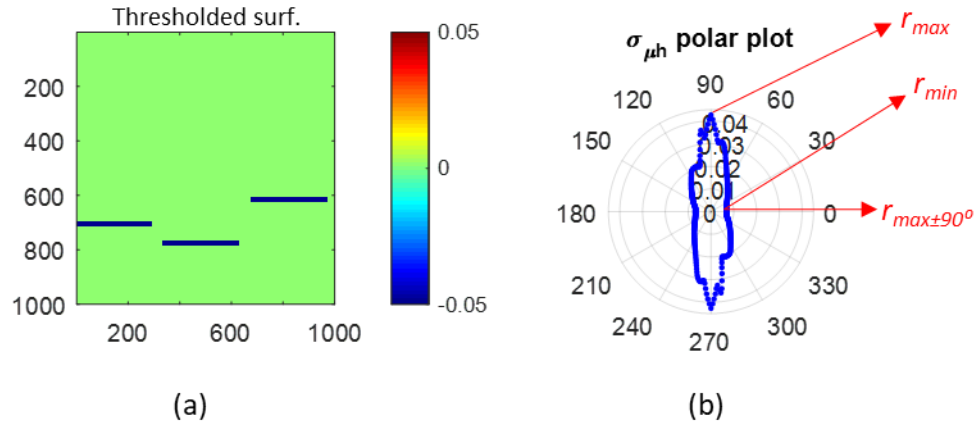


Figure 6-62: A thresholded surface with three parallel scratches without overlapping, and b) its $\sigma_{\mu h}$ polar plot.

The number of feature-related pixels in the feature-related columns is maximum when the surface is rotated 90° from its initial orientation, and the features are vertical. The angle between the features and the horizontal axis at the initial orientation of the surface is equal to 0° , and the critical angle of each of these features based on equation 6-32 is equal to 87.13° , since 90° is larger than the critical angle, the maximum radius of the polar plot can be calculated from equation 6-37, by substituting the total area of features from equation 6-26 in this formula the length of features can be calculated which is equal to:

$$L = \frac{4n^4 r_{\max}^2 + A_{\text{total_scr}}^2 d^2}{\sqrt{2n} A_{\text{total_scr}} d^2} \quad (6-42)$$

Where r_{\max} is the maximum radius of the polar plot.

Based on the geometrical analysis of the features the only angle at which the number of feature-related pixels in the feature related-columns is minimum, equal to the width of scratches, w , is when they are horizontal, and thus the radius of the polar plot is minimum at this angle. At this angle by substituting the total area of features from equation 6-26 in equation 6-34 the width of each feature can be calculated:

$$w = \frac{4n^4 r_{\min}^2 + A_{\text{total_scr}}^2 d^2}{\sqrt{2n} A_{\text{total_scr}} d^2} \quad (6-43)$$

Where r_{min} is the minimum radius of the polar plot.

After calculating the length, L , and the width, w , of the scratches, the only unknown is the quantity of features, α_{scr} , that can be calculated from equation 6-26.

When features have the same width but are different in terms of their length, Figure 6-63, then their width can be calculated via equation 6-43, but the length of each individual feature cannot be determined via equation 6-42, and only the cumulative length can be calculated using equation 6-26.

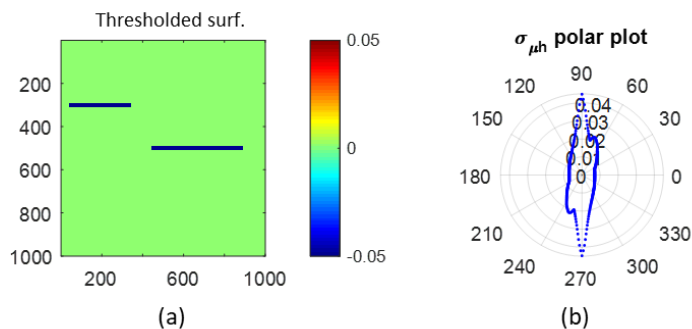


Figure 6-63: a) A thresholded surface with two non-overlapping scratches with the same width but different lengths, and b) its $\sigma_{\mu h}$ polar plot.

When the non-overlapping features have different widths and length, see Figure 6-64, then no information about the quantity, width, and their length can be obtained from the polar plots.

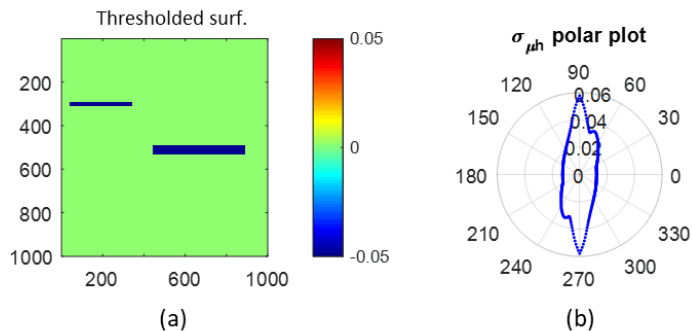


Figure 6-64: A thresholded surface with two non-overlapping scratches with different widths and lengths, and b) its $\sigma_{\mu h}$ polar plot.

Characteristics of the $\sigma_{\mu h}$ polar plot, see Figure 6-62(b), of the surfaces containing this configuration of identical features are:

- More than two lobes are present on the polar plot.
- R_{max} occur at the angles where the features are vertical.
- $r_{min} = r_{max \pm 90^\circ}$

6.3.4.4 Randomly located, no restrictions about overlapping

This case is depicted in Figure 6-65(a) where parallel and identical scratches with 300 pixels length and 20 pixels width are randomly located on the surface, overlapping exists between all or some number of scratches. Typical $\sigma_{\mu h}$ polar plot of this surface is shown in Figure 6-65(b).

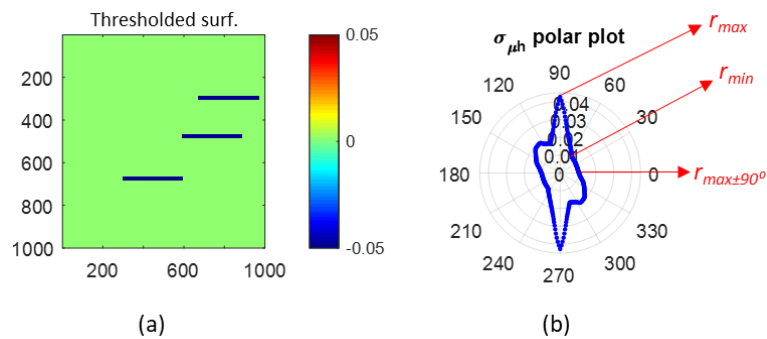


Figure 6-65: a) A thresholded surface with three parallel scratches, and b) its $\sigma_{\mu h}$ polar plot.

Similar to the previous cases the maximum number of feature-related pixels in the feature-related columns happens when all of the features are vertical, i.e. $\theta=90^\circ$ in Figure 6-65(a).

The angle between the features and the horizontal axis at the initial orientation of the surface is equal to 0° , the critical angle of each of these features based on equation 6-32 is equal to 87.13° , since 90° is larger than the critical angle, the maximum radius of the polar plot can be calculated from equation 6-34, by substituting the total area of features in this formula the length of features can be calculated via equation 6-42. Once the length is calculated the cumulative width, w_{total} , can also be achieved from equation 6-36.

Since the location of the features on the surface in this case is random, the angle at which the number of feature-related pixels in the feature-related columns is minimum cannot be formulized; and completely depends on the placement of the scratches. Therefore, it is not possible to find out the spacing between features as well as the quantity of them.

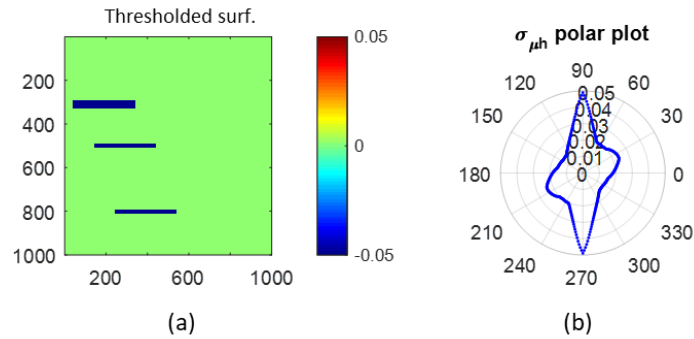


Figure 6-66: a) A thresholded surface with three randomly located scratches with equal length but different width, and b) its $\sigma_{\mu h}$ polar plot.

In this case of parallel scratches when the length of all of the features is equal to each other but their width is different as shown in Figure 6-66, the length of them can be calculated via equation 6-42, however, the cumulative width or the quantity of the scratches cannot be determined.

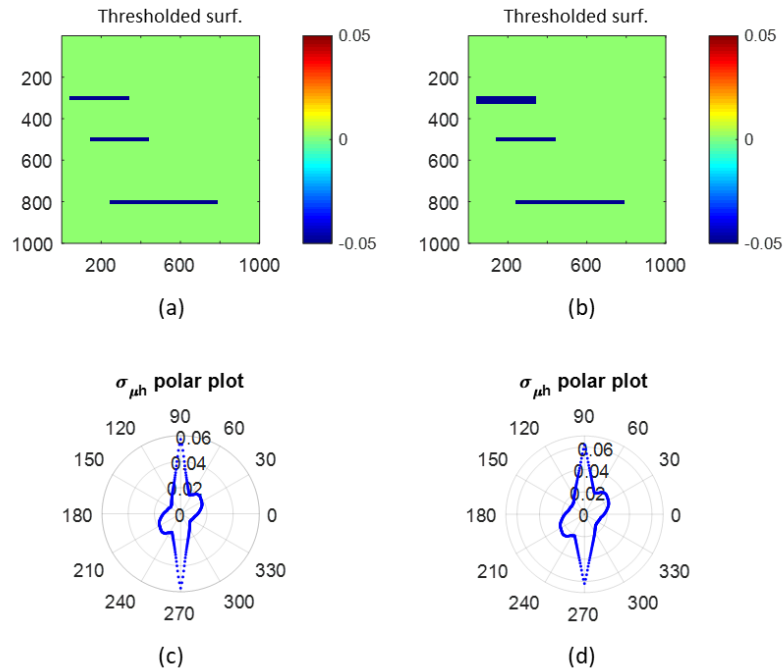


Figure 6-67: A thresholded surface with three randomly located scratches with a) equal width but different length, b) different widths and lengths, and c) and d) their $\sigma_{\mu h}$ polar plots.

When features have the same width but are different in terms of their length, Figure 6-67(a), no information regarding their length, width and quantity can be obtained from polar plots. So is the case when features are different from each other in terms of both length and width, Figure 6-67(b).

Characteristics of the $\sigma_{\mu h}$ polar plot, see Figure 6-65(b), of the surfaces containing this configuration of features are:

- More than two lobes are present on the polar plot.
- R_{max} occur at the angles where the features are vertical.
- $r_{min} \neq r_{max \pm 90^\circ}$

6.3.5 non-straight scratches

In this case where features are not rectangular, i.e. curved scratches it is possible to find out their major directionality as well as their quantity. However, estimating their length and width is

not possible from polar plots as it is highly dependent on the geometry of features, i.e. radius of the curvature.

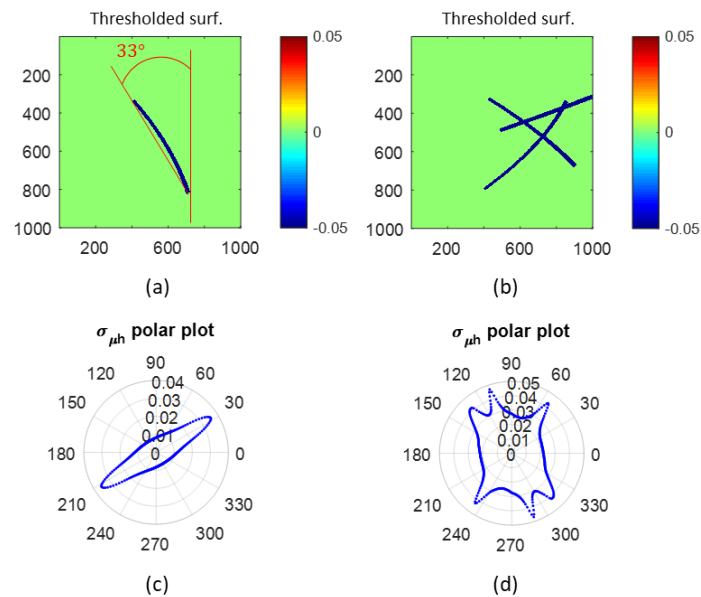


Figure 6-68: a) A thresholded surface with a single non-straight scratch, b) a thresholded surface containing three non-straight scratches, c) and d) their $\sigma_{\mu h}$ polar plots.

Figure 6-68(a) depicts a thresholded surface with a curved scratch, the $\sigma_{\mu h}$ polar plot of this surface is shown in Figure 6-68(c), from this polar plot the major directionality of this feature that is the angle enclosed between the straight line connecting both ends of the feature and the vertical axis is equal to 33° . This means that the number of feature-related pixels in the feature-related columns at this angle is at its maximum.

Figure 6-68(b) depicts a thresholded surface containing three non-straight scratches, and its $\sigma_{\mu h}$ polar plot is shown in Figure 6-68(d), this polar plot has six peaks that leads to the quantity of the features equal to three, and the angle of each peak points at the major directionality of each one of the features.

6.3.6 Analysis of a real surface with a single scratch

In section 5.3.3 a real surface from NIST scratch dig standard with a single linear feature was analyzed based on its σ_{Rq} polar plot, and its length, width, and depth were estimated equal to 90.4

μm (226 pixels), $10 \mu\text{m}$ (25 pixels), and $0.060 \mu\text{m}$ respectively. The same surface can also be analyzed with its $\sigma_{\mu h}$ polar plot and using equation 6-10.

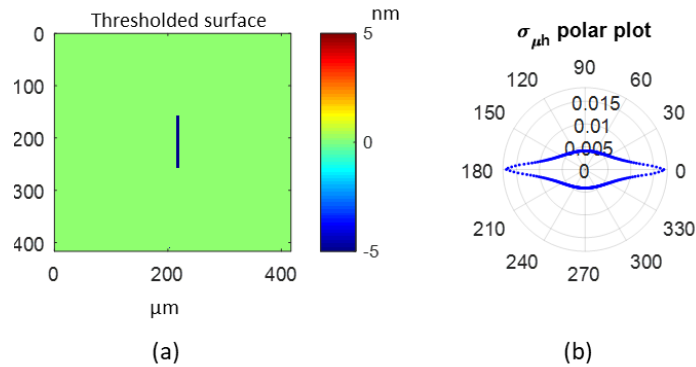


Figure 6-69: a) The thresholded surface with the single negative linear feature, b) its $\sigma_{\mu h}$ polar plot.

For this surface the threshold depth is selected equal to $5 \mu\text{m}$, every height value smaller than this limit is set to zero and every value larger than this limit is set to 1, i.e. $d = 1$. This thresholded surface is shown in Figure 6-69(a), and its $\sigma_{\mu h}$ polar plot in Figure 6-69 (b). The maximum and minimum radius of the $\sigma_{\mu h}$ polar plot is equal to 0.0172 nm and 0.0041 nm respectively. From the computer system the total number of non-zero pixels, i.e. total area of the feature is equal to 3912 pixels. Putting the maximum radius, r_{max} , and the total area, A_{total_scr} into equation 6-42 the length is equal to:

$$L = \frac{4 \times 1024^4 \times 0.0172^2 + 3912^2 \times 1^2}{\sqrt{2} \times 1024 \times 3912 \times 1^2} \rightarrow L = 232.37$$

Considering the discrete nature of the pixels the length is estimated equal to 232 pixels, which is equal to $92.8 \mu\text{m}$. Similarly, the width, w , of the scratch can be calculated via equation 6-43 and is equal to:

$$w = \frac{4 \times 1024^4 \times 0.0041^2 + 3912^2 \times 1^2}{\sqrt{2} \times 1024 \times 3912 \times 1^2} \rightarrow w = 15.75$$

The width is estimated equal to 16 pixels, which is equivalent of 6.4 μm when considering the pixel resolution of the 20 \times objective.

In order to find out the depth of the feature in the thresholding procedure the height values that are greater than the threshold height value remain unchanged, and only those that are smaller than the threshold will be set to zero. The $\sigma_{\mu h}$ polar plot of this surface is shown in Figure 6-70.

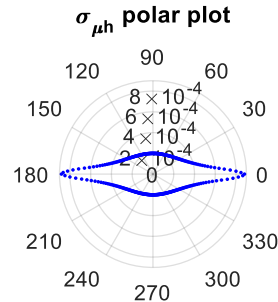


Figure 6-70: $\sigma_{\mu h}$ polar plot of the thresholded surface with the negative linear feature.

The maximum and minimum radius of this polar plot, Figure 6-70, is equal to 0.00088 μm and 0.00019 μm respectively. Now that the length and width are known values either of the equations 6-42 or 6-43 can be used to obtain the depth of the scratch. Based on equation 6-42 the depth is calculated equal to 0.051 μm .

$$232.37 = \frac{4 \times 1024^4 \times 0.00088^2 + 3912^2 \times d^2}{\sqrt{2} \times 1024 \times 3912 \times d^2} \rightarrow d = 0.051$$

The reason for this error could be due to the fact that the bottom of the scratch in the thresholded surface is not perfectly a flat plane, and has variations in magnitude. Also the estimated length is less than the measured length with the software, and thus this difference induces error on the $\sigma_{\mu h}$ polar plot which its maximum radius was used to estimate the depth.

6.3.7 Analysis of real surfaces with multiple scratches

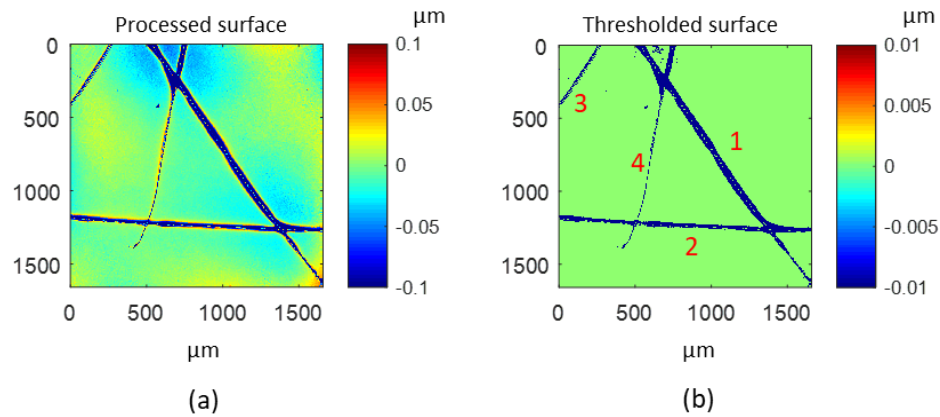


Figure 6-71: a) Polished glass surface measured with CSI 5 \times after processing, and b) the same surface after it is thresholded.

Figure 6-71(a) depicts a BK7 glass polished sample that was measured with Zygo Zegage coherence scanning interferometer (CSI) 5 \times objective with 1.6 mm \times 1.6 mm field of view. Piston, tilt, and a 4th order polynomial are removed from the initial height map. Sq surface roughness of the surface excluding defects is equal to 0.005 μm . The surface is thresholded with the threshold height equal to 0.016 μm and is shown in Figure 6-71(b); this threshold value is selected to be 3.2 times larger than the Sq of the surface because in a surface with Gaussian distribution of heights 3.2 times the standard deviation covers 99.9% of the data, and any value above it is considered as a outlier, i.e. defect. From the thresholded surface four scratches are visible labeled as 1, 2, 3, and 4. In this surface all of the height values above the threshold height are set to 1, and all of them that are smaller than the threshold height are set to zero.

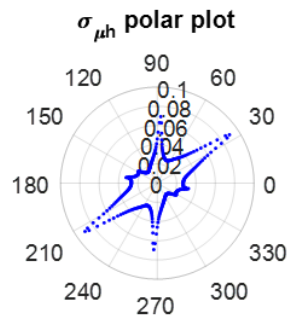


Figure 6-72: $\sigma_{\mu h}$ polar plot of the surface with four scratches.

The $\sigma_{\mu h}$ polar plot of the thresholded surface is shown in Figure 6-72, eight peaks are visible in this plot, which shown that there are four non-parallel scratches on the surface.

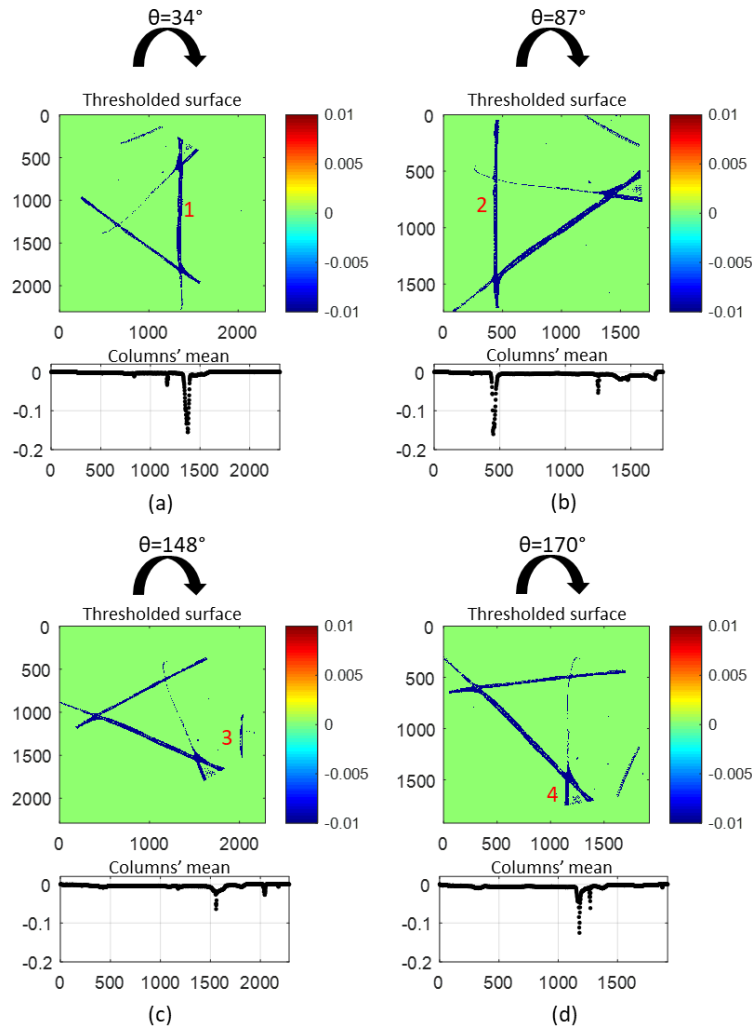


Figure 6-73: a) Thresholded surface rotated 34° clockwise, b) thresholded surface rotated 87° clockwise, c) thresholded surface rotated 148° , and d) thresholded surface rotated 170° clockwise along with their columns mean height graph.

To estimate the length and depth the original surface is rotated based on the angular location of the peaks in the upper half of the polar plot, at each rotation only one scratch becomes vertical. From the columns mean height graph it is possible to find out the width of each feature. In Figure 6-73(a) the width and length of the scratch is estimated to be 30 pixels ($48 \mu\text{m}$ when considering the pixel resolution of the $5\times$ objective) and from equation 6-27 the length is equal to 1143 pixels, which is equal to 1.83 mm. Similarly for the surfaces in Figure 6-73(b), (c), and (d) the width and

length is estimated to be 20×1023 pixels, 3×291 pixels, and 5×670 pixels respectively, (32×1.64 mm, $4.8 \mu\text{m} \times 465 \mu\text{m}$, and 8×1.07 mm). In order to find the depth of the features in the thresholding process the height values below the threshold limit is set to zero, while all the values above the threshold limit remain unchanged from the initial height values. Now by using equation 6-27 the depth of features 1, 2, 3, and 4 can be estimated as $0.12 \mu\text{m}$, $0.14 \mu\text{m}$, $0.12 \mu\text{m}$, and $0.08 \mu\text{m}$ respectively.

Table 6-3: Scratches' properties from CSI and polar plots.

Scratch #	$l \times w \times d$	$l \times w \times d$
	(pixel \times pixel \times μm) from CSI	(pixel \times pixel \times μm) from polar plot
1	$1177 \times 35 \times 0.15$	$1143 \times 30 \times 0.12$
2	$1018 \times 22 \times 0.15$	$1023 \times 20 \times 0.14$
3	$313 \times 4 \times 0.14$	$291 \times 3 \times 0.12$
4	$780 \times 9 \times 0.11$	$670 \times 5 \times 0.08$

Scratches' properties from CSI that were measured manually with the instrument software and from polar plots are given in Table 6-3, it should be noted that in this table the values from CSI are average values.

6.4 Multiple linear and circular features on the surface

When there are both linear and circular features on the surface their effect is reflected on the surface's polar plot. This section details the effect of a single linear, and a single circular feature present on the surface simultaneously on the polar plots, then expands the analysis to more complex cases consisting of multiple linear and circular features. Threshold limit for distinguishing scratch and dig related peaks on the polar plots will be explained.

6.4.1 Building blocks for polar plots of multiple linear and circular features

Based on the previous sections of this chapter a linear feature will create two peaks on the polar plot at the angle where the feature becomes vertical Figure 6-74(a), also a single circular feature only increases the radius of the polar plot, Figure 6-74(b), while two circular features not only increase the radius of the polar plot but also create two peaks on it, Figure 6-74(c).

To analyze the behavior of the polar plots in their general form where the surface contains multiple linear and circular features, another case must be studied which is the combination of a linear and a circular feature on the surface and its effect on the polar plots.

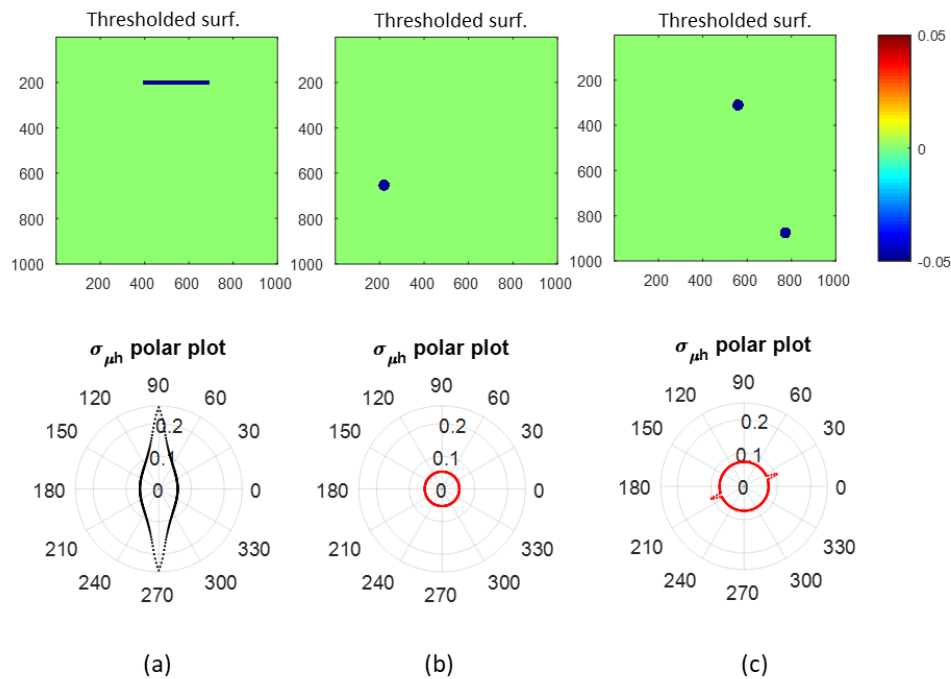


Figure 6-74: a) A thresholded surface with a linear feature, b) a thresholded surface with a single negative circular feature, and c) a thresholded surface with two negative circular features and their $\sigma_{\mu h}$ polar plot.

6.4.2 A circular and a linear feature on the surface

The polar plot of a surface that contains both a single circular and a single linear feature is shown in Figure 6-75(b). There are two sharp peaks in this polar plot that are created by the presence of the single scratch, however, since the single circular feature does not create any number

of lobes, its presence is reflected on the polar plot in another way. The standard deviation of the columns mean values, μh histogram, that is the radius of the $\sigma_{\mu h}$ polar plot, is directly related to the number of feature-related pixels in the feature-related columns, so during the rotation process when those columns that include the entire circular feature also include sections of the linear feature, the standard deviation of the μh histogram increases. This increase of standard deviation continuous until the angle where the columns again begin to cross only one feature. The step-like behavior of the polar plot that is depicted in Figure 6-75(c) is the result of this phenomenon. The slope of this step-like peak in the polar plot is also related to the geometry of the features and their configuration with respect to each other, this slope decreases as the features are closer together and vice versa. Further analysis is required to capture more information from this feature of the polar plots of surfaces with mixed features.

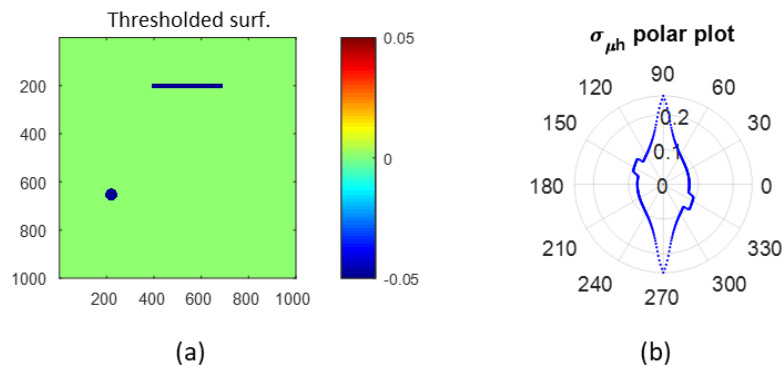


Figure 6-75: a) A thresholded surface with a negative circular feature and a scratch, b) its $\sigma_{\mu h}$ polar plot.

The minimum and maximum radius of this polar plot is larger than polar plots of surfaces with the single feature, however, it is not equal to the summation of their radii at any angle, i.e. it is not equal to the superposition of the two, Figure 6-76.

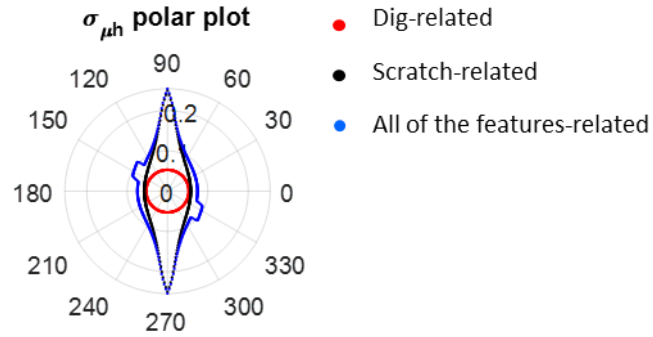


Figure 6-76: $\sigma_{\mu h}$ polar plot of the surface in Figure 6-75(a) with its constituent elements.

Geometrical analysis of the location of the scratch and the circular feature on the surface can estimate the width of this step-like peak on the polar plot, $\Delta\theta$ in Figure 6-77(a), and (b). Considering the upper half of the polar plot of Figure 6-77(b) the step-like peak begins at $\theta=136^\circ$, at this angle feature-related columns begin to include sections of both of the features, Figure 6-77(c), this behavior continuous until $\theta = 156^\circ$ which is the last angle that columns are including both features, and after that the feature-related columns only contain sections of just one feature. The difference between these two angles is the angle enclosed between the two lines connecting the center of the circular feature to the both end of the scratch.

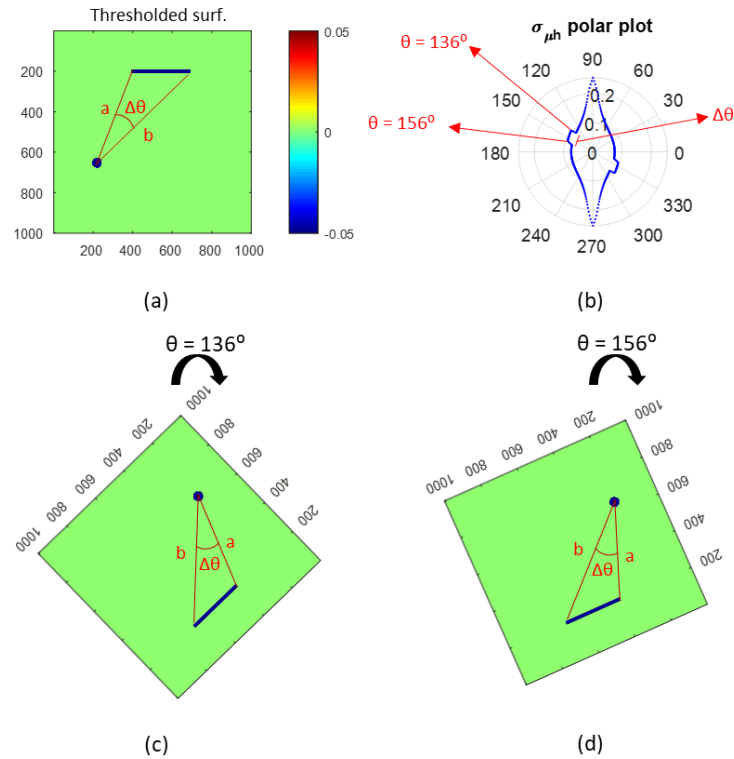


Figure 6-77: a) A thresholded surface with a negative circular and a linear feature, b) its $\sigma_{\mu h}$ polar plot, c) the same surface when it is rotated 136° , and d) when rotated 156° .

From the polar plot it is not possible to estimate the geometry of each of the features since a and b are unknown. However, it could be concluded that the maximum radius of the polar plot occurs at the angle where the linear feature is vertical, and the indicator of the presence of a single circular feature is the step-like peak behavior of the polar plot. The width of this step is a function of the location of the features with respect to each other, and as they get closer to each other, the step-like peak becomes wider, and vice versa.

6.4.3 Deconstructing complex cases using building blocks

From the result of the previous section, during the rotation procedure whenever the feature-related columns begin to include sections of both features, i.e. the number of feature-related pixels in the feature-related columns increases, there will be a step-like peak on the polar plot. By breaking down the case where two circular features and a linear feature are present on the thresholded surface

the behavior of the polar plot can be predicted and explained. It should be noted that these features do not have to have equal areas, i.e. there is no limitation on the geometry of the features. The linear feature will create two sharp peaks at the angle when it becomes vertical, the two circular features will create two peaks at the angle where they are contained within the same number of columns. Based on the geometrical analysis of the features each time that the scratch and one of the digs are included in the feature-related columns there will be a step-like peak; therefore since this situation is possible to occur two times, then the number of step-like peaks is equal to four, see Figure 6-78.

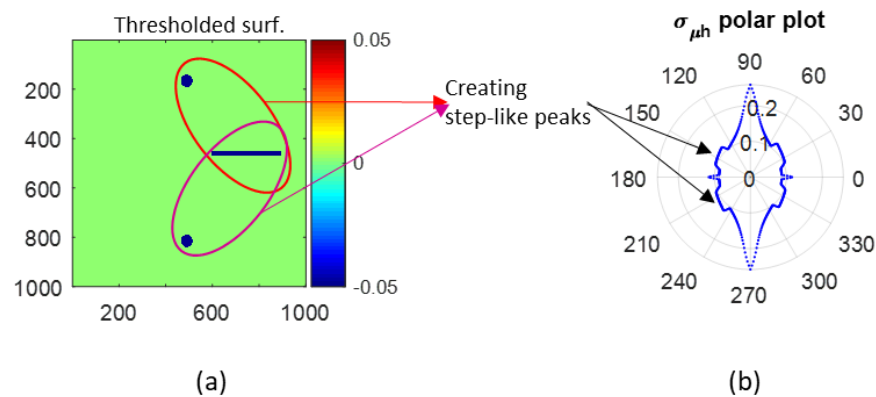


Figure 6-78: a) A thresholded surface with a pair of negative circular features, and a scratch, and b) its $\sigma_{\mu h}$ polar plot.

It should be noted that the peaks on the polar plots are generally dominated by linear features rather than circular features. This is due to the fact that when linear features are in vertical position they will increase the number of feature-related pixels in the feature-related columns far more than a pair of aligned circular features. This is depicted in Figure 6-78(b) where the radius of the polar plot at the angle of two scratch-related peaks at 90° and 270° are significantly larger than the two dig-related peaks at 0° and 180° .

6.4.4 General case of multiple circular and linear features on the surface

The radius of the $\sigma_{\mu h}$ polar plot only depends on the number of feature-related pixels in the feature-related columns, and this number is a function of the quantity of features and their relative

position with respect to each other. It should be noted that the areas of the features do not have to be equal to each other and the following discussion holds true in general.

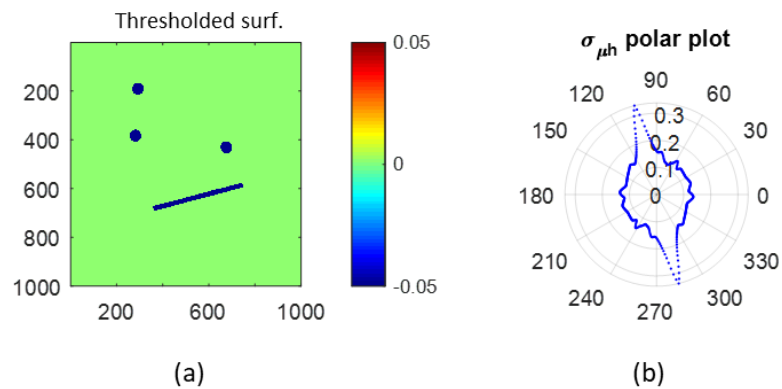


Figure 6-79: a) A thresholded surface with three negative circular features and one linear feature, b) its $\sigma_{\mu h}$ polar plot.

The surface in Figure 6-79(a) contains three negative circular features and one linear feature, considering only circular features six peaks are expected on the polar plot, each pair of a circular and linear feature creates two step-like peaks, and there is three possible pairs of this kind, so total of six step-like peaks. Finally the linear feature itself generates two peaks on the polar plot. The total of 14 peaks are expected to be on the polar plot, see Figure 6-79(b).

Figure 6-80 breaks down the polar plot shown in the Figure 6-79(b) to two of its constituent elements, one is all the peaks that are created by the circular features, the other is the peaks that are created by the linear scratch. All of the 14 peaks are numbered in this polar plot.

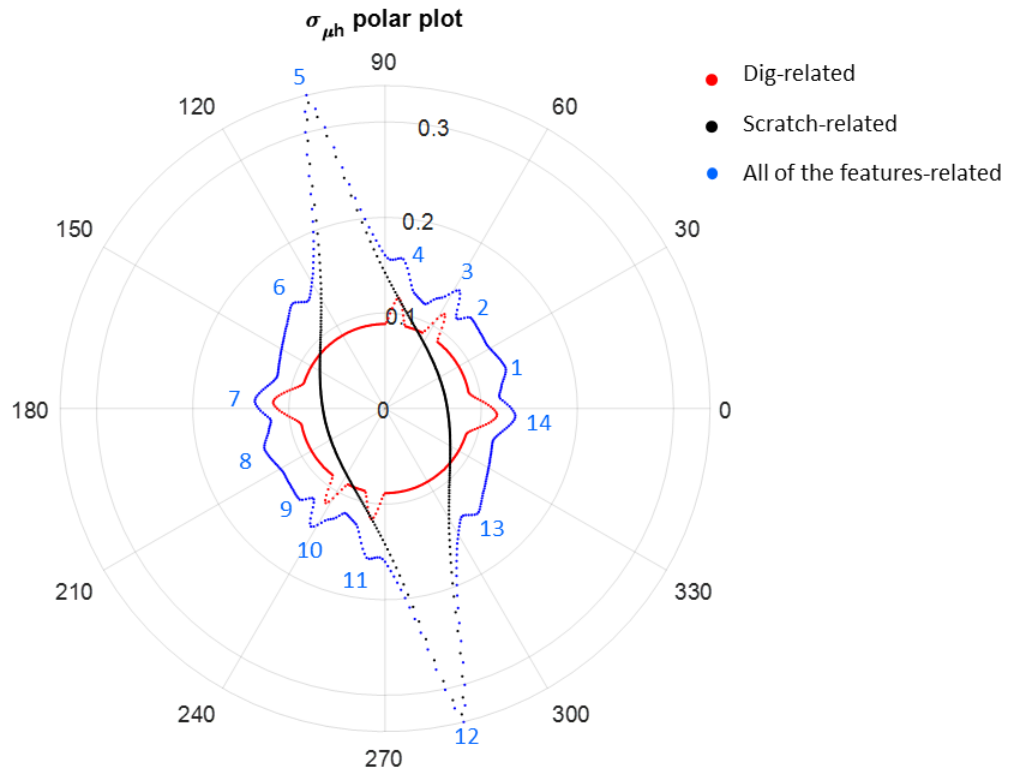


Figure 6-80: $\sigma_{\mu h}$ polar plot of the surface shown in Figure 6-79(a).

As the number of the features on the surface increases the complexity of the behavior of the polar plots increases significantly such that it might not be possible to identify all of the possible peaks that can exist on the polar plots, and also it might not be feasible to distinguish the specific type of peaks, that is to tell what kind of combination of features have created the peak.

However, analyzing each detected peak on the polar plot can provide some insights about the different types of features present on the surface.

6.4.5 Peak analysis

A criterion has to be defined in order to analyze each detected peak and identify the specific feature or combination of features that created it. Again, the two key metrics from the polar plots can be used to define this criterion, that are maximum and minimum radius of the $\sigma_{\mu h}$ polar. The following discussion in this section details the steps required for setting the criterion for identifying

different types of peaks, it assumes that the cumulative area of the pair of circular features, and the area of the single linear feature are equal to each other. It should be noted that these constraints have to be made to explain the general idea of the procedure, however, they do not result in the foolproof results; and therefore further study is required in this area.

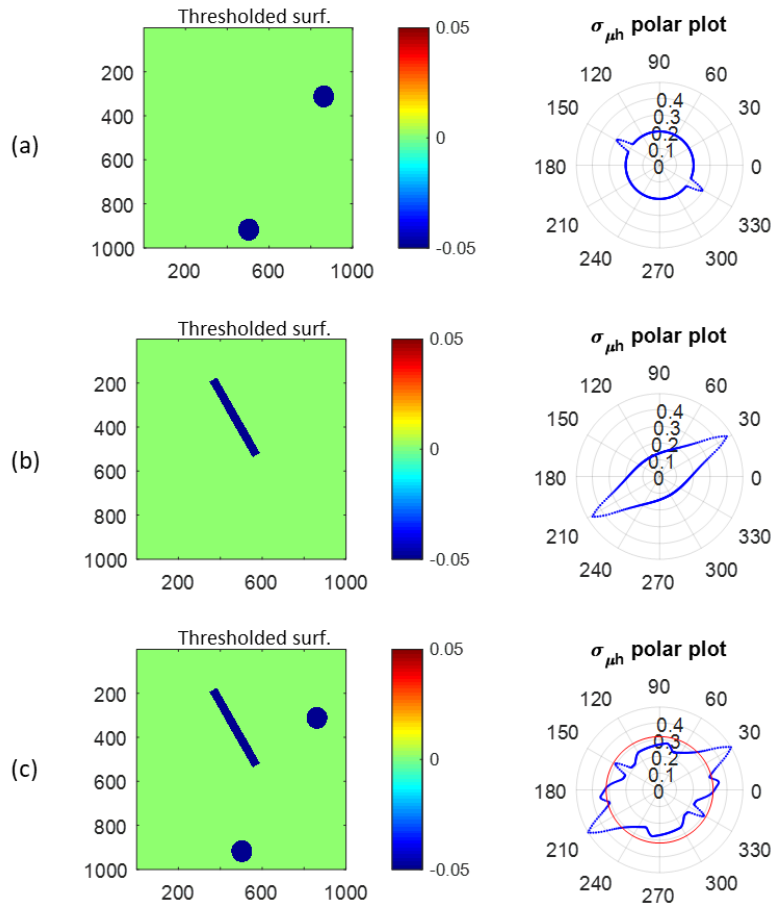


Figure 6-81: a) A thresholded surface with two negative circular features, b) a thresholded surface with a scratch, c) a thresholded surface with two circular and a linear feature, and their $\sigma_{\mu h}$ polar plots.

Figure 6-81(a) shows a thresholded surface with two negative circular features with their radius equal to 50 pixels and its $\sigma_{\mu h}$ polar plot. Figure 6-81(b) depicts another thresholded surface with a linear feature present on it with its area equal to the area of the two circular feature (400 pixels length and 40 pixels width), and its $\sigma_{\mu h}$ polar plot, the depth of the features are equal and is 0.1 μm . When these three features are present on another thresholded surface they will generate eight peaks on the polar plot, see Figure 6-81(c).

A peak is considered a scratch-related peak if it goes outside of a threshold circle whose radius is 1.5 times the minimum radius of the polar plot. This threshold circle is demonstrated in red in Figure 6-81(c). If a peak is inside this threshold circle then it is considered a dig-related peak, or a scratch-dig-related peak, see equation 6-44.

$$\frac{r_{peak}}{r_{min}} > 1.5 \rightarrow \text{scratch} - \text{related}$$

$$\frac{r_{peak}}{r_{min}} \leq 1.5 \rightarrow \text{dig} - \text{related}$$
(6-44)

Where r_{peak} is the radius of the $\sigma_{\mu h}$ polar plot at each peak.

The 1.5 constant in equation 6-44 is chosen based on the fact that the two circular features and the single linear feature of Figure 6-81(a) have equal areas, and when all three features are present on the surface the ratio of the radius of the polar plot at the dig-related peak to the minimum radius of the polar plot is close to 1.5. However, this constant would have to be changed and adjusted based on the required sensitivity of detecting features on the part.

Based on equation 6-44 a feature is considered a scratch if the ratio of its maximum radius of $\sigma_{\mu h}$ polar plot to the minimum radius is larger than 1.5. From this definition and based on equations 6-31 for r_{max} , and 6-28 for r_{min} for a single scratch the minimum ratio of the length of a scratch to its width should be:

$$\frac{L}{w} > 2.25$$
(6-45)

Where L is the length and w is the width of the scratch.

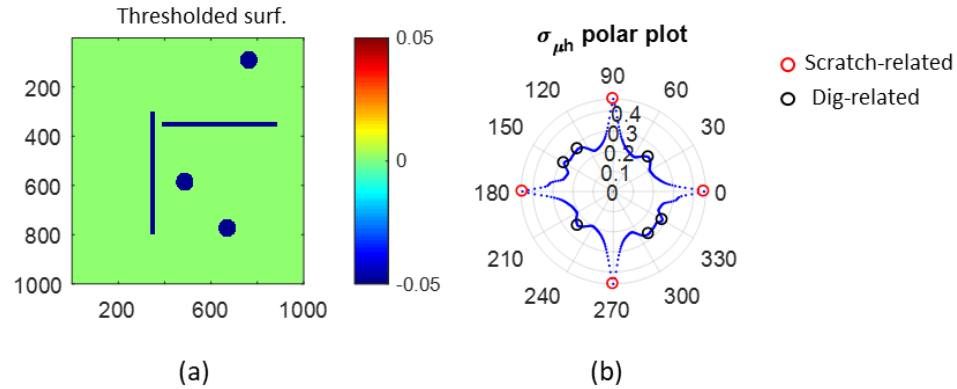


Figure 6-82: a) A thresholded surface with three negative circular, and two linear features, b) its $\sigma_{\mu h}$ polar plot.

Figure 6-82(a) depicts a thresholded surface with three negative circular, and two linear features. From this surface and its features six dig-related peaks, four scratch-related peaks, and 12 scratch-dig-related peaks are expected to be on the surface's $\sigma_{\mu h}$ polar plot, the total of 22 peaks. However, only ten peaks are counted on the polar plot, and among these peaks four are caused by the scratches, and six are caused by the presence of the three circular features. Despite the fact that not all the required peaks are reflected on the polar plot, the correct quantity of each type of features can be calculated. This is because six circular feature-related peaks on the polar plot will result in three number of circular features on the surface (equation 6-2), and four scratch-related peaks on the polar plot will result in two number of linear scratches (equation 6-27), so while all of the expected 22 peaks are not detected still the correct number of features are estimated from the $\sigma_{\mu h}$ polar plot.

In summary the signature peak of each type of features is shown in Figure 6-83.

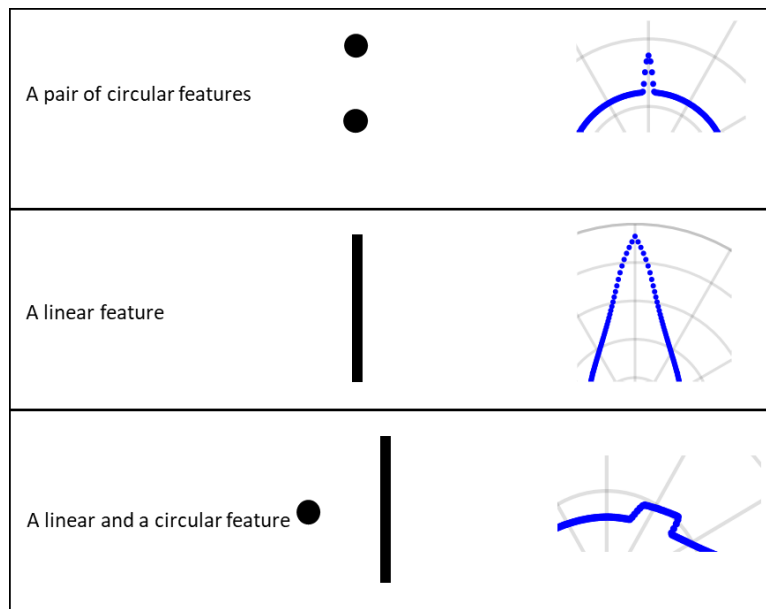


Figure 6-83: Signature peak of each type of features' combination.

6.4.6 Analysis of a real surface with mixed features

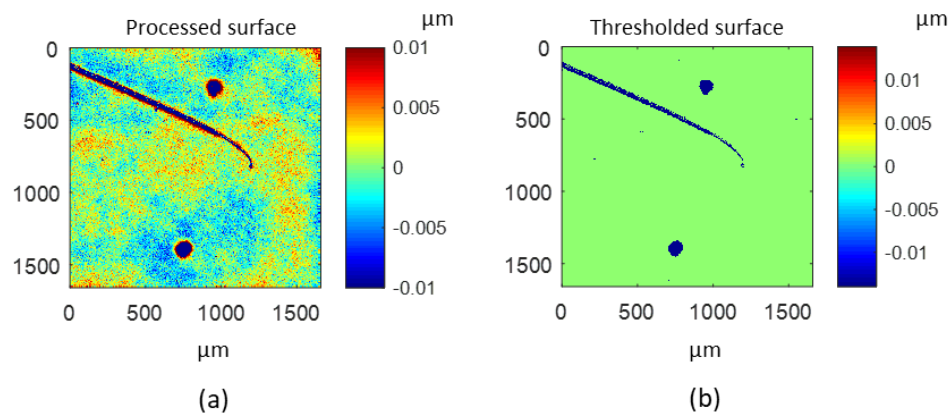


Figure 6-84: a) Polished glass surface measured with CSI 5 \times after processing, and b) the same surface after it is thresholded.

Figure 6-84(a) depicts a BK7 glass polished sample that was measured with Zygo Zegage coherence scanning interferometer (CSI) 5 \times objective with 1.6 mm \times 1.6 mm field of view. Piston, tilt, and a 4th order polynomial are removed from the initial height map. S_q surface roughness of the surface excluding defects is equal to 0.005 μm . The surface is thresholded with the threshold height equal to 0.016 μm and is shown in Figure 6-84(b); this threshold value is selected to be 3.2 times larger than the S_q of the surface because in a surface with Gaussian distribution of heights

3.2 times the standard deviation covers 99.9% of the data, and any value above it is considered as an outlier, i.e. defect. From the thresholded surface two near-circular and one near-linear features are visible.

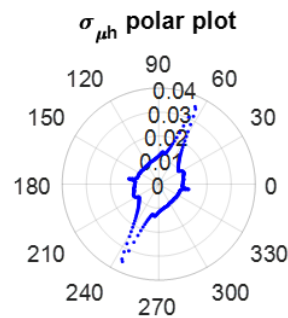


Figure 6-85: $\sigma_{\mu h}$ polar plot of the surface with mixed features.

Figure 6-85 shows the $\sigma_{\mu h}$ polar plot of the thresholded surface, from this polar plot the presence of the step-like peak on the plot is an indicator of a surface with mixed features, from the same peak it can be concluded that there is at least one scratch and one dig on the surface. The magnitude of the first peak in the upper half of the polar plot is larger than the second peak, therefore it is caused by a linear or near-linear feature, i.e. scratch, the second peak in the upper region of the polar plot is caused by presence of a pair of digs. The conclusion of presence of two digs on the surface is based on the fact that there is two low magnitude peaks on the polar plot. Finally, it can be concluded that the surface contains one near-linear feature and two near-circular features.

6.5 Obtainable information about the surface from the polar plots

In this section the question sought to be answered is how much information about surface texture and features is obtainable only from the polar plot's information without a prior knowledge of the analyzed surface? In order to answer this question, the first step is to pay attention to the specific type of the available polar plot. The σ_{Rq} polar plot for a defect-free surface with Gaussian distribution of heights with its Sq equal to $1.02 \mu\text{m}$ has the same average radius as the σ_{Rq} polar plot

of a surface with its Sq equal to $0.01 \mu\text{m}$ with a negative circular feature with its depth and diameter equal to $5 \mu\text{m}$ and 50 pixels respectively as shown in Figure 6-86.

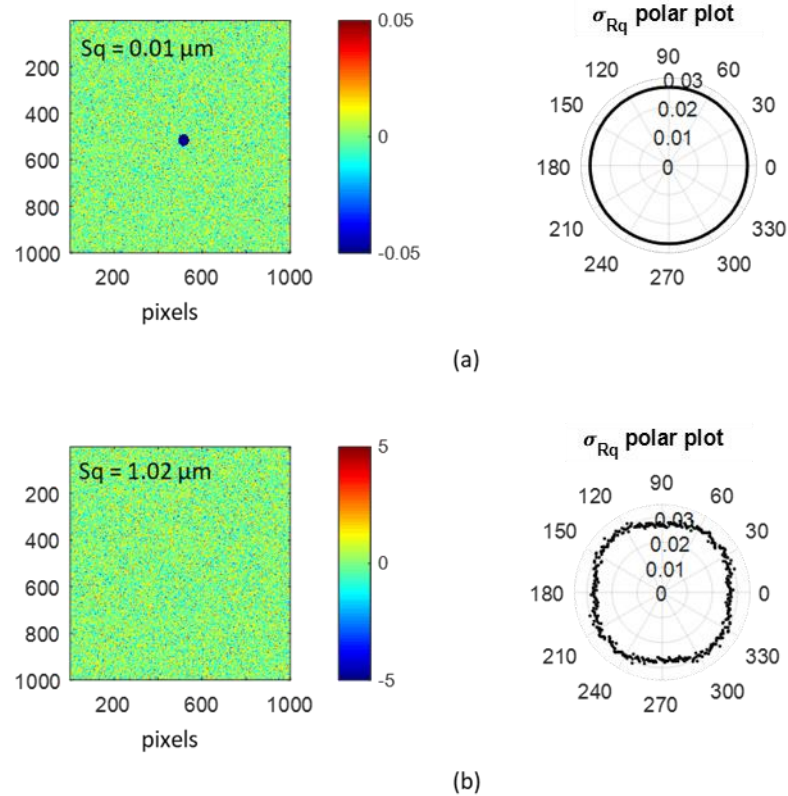


Figure 6-86: a) A MATLAB generated surface with Gaussian distribution of heights with a defect and its σ_{Rq} polar plot, and a defect free surface with Gaussian distribution of heights along with its σ_{Rq} polar plot.

In this case despite the equal average radius of the polar plot of the surfaces the overall shape of them can distinguish between a defect-free surface and a surface containing a defect; the deviations of the σ_{Rq} polar plot's data of the defect free surface is higher than the same polar plot for a surface that contains a defect. However, if the $\sigma_{\mu h}$ polar plot of the surfaces are used the difference can be easily observed. A defect-free surface after thresholding has its $\sigma_{\mu h}$ polar plot's radius equal to zero, whereas a surface that contains a defect has a non-zero value radius (with the same threshold height value). In general when the radius of the $\sigma_{\mu h}$ polar plot of a surface has a non-zero value it is an indication of the presence of the features or texture on the surface.

Key features from the polar plots that need to be analyzed in order to obtain information about the surface are the average radius, number of lobes, maximum radius at the lobe's angular location, the radius 90° before or after the maximum radius, angle between maximum and minimum radius, minimum radius of the polar plot, and the general shape of the lobes on the polar plots.

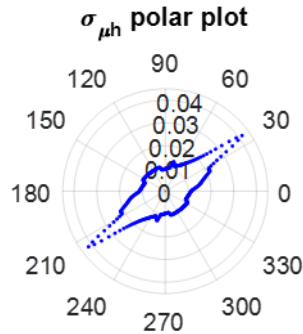


Figure 6-87: $\sigma_{\mu h}$ polar plot of a surface.

Figure 6-87 shows a $\sigma_{\mu h}$ polar plot of a thresholded surface, the polar plot does not have a nominally circular shape and therefore it could be concluded that the surface contains some features. There is a sharp peak at $\theta=34^\circ$ in the upper half of the polar plot, this shows that a scratch is present on the surface whose direction is 34° when measured from the vertical axis. There are four step-like peaks on the surface indicating that the surface contains mixed features and number four informs that there are two pairs of a circular and linear feature on the surface. Combining all the information it can be concluded that the surface contains two circular features and one linear one. This surface is shown in Figure 6-88.

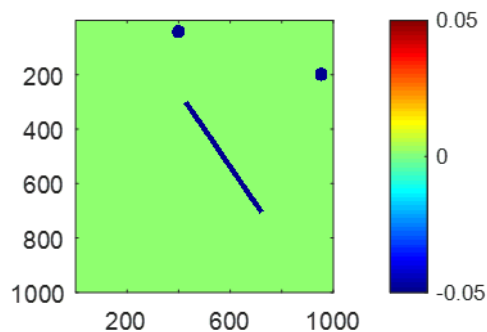


Figure 6-88: A thresholded surface with two negative circular and one negative linear feature.

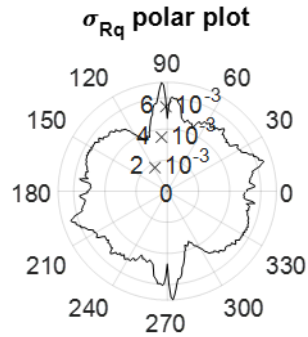


Figure 6-89: σ_{Rq} polar plot of an unknown sample.

6.6 Analyzing polar plots of unknown samples (blind testing)

In this section the only information given to the author were the σ_{Rq} polar plots for a number of surfaces, each polar plot will be analyzed individually, and its key metrics will be identified. Based on the identified key metrics insights of the surface will be provided. At the end of this section the samples that were used to create the polar plots will be given.

Figure 6-89 depicts a σ_{Rq} polar plot of a surface or a grayscale image, from the upper half of this polar plot the key features are: a local minimum at $\theta=90^\circ$ and the radius of the polar plot 90° after the angular location of this local minimum. From these two metrics it can be concluded that the surface contains a major directional feature, the angle enclosed between the directional feature and the vertical axis is 90° ; and that the surface does not contain an organized repeating structure on its surface because the radius of the polar plot 90° after the local minimum is not a close to zero value. Therefore, the sample could be ground surface with horizontal grinding marks, or a surface with the similar nature.

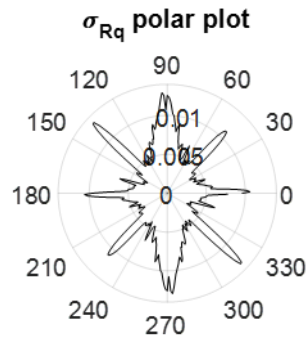


Figure 6-90: σ_{Rq} polar plot of an unknown sample.

Figure 6-90 depicts a σ_{Rq} polar plot of a surface or a grayscale image, from the upper half of this polar plot the key features are: a local minimum at $\theta=90^\circ$, and five local maximums at $\theta\approx 0^\circ$, 45° , 88° , 92° and 135° . The local minimum in between $\theta\approx 88^\circ$ and 92° could be caused by a major horizontal feature or features on the surface. This situation is similar to a surface containing a periodic structure such as a typical milled surface with horizontal tooling marks where there is a local minimum in the polar plot when the surface texture becomes vertical.

From this polar plot it can be concluded that the surface is a highly structured surface that contains multiple directional features with their angles measured from the vertical axis equal to the angular location of the peaks; the shape of the polar plot is similar to the textured surface shown in Figure 4-16(a), therefore it is likely that the surface contains an organized circular or near circular features.

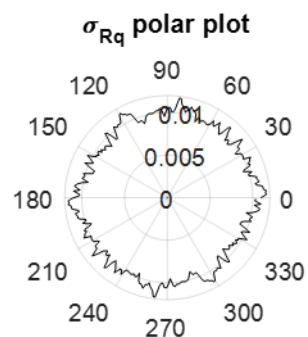


Figure 6-91: σ_{Rq} polar plot of an unknown sample.

Figure 6-91 depicts the σ_{Rq} polar plot of another sample, the radius of this polar plot does not change significantly, and the polar plot does not have any dominant peaks or local minimums. Thus the surface is thought to be an isotropic surface without any directional features.

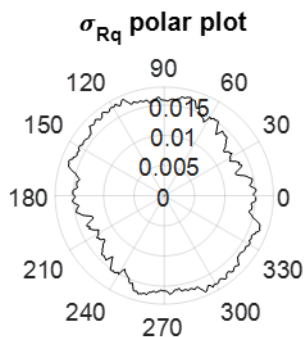


Figure 6-92: σ_{Rq} polar plot of an unknown sample.

In Figure 6-92 the polar plot does not have any dominant peaks or local minima, therefore it is thought that it lacks any linear features or major directional feature. However, the overall shape of the polar plot is not a nominally circular one, and it cannot be concluded that the surface is a highly isotropic one.

The surfaces of these four polar plots (Figures 6-89 to Figure 6-92) that were analyzed are illustrated below in Figures 6-94 to Figure 6-97.



Figure 6-93: Image of the sample of the polar plot shown in Figure 6-89.

The grayscale image of the sample whose σ_{Rq} polar plot was shown in Figure 6-89 is depicted in Figure 6-93. This is a grayscale photo taken from the pavement along the National Mall in Washington DC. The presence of the horizontal feature on the surface was detected from the presence of the local minimum at 90° in the upper half of the polar plot. However, detection of the near-vertical feature was missed, by reanalyzing the polar plot, there is another local minimum in the upper half of the polar plot close to 180° that is caused by this near-vertical feature. Therefore, the effect of this feature was present on the polar plot, but missed by the author.

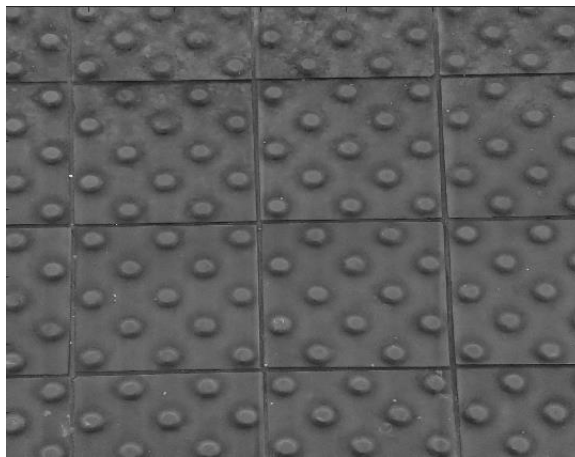


Figure 6-94: Image of the sample of the polar plot shown in Figure 6-90.

Figure 6-94 shows the image of the tiles at the edge of the platform in the DC metro station whose polar plot is shown in Figure 6-90. Highly structured nature of the surface and the general type of the features on its surface (near circular) were correctly detected from the polar plot's key features, however, the periodicity was missed. The local minimum between $\theta \approx 88^\circ$ and 92° on the polar plot was caused by the horizontal lines separating the tiles in the image. The result of using the β value equal to 2° (the difference between the angular location of the local minimum and maximum) and equations 4-9 and 4-11 to 4-14 would not match the wavelength of any structure on the surface, see table 6-4, in these calculations the length of the shorter side of the image is equal to 422 pixels, $n=422$. On the surface the wavelength of the straight horizontal lines is 130 pixels, vertical lines equal to 170 pixels, and the wavelength of near circular features is about 60 pixels.

This is because the constant coefficient in these formulas completely depends on the nature of the periodic structure, i.e. sine wave, cusp, grating, etc..

Table 6-4: Calculated wavelength for different structures based on $\beta=2.0^\circ$.

Sinewave	$\lambda_{\text{sinewave}} = \text{round} \left[\frac{422}{0.435\sqrt{2}} \sin 2.0 \right] = 24$
Sawtooth structure	$\lambda_{\text{sawtooth}} = \text{round} \left[\frac{422}{0.565\sqrt{2}} \sin 2.0 \right] = 18$
Cusp structure	$\lambda_{\text{cusp}} = \text{round} \left[\frac{422}{0.456\sqrt{2}} \sin 2 \right] = 23$
Grating structure	$\lambda_{\text{grating}} = \text{round} \left[\frac{422}{0.278\sqrt{2}} \sin 2.0 \right] = 37$
Step wave structure	$\lambda_{\text{stepwave}} = \text{round} \left[\frac{422}{0.269\sqrt{2}} \sin 2.0 \right] = 39$

At this angle, $\theta=90^\circ$, there are two major directional features, i.e. the lines and the near circular features, this situation of directional features on the surface was not studied in this dissertation, and requires further investigation.

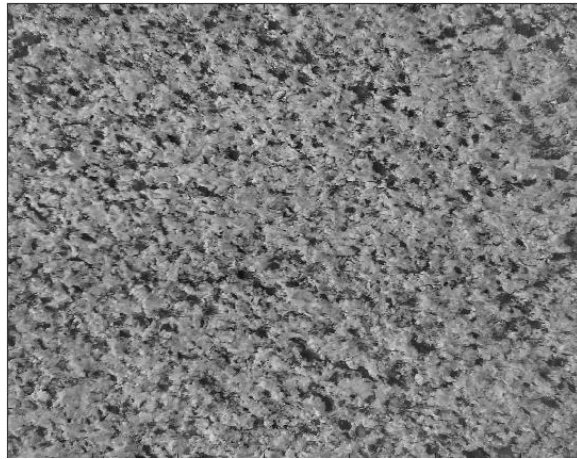


Figure 6-95: Image of the sample of the polar plot shown in Figure 6-91.

Another grayscale image of the pavement along the National Mall is shown in Figure 6-95, and its σ_{Rq} polar plot is depicted in Figure 6-91. The isotropic nature of this image and its lack of any directional features was correctly detected from its polar plot key metrics.

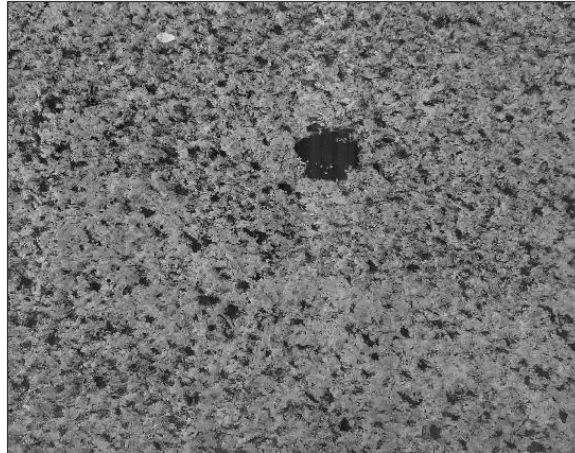


Figure 6-96: Image of the sample of the polar plot shown in Figure 6-92.

Figure 6-96 is an another grayscale image of the pavement along the National Mall with a single non-circular feature. The σ_{Rq} polar plot of this image is depicted in Figure 6-92. Lack of major directional features on the surface was detected by analyzing polar plot's key metrics, however, the presence of the single feature also could have been detected if the average radius of the polar plot had been compared to the radius of the defect free sample (shown in Figure 6-95). The increase of the average radius is an indicator of the presence of the single feature.

In general, without a prior knowledge of the surface it is not possible to exactly reconstruct the surface solely based on the information of the polar plots, however, by identifying and analyzing the key metrics extracted from polar plots a reliable and practical determination of various surface characteristics such as directional features, periodic features, and imperfections is possible. One obvious limitation of polar plots is identifying the location of a feature on its surface. Also, the limitations of the polar plots when there are several parallel linear features and their different configurations on the surface was discussed in section 6.3.4.

In this dissertation the focus was to understand the fundamentals of the behavior of the polar plots, and to realize the relationship between surface features and polar plot's key metrics. Exploring the limitations in recreating the original surface features from the polar plots has not been explored, however, at an initial first pass the polar plots can perform substantially better than common statistical based parameters (Sq , Ssk etc.) used in the majority of industrial and research applications.

6.7 Summary

In this chapter the effect of multiple linear and circular features on polar plot was detailed. Approach was modified by using the standard deviation of columns mean histogram instead of standard deviation of columns Rq histogram in order to increase the sensitivity of peak detection, and simplifying formulization of the radius of the polar plots.

Two methods were developed for the case when there are multiple circular features on the surface, the first one was to estimate the number of features based on the number of lobes that they create on the polar plots. This could be called the general form since it does not require the features to be identical, however, features' configuration should be in a way that in any orientation there is only one pair of them aligned and not more. Violation of this constraints decreases the accuracy of the estimated quantity of the features, also to resolve the issue of having more than one pair of features aligned at each angle the surface was distorted. Distortion of the surface makes sure that features' configuration is changed such that the probability of having more than one pair of aligned features decreases without harming the generality of the approach. Standard deviation of the columns' mean values was used to enhance the magnitude of the lobes and help identifying and counting them. It was also shown that the application of the approach can be broaden by thresholding the surface, and also the analysis of the entire field of view becomes possible by performing this technique.

The number of lobes on the polar plots, however, is only able to give insights about the quantity of the features on the surface, and is unable to provide information about the geometrical properties of them.

In order to obtain information about the quantity of the features as well as their geometrical attributes another approach was introduced based on the minimum radius of the polar plots. This second approach has two constraints, 1) the surface features are symmetric with respect to vertical and horizontal axis, and 2) there should not be any collinearity between features in at least one orientation. Based on these two constraints the relationship between the minimum radius of the $\sigma_{\mu h}$ polar plot, and the quantity of the symmetric features on the surface was established. From the system of equations of the r_{min} of the surface containing multiple symmetric features and the r_{min} of the surface with a single square feature (with equal areas), the quantity and radius of all of the identical features can be calculated. The advantage of this approach of estimating the quantity of the features over the estimation based on the number of the lobes of the polar plot is that it does not require to have only a pair of features align at each angle, also it is independent of the number of lobes on the polar plots. However, this method requires the features to be identical and be non-collinear on at least one orientation.

The r_{min} of the polar plots can also be taken advantage from in quality control processes. The r_{min} of the surface that is being assessed can be compared to the r_{min} of a surface with an accepted feature, the passing criterion can be defined as if the r_{min} of the surface is smaller than the r_{min} of the surface with the accepted surface, and failing is when this value is larger than the r_{min} of the surface with the accepted surface.

It was shown that if the r_{min} value is the base of calculation, violation of its requirements causes the inaccuracy of the results; if the features are non-identical then the calculated number of features is always underestimated. And if the non-collinearity requirement is not met then again the estimated number of features is less than the actual number of them on the surface.

Similar to the multiple circular features on the surface, polar plots are able to provide insights about surfaces containing linear features. Analysis of the surface with multiple linear features is divided into two sections, 1) when none of the features are parallel to each other, and 2) when there is only parallel scratches on the surface. In the first case the number of lobes on the polar plot divided by two will result in the number of the features on the surface, from the angular location of each lobe it is possible to estimate the width of the scratch and also find out its length. All the information about each feature's length, width, and depth can be obtained from the polar plots as long as none of them are parallel to each other. However, the special case of solely parallel scratches has to be broken down to four different scenarios namely 1) all identical and below each other when they are horizontal, 2) all identical and aligned when they are horizontal, 3) all identical and there is no overlapping between them when they are horizontal, and 4) all identical without any restriction. Each one of the cases were detailed and the obtainable information from polar plots were introduced. Identity of the linear features is the key requirement in this case and makes the interpretation of the results meaningful. Once this criterion is not met, the polar plots are not able to give insights about the surface features. Failure of this requirement was detailed at the end of each case of parallel scratches.

The last case of analysis of surfaces with multiple features is the case where there are mixed features on the surface, i.e. circular and linear features together. This situation was analyzed with the simplest case where only a scratch and a dig are present on the surface, the signature step-like peak created by their presence was detailed. Based on the specific type of lobes created by a pair of circular features and the lobe created by a linear feature the criterion for distinguishing different types of peaks was introduced. This criterion mathematically defines what feature is considered as a scratch.

Analysis of the specific type of lobes on the polar plots can provide information about the specific features that created them, and an estimate of their quantity. However, when the number

CHAPTER 7: CONCLUSIONS AND FUTURE DIRECTIONS

7.1 Conclusions

In this dissertation a novel approach for characterizing surface characteristics and surface features by using polar plots was presented. The surface is considered as a set of constituent profiles, the statistical parameter of choice for each profile is calculated, and the resulting distribution is then quantified by its standard deviation, skewness, and kurtosis. In the next step the surface rotates around its center and the process of calculating the statistical parameter of choice is again carried out. The whole process repeats until a 180° rotation of the surface is done. The calculated distribution properties are plotted versus the angle of rotation at which they were calculated in a polar plot formation, symmetry of the results is utilized to create a complete polar plot.

The following lists the capabilities of the polar plots and what information about the surface topography can be achieved by analyzing the polar plots, and their features.

Table 7-1: Polar plot's key features.

Feature(s)	r_{max}	r_{min}	$r_{max\pm 90^\circ}$	Local r_{min}	Angle between r_{max} and r_{min}	Angle between r_{max} and local r_{min}	# peaks	Rate of slope change
Surface Sq (Gaussian dist. of heights)								
Isotropy, directionality								
Periodicity								
Single circular feature								
Single linear feature								
Multiple digs simple								
Multiple digs threshold								
Multiple non-circular digs								
Multiple scratches – non parallel								
Multiple non-parallel, non-straight scratches								
Multiple scratches - parallel								
Mixed features								

For a surface with a Gaussian distribution of heights the Sq roughness of the surface can be calculated from the average radius of a nominally circular σ_{Rq} polar plot; it should be noted that any deviation of the surface height distribution from the ideal normal distribution induces error on the calculated Sq value of the surface from the polar plot radius. Isotropy and texture directionality of surfaces that are reported by Str and Std in ISO 25178-2 can also be captured by using the key

features of the polar plots. Maximum and minimum radius of the polar plots of an isotropic surface are reasonably close together, and thus the nominally circular shape of the polar plots is an indicator of an isotropic surface (equivalent of *Str*). Major surface directionality is reflected on the polar plots by creating a pair of lobes or local minimums in the lobe region of the polar plots, the angle of the lobe or the local minimum in the upper half of the polar plot indicates the angle enclosed between the surface texture and the vertical axis. This property of the polar plots is equivalent of the surface texture direction parameter of the ISO 25178-2 standard, *Std*. When there are several directionalities on the surface, the presence of all of them will be reflected on the polar plots as lobes or local minimums. While the *Std* parameter for these type of surfaces only indicates the directionality of the major surface texture, the angle of lobes or the local minimums of the polar plots shows the directionality of all of the directional features on the surface.

It was shown that from polar plots it is possible to calculate the wavelength of a periodic structure present on the surface and the nature of the repeating structure (sinewave, cusp, etc.) by using the minimum radius of the polar plot and the angle difference between the maximum radius and the local minimum. The advantage of calculating the wavelength of periodic features on the surface with polar plots over the power spectral analysis, PSD, is that polar plots are independent of the orientation of the surface texture, whereas the 1D PSD will result in accurate answer if it is taken perpendicular to the surface texture. It should be noted that in calculating the periodicity of the periodic structure on the surface the magnitude of the deviations of the real surface from the theoretical model such as curved tooling marks (in a milled surface), irregularities in the repetitive pattern on the surface, etc. could induce errors on the results.

Single circular features on the surface will increase the diameter of the polar plots, i.e. changes the minimum radius of the σ_{Rq} polar plot, and by analyzing the polar plot their depth and diameter can be back calculated. In a conservative approach a detectability threshold graph for a specific surface size can be generated. If the diameter and depth of a circular feature is in the detectable region not only the defect is detectable, but also its diameter can be estimated with two pixels

margin of error. It is also possible to identify whether the feature is on the surface such as a piece of dirt, or below the surface such as a dig by using the skewness of the columns Rsk histogram, Sk_{Rsk} polar plot.

Similar to the single circular feature, a single linear feature, i.e. a scratch will also affect the polar plots by increasing the average radius of the polar plot as well as creating a pair of lobes or local minimums, in this case the angle difference between the maximum radius and the lobe or local minimum is equal to 90° . The presence of a sharp peak or a local minimum in the lobe region is a function of the scratch's geometry, i.e. its length, depth, and width. The angular location of the lobe or the local minimum indicates the angle enclosed between the feature and the vertical axis. The presence of a linear feature on a surface is detected by comparing its polar plot with the same type of polar plots of an ideal defect-free surface, presence of a pair lobes or local minimums is an indicator that the surface contains a linear feature. The scratch detectability threshold graph can also be generated for a specific surface size based on the information of the columns Rq histogram. Presence of a pair of lobes in the polar plots of surfaces containing a single linear scratch can be taken advantage of to increase the sensitivity of the feature detection. Instead of the standard deviation of Rq histogram, if the skewness and kurtosis of the Rq histogram is used the sensitivity of the feature detection will increase. Also using Sk_{Rsk} polar plot provides information about whether a linear feature is on the surface or below it such as a scratch.

It was shown that for surfaces containing multiple features polar plots can also be used to achieve information about the surface features. For the case of only circular features on the surface two different methods were introduced, the first one used the number of peaks on the polar plots to estimate the quantity of the features on the surface, thresholding, distortion of the surface, and using the columns mean height value instead of their Rq values was done to improve the peak detection and consequently the accuracy of the feature estimation. The second method of estimating the quantity of the features as well as their depth and diameter was using the minimum radius of their $\sigma_{\mu h}$ polar plot.

Similar to the surfaces with circular features, polar plots can provide information about the surfaces containing multiple linear features. For the situation where none of the features is parallel to each other the number of lobes on the polar plot divided by two results in the quantity of the features on the surface. Different cases of surfaces containing multiple parallel scratches were analyzed and the obtainable information from polar plot for each case was detailed. In all of these cases the assumption was that the features are identical, it was also discussed how the violation of this assumption will affect the result.

In terms of single and multiple surface features some assumptions have to be made in order to be able to analyze the surface with this approach. The first assumption that applies to all of the surface features analysis is that the magnitude of the features, i.e. deviations from the nominal surface, is a constant value.

When multiple linear features are present on the surface and none of them are parallel to each other the only limitation of the approach is the maximum number of detectable lobes on the polar plots and there is no limitation on the geometry of linear features. However, when linear features are parallel to each other the main assumption is that they have to be identical in order to be able to meaningfully interpret the results of the polar plots. When this constraint is not met polar plots are not able to provide insight on the surface features.

In terms of estimating the number of circular features from the number of lobes on the polar plots the only requirement was having only two features aligned at each angle, violation of this requirement will cause an underestimation of the estimated value. For the case of multiple circular features estimation based on the minimum radius of the $\sigma_{\mu h}$ polar plot the approach results in accurate results if the features are all identical and non-collinear at one orientation at least. If these two requirements are not met the result are always underestimated.

Also polar plots of the surfaces that have multiple circular and linear features were analyzed, maximum and minimum radius of the polar plots as well as their number of peaks could provide information about the surface features. The simplest case was detailed where there is one scratch

and one dig on the surface, the resulting peaks on the polar plots and their formation was explained. From this simple case identifying different types of peaks on a given polar plot is possible.

Finally, all the above mentioned capabilities of the polar plots is applicable to grayscale images as well, however, it should be noted that the form and waviness of the image must be removed prior to their processing, and obviously no information about the depth of features can be obtained from the grayscale images.

7.2 Processing time of the approach

One of the strong points of this approach is its great capabilities in automatic quality control processes where time is among the most important matters. The entire amount of time to process a typical 1024×1024 pixels height map, and produce its different polar plots is about 10 seconds in MATLAB. It is believed that using other programming platforms (such as C++) to rotate the surface, which is the most time-consuming step of the calculations, can increase the speed of calculations, and thus benefits the in-situ assessment of the surface height maps or grayscale images in quality control systems.

7.3 Future directions

The approach that was developed and discussed in this dissertation outlines statistically based analysis of the surface topography, and focused on understanding the geometrical relationship between the rotated surface features and textures and the resulting polar plots.

It is believed that polar plots have a lot more potential capabilities and further studies are needed to explore them, suggested areas of the continuation of this work are listed below:

7.3.1 Processing aspects

- The nearest-neighborhood algorithm was used in order to rotate the surface around its center, however, other algorithms also need to be studied such as bilinear and bicubic interpolation methods, and their effect on the polar plots should be investigated.
- Peak detection is an important aspect of analyzing the polar plots, the maximum value of a moving window was used in this work in order to detect peaks, however, it is believed that other methods of peak detection should be investigated, such as assigning a probability value to each data point of a polar plot and setting a limit for differentiating peak-related points from other points. This becomes crucial and important when analyzing surfaces with mixed features, i.e. digs and scratches.
- Sensitivity of the approach increases as the higher order moments of data are used when quantifying the columns' statistical parameter histogram, for example columns Rq histogram, it is worth investigating the use of higher than fourth order moments of data (that are stable, and can meaningfully be related to the data distribution).
- It is believed that a machine learning approach can be applied to the polar plots for obtaining insights on the quantity and geometrical properties of the surface features. This is very helpful for surfaces containing multiple linear and circular features where the behavior of the polar plots become complicated. It is also very beneficial for automatic surface inspection systems, and classification of surface quality.

7.3.2 Applications aspects

- It is believed that the polar plots for highly structured surfaces have the potential to capture pattern irregularities on the surface structure, as well as the frequency of multiple repeating structures. Behavior of polar plots when analyzing these types of surfaces should be investigated.

- In this dissertation the method was applied on the processed surface, however, analysis of the unprocessed surface should be investigated, and potential capabilities of the polar plots, such as checking if the form or waviness is sufficiently removed from the surface, in this manner is worth exploring.
- In this dissertation when analyzing surfaces with multiple features the assumption was that the features have to be identical, and none-overlapping in at least one orientation, however, the use of minimum radius of the $\sigma_{\mu h}$ polar plot, or other polar plots, should be investigated when circular features are not identical.

REFERENCES

- [1] Leach, R., *Characterisation of areal surface texture*. 2013: Springer.
- [2] Blunt, L. and X. Jiang, *Advanced techniques for assessment surface topography: development of a basis for 3D surface texture standards" surfstand"*. 2003: Elsevier.
- [3] Bhushan, B., *Principles and applications of tribology*. 1999: John Wiley & Sons.
- [4] Meine, K., T. Schneider, D. Spaltmann and E. Santner, *The influence of roughness on friction: Part I: The influence of a single step*. *Wear*, 2002. **253**(7-8): p. 725-732.
- [5] Whitehouse, D.J., *Handbook of surface and nanometrology*. 2010: CRC press.
- [6] Jiang, X., P.J. Scott, D. Whitehouse and L. Blunt, *Paradigm shifts in surface metrology. Part I. Historical philosophy*. *Proceedings of the Royal Society A: Mathematical, Physical and Engineering Sciences*, 2007. **463**(2085): p. 2049-2070.
- [7] Leach, R., *Fundamental principles of engineering nanometrology*. 2014: Elsevier.
- [8] Lonardo, P., H. Trumpold and L. De Chiffre, *Progress in 3D surface microtopography characterization*. *CIRP annals*, 1996. **45**(2): p. 589-598.
- [9] Jiang, X., P.J. Scott, D. Whitehouse and L. Blunt, *Paradigm shifts in surface metrology. Part II. The current shift*. *Proceedings of the Royal Society A: Mathematical, Physical and Engineering Sciences*, 2007. **463**(2085): p. 2071-2099.
- [10] 25178-2, I., *Geometrical product specifications (GPS)–surface texture: areal–part 2: terms, definitions and surface texture parameters*. 2012.
- [11] Dong, W., P. Sullivan and K. Stout, *Comprehensive study of parameters for characterizing three-dimensional surface topography I: Some inherent properties of parameter variation*. *Wear*, 1992. **159**(2): p. 161-171.
- [12] Chattopadhyay, R., *Surface wear: analysis, treatment, and prevention*. 2001: ASM international.
- [13] Javidi, A., U. Rieger and W. Eichlseder, *The effect of machining on the surface integrity and fatigue life*. *International Journal of fatigue*, 2008. **30**(10-11): p. 2050-2055.
- [14] F Azimi, B Young and B. Mullany, *Statistical Analysis of Surface Measurements and Images*, in *American Society for Precision Engineering*. 2017: Charlotte, NC, USA.
- [15] Azimi, F. and B. Mullany, *Geometric surface feature detection using statistical based metrics*. *Precision Engineering*, 2019. **60**: p. 602-609.
- [16] Leach, R., *Optical measurement of surface topography*. Vol. 14. 2011: Springer.
- [17] Persson, B., O. Albohr, U. Tartaglino, A. Volokitin and E. Tosatti, *On the nature of surface roughness with application to contact mechanics, sealing, rubber friction and adhesion*. *Journal of Physics: Condensed Matter*, 2004. **17**(1): p. R1.
- [18] Archard, J., *Friction between metal surfaces*. *Wear*, 1986. **113**(1): p. 3-16.
- [19] Greenwood, J. and J. Tripp, *The contact of two nominally flat rough surfaces*. *Proceedings of the institution of mechanical engineers*, 1970. **185**(1): p. 625-633.
- [20] Hamrock, B.J., S.R. Schmid and B.O. Jacobson, *Fundamentals of fluid film lubrication*. 2004: CRC press.
- [21] Wang, W.-Z., H. Chen, Y.-Z. Hu and H. Wang, *Effect of surface roughness parameters on mixed lubrication characteristics*. *Tribology international*, 2006. **39**(6): p. 522-527.
- [22] Patir, N. and H. Cheng, *An average flow model for determining effects of three-dimensional roughness on partial hydrodynamic lubrication*. *Journal of lubrication Technology*, 1978. **100**(1): p. 12-17.
- [23] Whitehouse, D., D. Bowen, V. Venkatesh, P. Lonardo and C. Brown, *Gloss and surface topography*. *CIRP Annals-Manufacturing Technology*, 1994. **43**(2): p. 541-549.
- [24] Davies, H., *The reflection of electromagnetic waves from a rough surface*. *Proceedings of the IEE-Part IV: Institution Monographs*, 1954. **101**(7): p. 209-214.

- [25] Holzer, J.A. and C. Sung, *Scattering of electromagnetic waves from a rough surface. II*. Journal of Applied Physics, 1978. **49**(3): p. 1002-1011.
- [26] Sung, C. and J. Holzer, *Scattering of electromagnetic waves from a rough surface*. Applied Physics Letters, 1976. **28**(8): p. 429-431.
- [27] Biot, M.A., *Some new aspects of the reflection of electromagnetic waves on a rough surface*. Journal of Applied Physics, 1957. **28**(12): p. 1455-1463.
- [28] Kivelson, M.G. and S. Moszkowski, *Reflection of electromagnetic waves from a rough surface*. Journal of Applied Physics, 1965. **36**(11): p. 3609-3612.
- [29] Ås, S.K., B. Skallerud and B.W. Tveiten, *Surface roughness characterization for fatigue life predictions using finite element analysis*. International Journal of Fatigue, 2008. **30**(12): p. 2200-2209.
- [30] Suraratchai, M., J. Limido, C. Mabru and R. Chieragatti, *Modelling the influence of machined surface roughness on the fatigue life of aluminium alloy*. International Journal of Fatigue, 2008. **30**(12): p. 2119-2126.
- [31] Novovic, D., R. Dewes, D. Aspinwall, W. Voice and P. Bowen, *The effect of machined topography and integrity on fatigue life*. International Journal of Machine Tools and Manufacture, 2004. **44**(2-3): p. 125-134.
- [32] Hashimoto, F., Y. Guo and A. Warren, *Surface integrity difference between hard turned and ground surfaces and its impact on fatigue life*. CIRP Annals-Manufacturing Technology, 2006. **55**(1): p. 81-84.
- [33] Lai, J., H. Huang and W. Buising, *Effects of microstructure and surface roughness on the fatigue strength of high-strength steels*. Procedia Structural Integrity, 2016. **2**: p. 1213-1220.
- [34] Maiya, P. and D. Busch, *Effect of surface roughness on low-cycle fatigue behavior of type 304 stainless steel*. Metallurgical Transactions A, 1975. **6**(9): p. 1761.
- [35] Li, W. and D. Li, *Influence of surface morphology on corrosion and electronic behavior*. Acta materialia, 2006. **54**(2): p. 445-452.
- [36] Walter, R. and M.B. Kannan, *Influence of surface roughness on the corrosion behaviour of magnesium alloy*. Materials & Design, 2011. **32**(4): p. 2350-2354.
- [37] Fuller, K. and D. Tabor, *The effect of surface roughness on the adhesion of elastic solids*. Proc. R. Soc. Lond. A, 1975. **345**(1642): p. 327-342.
- [38] Persson, B. and S. Gorb, *The effect of surface roughness on the adhesion of elastic plates with application to biological systems*. The Journal of chemical physics, 2003. **119**(21): p. 11437-11444.
- [39] Linez-Bataillon, P., F. Monchau, M. Bigerelle and H. Hildebrand, *In vitro MC3T3 osteoblast adhesion with respect to surface roughness of Ti6Al4V substrates*. Biomolecular engineering, 2002. **19**(2-6): p. 133-141.
- [40] Deligianni, D.D., N.D. Katsala, P.G. Koutsoukos and Y.F. Missirlis, *Effect of surface roughness of hydroxyapatite on human bone marrow cell adhesion, proliferation, differentiation and detachment strength*. Biomaterials, 2000. **22**(1): p. 87-96.
- [41] Whitehouse, D., *The parameter rash—is there a cure?* Wear, 1982. **83**(1): p. 75-78.
- [42] Lonardo, P., D. Lucca and L. De Chiffre, *Emerging trends in surface metrology*. CIRP Annals-Manufacturing Technology, 2002. **51**(2): p. 701-723.
- [43] Sherrington, I. and E. Smith, *Modern measurement techniques in surface metrology: part I: stylus instruments, electron microscopy and non-optical comparators*. Wear, 1988. **125**(3): p. 271-288.
- [44] Brown, L. and L. Blunt, *Surface metrology for the automotive industry*. 2008.
- [45] Binnig, G., C.F. Quate and C. Gerber, *Atomic force microscope*. Physical review letters, 1986. **56**(9): p. 930.
- [46] Whitehouse, D.J., *Surface metrology*. Measurement Science and Technology, 1997. **8**(9): p. 955.

- [47] Leach, R., *The measurement of surface texture using stylus instruments*. NPL, 2001: p. 54-61.
- [48] 3274, I., *Geometrical Product Specifications (GPS) -- Surface texture: Profile method -- Nominal characteristics of contact (stylus) instruments*. 1996.
- [49] Whitehouse, D.J., *Surfaces and their Measurement*. 2004: Elsevier.
- [50] Nugent, P., *Skimming the Surface of Surface Finish*. 2016, Quality Magazine.
- [51] Hocken, R., N. Chakraborty and C. Brown, *Optical metrology of surfaces*. CIRP Annals-Manufacturing Technology, 2005. **54**(2): p. 169-183.
- [52] ISO, E., *4288—Geometrical product specifications (GPS)—surface texture: profile method—rules and procedures for the assessment of surface texture*. International Organization for Standardization, Genève, 1996.
- [53] Wyant, J.C. *Optical profilers for surface roughness*. in *Measurement and Effects of Surface Defects & Quality of Polish*. 1985. International Society for Optics and Photonics.
- [54] 4287, I., *Geometrical Product Specifications (GPS) -- Surface texture: Profile method -- Terms, definitions and surface texture parameters*. 1997.
- [55] Standard, I. and B. ISO, *4287/1997. Geometrical product specifications (GPS)—Surface texture: Profile method—Terms, definitions and surface texture parameters*, 1997.
- [56] De Chiffre, L., P. Lonardo, H. Trumpold, D. Lucca, G. Goch, C. Brown, J. Raja and H.N. Hansen, *Quantitative characterisation of surface texture*. CIRP Annals-Manufacturing Technology, 2000. **49**(2): p. 635-652.
- [57] Bennett, J.M., *Recent developments in surface roughness characterization*. Measurement Science and Technology, 1992. **3**(12): p. 1119.
- [58] Dong, W., P. Sullivan and K. Stout, *Comprehensive study of parameters for characterising three-dimensional surface topography: III: Parameters for characterising amplitude and some functional properties*. Wear, 1994. **178**(1-2): p. 29-43.
- [59] Dong, W., P. Sullivan and K. Stout, *Comprehensive study of parameters for characterising three-dimensional surface topography: IV: parameters for characterising spatial and hybrid properties*. Wear, 1994. **178**(1-2): p. 45-60.
- [60] Dong, W., P. Sullivan and K. Stout, *Comprehensive study of parameters for characterizing three-dimensional surface topography II: Statistical properties of parameter variation*. Wear, 1993. **167**(1): p. 9-21.
- [61] Scott, P.J., *Feature parameters*. Wear, 2009. **266**(5-6): p. 548-551.
- [62] Stout, K., L. Blunt, W. Dong, E. Mainsah, N. Luo, T. Mathia, P. Sullivan and H. Zahouani, *Development of Methods for Characterisation of Roughness in Three Dimensions* First ed. 2000: ELSEVIER. 384.
- [63] Huang, S.-H. and Y.-C. Pan, *Automated visual inspection in the semiconductor industry: A survey*. Computers in industry, 2015. **66**: p. 1-10.
- [64] Scholz-Reiter, B., D. Weimer and H. Thamer, *Automated surface inspection of cold-formed micro-parts*. Cirp annals-manufacturing technology, 2012. **61**(1): p. 531-534.
- [65] Cao, Z., F. Cui and C. Zhai, *Vision system with high dynamic range for optical surface defect inspection*. Applied Optics, 2018. **57**(34): p. 9981-9987.
- [66] Mital, A., M. Govindaraju and B. Subramani, *A comparison between manual and hybrid methods in parts inspection*. Integrated Manufacturing Systems, 1998. **9**(6): p. 344-349.
- [67] Bartkowiak, T. and C.A. Brown, *Multiscale 3D Curvature Analysis of Processed Surface Textures of Aluminum Alloy 6061 T6*. Materials, 2019. **12**(2): p. 257.
- [68] Kopardekar, P., A. Mital and S. Anand, *Manual, hybrid and automated inspection literature and current research*. Integrated Manufacturing Systems, 1993. **4**(1): p. 18-29.
- [69] Tsai, D.-M. and C.-Y. Hsieh, *Automated surface inspection for directional textures*. Image and vision computing, 1999. **18**(1): p. 49-62.
- [70] Buehlmann, U. and R.E. Thomas, *Impact of human error on lumber yield in rough mills*. Robotics and computer integrated manufacturing. 18: 197-203., 2002. **18**.

- [71] Ruz, G.A., P.A. Estevez and P.A. Ramirez, *Automated visual inspection system for wood defect classification using computational intelligence techniques*. International Journal of Systems Science, 2009. **40**(2): p. 163-172.
- [72] Neogi, N., D.K. Mohanta and P.K. Dutta, *Review of vision-based steel surface inspection systems*. EURASIP Journal on Image and Video Processing, 2014. **2014**(1): p. 50.
- [73] Aikens, D.M. *Meaningful surface roughness and quality tolerances*. in *International Optical Design Conference*. 2010. Optical Society of America.
- [74] 14997, I., *Optics and photonics - Test methods for surface imperfections of optical elements*. 2003.
- [75] 7, I.-. *Optics and photonics -- Preparation of drawings for optical elements and systems -- Part 7: Surface imperfections*. 2008.
- [76] Herman, E., R.N. Youngworth and D.M. Aikens. *Modern optics drawings: the journey from MIL to ANSI to ISO drawing formats*. in *Optical Manufacturing and Testing XII*. 2018. International Society for Optics and Photonics.
- [77] ARDEC, U.A., *MIL-PRF-13830B American military standards*. United States Department of Defense, 1992.
- [78] ARDEC, U.A., *MIL-O-13830 American military standards*. United States Department of Defense, 1954.
- [79] Aikens, D.M. *The truth about scratch and dig*. in *Optical Fabrication and Testing*. 2010. Optical Society of America.
- [80] Aikens, D. *Objective measurement of scratch and dig*. in *Optical Fabrication and Testing*. 2012. Optical Society of America.
- [81] Cormier, A. *Assessment of current scratch standards*. in *Optical Components and Systems*. 1987. International Society for Optics and Photonics.
- [82] Young, M. *The scratch standard is only a cosmetic standard*. in *Surface Characterization and Testing II*. 1989. International Society for Optics and Photonics.
- [83] Institute, A.N.S., *Optics and Electro-Optical Instruments – Optical Elements and Assemblies – Surface Imperfections*. 2017.
- [84] Newman, T.S. and A.K. Jain, *A survey of automated visual inspection*. Computer vision and image understanding, 1995. **61**(2): p. 231-262.
- [85] Chin, R.T. and C.A. Harlow, *Automated visual inspection: A survey*. IEEE transactions on pattern analysis and machine intelligence, 1982(6): p. 557-573.
- [86] Xie, X., *A review of recent advances in surface defect detection using texture analysis techniques*. ELCVIA Electronic Letters on Computer Vision and Image Analysis, 2008. **7**(3): p. 1-22.
- [87] Kumar, A., *Computer-vision-based fabric defect detection: A survey*. IEEE transactions on industrial electronics, 2008. **55**(1): p. 348-363.
- [88] Bartkowiak, T. *Characterization of 3D surface texture directionality using multi-scale curvature tensor analysis*. in *ASME 2017 International Mechanical Engineering Congress and Exposition*. 2017. American Society of Mechanical Engineers.
- [89] Xie, X., M. Mirmehdi and B. Thomas, *Colour tonality inspection using eigenspace features*. Machine Vision and Applications, 2006. **16**(6): p. 364-373.
- [90] Broadhurst, R., J. Stough, S. Pizer and E. Chaney. *Histogram statistics of local image regions for object segmentation*. in *International workshop on deep structure, singularities, and computer vision*. 2005. Citeseer.
- [91] Tsai, I.-S., C.-H. Lin and J.-J. Lin, *Applying an artificial neural network to pattern recognition in fabric defects*. Textile Research Journal, 1995. **65**(3): p. 123-130.
- [92] Bodnarova, A., J.A. Williams, M. Bennamoun and K.K. Kubik. *Optimal textural features for flaw detection in textile materials*. in *TENCON'97. IEEE Region 10 Annual Conference. Speech and Image Technologies for Computing and Telecommunications., Proceedings of IEEE*. 1997. IEEE.

- [93] Siew, L.H., R.M. Hodgson and E.J. Wood, *Texture measures for carpet wear assessment*. IEEE Transactions on Pattern Analysis and Machine Intelligence, 1988. **10**(1): p. 92-105.
- [94] Iivarinen, J., J. Rauhamaa and A. Visa. *Unsupervised segmentation of surface defects*. in *Pattern Recognition, 1996., Proceedings of the 13th International Conference on*. 1996. IEEE.
- [95] Khodabandehlou, H. and M.S. Fadali. *A quotient gradient method to train artificial neural networks*. in *2017 International Joint Conference on Neural Networks (IJCNN)*. 2017. IEEE.
- [96] Odemir, S., A. Baykut, R. Meylani, A. Erçil and A. Ertuzun. *Comparative evaluation of texture analysis algorithms for defect inspection of textile products*. in *Pattern Recognition, 1998. Proceedings. Fourteenth International Conference on*. 1998. IEEE.
- [97] Khodabandehlou, H. and M.S. Fadali, *Echo State versus Wavelet Neural Networks: Comparison and Application to Nonlinear System Identification*. IFAC-PapersOnLine, 2017. **50**(1): p. 2800-2805.
- [98] Mäenpää, T. and M. Pietikäinen, *Texture analysis with local binary patterns*, in *Handbook of pattern recognition and computer vision*. 2005, World Scientific. p. 197-216.
- [99] Niskanen, M., O. Silvén and H. Kauppinen. *Color and texture based wood inspection with non-supervised clustering*. in *Proceedings of the scandinavian Conference on image analysis*. 2001.
- [100] Vilnrotter, F.M., R. Nevatia and K.E. Price, *Structural analysis of natural textures*. IEEE Transactions on Pattern Analysis & Machine Intelligence, 1986(1): p. 76-89.
- [101] Chen, J. and A.K. Jain. *A structural approach to identify defects in textured images*. in *Systems, Man, and Cybernetics, 1988. Proceedings of the 1988 IEEE International Conference on*. 1988. IEEE.
- [102] Fricout, G., D. Jeulin, P.-J. Krauth and T. Jacquot, *Automatic on-line inspection of non-smooth surface*. Wear, 2008. **264**(5-6): p. 416-421.
- [103] Zheng, H., L.X. Kong and S. Nahavandi, *Automatic inspection of metallic surface defects using genetic algorithms*. Journal of materials processing technology, 2002. **125**: p. 427-433.
- [104] Bailey, W.B. and J. Cummins, *Statistics*. 1917.
- [105] Forbes, C.S., *Statistical distributions Catherine Forbes ... [et al.]*. 2011, Wiley: Hoboken, N.J. p. 1 online resource.
- [106] Press, W.H., *Numerical recipes in C : the art of scientific computing*. 2nd ed. 1997, Cambridge [Cambridgeshire] ; New York: Cambridge University Press. xxvi, 994 p.

APPENDIX A: STATISTICAL TOOLS

Some of the statistical concepts that were discussed in this survey as well as those that will be used in next chapters of this thesis will be introduced here.

A.1 Moment of data

The property of the tendency of a set of discrete values to cluster around a specific number can be used to characterize the set by a few numbers related to its moments. The first moment is the mean value which is the sum of a set of numbers divided by the quantity of numbers in that set denoted by μ or \bar{x} . Mean estimates the value around which the central clustering happens. Second central moment of data that measures the dispersion of the data around the mean value (first moment) is the variance which is given in equation 0-1 [104, 105].

$$var = \frac{1}{n} \sum_{i=1}^n (x_i - \mu)^2 \quad (0-1)$$

The square root of the variance is called standard deviation and is denoted by σ . The third moment of data is skewness which characterizes the symmetry of a distribution around its mean; it is defined in such a way that is dimensionless and is given in equation 0-2.

$$skewness = \frac{1}{n} \sum_{i=1}^n \left[\frac{x_i - \mu}{\sigma} \right]^3 \quad (0-2)$$

Skewness value equal to zero means that the distribution is completely symmetric around the mean value.

The fourth moment of the data is kurtosis which is a measure of peakedness or flatness of a distribution, kurtosis is also a positive dimensionless value and is given in equation 0-3.

$$kurtosis = \frac{1}{n} \sum_{i=1}^n \left[\frac{x_i - \mu}{\sigma} \right]^4 \quad (0-3)$$

And in general, the N^{th} moment of data can be calculated based on equation 0-4.

$$N^{th} \text{moment} = \frac{1}{n} \sum_{i=1}^n \left[\frac{x_i - \mu}{\sigma} \right]^N \quad (0-4)$$

It should be noted that all these moments are normalized with respect to standard deviation of the distribution [105, 106].

A.2 Normal distribution

One of the most important distributions in the study of probability and statistics is the Normal (Gaussian) probability distribution, a random variable is said to have a Normal probability distribution if its probability density function (PDF) is given by equation 0-5 [105]:

$$f(x | \mu, \sigma^2) = \frac{1}{\sqrt{2\pi\sigma^2}} e^{-\frac{(x-\mu)^2}{2\sigma^2}} \quad (0-5)$$

Subtracting the mean value from the values of all of the data set with mean equal to μ and variance equal to σ , $X \sim (\mu, \sigma^2)$, and dividing the result by the standard deviation makes a standard normal distribution with mean equal to zero and variance equal to one, i.e. $X \sim N(0,1)$.

Histogram: is a graphical representation of a distribution of a set of values. x-axis in a histogram is the range of values divided into equal or unequal non-overlapping bins, and the y-axis shows the total number of values (the count) of the set that have the value of the bin. A normal distribution has a bell shape histogram [105].

A.3 Chi distribution

Chi distribution is a distribution of the sum of the square of values from a standard normal distribution which explains the additive property of independent *Chi* squared variables, and the square root of this distribution is called *Chi* distribution [105]. The mean value of *Chi* distribution can be calculated based on equation 0-6 and the variance is based on equation 0-7 [105].

$$\mu = \sqrt{2} \frac{\Gamma((k+1)/2)}{\Gamma(k/2)} \quad (0-6)$$

$$\sigma^2 = k - \mu^2 \quad (0-7)$$

Where k is the degree of freedom and Γ is the Gamma function.

APPENDIX B: PUBLICATIONS

- F. Azimi, B. Mullany, “Geometric surface feature detection using statistical based metrics” *Journal of Precision Engineering*, Volume 60, November 2019, 602-609.
- F. Azimi, Benjamin Young, Brigid Mullany, “Statistical Analysis of Surface Measurements and Images”, ASPE conference, Charlotte, NC. November 2017.
- F. Azimi, E. Fleischhauer, P. Tkacik, R. Keanini ,B. Mullany, “Correlations Between Media-Workpiece Contact Modes Occurring During Vibrational Finishing and the Resulting Workpiece Topography”, 15th International Conference on Metrology and Properties of Engineering Surfaces, Charlotte, NC. March 2015.

APPENDIX C: MATLAB CODES

The key MATLAB codes that were used in this work are presented here.

`Polars`: This function takes the matrix and calculates the standard deviation, skewness, and kurtosis of columns *Rq* histogram as well as the standard deviation of the columns mean height histogram by rotating the surface 180°.

```
function [std_mean_matrix, std_rq_matrix, sk_rq_matrix, ku_rq_matrix,
sk_rsk_matrix, T]= Polars(a,stp)

% INPUTS:      a: surface/image matrix
%              stp: Resolution of rotation

center_point = round(length(a)/2);           %finds the center of the matrix
limiit = round(length(a)/sqrt(2)/2);        %calculates the half size of
the superimposed rectangle
ct = 0;
begining_angle = 0;
end_angle = 180;
rq_columns = zeros(end_angle/stp , 2*limiit); %assigning zero
matrices for speeding up the loop
mean_columns = zeros(end_angle/stp , 2*limiit); %assigning zero
matrices for speeding up the loop
for lp=begining_angle:stp:end_angle
    c = imrotate(a,-(lp));                    %rotates the surface
    center_point = floor(length(c)/2);
    c = c(center_point-limiit:center_point+limiit-1,center_point-
limiit:center_point+limiit-1);
    ct=ct+1;

    rq_columns(ct,:) = std(c);
    mean_columns(ct,:) = mean(c);
    sk_columns(ct,:) = skewness(c);
end
std_mean_matrix = std(mean_columns'); %calculates the std of columns
mean
std_rq_matrix = std(rq_columns'); %calculates the std of columns
Rq
sk_rq_matrix = skewness(rq_columns'); %calculates the skewness of
columns Rq
ku_rq_matrix = kurtosis(rq_columns'); %calculates the kurtosis of
columns Rq
sk_rsk_matrix = skewness(sk_columns'); %calculates the skewness of
columns Rsk
%%-----
% using the angular symmetry to create the second half of the polar
plot
std_mean_matrix = [std_mean_matrix, std_mean_matrix(2:end-1)];
```

```

std_rq_matrix = [std_rq_matrix, std_rq_matrix(2:end-1)];
sk_rq_matrix = [sk_rq_matrix, sk_rq_matrix(2:end-1)];
ku_rq_matrix = [ku_rq_matrix, ku_rq_matrix(2:end-1)];
sk_rsk_matrix = [sk_rsk_matrix, sk_rsk_matrix(2:end-1)];

```

```

T = (0:stp:(2*end_angle)-stp)*pi/180; %angles for plotting the
results in polarplot command

```

Fast_Polars: This function takes the matrix and calculates the standard deviation, skewness, and kurtosis of columns *Rq* histogram as well as the standard deviation of the columns mean height histogram, but rotates the surface only 90°.

```

function [std_mean_matrix, std_rq_matrix, sk_rq_matrix, ku_rq_matrix,
sk_rsk_matrix, T]= Fast_Polars(a,stp)

```

```

% this function rotates the surface 90 degrees and creates complete
polar plots.

```

```

center_point = round(length(a)/2); %finds the center of the matrix
limiit = round(length(a)/sqrt(2)/2); %calculates the half size of
the superimposed rectangle
ct = 0;
begining_angle = 0;
end_angle = 90-stp;
rq_columns = zeros(end_angle/stp , 2*limiit); %assigning zero
matrices for speeding up the loop
mean_columns = zeros(end_angle/stp , 2*limiit); %assigning zero
matrices for speeding up the loop

```

```

for lp=begining_angle:stp:end_angle
    c = imrotate(a,-(lp)); %rotates the surface
    center_point = floor(length(c)/2);
    c = c(center_point-limiit:center_point+limiit-1,center_point-
limiit:center_point+limiit-1);
    ct=ct+1;

```

```

    rq_columns(ct,:) = std(c,0,1);
    rq_columns(90/stp+ct,:) = std(c,0,2);

```

```

    mean_columns(ct,:) = mean(c,1);
    mean_columns(90/stp+ct,:) = mean(c,2);

```

```

    sk_columns(ct,:) = skewness(c,0,1);
    sk_columns(90/stp+ct,:) = skewness(c,0,2);

```

```

end

```

```

std_mean_matrix = std(mean_columns'); %calculates the std of
columns Rq

```

```

std_rq_matrix = std(rq_columns');           %calculates the std of columns
Rq
sk_rq_matrix = skewness(rq_columns');      %calculates the skewness of
columns Rq
ku_rq_matrix = kurtosis(rq_columns');      %calculates the kurtosis of
columns Rq
sk_rsk_matrix = skewness(sk_columns');     %calculates the skewness of
columns Rsk
%%-----
-----
% using the angular symmetry to create the second half of the polar
plot
std_mean_matrix = [std_mean_matrix, std_mean_matrix(1:end)];
std_rq_matrix = [std_rq_matrix, std_rq_matrix(1:end)];
sk_rq_matrix = [sk_rq_matrix, sk_rq_matrix(1:end)];
ku_rq_matrix = [ku_rq_matrix, ku_rq_matrix(1:end)];
sk_rsk_matrix = [sk_rsk_matrix, sk_rsk_matrix(1:end)];

T = (0:stp:(4*(end_angle+stp))-stp)*pi/180; %angles for plotting the
results in polarplot command

```

SQRT_Polars: The input of this function is the thresholded surface and the outcome is the standard deviation of the columns mean height values, it analyzes the entire field of view.

```

function[std_mean_matrix, T] = SQRT2_Polars(a, stp)

%this function is like Polars function with the difference that it
creates
%a matrix 1.414 times the input matrix, zeros, and puts the rotated
matrix
%at the center of it (called bigger_matrix), and it does the
calculations.
%the input matrix has to be after thresholding (= all zeros except
features
%on the surface)

N = round(sqrt(2)*length(a));           %analyzing the entire field of view
ct = 0;
begining_angle = 1;
end_angle = 180;
for lp=begining_angle:stp:end_angle %loop for calculation of std
    c = imrotate(a,-(lp));
    bigger_matrix = zeros(N,N);        %bigger matrix to cover the initial
input surface
    Start = round((N - length(c))/2);
    bigger_matrix(Start:Start+length(c)-1 , Start:Start+length(c)-1) =
c;
    ct=ct+1;
    mean_columns(ct,:) = mean(bigger_matrix);
end

```

```

%%-----
----
% using the angular symmetry to create the second half of the polar
plot
std_mean_matrix = std(mean_columns');
std_mean_matrix = [std_mean_matrix, std_mean_matrix(1:end)];
T = (1:stp:(2*end_angle))*pi/180; %angles for plotting the results in
polarplot command

```

whole_location_creator: This function creates random location for surface features on the entire field of view

```
function[xc, yc] = whole_location_creator(a, no_of_digs, diameter, uni)
```

```
% this function creates coordinates for un-overlapped features on the
% surface, doesn't care if the feature is circle or square.
```

```

%outputs are two vectors, xc and yc.
dig = zeros(diameter,diameter); %matrix
of dig, dimensions = diameter of the dig
temp = zeros(length(a) , length(a)); %temp
matrix to check for overlapping
dig_binary = zeros(diameter,diameter); %temp
binary dig matrix to check for overlapping

flag = 1;
ct = 0;
if uni == 1
    xc = ones(1,no_of_digs);
    yc = ones(1,no_of_digs);
else
    while flag == 1 && ct < 500 %500
    try to solve dig overlapping issue

        for i = 1:length(dig)
%assigning depth to the dig
            for j = 1:length(dig)
                if (i-(0.5*diameter))^2 + (j-(0.5*diameter))^2 <
(0.5*diameter)^2
                    dig_binary(i,j) = 1;
%assigning 1 to binary dig matrix
                end
            end
        end

        xc = randi([1 , length(a) - length(dig)], 1, no_of_digs);
        yc = randi([1 , length(a) - length(dig)], 1, no_of_digs);

        for i = 1:length(xc)
            temp(xc(i) : xc(i) + diameter-1 , yc(i) : yc(i) + diameter-
1 )= temp(xc(i) : xc(i) + diameter-1 , yc(i) : yc(i) + diameter-1) +
dig_binary ; %if 2 digs overlap the value of temp goes up
            end
            ct = ct + 1;

```

```

        if max(temp(:)) > 1 % 1 ---> overlap checking, max(temp(:)) >
1 means there is at least one overlap, do the dig creation again
            flag = 1;
        else
            flag = 0;          %0 ---> there is no overlapping. GOOD TO
GO
        end
    end
    if flag ==1
        error('overlapping exist');
    end
end
end

```

dig_creator: This function creates circular features on the surface.

```

function[a] = dig_creator(a, xc, yc, diameter, depth, uni)

dig = zeros(diameter,diameter);      %matrix of dig, dimensions =
diameter of the dig

b = zeros(length(a), length(a));
b = logical(b);

for i = 1:length(dig)                %assigning depth to the dig
    for j = 1:length(dig)
        if (i-(0.5*diameter))^2 + (j-(0.5*diameter))^2 <=
(0.5*diameter)^2
            dig(i,j) = depth;
        end
    end
end
if uni == 0
    for i = 1:length(xc)
        b(xc(i) : xc(i) + diameter-1 , yc(i) : yc(i) + diameter-1 ) =
dig;
        c = logical(b);
        a(c) = depth;
    end
else
    n = round((length(a)-diameter)/(length(xc)-1))-1;
    containing_row = round(length(a)/2);
    for i = 1:length(xc)
        b((i-1)*n+1:(i-1)*n+diameter , containing_row-
diameter/2:containing_row+diameter/2-1) = dig;
        c = logical(b);
        a(c) = depth;
    end
%    a = imrotate(a,90);
end

```

scratch_creator: This function creates multiple linear features on the surface.

```

function [a, theta] = scratch_creator(a, no_of_scratches, Length,
width, depth, vert, teta)
% this function takes matrix "a" and put some random scratches on it
based
% on input dimensions
d = zeros(no_of_scratches,no_of_scratches);
b = zeros(length(a), length(a));
b = logical(b);
temp = ones(width, Length)*depth;
temp = logical(temp);
m = cell(1, no_of_scratches) ;
incr = round(180/no_of_scratches);
flag = 0;
if vert == 0
    while flag == 0
        theta = randi([1 , 180], 1, no_of_scratches);
        for i = 1:length(theta)
            d(i,:) = abs(theta(i) - theta);
        end
        for u = 1:length(d)
            d(u,u) = 360;
        end
        d = d(:)';
        if max(d < 5) == 1
            flag = 0;
            clear d;
        else
            flag = 1;
        end
    end
elseif vert == 1
    theta = ones(1, no_of_scratches)*90;
elseif vert == 2
    theta = (0:incr:180);
    theta = theta(1:no_of_scratches);
else
    theta = teta;
end

xc = randi([length(a) - round(length(a)/sqrt(2)) , length(a)-Length],
1, no_of_scratches);
yc = randi([length(a) - round(length(a)/sqrt(2)) , length(a)-Length],
1, no_of_scratches);

for i = 1:no_of_scratches
    m[95] = imrotate(temp, theta(i));
    [dx, dy] = size(m{i});
    b(xc(i):xc(i)+dx-1 , yc(i):yc(i)+dy-1) = b(xc(i):xc(i)+dx-1
, yc(i):yc(i)+dy-1) + m{i};
    c = logical(b);
    a(c) = depth;

end
end

```